Higher order global differentiability local approximations for 2-D and 3-D distorted element geometries

by

Rajesh Kumar Maduri

B.E., Osmania University, India, 2001

M.S. (Mechanical Engineering), University of Kansas, 2004

Submitted to the Department of Mechanical Engineering and the Faculty of the Graduate School of the University of Kansas in partial fulfillment of the requirements for the Degree of Doctor of Philosophy

---

Dr. Karan S. Surana, (Chairperson)

Dr. Peter W. TenPas

Dr. Ray Taghavi

Dr. Robert Sorem

Dr. Albert Romkes

Date defended

The Thesis committee for Rajesh Kumar Maduri certifies that this is the approved version of the following thesis:

Higher order global differentiability local approximations for 2-D and 3-D distorted element geometries

Committee:

Dr. Karan S. Surana, (Chairperson)

Dr. Peter W. TenPas

Dr. Ray Taghavi

Dr. Robert Sorem

Dr. Albert Romkes

Date approved

This thesis is dedicated to my sister's love and friendship

Acknowledgments

I would like to express my sincere gratitude to Dr. Karan S. Surana for providing invaluable guidance and constant encouragement during the course of my study. Dr.Surana's exhaustive knowledge and enthusiasm for the subject has helped me immensely in successful completion of this work. I extend my thanks to Dr. Surana for providing me financial support. I would also like to thank my committee members for taking time to serve on my thesis committee.

The financial support provided by DEPSCoR/AFOSR through grant numbers F49620-03-01-0298 to the University of Kansas, Department of Mechanical Engineering and through grant number F49620-03-01-0201 to Texas A & M University is gratefully acknowledged. The seed grant provided by ARO through grant number FED46680 to the University of Kansas, Department of Mechanical Engineering is also acknowledged. The computing facilities of the Computational Mechanics Laboratory (CML) of the Department of Mechanical Engineering Department and the software development infrastructure in CML has been instrumental in conducting the numerical studies. I thank Dr. Ron Dougherty, Chairman, Mechanical engineering Department for the invaluable scholarships and Graduate teaching assistantship positions provided to me through the course of study. I will always cherish the GTA experience which has given me a new perspective of school life.

I am grateful to Carol Gonce and Lucas Jacobsen, M.E Department staff who have withstood my constant barging into the M.E. Office: Carol, with love and affection, Lucas with constant criticism and sarcasm. I greatly appreciate all the help they have provided.

I thank all the friends who have directly or indirectly helped me in achieving this goal. This work would not have been successful if not for the discussions I had with my colleagues. My special thanks go to Abhijit for his never-give up attitude which he could rub on to me. I will cherish the time spent with my special friend, Salahi. I respect your authoritaah. I thank my roommate Jabbar for being a great friend. I also appreciate the help of Kedar and Srikanth.

I would like to thank my parents for their incessant support, patience and under-

standing. They have always been there for me and I greatly appreciate their love and admire them for being a constant source of inspiration.

The last words of appreciation are reserved for the most important person in my life, my sister and dearest friend Anupama Maduri (Munni). I could not have done this without her support and encouragement. There can be no situation in life in which conversation with my sister will not administer some comfort to me. There is no better friend than a sister. And there is no better sister than you.

Abstract

The primary focus of this thesis is to present a framework to develop higher order global differentiability local approximations for 2-D and 3-D distorted element geometries. The necessity and superiority of higher order global differentiability approximations in designing finite element computational processes has been demonstrated by Surana and co-workers [1–4]. It has been shown by Surana et al. [5] that when the element geometry is rectangular, higher order global differentiability approximations can be easily derived using tensor product of 1-D higher order continuity approximations. When the element geometries are distorted, the tensor product approach cannot be utilized in deriving these approximation functions. This thesis presents a systematic procedure for deriving desired order global differentiability approximations for 2-D and 3-D elements of distorted geometries.

The curved element in 2-D xy or 3-D xyz physical coordinate space is mapped to a master element in $\xi\eta$ or $\xi\eta\zeta$ natural coordinate space. The master elements considered for 2-D quadrilateral, 2-D triangular and 3-D hexahedral elements are a 2 unit square, a 2 unit equilateral triangle and a 2 unit cube respectively. For the master element, 2-D C^{00} or 3-D C^{000} p-version local approximations are considered and appropriate degrees of freedom and the corresponding approximation functions from appropriate nodes are borrowed to derive the higher order approximations and the corresponding derivative degrees of freedom at the corner nodes. These degrees of freedom can be transformed from natural coordinate space to the physical coordinate space by using Jacobians of transformations for the derivatives of various orders. The choice of these degrees of freedom and the corresponding functions being borrowed in deriving these desired functions for the derivative dofs is not arbitrary and must be made in such a way that all lower degree admissible functions and the corresponding dofs are borrowed before considering the higher degree functions and the corresponding dofs. Pascal's rectangle, Pascal's triangle and Pascal's pyramid provide a systematic selection process for accomplishing this selection process for 2-D quadrilateral, 2-D triangular and 3-D hexahedral geometries respectively.

Numerical studies are presented to illustrate the behavior and performance of the

approximations developed. The applicability of the developed approximation functions to all physical problems is demonstrated by solving model problems which are described by self-adjoint, non self-adjoint and non-linear differential operators. In all cases, various finite element quantities of interest (error or residual functional, error norms) are computed and a study of their convergence rates with h, p and k refinement is made.

Contents

List of Tables

List of Figures

Chapter 1

Introduction

The mathematical theory of finite element method has been developed using Sobolev spaces, theory of distribution and measures based on Lebesgue integrals. In this approach, the behaviors over sets of measure zero can be ignored. Thus, when a domain of definition is discretized into sub-domains (finite elements), the integrand behavior over inter sub-domain boundaries is neglected in the formulations as well as computations. This approach permits use of C^0 local approximations in space as well as time if the integrands in the integral forms contain only first order derivatives. If the governing differential equations (GDEs) contain higher order derivatives (higher than one), they are recast as a system of first order differential equations through the use of integration by parts in Galerkin method with weak form or auxiliary variables and auxiliary equations in least squares processes. These approaches ensure that integrand have only first order derivatives so that C^0 local approximations can be employed. In such weak formulations that require C^0 interpolations, one must establish the convergence of the solution to the strong solution (at least in weak sense). This is possible in simple cases [6–10] but is difficult to establish when the differential operators in the GDEs are highly complex or non-linear.

Convergence of the approximation in a finite element process has been conventionally studied in two ways. (i) increasing the number of elements such that the finite element characteristic length approaches zero while maintaining a fixed degree of the local approximation. This is referred to as the 'h' version of finite element method

(ii) increasing the degree of the local approximation while maintaining a fixed finite element characteristic length. This is referred to as the 'p' version of finite element method. Surana et al. [1–4] have shown that global differentiability of order (k-1) resulting from local approximations in scalar product spaces of order 'k' is an independent parameter in all finite element processes. This led to the development of the 'k' version of finite element method in which k is an independent finite element framework in addition to h and p. Authors [1–4] have shown that higher order global differentiability local approximations: (1) allow us to incorporate the desired physics in the design of a computational process (2) eliminate the need for auxiliary equations and auxiliary variables in least squares processes, thereby reducing the number of variables significantly especially for 2-D and 3-D cases. (3) with the proper choices of the order k of the approximation space all integrals in the formulation become Riemann integrals as apposed to Lebesgue integrals. (4) improved accuracy is achieved for the same number of degrees of freedom compared to C^0 processes. (5) higher order global differentiability local approximations is rather a natural way to design a computational process with desired continuity and differentiability features that are dictated by the physics.

In the hpk mathematical and computational framework [1–4], higher order derivatives of the dependent variables may be retained in the integral forms yet preserving the continuity of the integrand over the whole discretization by appropriate choice of k, the order of the approximation space. Since higher order spaces contain higher order global differentiability local approximations, construction of such local approximations for 2-D and 3-D elements with distorted geometries in xy and xyz spaces is critical and constitutes the main focus of this work.

1.1 Literature review

The approximation functions in the finite element method are usually associated with a mesh entity (e.g. vertex, edge, face, region) and their selection can greatly influence the quality of finite element solution. Use of C^0 local approximations for boundary

value problems (in which independent variables are x, y and z) and initial value problems (in which independent variables are x, y, z and t) has remained the basis of the finite element literature over the last forty years. C^0 local approximations based on Lagrange, Legendre or Chebyshev functions have dominated the up to date developments in finite element processes [11–14]. With the development of p-version of the finite element method, hierarchical approximation functions became popular as they removed the need for new functions for every p-level for an element. Hierarchical basis has the feature of obtaining the basis of degree p+1 as a correction to the degree p basis. The shape functions also resulted in (i) improved conditioning (conditioning number of the stiffness matrix improved by orders of magnitude) (ii) faster rate of convergence (iii) immediate estimate of the error in solution [15–19]. p-version hierarchical local approximations for various kinds of elements (triangular, quadrilateral, tetrahedral, hexahedral) based on Lagrange, Legendre or Chebyshev polynomials for fixed node configurations in 1-D, 2-D and 3-D revolutionized the finite element computations [20–30] . These developments permitted convergence studies with progressively increasing p-levels without rediscretizations.

Due to the wide acceptance of the C^0 basis functions in finite element processes, developments in the area of higher order global differentiability local approximations remained virtually non-existent. However, the concept of higher order global differentiability and the benefits of using it have been recognized long ago and implemented to some extent.

Strang [31] pointed out that the jumps produced in the first derivatives normal to the inter-element boundaries constitute the fundamental weakness of C^0 approximation functions. According to him, these jumps provide a measure of deviation of the computed solution from the true C^1 behavior. Bazeley et al. [32] suggested that if such elements pass the "patch test", then the weak convergence of C^0 solution to C^1 is guaranteed. Strang [31] proved that this indeed is the case and also pointed out that with the inter-element discontinuity of the first derivatives, the strain energy becomes unbounded and therefore such approximation functions are not admissible in the true mathematical sense. However, if the theory of distribution and the notion

of generalized derivatives is followed, the strain energy remains finite since the integrals are evaluated in the Lebesgue sense. Although the weak convergence to C^1 can be achieved with C^0 approximation functions using h, p and hp adaptive processes, adaptivity may be completely avoided by employing basis functions of class C^1.

Although, global differentiability has been recognized as an important aspect in all numerical computations, very little has been done to design mathematical and computational processes in which higher-order global smoothness is achievable. Alternative techniques such as the diffuse element method [33] and the element free methods [34] have been proposed to smoothen the higher order continuity requirement. Hermite basis functions and associated higher order finite elements have been used in solid mechanics (e.g. classical beam and plate bending elements) and other areas. Some literature on these can be found in Reference [35]. If C^1 continuity is required as in case of plate bending, compatibility has been traditionally enforced by separate constraint equations. Peano [36] presented the simplest form of these constraints while formulating hierarchical basis for C^1 element. Wang et. al. [37] implemented C^1 triangular element based on p-version of finite element method by adding corrective rational functions to the polynomial basis. Other references to higher order elements can be found in References [38–41].

Surana et al. [5] presented a systematic development of higher order global differentiability p-version 1-D C^i; $i = 0, 2, \ldots k$ local approximations based on lagrange monomials. The authors utilized tensor product in 2-D xy spaces and 3-D xyz spaces to derive local approximations of classes C^{ij} and C^{ijk} in which i, j and k can be chosen arbitrarily. These developments are restricted to rectangular family of elements in which the natural coordinate axes ξ, η, ζ must be parallel to x, y, z axes and pointing in the same directions as xyz axes. In other words, when the element geometries are distorted with curved sides and faces, the tensor product approach fails. This obviously limits the usefulness of higher order global differentiability local approximations for domains with boundaries parallel to x, y and z axes. C^i, C^{ij}, C^{ijk} local approximations have been successfully utilized by Surana et al. [42, 43] in a variety of applications, some of which are discussed in the following.

While solving the gas dynamics equations using the space-time least squares finite element method with the p-version C^{00} basis functions in space and time, Surana and Van Dyne [42, 43] noted that the presence of discontinuities in the first derivatives of dependent variables in space and time generate solution perturbations that amplify with time marching and eventually leads to the failure of the computational process. This problem was eliminated by using C^{11} basis functions in space and time, thereby enforcing continuity of the first normal derivatives of dependent variables at the inter-element boundaries strongly. The necessity and merits of using C^{11} basis functions in 2-D incompressible Newtonian flows and polymer flows have been reported by Nayak [44]. Surana and Bona [45] reported solutions of class C^1 and C^{11} for stationary and transient one dimensional convection-diffusion and Burgers equation which demonstrated superior performance of C^1 and C^{11} approximations over the traditionally accepted C^0 and C^{00} solutions. Remarkable success of C^1 and C^{11} basis functions in boundary value problems and initial value problems has been the motivating factor in generalization of these concepts and the subsequent development of hpk framework of finite element method. A major limitation in all the papers discussed on k version of finite element method is that the domains of definition need to be rectangular. Successful application of hpk framework to physical problems requires development of local approximations which enforce inter-element continuity of desired order derivative of the dependent variables for any arbitrary geometric shape of the elements.

1.2 Scope of present study

The use of hpk mathematical and computational framework for boundary value problems and initial value problems with arbitrary irregular domains necessitates the development of higher order global differentiability C^{ij} and C^{ijk} local approximations for distorted element geometries in 2-D xy and 3-D xyz spaces and is the main thrust of the work presented here. Ahmadi, Surana and Reddy [46] presented a systematic procedure for deriving higher order global differentiability C^{ij} p-version local approximations for distorted 2-D quadrilateral elements in x, y space based on lagrange

monomials. This work is summarized in this thesis and is extended for legendre and chebyshev functions as well. A framework and complete derivation is presented for higher order global differentiability C^{ij} local approximations for distorted triangular elements in xy space using L_1, L_2, L_3 area coordinates. C^{00} p-version hierarchical local approximations are used as starting point and the basis for the developments of C^{ij} local approximations. C^{ijk} higher order global differentiability local approximations are also developed for 3-D distorted elements of hexahedral family in xyz space. C^{000} p-version local approximation of lagrange, legendre and chebyshev type are used as a starting point and basis for the development of C^{ijk} local approximations.

In all cases, various model problems and pertinent finite element quantities of interest (error or residual functional, L_2 norm of error in solution etc.) are used to assess the validity and performance of the developed approximations. Comparisons of the numerical results will be made with C^{ij}, C^{ijk} local approximations [5] based on tensor product approach for model problems in which the boundaries of the domains are parallel to global x, y, z axes.

Chapter 2

Higher order global differentiability local approximations for 2-D distorted element geometries

2.1 Introduction

In this chapter we present derivations of higher order global differentiability local approximations for 2-D distorted element geometries. We consider 2-D distorted quadrilateral elements as well as triangular elements. Surana et al. [5] have presented 1-D higher order continuity local approximations based on 1-D C^0 p-version hierarchical local approximations of Lagrange, Legendre or Chebyshev type. Authors in reference [5] also presented derivation of 2-D and 3-D higher order global differentiability local approximations of arbitrary order using tensor product of 1-D higher order continuity local approximations. These approximation functions require the element geometries to be rectangular and the natural coordinate axes ξ, η and ζ to be parallel to physical coordinate axes x, y, z as well as pointing in the same directions. This obviously limits the usefulness of these elements to domains in which the boundaries of the domain are parallel and perpendicular to the global xyz axes. Irregular domains with irregular boundaries obviously require the use of distorted element geometries in the discretizations.

The higher order global differentiability local approximations for distorted geometries cannot be derived using the tensor product approach utilized in reference [5]. In this chapter, we present derivations of the higher order global differentiability local approximations for distorted quadrilateral and triangular family of elements. Ahmadi, Surana and Reddy [46] developed basic strategy for distorted quadrilateral elements using Lagrange monomials. This work is extended for Legendre and Chebyshev monomials. This work is further modified and extended for 2-D triangular elements of distorted geometries.

2.2 Higher order global differentiability local approximations for distorted quadrilateral elements

First we consider 2-D higher order global differentiability approximations (HGDA) for rectangular family of undistorted elements. Following reference [5], we begin with 1-D HGDA in x and y and the corresponding nodal operators shown in Figure 2.1(a) derived using 1-D C^0 p-version hierarchical approximations. A tensor product of the 1-D nodal operators and the corresponding 1-D HGDA yields the desired 2-D nodal operators and the corresponding HGDA (Figure 2.1(b)). The 2-D C^{ij} tensor product element in Figure 2.1(b) has four corner nodes (1,3,5,7), four mid-side nodes (2,4,6,8) and one center node (9). The mid-side nodes are hierarchical in one direction (nodes 2 and 6 along ξ direction and nodes 4 and 8 along η direction) and the center node is hierarchical in two directions (along ξ and η). The tensor product element is characterized by function value and its derivatives with respect to x and y as degrees of freedom at the corner nodes. The choice of 1-D C^0 p-version hierarchical approximation functions i.e. Lagrange, Legendre or Chebyshev determines whether the corresponding 2-D HGDA are Lagrange, Legendre or Chebyshev type. This approach requires the elements in the xy space to be rectangular with x and y axes parallel to ξ and η and point in the same direction.

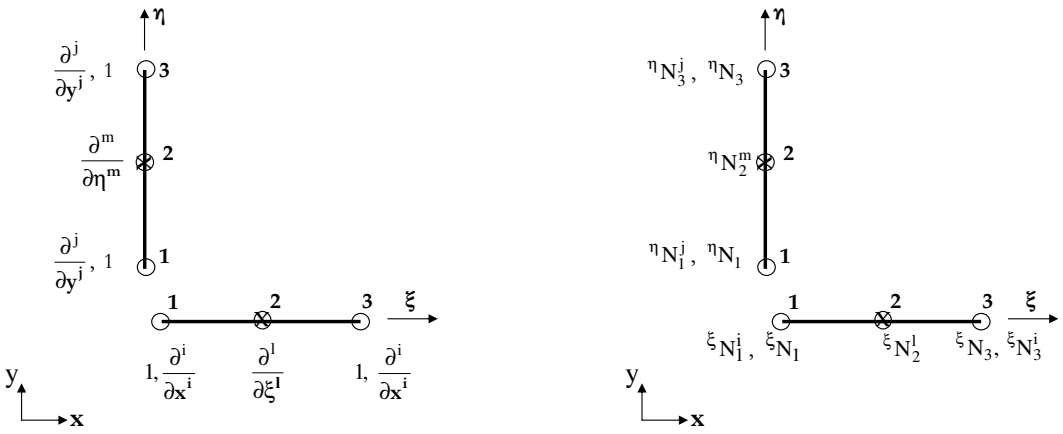

(a) 1 – D nodal operators and higher order global differentiability approximation functions

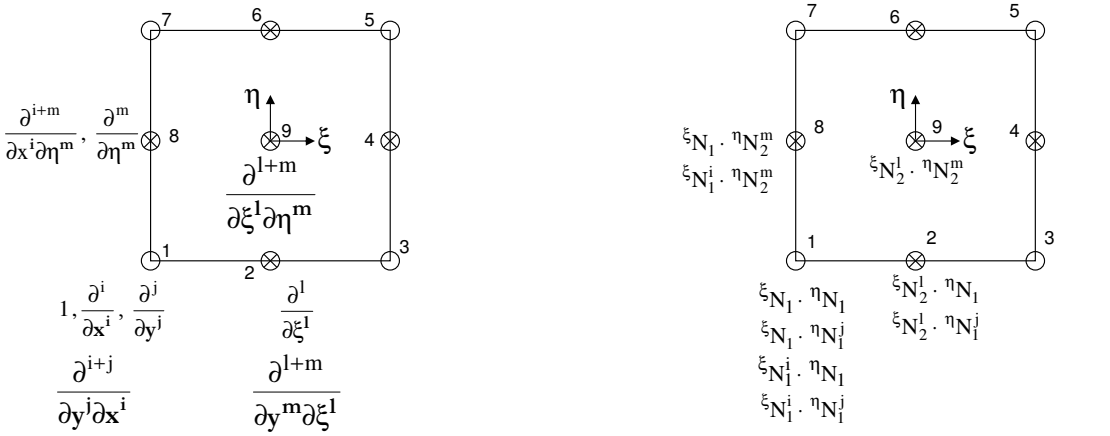

(b) 2 - D higher order nodal operators and approximation functions

Figure 2.1: 1-D nodal and 2-D higher order global differentiability (Tensor product) approximations and nodal operators

If the elements in xy space are distorted, we could possibly discuss an alternative. The curved element is first mapped from xy physical coordinate space to 2 unit square in $\xi\eta$ natural coordinate space. We can consider 1-D higher order global differentiability approximations in ξ, η space as shown in Figure 2.2(a). Comparing to Figure 2.1(a), we notice that degrees of freedom at the corner nodes are now derivatives with respect to ξ and η as apposed to x and y. A tensor product of these 1-D approximations would yield higher order differentiability approximations in ξ, η space as illustrated in Figure 2.2(b). The approximation functions $\tilde{N}$ correspond to derivative degrees of freedom with respect to ξ and η and are different from N.

The requirement of higher order global differentiability in xy space necessitates that the derivative degrees of freedom at the corner nodes (and some at mid-side nodes) be transformed from $\xi\eta$ space to xy space. For example, in case of C^{11} HGDA, $\frac{\partial}{\partial\xi}$, $\frac{\partial}{\partial\eta}$, $\frac{\partial^2}{\partial\xi\partial\eta}$ need to be transformed to $\frac{\partial}{\partial x}$, $\frac{\partial}{\partial y}$, $\frac{\partial^2}{\partial x\partial y}$ and for C^{22} HGDA, $\frac{\partial}{\partial\xi}$, $\frac{\partial}{\partial\eta}$, $\frac{\partial^2}{\partial\xi^2}$, $\frac{\partial^2}{\partial\eta^2}$ $\frac{\partial^2}{\partial\xi\partial\eta}$, $\frac{\partial^3}{\partial\xi^2\partial\eta}$, $\frac{\partial^3}{\partial\xi\partial\eta^2}$, $\frac{\partial^4}{\partial\xi^2\partial\eta^2}$ need to be transformed into $\frac{\partial}{\partial x}$, $\frac{\partial}{\partial y}$, $\frac{\partial^2}{\partial x^2}$, $\frac{\partial^2}{\partial y^2}$ $\frac{\partial^2}{\partial x\partial y}$, $\frac{\partial^3}{\partial x^2\partial y}$, $\frac{\partial^3}{\partial x\partial y^2}$, $\frac{\partial^4}{\partial x^2\partial y^2}$. Due to the fact that degrees of freedom (dofs) in $\xi\eta$ space for C^{ij} higher order approximations are not complete sets, this transformation is not possible. For C^{11} case, $\frac{\partial}{\partial\xi}$, $\frac{\partial}{\partial\eta}$ can be transformed into $\frac{\partial}{\partial x}$, $\frac{\partial}{\partial y}$ but there is no feasible resolution for transforming $\frac{\partial^2}{\partial\xi\partial\eta}$ into $\frac{\partial^2}{\partial x\partial y}$. In case of C^{22}, we can transform $\frac{\partial}{\partial\xi}$, $\frac{\partial}{\partial\eta}$ to $\frac{\partial}{\partial x}$, $\frac{\partial}{\partial y}$ and $\frac{\partial^2}{\partial\xi^2}$, $\frac{\partial^2}{\partial\eta^2}$, $\frac{\partial^2}{\partial\xi\partial\eta}$ to $\frac{\partial^2}{\partial x^2}$, $\frac{\partial^2}{\partial y^2}$, $\frac{\partial^2}{\partial x\partial y}$. However, we cannot transform $\frac{\partial^3}{\partial\xi^2\partial\eta}$, $\frac{\partial^3}{\partial\xi\partial\eta^2}$, $\frac{\partial^4}{\partial\xi^2\partial\eta^2}$ into their counterparts in xy space. Similar situation exists for orders higher than two as well. Thus, the derivation of HGDA for 2-D distorted elements in xy space requires a fundamentally different approach.

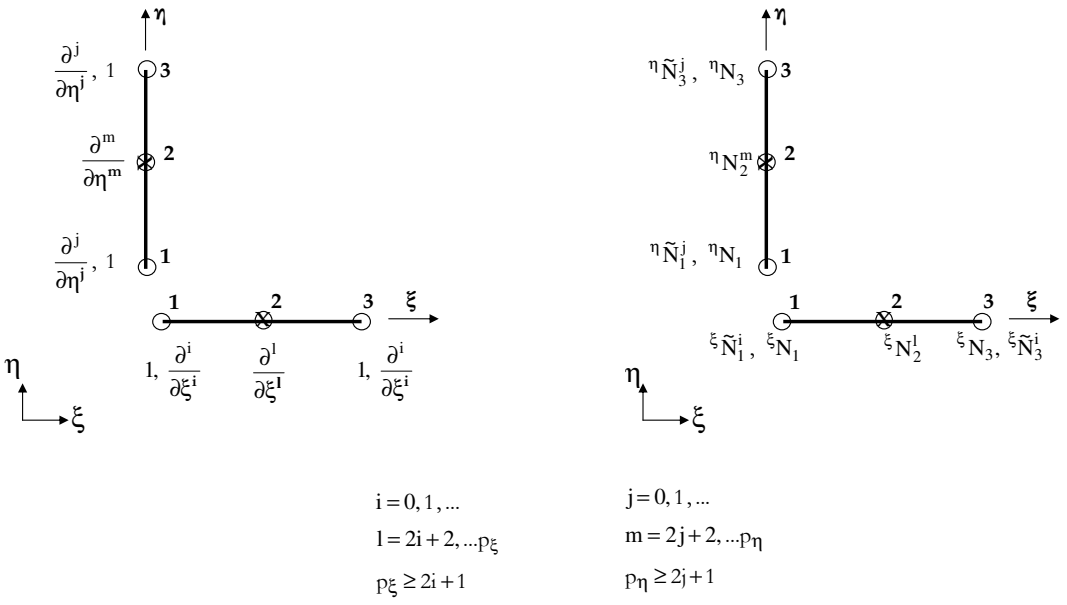

$i = 0, 1, ...$
$l = 2i + 2, ...p_\xi$
$p_\xi \geq 2i + 1$

$j = 0, 1, ...$
$m = 2j + 2, ...p_\eta$
$p_\eta \geq 2j + 1$

(a) 1 – D nodal operators and higher order global differentiability approximation functions (along ξ and η directions)

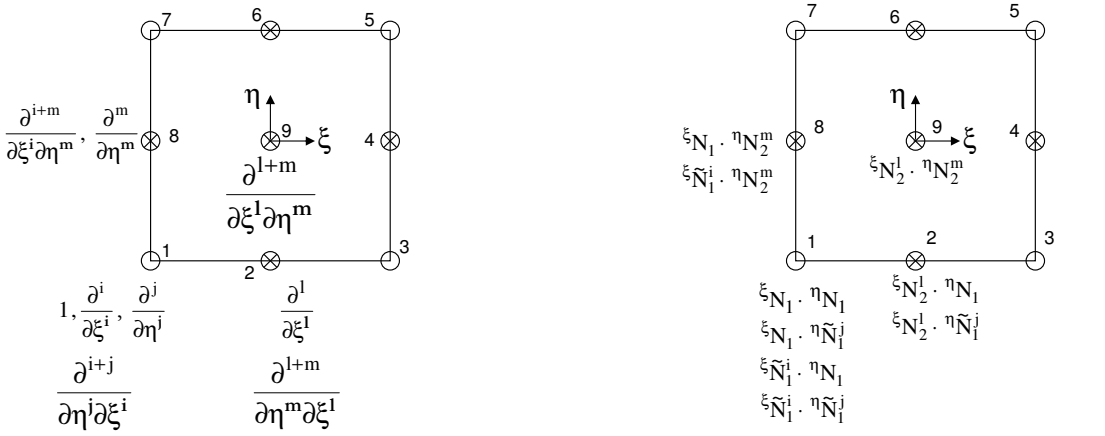

(b) 2 - D higher order nodal operators and approximation functions (along ξ and η directions)

Figure 2.2: 1-D nodal and 2-D higher order global differentiability (Tensor product) approximations and nodal operators in $\xi\eta$ space

2.2.1 Guidelines:

In deriving the desired HGDA for 2-D distorted elements of quadrilateral family in xy space, we obey the following guidelines.

(a) The distorted element geometry is mapped from xy physical coordinate space into $\xi\eta$ natural coordinate space, which for quadrilateral geometry is a 2 unit square (Figure 2.3(a) and (b)). The origin of the ξ, η coordinate system is located at the center of the map and we have the following for the mapping of points,

$$\left\{ \begin{array}{c} x \\ y \end{array} \right\} = \sum_{i=1}^{n} \underset{\sim}{N}_i(\xi, \eta) \left\{ \begin{array}{c} x_i \\ y_i \end{array} \right\} \tag{2.1}$$

In which, (x_i, y_i) are the cartesian coordinates of the nodes and $\underset{\sim}{N}_i(\xi, \eta)$ are the shape functions. We could use eight node configuration (i.e. n=8) with serendipity functions [47] for this purpose.

(b) If possible, we would like to consider C^{00} p-version hierarchical local approximation as a starting point in the derivation of 2-D HGDA. Figure 2.3(c) shows nodal degrees of freedom for a standard C^{00} p-version hierarchic element in which φ is the field variable being interpolated. The degrees of freedom at the corner nodes of this element consists of only function values.

(c) Different degrees of freedom are needed at the corner nodes than those for the 2-D HGDA generated using tensor product. This is due to the fact that dofs in tensor product 2-D HGDA do not transform from xy to $\xi\eta$ or vice-versa. Obviously the choices of the dofs at the corner nodes are dictated by the transformation between xy and $\xi\eta$ spaces.

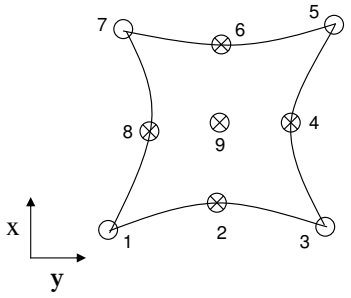

(a) Nine - node 2 D distorted quadrilateral in xy space

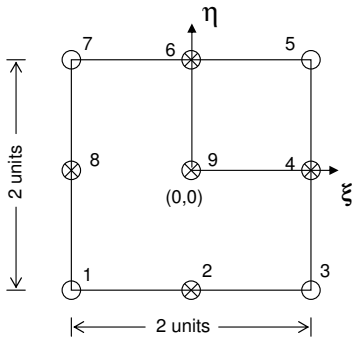

(b) Map of the element of (a) in natural coordinate space ξη

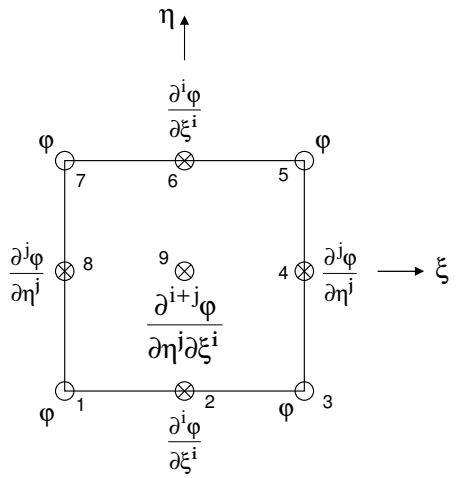

$i = 2, 3, \ldots p_\xi \quad ; \quad j = 2, 3, \ldots p_\eta$

(c) Dofs for C^{00} p-version hierarchical element with p - levels p_ξ and p_η in ξ and η directions

Figure 2.3: 2-D distorted p version hierarchical element with p - levels p_ξ and p_η in ξ and η directions

(d) The degrees of freedom for 2-D HGDA element should be such that they can be transformable using standard Jacobians of transformation from natural coordinate space to physical coordinate space. The choices of nodal operators (or dofs) at the corner nodes listed in Table 2.1 for C^{11}, C^{22} and C^{33} HGDA satisfy this requirement. We note that for C^{11}, the derivative operators are a complete set of first order operators. For C^{22} HGDA, the set of C^{11} is augmented by a complete second order set and so on.

(e) Since C^{00} p-version hierarchical approximations are used as a starting point and that in these local approximations function value is the only degree of freedom at the corner nodes, we must establish some rules that allow us to borrow some dofs from C^{00} p-version hierarchical approximations to generate the desired dofs at the corner nodes of the 2-D HGDA distorted element.

Table 2.1: Choices of nodal operators at the corner nodes for C^{ij} 2-D distorted quadrilateral elements in xy space

Type of HGDA	Nodal Operators at the corner nodes
C^{11}	$1\ ,\ \frac{\partial}{\partial x}\ ,\ \frac{\partial}{\partial y}$
C^{22}	$1\ ,\ \frac{\partial}{\partial x}\ ,\ \frac{\partial}{\partial y}\ ,\quad \frac{\partial^2}{\partial x^2}\ ,\ \frac{\partial^2}{\partial y \partial x}\ ,\ \frac{\partial^2}{\partial y^2}$
C^{33}	$1\ ,\ \frac{\partial}{\partial x}\ ,\ \frac{\partial}{\partial y}\ ,\quad \frac{\partial^2}{\partial x^2}\ ,\ \frac{\partial^2}{\partial y \partial x}\ ,\ \frac{\partial^2}{\partial y^2}\ ,\quad \frac{\partial^3}{\partial x^3}\ ,\ \frac{\partial^3}{\partial y \partial x^2}\ ,\ \frac{\partial^3}{\partial y^2 \partial x}\ ,\ \frac{\partial^3}{\partial y^3}$

2.2.2 Transformation matrices

In this section we present details of the transformation matrices essential to derive 2-D HGDA for distorted quadrilateral geometries in xy space. Figure 2.3(c) shows nodal degrees of freedom for C^{00} p-version hierarchical element in which φ is dependent variable. From Equation (2.1), we obtain the following for mapping of lengths in (ξ, η) and (x, y) spaces,

$$\left\{ \begin{array}{c} dx \\ dy \end{array} \right\} = [J] \left\{ \begin{array}{c} d\xi \\ d\eta \end{array} \right\} \tag{2.2}$$

Using Murnaghan's notation [48] we can write,

$$[J] = \left[\frac{x \; y}{\xi \; \eta} \right] \tag{2.3}$$

in which the quantities in numerator define a row and those in the denominator define column wise differentiation of the terms in numerator. Thus,

$$[J] = \left[\frac{x \; y}{\xi \; \eta} \right] = \left[\begin{array}{cc} x_\xi & x_\eta \\ y_\xi & y_\eta \end{array} \right] \tag{2.4}$$

where subscript denotes differentiation, i.e. $x_\xi = \frac{\partial x}{\partial \xi}$, $x_\eta = \frac{\partial x}{\partial \eta}$ etc.

Using the C^{00} p-version hierarchical approximations for a nine node element (Figure 2.3(c)), the field variable φ can be approximated as [24],

$$\varphi(\xi, \eta) = [N(\xi, \eta)]\{\delta^e\} \tag{2.5}$$

in which $[N(\xi, \eta)]$ is a row matrix of C^{00} p-version hierarchical local approximations and $\{\delta^e\}$ are the corresponding nodal dofs (arranged in some suitable fashion).

We define,

$$\{\varphi\}_1^{\xi\eta} = \left[\frac{\partial\varphi}{\partial\xi}\ ,\ \frac{\partial\varphi}{\partial\eta}\right]^T \tag{2.6}$$

$$\{\varphi\}_1^{xy} = \left[\frac{\partial\varphi}{\partial x}\ ,\ \frac{\partial\varphi}{\partial y}\right]^T \tag{2.7}$$

$$\{\varphi\}_2^{\xi\eta} = \left[\frac{\partial^2\varphi}{\partial\xi^2}\ ,\ \frac{\partial^2\varphi}{\partial\eta\partial\xi}\ ,\ \frac{\partial^2\varphi}{\partial\eta^2}\right]^T \tag{2.8}$$

$$\{\varphi\}_2^{xy} = \left[\frac{\partial^2\varphi}{\partial x^2}\ ,\ \frac{\partial^2\varphi}{\partial y\partial x}\ ,\ \frac{\partial^2\varphi}{\partial y^2}\right]^T \tag{2.9}$$

$$\{\varphi\}_3^{\xi\eta} = \left[\frac{\partial^3\varphi}{\partial\xi^3}\ ,\ \frac{\partial^3\varphi}{\partial\eta\partial\xi^2}\ ,\ \frac{\partial^3\varphi}{\partial\eta^2\partial\xi}\ ,\ \frac{\partial^3\varphi}{\partial\eta^3}\right]^T \tag{2.10}$$

$$\{\varphi\}_3^{xy} = \left[\frac{\partial^3\varphi}{\partial x^3}\ ,\ \frac{\partial^3\varphi}{\partial y\partial x^2}\ ,\ \frac{\partial^3\varphi}{\partial y^2\partial x}\ ,\ \frac{\partial^3\varphi}{\partial y^3}\right]^T \tag{2.11}$$

where T denotes transpose of a matrix.

We note that Equations (2.6) and (2.7) are complete first order derivative sets, Equations (2.8) and (2.9) are complete second order derivative sets and Equations (2.10) and (2.11) are complete third order derivative sets in $\xi\eta$ and xy coordinate spaces. In this manner, we can define $\{\varphi\}_i^{\xi\eta}$ and $\{\varphi\}_i^{xy}$ as complete sets of the derivatives of order 'i' in (ξ, η) and (x, y) spaces. Next we define the rules of transformation between the sets of different order derivatives in (ξ, η) and (x, y) spaces.

$$\{\varphi\}_i^{\xi\eta} = [J_i]\{\varphi\}_i^{xy} \tag{2.12}$$

Obviously,

$$[J_1] = \begin{bmatrix} x_\xi & y_\xi \\ x_\eta & y_\eta \end{bmatrix} = [J]^T \tag{2.13}$$

Using chain rule of differentiation, we can determine the transformation matrices for higher order derivatives of the dependent variable. We will use the following notations for higher order derivatives of physical coordinate x with respect to natural coordinates ξ and η

$$x_\xi = \frac{\partial x}{\partial \xi} \;\; ; \;\; x_\xi^i = \left(\frac{\partial x}{\partial \xi}\right)^i \;\; ; \;\; x_{\xi^i} = \frac{\partial^i x}{\partial \xi^i} \;\; ; \;\; x_{\xi^i\eta^j} = \frac{\partial^{i+j} x}{\partial \xi^i \partial \eta^j} \tag{2.14}$$

and

$$x_\eta = \frac{\partial x}{\partial \eta} \;\; ; \;\; x_\eta^i = \left(\frac{\partial x}{\partial \eta}\right)^i \;\; ; \;\; x_{\eta^i} = \frac{\partial^i x}{\partial \eta^i} \;\; ; \tag{2.15}$$

Similarly, the following notations hold for derivatives of physical coordinate y with respect to natural coordinates ξ and η.

$$y_\xi = \frac{\partial y}{\partial \xi} \;\; ; \;\; y_\xi^i = \left(\frac{\partial y}{\partial \xi}\right)^i \;\; ; \;\; y_{\xi^i} = \frac{\partial^i y}{\partial \xi^i} \;\; ; \;\; y_{\xi^i\eta^j} = \frac{\partial^{i+j} y}{\partial \xi^i \partial \eta^j} \tag{2.16}$$

and

$$y_\eta = \frac{\partial y}{\partial \eta} \;\; ; \;\; y_\eta^i = \left(\frac{\partial y}{\partial \eta}\right)^i \;\; ; \;\; y_{\eta^i} = \frac{\partial^i y}{\partial \eta^i} \;\; ; \tag{2.17}$$

Following these notations, the transformation matrices for the second order derivatives are as follows:

$$\{\varphi\}_2^{xy} = [J_2]^{-1}\left[\{\varphi\}_2^{\xi\eta} - [J_2^1]\{\varphi\}_1^{xy}\right] \tag{2.18}$$

$$[J_2] = \begin{bmatrix} {x_\xi}^2 & 2x_\xi y_\xi & {y_\xi}^2 \\ x_\xi x_\eta & x_\xi y_\eta + x_\eta y_\xi & y_\eta y_\xi \\ {x_\eta}^2 & 2x_\eta y_\eta & {y_\eta}^2 \end{bmatrix} \qquad [J_2^1] = \begin{bmatrix} x_{\xi^2} & y_{\xi^2} \\ x_{\xi\eta} & y_{\xi\eta} \\ x_{\eta^2} & y_{\eta^2} \end{bmatrix} \tag{2.19}$$

Similarly, transformation matrices for the third order derivatives are as follows:

$$\{\varphi\}_3^{xy} = [J_3]^{-1}\left[\{\varphi\}_3^{\xi\eta} - [J_3^1]\{\varphi\}_2^{xy} - [J_3^2]\{\varphi\}_1^{xy}\right] \tag{2.20}$$

$$[J_3] = \begin{bmatrix} {x_\xi}^3 & 3{x_\xi}^2 y_\xi & 3x_\xi {y_\xi}^2 & {y_\xi}^3 \\ {x_\xi}^2 x_\eta & 2x_\eta x_\xi y_\xi + {x_\xi}^2 y_\eta & 2x_\xi y_\eta y_\xi + {y_\xi}^2 x_\eta & y_\eta {y_\xi}^2 \\ {x_\eta}^2 x_\xi & 2x_\eta x_\xi y_\eta + {x_\eta}^2 y_\xi & 2x_\eta y_\eta y_\xi + {y_\eta}^2 x_\xi & y_\xi {y_\eta}^2 \\ {x_\eta}^3 & 3{x_\eta}^2 y_\eta & 3x_\eta {y_\eta}^2 & {y_\eta}^3 \end{bmatrix} \tag{2.21}$$

$$[J_3^1] = \begin{bmatrix} 3x_\xi x_{\xi^2} & 3x_{\xi^2} y_\xi + 3y_{\xi^2} x_\xi & 3y_\xi y_{\xi^2} \\ x_\eta x_{\xi^2} + 2x_\xi x_{\xi\eta} & x_{\xi^2} y_\eta + 2x_{\xi\eta} y_\xi + x_\eta y_{\xi^2} + 2x_\xi y_{\xi\eta} & y_\eta y_{\xi^2} + 2y_\xi y_{\xi\eta} \\ x_\xi x_{\eta^2} + 2x_\eta x_{\xi\eta} & x_\xi y_{\eta^2} + 2x_{\xi\eta} y_\eta + x_{\eta^2} y_\xi + 2x_\eta y_{\xi\eta} & y_{\eta^2} y_\xi + 2y_\eta y_{\xi\eta} \\ 3x_\eta x_{\eta^2} & 3x_{\eta^2} y_\eta + 3y_{\eta^2} x_\eta & 3y_\eta y_{\eta^2} \end{bmatrix} \tag{2.22}$$

$$[J_3^2] = \begin{bmatrix} x_{\xi^3} & y_{\xi^3} \\ x_{\xi^2\eta} & y_{\xi^2\eta} \\ x_{\xi\eta^2} & y_{\xi\eta^2} \\ x_{\eta^3} & y_{\eta^3} \end{bmatrix} \tag{2.23}$$

From Equation (2.12) we can write

$$\{\varphi\}_i^{xy} = [J_i]^{-1}\{\varphi\}_i^{\xi\eta} \tag{2.24}$$

2.2.3 C^{11} HGDA for 2-D distorted quadrilateral elements in xy space

In order to show specific details of the development, we consider C^{11} HGDA. Figure 2.4(a) shows the dofs at the corner nodes of C^{11} HGDA element (subscript indicates differentiation). Comparing Figure 2.4(a) with C^{00} p-version element of Figure 2.3(c), we note that the element of Figure 2.4(a) requires φ_x and φ_y as additional dofs at each of the four corner nodes i.e. a total of eight dofs for the four corner nodes. We need to borrow eight dofs and the corresponding C^{00} p-version approximation functions to generate these dofs and the corresponding approximation functions for the 2-D C^{11} HGDA element. This would obviously result in reduction of dofs at the hierarchical nodes of the 2-D HGDA element. In doing so we must follow a systematic procedure. For this case, the choice of dofs from C^{00} element is rather straightforward. We borrow two dofs which are associated with the lowest p-levels (i.e. p = 2 and 3) and the corresponding approximation functions from each of the four mid-side nodes. This implies that the degrees of freedom corresponding to $\frac{\partial^2\varphi}{\partial\xi^2}$, $\frac{\partial^3\varphi}{\partial\xi^3}$ from nodes 2, 6 and $\frac{\partial^2\varphi}{\partial\eta^2}$, $\frac{\partial^3\varphi}{\partial\eta^3}$ from nodes 4 and 8 and the corresponding approximation functions are borrowed. These dofs must be eliminated to generate the derivative dofs at the corner nodes of 2-D C^{11} HGDA element (Figure 2.4(a)). Figure 2.4(b) shows the dofs at the hierarchical nodes of the 2-D HGDA element. The derivation of the 2-D C^{11} HGDA element is shown in a later section.

We note that the dofs removed from the mid side nodes of the C^{00} p-version element correspond to p-levels 2 and 3 and hence consistent with the tensor product C^{11} element. The first degree of freedom at the mid side nodes of the C^{11} HGDA element corresponds to p-level of 4. For C^{11} HGDA element, we do not need to borrow any dofs from the center node of C^{00} p-version element.

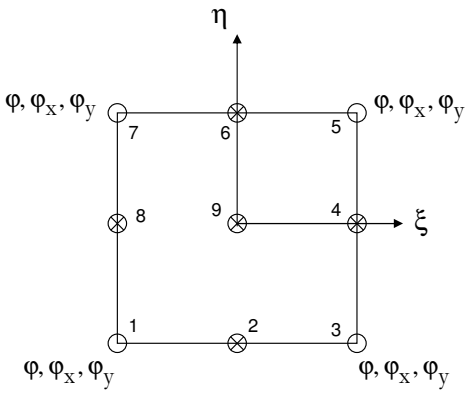

(a) Nodal dofs at the corner nodes of a 2-D C[11] HDGA element

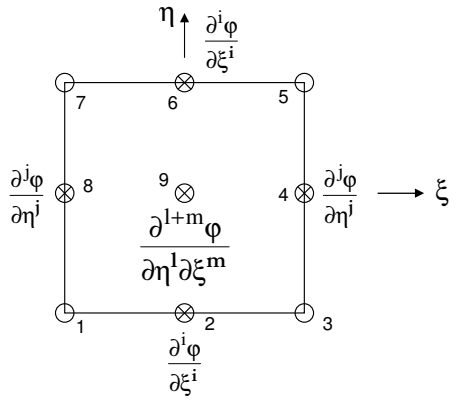

(b) Dofs at the hierarchical nodes of 2-D C[11] HGDA element

Figure 2.4: Nodal dofs for 2-D C^{11} HGDA distorted quadrilateral element

2.2.4 C^{22} HGDA for 2-D distorted quadrilateral elements in xy space

Here we consider 2-D C^{22} HGDA for distorted quadrilateral elements in xy space. Figure 2.5(a) shows dofs at the corner nodes of the element. Comparing this with C^{00} HGDA of Figure 2.3(c), we note that φ_x, φ_y, φ_{x^2}, φ_{xy} and φ_{y^2} are additional dofs at each of the four corner nodes, i.e. a total of twenty. We need to borrow twenty dofs and the corresponding C^{00} p-version approximation functions to generate these dofs and the corresponding approximation functions for the 2-D C^{22} HGDA element. This would obviously result in reduction of dofs at the hierarchical nodes of the 2-D HGDA element. For this case, the choice of dofs from C^{00} element is a little involved. We borrow four dofs which are associated with the p-levels 2, 3, 4 and 5 and the corresponding approximation functions from each of the four mid-side nodes to maintain conformity with C^{22} tensor product element. This implies that the degrees of freedom corresponding to $\frac{\partial^2\varphi}{\partial\xi^2}$, $\frac{\partial^3\varphi}{\partial\xi^3}$, $\frac{\partial^4\varphi}{\partial\xi^4}$, $\frac{\partial^5\varphi}{\partial\xi^5}$ from nodes 2, 6 and $\frac{\partial^2\varphi}{\partial\eta^2}$, $\frac{\partial^3\varphi}{\partial\eta^3}$, $\frac{\partial^4\varphi}{\partial\eta^4}$, $\frac{\partial^5\varphi}{\partial\eta^5}$ from nodes 4 and 8 and the corresponding approximation functions are borrowed. This would result in a total of 16 degrees of freedom.

The remaining four degrees of freedom required are borrowed from the center node (node 9). The degrees of freedom are borrowed from center node of the C^{00} tensor product element in such a way that the dofs corresponding to a lower p-level are selected before those corresponding to higher p-levels. Figure 2.6 shows the dofs generated at the center node of a C^{00} element corresponding to p-levels p_ξ (along ξ direction) and p_η (along η direction). The dofs illustrated with a circle are selected in deriving a C^{22} HGDA element. They correspond to (p_ξ, p_η) pairs of $(2,2)$, $(3,2)$, $(2,3)$ and $(3,3)$. Degree of freedom corresponding to p-level pair of $(3,3)$ is chosen over $(4,2)$ or $(2,4)$ to ensure symmetry with respect to p_ξ and p_η. Symmetry in the degrees of freedom pairs is maintained to preserve the symmetry of finite element solutions for symmetric discretizations. These dofs must be eliminated from C^{00} p-version approximations to generate the derivative dofs at the corner nodes of 2-D C^{11} HGDA element (Figure 2.5(a)). Figure 2.5(b) shows the dofs at the hierarchical nodes of the 2-D HGDA element.

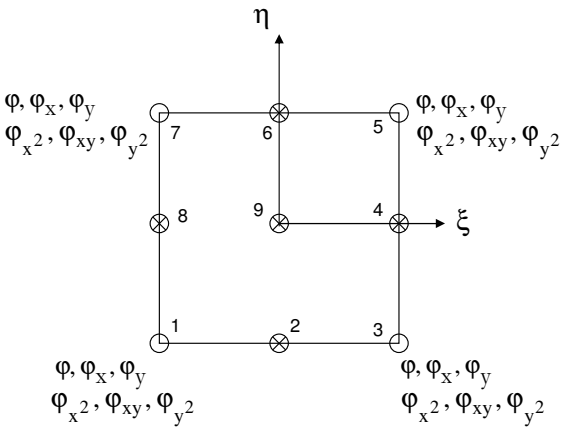

(a) Nodal dofs at the corner nodes of a 2-D C^{22} HGDA element

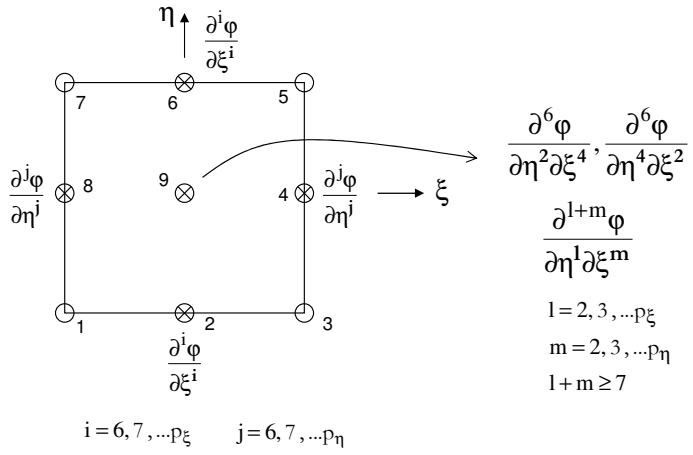

(a) Nodal dofs at the hierarchical corner nodes of a 2-D C^{22} HGDA element

Figure 2.5: Nodal dofs for 2-D C^{22} HGDA distorted quadrilateral element

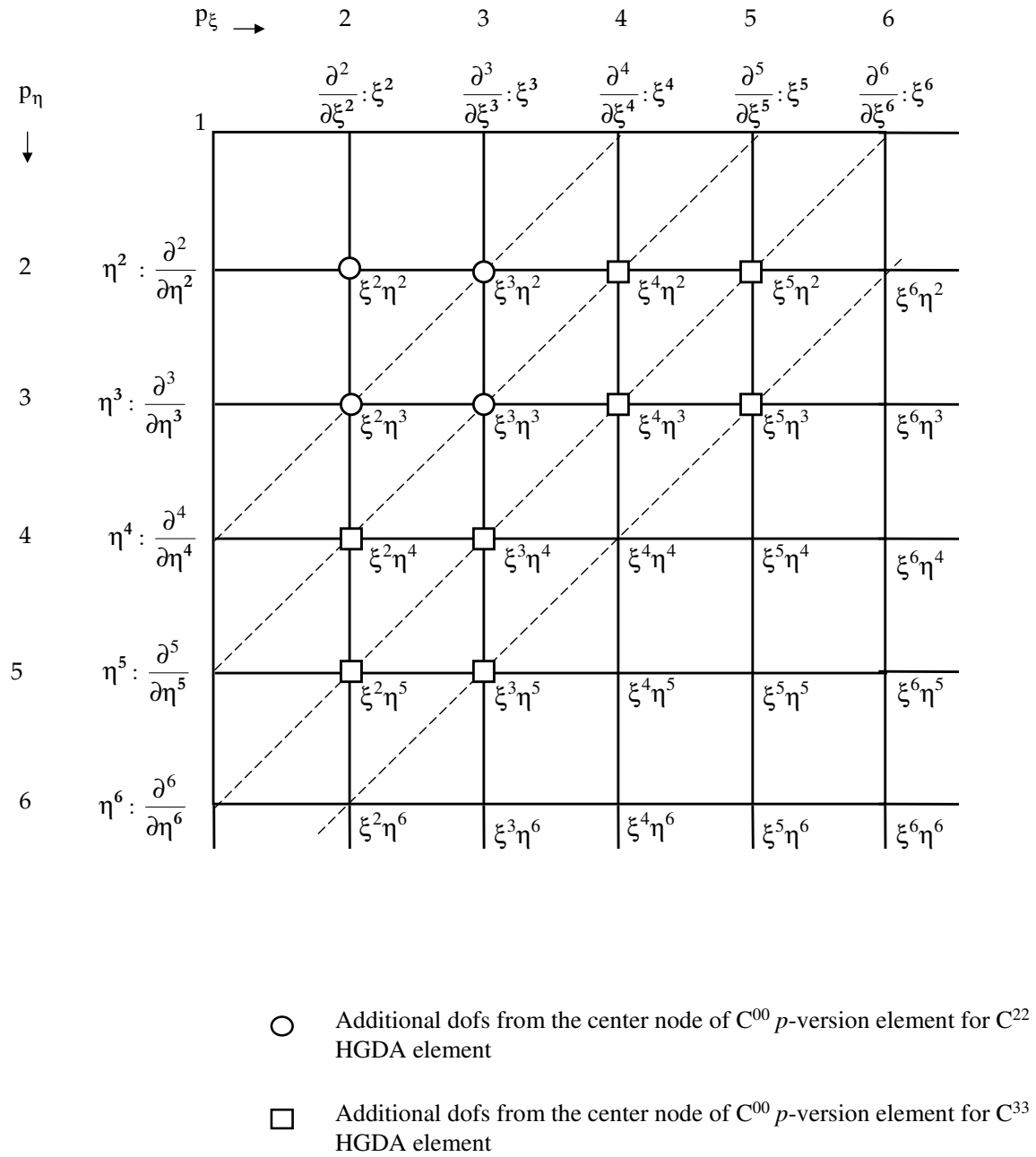

Figure 2.6: Dofs at the center node of a C^0 p-version hierarchical element

2.2.5 C^{33} HGDA for 2-D distorted quadrilateral elements in xy space

Here we consider 2-D C^{33} HGDA for distorted quadrilateral elements in xy space. Compared to a C^{00} HGDA of Figure 2.3(c), we note that φ_x, φ_y, φ_{x^2}, φ_{xy}, φ_{y^2}, φ_{x^3}, φ_{x^2y}, φ_{xy^2} and φ_{y^3} are additional dofs at each of the four corner nodes, i.e. a total of thirty six. Hence, we need to borrow thirty six dofs from the hierarchical nodes of C^{00} HGDA element, keeping in mind that the remaining dofs at the mid side nodes must begin with p-level of eight. This is to ensure that C^{33} HGDA is in conformity with C^{33} tensor product element. This allows us to borrow twenty four dofs (corresponding to p-levels of 2, 3, 4, 5, 6 and 7) from each of the mid side nodes (nodes 2, 4, 6, 8) of Figure2.3(c), making a total of twenty four. The remaining twelve dofs needed to generate the dofs at the corner nodes of C^{33} HGDA element must come from the center node (node 9).

From Figure 2.6, the dofs illustrated with circle and square are the dofs selected from the center node of C^{00} tensor product element in deriving a C^{33} HGDA element. The additional dofs correspond to (p_ξ, p_η) pairs of $(2,2)$, $(3,2)$, $(2,3)$, $(3,3)$, $(2,4)$, $(2,5)$, $(3,4)$, $(3,5)$, $(4,2)$, $(4,3)$, $(5,2)$ and $(5,3)$. These degrees of freedom are chosen in such a way that symmetry is ensured with respect to p_ξ and p_η.

With the discussion of the concepts relating to the transformation of the matrices, selection of the dofs and appropriate guidelines, we now proceed to the derivation of the C^{ij} approximations for distorted quadrilateral elements.

2.2.6 Derivation of C^{ij} approximations for distorted quadrilateral elements

We describe a new methodology which utilizes C^{00} p-version hierarchical interpolation functions as a starting point to generate desired order global differentiability approximations for distorted quadrilateral elements. Since the approximation functions are functions of natural coordinates ξ, η, i.e. $N_i = N_i(\xi, \eta)$, the desired derivative degrees of freedom need to be generated first in $\xi\eta$ space and then transformed into xy space. The matrices described in Section 2.2.2 assist us in transforming the desired derivative degrees of freedom from one coordinate space to another.

The dofs in $\{\delta^e\}$ of a nine node C^{00} p-version hierarchical element from Equation(2.5) are separated into those corresponding to corner nodes (denoted by co), mid-side nodes (m) and center node (denoted by c) as follows:

$$\varphi(\xi, \eta) = [a]\{\delta^e_{co}\}_{r_1} + [b]\{\delta^e_{mc}\}_{el} + [c]\{\delta^e_{m}\}_{r_2} + [d]\{\delta^e_{c}\}_{r_3} \tag{2.25}$$

where the subscript 'r_1' denotes the degrees of freedom retained from the corner nodes. Subscript 'el' corresponds to the degrees of freedom borrowed from the mid-side nodes and the center node to derive the new derivative degrees of freedom at the corner nodes of a C^{ij} HGDA element. Finally, subscripts 'r_2' and 'r_3' denote the remaining degrees of freedom from mid-side nodes and center node (after borrowing the required degrees of freedom). $[a]$, $[b]$, $[c]$ and $[d]$ are row matrices containing C^{00} p-version local approximations corresponding to the dofs in the r_1, el, r_2, r_3 sets respectively.

For a C^{11} HGDA element, $\{\delta^e_{mc}\}_{el}$ consists of dofs from mid-side nodes only since we do not need any dofs from the center node, i.e. $\{\delta^e_{mc}\}_{el}$ =$\{\delta^e_{m}\}_{el}$, which consists of the following:

$$\{\delta^e_m\}_e = \left\{ \left.\frac{\partial^2\varphi}{\partial\xi^2}\right|_2 , \left.\frac{\partial^3\varphi}{\partial\xi^3}\right|_2 , \left.\frac{\partial^2\varphi}{\partial\eta^2}\right|_4 , \left.\frac{\partial^3\varphi}{\partial\eta^3}\right|_4 , \left.\frac{\partial^2\varphi}{\partial\xi^2}\right|_6 , \left.\frac{\partial^3\varphi}{\partial\xi^3}\right|_6 , \left.\frac{\partial^2\varphi}{\partial\eta^2}\right|_8 , \left.\frac{\partial^3\varphi}{\partial\eta^3}\right|_8 \right\}^T \tag{2.26}$$

For classes higher than C^{11}, $\{\delta^e_{mc}\}_{el}$ will consist of dofs from mid-side nodes as well

as center node as discussed in Sections 2.2.4 and 2.2.5.

Let the desired new derivative dofs at the corner nodes of a C^{ij} HGDA element be denoted by $\{\delta^e\}_n^{xy}$. In case of a C^{11} HGDA element, these dofs will consist of complete set of first order derivatives of the dependent variable evaluated at the four corner nodes, i.e.

$$\{\delta^e\}_n^{\xi\eta} = \left\{\varphi_\xi|_1 \ , \ \varphi_\eta|_1 \ , \ \varphi_\xi|_3 \ , \ \varphi_\eta|_3 \ , \ \varphi_\xi|_5 \ , \ \varphi_\eta|_5 \ , \ \varphi_\xi|_7 \ , \ \varphi_\eta|_7 \right\}^T \tag{2.27}$$

where subscript denotes differentiation i.e. $\varphi_\xi|_1 = \frac{\partial\varphi}{\partial\xi}|_{\text{node 1}} = \frac{\partial\varphi}{\partial\xi}|_{(\xi=-1\ ,\ \eta=-1)}$

For classes higher than C^{11}, the new derivative dofs at the corner nodes will be augmented with the complete sets of derivatives up to the class being derived.

Differentiating Equation (2.25) with respect to ξ and η and evaluating the resulting expression at each of the four corner nodes, we get

$$\{\delta^e\}_n^{\xi\eta} = [A]\{\delta^e_{co}\}_{r_1} + [B]\{\delta^e_{mc}\}_{el} + [C]\{\delta^e_m\}_{r_2} + [D]\{\delta^e_c\}_{r_3} \tag{2.28}$$

Solving for the degrees of freedom to be eliminated i.e. $\{\delta^e_{mc}\}_{el}$ in Equation (2.28), we get

$$\{\delta^e_{mc}\}_{el} = [B]^{-1}\{\delta^e\}_n^{\xi\eta} - [B]^{-1}[A]\{\delta^e_{co}\}_{r_1} - [B]^{-1}[C]\{\delta^e_m\}_{r_2} - [B]^{-1}[D]\{\delta^e_c\}_{r_3} \tag{2.29}$$

Substituting Jacobian of transormation from Equation (2.24) into the above equation, we can transform the new derivative dofs from $\xi\eta$ space to xy space. Equation (2.29) can thus be written as

$$\{\delta^e_{mc}\}_{el} = [B]^{-1}[J_i]\{\delta^e\}_n^{xy} - [B]^{-1}[A]\{\delta^e_{co}\}_{r_1} - [B]^{-1}[C]\{\delta^e_m\}_{r_2} - [B]^{-1}[D]\{\delta^e_c\}_{r_3} \tag{2.30}$$

Now, substituting $\{\delta^e_{mc}\}_{el}$ from Equation (2.30) into Equation (2.25),

$$\begin{aligned}\varphi(\xi,\eta) = [a]\{\delta^e_{co}\}_{r_1} + [b]\Big(& [B]^{-1}[J_i]\{\delta^e\}_n^{xy} - [B]^{-1}[A]\{\delta^e_{co}\}_{r_1} \\ & -[B]^{-1}[C]\{\delta^e_m\}_{r_2} - [B]^{-1}[D]\{\delta^e_c\}_{r_3}\Big) + [c]\{\delta^e_m\}_{r_2} + [d]\{\delta^e_c\}_{r_3}\end{aligned} \tag{2.31}$$

Collecting terms in the Equation (2.31), we get the final form of the C^{ij} HGDA local approximations as follows:

$$\begin{aligned}\varphi(\xi,\eta) = \big([a]-[b][B]^{-1}[A]\big)\{\delta^e_{co}\}_{r_1} + [b][B]^{-1}[J_i]\{\delta^e\}^{xy}_n \\ + \big([c]-[b][B]^{-1}[C]\big)\{\delta^e_m\}_{r_2} + \big([d]-[b][B]^{-1}[D]\big)\{\delta^e_c\}_{r_3}\end{aligned} \tag{2.32}$$

2.2.7 Limitations of 2-D C^{11} global differentiability local approximations for distorted quadrilateral elements

In the proposed framework, 2-D C^{ij} global differentiability local approximations are derived by borrowing appropriate degrees of freedom and the corresponding approximation functions from the hierarchical nodes of C^{00} element. In Equation 2.32, $[a]$, $[c]$ and $[d]$ contain C^{00} local approximations which are retained at corner, mid-side and center nodes whereas $[b]$ contains C^{00} local approximation functions which are borrowed from mid-side and center nodes. $[A]$, $[B]$, $[C]$ and $[D]$ are matrices containing derivatives of C^{00} approximations collected in $[a]$, $[b]$, $[c]$ and $[d]$ with respect to ξ and η evaluated at the corner nodes. The approximation functions for the C^{11} distorted element at the corner, mid-side and center nodes (which are retained) are obtained by modifying the corresponding functions for the C^{00} element by $[b][B]^{-1}[A]$, $[b][B]^{-1}[C]$ and $[b][B]^{-1}[D]$ respectively.

In case of 2-D C^{11} HGDA element, the new derivative degrees of freedom introduced at the corner nodes are first order derivatives with respect to x and y. The nature of the C^{00} local approximation functions and the coordinates of the corner nodes (ξ and η coordinates are either $+1$ or -1) always result in all the coefficients of $[D]$ matrix to be zeros regardless of the p-level. The coefficients of matrices $[A]$, $[B]$, $[C]$ however are not all zero. This results in the approximation functions at the center node of C^{11} distorted element to coincide with those corresponding to C^{00} element (since $[b][B]^{-1}[D]$ is a row matrix containing all zeros). As a consequence, we have an incomplete C^{11} HGDA distorted element, which is prone to yield inaccurate results for coarser discretizations. When we derive approximation functions for C^{22} and higher order elements, the derivative degree of freedoms introduced at the corner nodes include mixed

derivatives with respect to x and y. The mixed derivatives of the C^{00} approximation functions in $[d]$ (center node) evaluated at the corner nodes are not all zero and hence we do have some non-zero coefficients in $[D]$ matrix. For the current work, we only consider 2-D C^{ij}; $i,\ j\ \geq 2$ and an alternative way to generate C^{11} HGDA element is under investigation.

Remarks

1. The derivation presented above is general and is independent of the nature of the C^{00} interpolation functions. Hence, $[a]$, $[b]$, $[c]$ and $[d]$ vectors can contain approximation functions of any kind (for example, Lagrange, Legendre or Chebyshev functions) The type of approximation functions chosen would determine the nature of the interpolation functions for the resulting 2-D C^{ij} HGDA element.

2. The matrices $[A]$, $[B]$, $[C]$, $[D]$ contain derivatives of C^{00} approximation functions with respect to ξ and η evaluated at the corner nodes. They can be precomputed once and used to generate approximation functions of any order $C^{ij};\ i,\ j\ \geq 2$ element.

3. The approximation functions being borrowed from the mid-side nodes and center node should be such that: (i) lowest degree admissible functions (corresponding to a lower p-level) should be selected first (ii) and a symmetric pattern maintained in selecting the approximation functions.

2.3 Higher order global differentiability approximations for distorted triangular elements

The framework presented to derive C^{ij} HGDA for distorted triangular elements is parallel to that used for 2-D distorted quadrilateral elements yet differs in many aspects due to the basic nature of the C^{00} p-version basis functions for triangular elements. This section presents development of higher order global differentiability local approximations for 2-D triangular elements using 2-D C^{00} p-version hierarchical approximations as a basis. The degrees of freedom and the corresponding approximation functions are borrowed from C^{00} p-version element to generate the derivative degrees of freedom and the corresponding approximation functions for C^{ij} triangular elements. The requirement of higher order global differentiability (in xy space) necessitates that the derivative degrees of freedom at the vertex or corner nodes (and some at mid-side nodes) be transformed from $\xi\eta$ space to xy space. The admissible choices of degrees of freedom and approximation functions is discussed and presented in deriving approximation functions for higher order continuity triangular elements of various orders. A systematic procedure is presented for accomplishing this ensuring the uniqueness of the C^{ij} approximations.

2.3.1 Guidelines

In deriving the desired HGDA for 2-D distorted elements of triangular family in xy space, we obey the following guidelines

(a) The distorted element geometry is mapped from xy physical coordinate space into $\xi\eta$ natural coordinate space. The master element in this case is a 2 unit equilateral triangle (Figure 2.7(a) and (b)). The master element consists of three vertex or corner nodes (nodes 1, 3 and 5), three mid-side nodes (nodes 2, 4 and 6) and one internal node (node 7). The mid-side and internal nodes are generally hierarchical in nature.

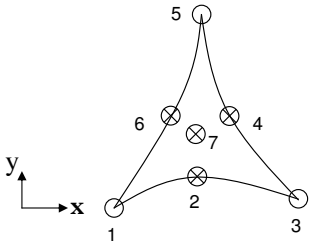

(a) 2 D distorted triangle in physical coordinate space xy

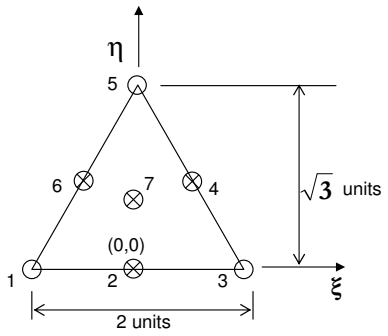

(b) Map of the element of (a) in natural coordinate space ξη

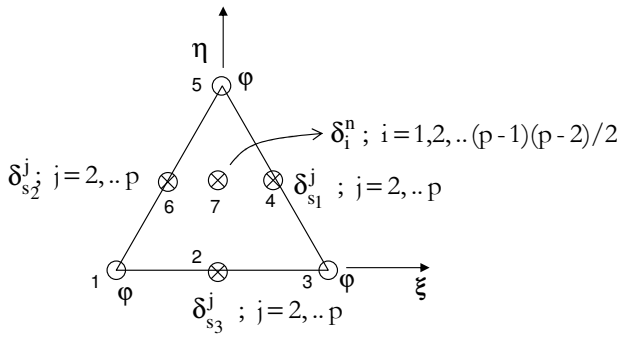

(c) Dofs for C^{00} p-version hierarchical element with p - levels p in ξ and η directions

Figure 2.7: 2-D distorted p version hierarchical triangular element with p - level $p_\xi = p_\eta = p$ in ξ and η directions

The origin of the ξ, η coordinate system is located at the node 2 of the equilateral triangle (Figure 2.7(b)) and we have the following for the mapping of points,

$$\left\{ \begin{array}{c} x \\ y \end{array} \right\} = \sum_{i=1}^{n} \bar{N}_i(L_1, L_2, L_3) \left\{ \begin{array}{c} x_i \\ y_i \end{array} \right\} \tag{2.33}$$

In Equation(2.33), (x_i, y_i) are the cartesian coordinates of the nodes and $\bar{N}_i(L_1, L_2, L_3)$ are the shape functions. The shape functions for triangle are in terms of standard barycentric or area coordinates L_1, L_2, L_3. We could use six node configuration with parabolic shape functions [47] for this purpose.

The area coordinates L_1, L_2, L_3 can be related to the orthogonal natural coordinates ξ, η, through the relations introduced by Szabo [26].

$$\begin{aligned} L_1 &= \tfrac{1}{2}(1 - \xi - \tfrac{\eta}{\sqrt{3}}) \\ L_2 &= \tfrac{1}{2}(1 + \xi - \tfrac{\eta}{\sqrt{3}}) \\ L_3 &= \tfrac{\eta}{\sqrt{3}} \end{aligned} \tag{2.34}$$

The relations in Equation (2.34) will be utilized to convert the approximation functions given in Equation (2.33) from barycentric coordinates L_1, L_2, L_3 to natural coordinates ξ, η. The relation to map points given in Equation (2.33) can be thus rewritten as follows

$$\left\{ \begin{array}{c} x \\ y \end{array} \right\} = \sum_{i=1}^{n} \bar{N}_i(\xi, \eta) \left\{ \begin{array}{c} x_i \\ y_i \end{array} \right\} \tag{2.35}$$

(b) If possible, we would like to consider C^{00} p-version hierarchical local approximation as a starting point in the derivation of 2-D HGDA. The choice of 2-D C^0 p-version hierarchical approximation functions i.e. Lagrange, Legendre or Chebyshev determines whether the corresponding 2-D HGDA are Lagrange, Legendre or Chebyshev type. Szabo and Babuska [26] presented a C^{00} p-version element based on Legendre polynomials which is shown in Figure 2.7(c). The approximation functions are separated into those corresponding to the vertex or corner

nodes, mid-side nodes and an internal node as follows:

1. Nodal shape functions

   Three nodal shape functions are chosen at the three vertices of the triangle (nodes 1, 3, 5).

$$\begin{aligned} N^1 &= L_1 \\ N^3 &= L_2 \\ N^5 &= L_3 \end{aligned} \tag{2.36}$$

2. Shape functions corresponding to Mid-Side nodes

   (p-1) mid-side shape functions are defined in terms of Legendre polynomials (P_i) at each of the three mid-side nodes (2, 4, 6) thus giving a total of $(3p-1)$ shape functions

$$\begin{aligned} N_i^2 &= L_1\, L_2\, \Psi_i(L_2 - L_1) \\ N_i^4 &= L_2\, L_3\, \Psi_i(L_3 - L_2) \\ N_i^6 &= L_1\, L_3\, \Psi_i(L_1 - L_3) \end{aligned} \tag{2.37}$$

   where Ψ is defined as follows

$$\Psi_i(\alpha) = \frac{P_i(\alpha) - P_{i-2}(\alpha)}{\sqrt{2(2i-1)}} \times \frac{4}{(1-\alpha^2)} \;; \quad i = 2, 3, \ldots p \tag{2.38}$$

   In the above equation, α assumes a value of $(L_2 - L_1)$, $(L_3 - L_2)$, $(L_1 - L_3)$ for mid-side shape functions corresponding to nodes 2, 4 and 6 respectively.

   The first few terms of $\Psi_i(\alpha)$ are:

$$\begin{aligned} &\Psi_2(\alpha) = -\sqrt{6}; \\ &\Psi_3(\alpha) = -\sqrt{10}\alpha; \\ &\Psi_4(\alpha) = -\sqrt{\tfrac{7}{8}}(5\alpha^2 - 1) \\ &\text{and so on} \end{aligned} \tag{2.39}$$

3. Internal shape functions

   From Pascal's triangle the total number of shape functions corresponding to an approximation of degree p requires to be equal to $\frac{(p+1)(p+2)}{2}$ for completeness. From the sum of approximation functions corresponding to nodal shape functions and side modes, we require $\frac{(p-1)(p-2)}{2}$ additional shape functions to satisfy this condition of completeness. These shape functions are defined at an internal node and have the characteristic of being non-zero only in the interior of the triangular domain and vanishing along all the three sides. The internal shape functions associated with the master element (at an internal node, node 7) for $p \geq 3$ are as follows

$$\begin{aligned} N_j^7\,(L_1, L_2, L_3) \;&=\; L_1\, L_2\, L_3\, P_{p-i-2}(L_2 - L_1)\, P_{i-1}(2L_3 - 1) \\ &\text{where}\;\; i = 1, 2, \ldots (p-2) \\ &\text{and}\;\; j = 1, 2, \ldots (p-1)(p-2)/2 \end{aligned} \tag{2.40}$$

For example, for a p-level of 3, we have one internal shape function

$$N_1^7 \;=\; L_1\, L_2\, L_3 \tag{2.41}$$

For a p-level of 4, we have the following three internal shape functions.

$$\begin{aligned} N_1^7 \;&=\; L_1\, L_2\, L_3 \\ N_2^7 \;&=\; L_1\, L_2\, L_3\, P_1(L_2 - L_1) \\ N_3^7 \;&=\; L_1\, L_2\, L_3\, P_1(2L_3 - 1) \end{aligned} \tag{2.42}$$

Therefore, the C^{00} triangular element consists of 55 shape functions (three nodal, 24 mid-side and 28 internal shape functions) for a p level of 9.

To preserve consistency of the coordinate system, we transform all the approximation functions presented for a C^{00} p-version element which are in terms of area coordinates to natural coordinates using the relations in Equation (2.34).

(c) Selection of the derivative degrees of freedom at the vertices of a 2-D HGDA triangular element is very critical and is dictated by the transformation between xy and $\xi\eta$ spaces. The following choices of nodal operators (or dofs) at the vertices listed in Table 2.2 for C^{11}, C^{22} and C^{33} HGDA satisfy the requirement. We note that for C^{11}, the derivative operators are a complete set of first order operators. For C^{22} HGDA, the set of C^{11} is augmented by a complete second order set and so on. This selection of degrees of freedom is consistent with the the framework developed for 2-D distorted quadrilateral elements.

(d) Since C^{00} p-version hierarchical approximations are used as a starting point, which have only function value as a degree of freedom at the vertices, we must establish some rules that allow us to borrow some dofs from C^{00} p-version hierarchical approximations to generate the desired dofs at the vertices of the 2-D HGDA for the distorted element.

Table 2.2: Choices of dofs at the corner nodes for C^{ij} 2-D distorted triangular elements in xy space

Type of HGDA	Nodal Operators at the corner nodes
C^{11}	$1\ ,\ \frac{\partial}{\partial x}\ ,\ \frac{\partial}{\partial y}$
C^{22}	$1\ ,\ \frac{\partial}{\partial x}\ ,\ \frac{\partial}{\partial y}\ ,\ \ \frac{\partial^2}{\partial x^2}\ ,\ \frac{\partial^2}{\partial y \partial x}\ ,\ \frac{\partial^2}{\partial y^2}$
C^{33}	$1\ ,\ \frac{\partial}{\partial x}\ ,\ \frac{\partial}{\partial y}\ ,\ \ \frac{\partial^2}{\partial x^2}\ ,\ \frac{\partial^2}{\partial y \partial x}\ ,\ \frac{\partial^2}{\partial y^2}\ ,\ \ \frac{\partial^3}{\partial x^3}\ ,\ \frac{\partial^3}{\partial y \partial x^2}\ ,\ \frac{\partial^3}{\partial y^2 \partial x}\ ,\ \frac{\partial^3}{\partial y^3}$

(e) The discussion presented in Section 2.2.2 on the transformation matrices for higher order derivatives of the dependent variable holds true for 2-D distorted triangular elements and hence is not repeated here. We note that the elements of transformation matrices presented for different order derivatives need to be evaluated using C^{00} p-version approximation functions corresponding to a triangle.

2.3.1.1 C^{11} HGDA for 2-D distorted triangular elements in xy space

In order to show specific details of the development, we consider C^{11} HGDA. Figure 2.8(a) shows the dofs at the vertices of C^{11} HGDA element (subscript indicates differentiation). Comparing 2.8(a) with C^{00} p-version element of Figure 2.7(c), we note that the C^{00} element requires φ_x and φ_y as additional dofs at each of the three vertices i.e. a total of six dofs for the three vertices. We borrow six dofs and the corresponding C^{00} p-version approximation functions to generate the desired derivative dofs and the corresponding approximation functions for the 2-D C^{11} HGDA element. This would obviously result in reduction of dofs at the hierarchical nodes of the 2-D HGDA element. In doing so we must follow a systematic procedure.

For this case, the choice of dofs from C^{00} element is rather straightforward. We borrow dofs corresponding to p levels 2, 3 from mid-side nodes 2, 4 and 6. These dofs must be eliminated from C^{00} p-version approximations to generate the derivative dofs at the vertices of 2-D C^{11} HGDA element as shown in Figure 2.8(a). Figure 2.8(b) shows the dofs at the hierarchical nodes of the 2-D HGDA element.

The first degree of freedom at the mid side nodes of the C^{11} HGDA element correspond to p-level of 4. For C^{11} HGDA element, we do not need to borrow any dofs from the internal node of C^{00} p-version element.

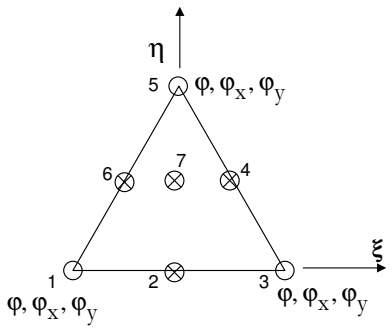

(a) Nodal dofs at the corner nodes of a 2-D C^{11} HGDA element

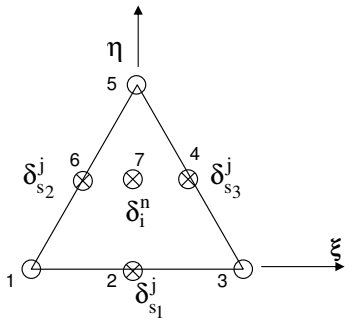

$$\text{where} \quad j = 4, .. p \ ;$$

$$i = 1,2,..(p-1)(p-2)/2$$

(b) Nodal dofs at the hierarchical nodes of a C^{11} HGDA element

Figure 2.8: Nodal dofs for C^{11} 2-D HGDA distorted triangular element

2.3.2 C^{22} HGDA for 2-D distorted triangular elements in xy space

Here we consider 2-D C^{22} HGDA for distorted triangular elements in xy space. Figure 2.9(a) shows dofs at the corner nodes of the element. Comparing this with C^{00} HGDA of Figure 2.7(c), we note that φ_x, φ_y, φ_{x^2}, φ_{xy} and φ_{y^2} are additional dofs at each of the three vertex nodes, a total of fifteen. Hence, we need to borrow fifteen dofs from the hierarchical nodes of C^{00} element shown in Figure 2.7(c), keeping in mind that the remaining dofs at the mid-side nodes C^{00} element must begin with p-level of six. This is due to the fact that a quintic polynomial describes a C^{22} approximation in 1-D. This allows us to borrow four dofs (corresponding to p-levels of 2, 3, 4 and 5) from each of the mid side nodes of Figure 2.7(c), making a total of twelve. The remaining three dofs needed to generate the dofs at the corner nodes of C^{22} HGDA element must come from the internal node.

The degrees of freedom are borrowed from internal node of the C^{00} p-version element in such a way that the dofs corresponding to a lower p-level are selected before those corresponding to higher p-levels. Figure 2.9(b) shows the dofs at the hierarchical nodes of the 2-D HGDA element.

With the discussion of the concepts relating to the selection of the dofs and appropriate guidelines, we now proceed to the derivation of the C^{ij} approximations for distorted triangular elements.

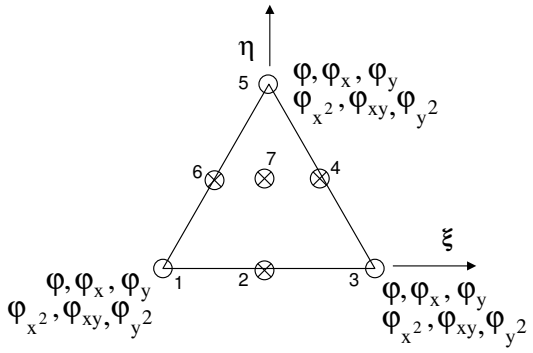

(a) Nodal dofs at the corner nodes of a C^{22} HGDA element

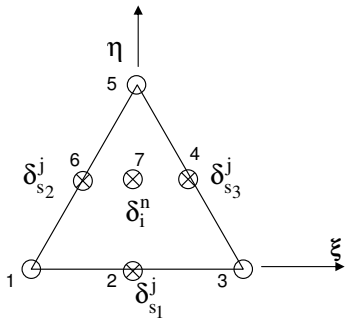

where $j = 6, .. p$;

$i = 3, 4, ... \frac{(p-1)(p-2)}{2}$

(b) Nodal dofs at the hierarchical corner nodes of a C^{22} HGDA element

Figure 2.9: Nodal dofs for 2-D C^{22} HGDA distorted triangular element

2.3.3 Derivation of C^{ij} approximations for distorted triangular elements

We propose a new methodology which utilizes C^{00} p-version hierarchical interpolation functions as a starting point and generates desired order global differentiability approximations for distorted triangular elements. Since the approximation functions are functions of natural coordinates ξ, η, i.e. $N_i = N_i(\xi, \eta)$, the desired derivative degrees of freedom need to be generated first in $\xi\eta$ space and then transformed into xy space. The matrices described in Section 2.2.2 assist us in transforming the desired derivative degrees of freedom.

Using the C^{00} p-version hierarchical approximations for a seven node element (Figure 2.7(c)), the field variable φ can be approximated as,

$$\varphi(\xi, \eta) = [N(\xi, \eta)]\{\delta^e\} \tag{2.43}$$

in which $[N(\xi, \eta)]$ is a row matrix of C^{00} p-version hierarchical local approximations and $\{\delta^e\}$ are the corresponding nodal dofs (arranged in some suitable fashion). The dofs in $\{\delta^e\}$ of Equation(2.43) are separated into those corresponding to vertex or corner nodes (denoted by co), mid-side nodes(denoted by m) and internal node (denoted by i) as follows:

$$\varphi(\xi, \eta) = [a]\{\delta^e_{co}\}_{r_1} + [b]\{\delta^e_{mi}\}_{el} + [c]\{\delta^e_m\}_{r_2} + [d]\{\delta^e_i\}_{r_3} \tag{2.44}$$

where a subscript 'r_1' denotes the degrees of freedom retained from corner nodes. Subscript 'el' corresponds to the degrees of freedom borrowed from the mid-side nodes and the internal node to derive the new derivative degrees of freedom at the corner nodes of a C^{ij} HGDA element. Finally, 'r_2' and 'r_3' denotes the degrees of freedom remaining from mid-side nodes and internal node (after borrowing the required degrees of freedom). $[a]$, $[b]$, $[c]$ and $[d]$ are vectors containing C^{00} p-version local approximations corresponding to the dofs in the r_1, el, r_2 and r_3 sets respectively.

For a C^{11} HGDA element, $\{\delta^e_{mi}\}_{el}$ consists of dofs from mid-side nodes only, since we do not need any from the internal node, i.e. $\{\delta^e_{mi}\}_{el}$ = $\{\delta^e_m\}_{el}$, which would contain

the following dofs:

$$\{\delta^e_m\}_e = \left\{\delta^2|_2\ ,\ \delta^3|_2\ ,\ \delta^2|_4\ ,\ \delta^3|_4\ ,\ \delta^2|_6\ ,\ \delta^3|_6\right\}^T \tag{2.45}$$

For classes higher than C^{11}, $\{\delta^e_{mi}\}_{el}$ will consist of dofs from mid-side nodes as well as internal node.

Let the desired new derivative dofs at the corner nodes of a C^{ij} HGDA element be denoted by $\{\delta^e\}^{xy}_n$. In case of a C^{11} HGDA element, these dofs will consist of complete set of first order derivatives of the dependent variable evaluated at the three corner nodes, i.e.

$$\{\delta^e\}^{\xi\eta}_n\ =\ \left\{\varphi_\xi|_1\ ,\ \varphi_\eta|_1\ ,\ \varphi_\xi|_3\ ,\ \varphi_\eta|_3\ ,\ \varphi_\xi|_5\ ,\ \varphi_\eta|_5\right\}^T \tag{2.46}$$

where subscript denotes differentiation i.e. $\varphi^\xi|_1\ =\ \frac{\partial\varphi}{\partial\xi}|_{node1} = \frac{\partial\varphi}{\partial\xi}|_{\xi=-1,\eta=0}$

For classes higher than C^{11}, the new derivative dofs at the corner nodes will be augmented with the complete sets of derivatives up to the class being derived.

Differentiating Equation (2.44) with respect to ξ and η and evaluating the resulting expression at each of the three corner nodes, we get

$$\{\delta^e\}^{\xi\eta}_n\ =\ [A]\{\delta^e_{co}\}_{r_1} + [B]\{\delta^e_{mi}\}_{el} + [C]\{\delta^e_m\}_{r_2} + [D]\{\delta^e_i\}_{r_3} \tag{2.47}$$

Solving for degrees of freedom to be eliminated i.e. $\{\delta^e_{mi}\}_{el}$ in Equation (2.47), we get

$$\{\delta^e_{mi}\}_{el} = [B]^{-1}\{\delta^e\}^{\xi\eta}_n - [B]^{-1}[A]\{\delta^e_{co}\}_{r_1} - [B]^{-1}[C]\{\delta^e_m\}_{r_2} - [B]^{-1}[D]\{\delta^e_i\}_{r_3} \tag{2.48}$$

Substituting Jacobian of transformation from Equation (2.24) into the above equation, we can transform the new derivative dofs from $\xi\eta$ space to xy space. Equation (2.48) can thus be written as

$$\{\delta^e_{mi}\}_{el} = [B]^{-1}[J_i]\{\delta^e\}^{xy}_n - [B]^{-1}[A]\{\delta^e_{co}\}_{r_1} - [B]^{-1}[C]\{\delta^e_m\}_{r_2} - [B]^{-1}[D]\{\delta^e_i\}_{r_3} \tag{2.49}$$

Now, substituting $\{\delta^e_{mi}\}_{el}$ from Equation (2.49) into Equation (2.44),

$$\begin{aligned}\varphi(\xi,\eta) = [a]\{\delta^e_{co}\}_{r_1} + [b]\Big(& [B]^{-1}[J_i]\{\delta^e\}^{xy}_n - [B]^{-1}[A]\{\delta^e_{co}\}_{r_1} \\ & -[B]^{-1}[C]\{\delta^e_m\}_{r_2} - [B]^{-1}[D]\{\delta^e_i\}_{r_3}\Big) + [c]\{\delta^e_m\}_{r_2} + [d]\{\delta^e_i\}_{r_3}\end{aligned} \tag{2.50}$$

Collecting terms in the Equation (2.50), we get the final form of the C^{ij} HGDA local approximations as follows:

$$\begin{aligned}\varphi(\xi,\eta) = \big([a] - [b][B]^{-1}[A]\big)\{\delta^e_{co}\}_{r_1} & + [b][B]^{-1}[J_i]\{\delta^e\}^{xy}_n \\ & + \big([c] - [b][B]^{-1}[C]\big)\{\delta^e_m\}_{r_2} + \big([d] - [b][B]^{-1}[D]\big)\{\delta^e_i\}_{r_3}\end{aligned} \tag{2.51}$$

2.3.4 Limitations of 2-D C^{11} global differentiability local approximations for distorted triangular elements

In the proposed framework, 2-D C^{ij} global differentiability local approximations are derived by borrowing appropriate degrees of freedom and the corresponding approximation functions from the hierarchical nodes of C^{00} element. In Equation 2.51, $[a]$, $[c]$ and $[d]$ contain C^{00} local approximations which are retained at corner, mid-side and internal nodes whereas $[b]$ contains C^{00} local approximations functions which are borrowed from mid-side and internal nodes. $[A]$, $[B]$, $[C]$ and $[D]$ are matrices containing derivatives of C^{00} approximations collected in $[a]$, $[b]$, $[c]$ and $[d]$ with respect to ξ and η evaluated at the corner nodes. The approximation functions for the C^{11} distorted element at the corner, mid-side and internal nodes (which are retained) are obtained by modifying the corresponding functions for the C^{00} element by $[b][B]^{-1}[A]$, $[b][B]^{-1}[C]$ and $[b][B]^{-1}[D]$ respectively.

In case of 2-D C^{11} HGDA element, the new derivative degrees of freedom introduced at the corner nodes are first order derivatives with respect to x and y. The nature of the C^{00} local approximation functions and the coordinates of the corner nodes (ξ and η coordinates are either $+1$, 0, $\sqrt{3}$ or -1) always result in all the coefficients of $[D]$ matrix to be zeros regardless of the p-level. The coefficients of matrices $[A]$, $[B]$, $[C]$ however are not all zero. This results in the approximation functions at the internal

node of C^{11} distorted element to coincide with those corresponding to C^{00} element (since $[b][B]^{-1}[D]$ is a row matrix containing all zeros). As a consequence, we have an incomplete C^{11} HGDA distorted element, which is prone to yield inaccurate results for coarser discretizations. When we derive approximation functions for C^{22} and higher order elements, the derivative degree of freedoms introduced at the corner nodes include mixed derivatives with respect to x and y. The mixed derivatives of the C^{00} approximation functions in $[d]$ (internal node) evaluated at the corner nodes are not all zero and hence we do have some non-zero coefficients in $[D]$ matrix. For the current work, we only consider 2-D C^{ij} ; $i,\ j\ \geq 2$ HGDA elements and an alternative way to generate C^{11} HGDA element is under investigation.

Remarks

1. The derivation presented above is general and is independent of the nature of the C^{00} interpolation functions. Hence, $[a]$, $[b]$, $[c]$ and $[d]$ vectors can contain approximation functions of any kind (for example, Lagrange, Legendre or Chebyshev functions) The type of approximation functions chosen would determine the nature of the interpolation functions for the resulting 2-D C^{ij} HGDA element.

2. The matrices $[A]$, $[B]$, $[C]$ and $[D]$ contain derivatives of C^{00} approximation functions with respect to ξ and η evaluated at the corner nodes. They can be precomputed once and used to generate approximation functions of any order C^{ij} element.

3. The approximation functions being borrowed from the mid-side nodes and internal node should be such that: (i) lowest degree admissible functions (corresponding to a lower p-level) should be selected first (ii) and a symmetric pattern maintained in selecting the approximation functions.

2.4 Summary

This chapter presents a framework to derive higher order global differentiability local approximations for 2-D distorted quadrilateral and triangular elements. The distorted element in physical coordinate space xy is mapped into a master element in natural coordinate space $\xi\eta$ which is a 2 unit square and 2 unit equilateral triangle for quadrilateral and triangular elements respectively. The higher order global differentiability approximations are first generated in $\xi\eta$ space and then transformed into xy space. 2-D C^{00} hierarchical approximations are used as a starting point and the basis for the developments of C^{ij} local approximations. C^{00} hierarchical elements have only function values of the field variable being approximated as a degree of freedom at the corner nodes (inter-element nodes). To derive higher order distorted elements, additional degrees of freedom which enforce desired order inter-element continuity need to be introduced at these corner nodes. The degrees of freedom chosen in developing the framework consists of a complete set of derivatives of order i (=j) in deriving C^{ij} global differentiability approximations. The approximation functions being borrowed from the mid-side nodes and internal node should be such that: (i) lowest degree admissible functions (corresponding to a lower p-level) should be selected first (ii) and a symmetric pattern maintained in selecting the approximation functions. In Chapter 3, derivation of 3-D C^{ijk} elements of hexahedral type is discussed by extending the framework presented in this chapter.

Chapter 3

Higher order global differentiability local approximations for 3-D distorted element geometries

3.1 Introduction

In this chapter we present derivations of higher order global local approximations for 3-D distorted element geometries of hexahedral type. Surana et. al. [5] presented derivation of 3-D higher order global differentiability local approximations of arbitrary order using tensor product of 1-D higher order continuity local approximations. These approximation functions require the element geometries to be rectangular and the natural coordinate axes ξ, η and ζ to be parallel to x, y, z as well as pointing in the same directions. This obviously limits the usefulness of these elements to domains in which the boundaries of the domain are parallel and perpendicular to the global xyz axes. Irregular domains with irregular boundaries obviously require the use of distorted element geometries in the discretizations.

The higher order global differentiability local approximations for distorted geometries cannot be derived using the tensor product approach utilized in reference [5]. In this chapter, we present derivations of the higher order global differentiability local approximations for distorted hexahedral family of elements. Ahmadi, Surana and Reddy

[46] developed basic strategy for distorted quadrilateral elements that also forms the basis for 3-D distorted elements.

Following reference [5], we begin with 1-D HGDA in x, y and z and the corresponding nodal operators shown in Figure 3.1(a) and (b) derived using C^0 p-version hierarchical 1-D approximations. A tensor product of the 1-D nodal operators and the corresponding 1-D HGDA yields the desired 3-D nodal operators and the corresponding HGDA. The choice of 1-D C^0 p-version hierarchical approximation functions i.e. Lagrange, Legendre or Chebyshev determines whether the corresponding 3-D HGDA are Lagrange, Legendre or Chebyshev type. This approach requires the elements in the xyz space to be straight sided with ξ , η and ζ axes parallel to x, y, z and point in the same direction. If the elements in xyz space are distorted then, we could possibly discuss an alternative. Consider 1-D higher order global differentiability approximations in ξ, η, ζ space (similar to Figure 3.1(a) and (b), but derivatives with respect to x, y, z become those with respect to ξ, η, ζ. A tensor product of these 1-D approximations would yield higher order differentiability approximations in ξ, η, ζ space. The requirement of higher order global differentiability (in xyz space) necessitates that the derivative degrees of freedom at the corner nodes (and some at mid-side and face nodes) be transformed from $\xi\eta\zeta$ space to xyz space. For example for C^{111} HGDA, $\frac{\partial}{\partial\xi}$, $\frac{\partial}{\partial\eta}$, $\frac{\partial}{\partial\zeta}$, $\frac{\partial^2}{\partial\xi\partial\eta}$, $\frac{\partial^2}{\partial\xi\partial\zeta}$, $\frac{\partial^2}{\partial\eta\partial\zeta}$, $\frac{\partial^3}{\partial\xi\partial\eta\zeta}$ need to be transformed to $\frac{\partial}{\partial x}$, $\frac{\partial}{\partial y}$, $\frac{\partial}{\partial z}$, $\frac{\partial^2}{\partial x\partial y}$, $\frac{\partial^2}{\partial x\partial z}$, $\frac{\partial^2}{\partial y\partial z}$ and $\frac{\partial^3}{\partial x\partial y\partial z}$. Due to the fact that degrees of freedom in ξ, η, ζ space for C^{ijk} higher order approximations are not complete sets, this transformation is not possible. For C^{111} case, $\frac{\partial}{\partial\xi}$, $\frac{\partial}{\partial\eta}$, $\frac{\partial}{\partial\zeta}$ can be transformed into $\frac{\partial}{\partial x}$, $\frac{\partial}{\partial y}$, $\frac{\partial}{\partial z}$ but there is no feasible resolution for transforming $\frac{\partial^2}{\partial\xi\partial\eta}$, $\frac{\partial^2}{\partial\xi\partial\zeta}$, $\frac{\partial^2}{\partial\eta\partial\zeta}$, $\frac{\partial^3}{\partial\xi\partial\eta\partial\zeta}$ into $\frac{\partial^2}{\partial x\partial y}$, $\frac{\partial^2}{\partial x\partial z}$, $\frac{\partial^2}{\partial y\partial z}$, $\frac{\partial^3}{\partial x\partial y\partial z}$. Similar situation exists for higher orders as well. Thus, the derivation of HGDA for 3-D distorted elements in xyz space requires a fundamentally different approach.

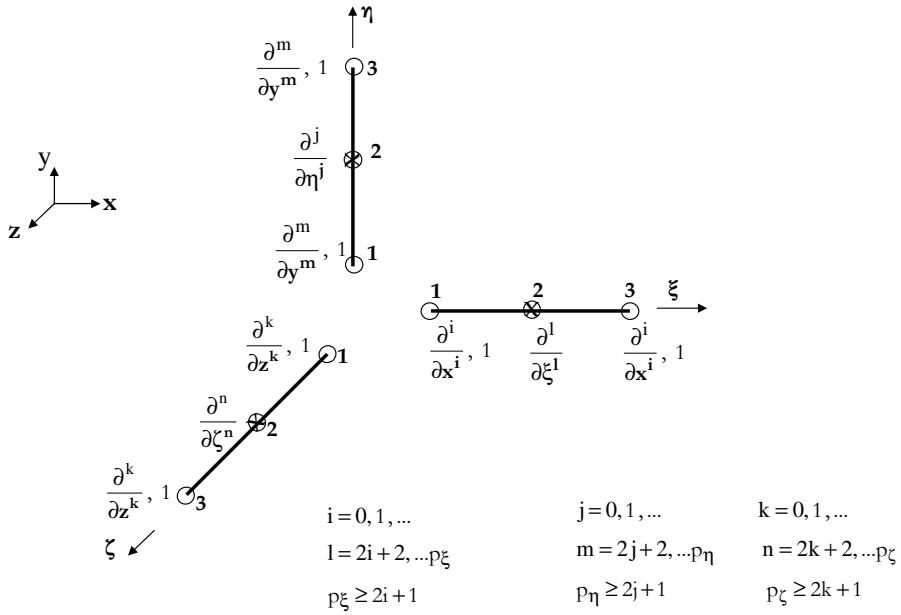

(a) 1 – D nodal operators

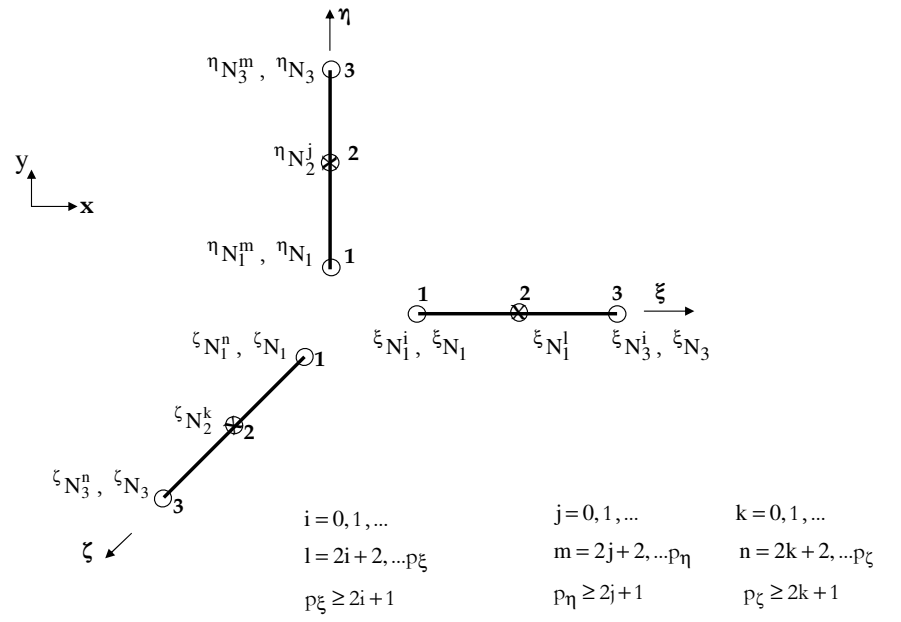

(b) 1-D Higher order global differentiability approximation functions

Figure 3.1: 1-D nodal operators and approximation functions in x, y and z

3.2 Guidelines:

In deriving the desired HGDA for 3-D distorted elements of hexahedral family in xyz space, we follow the ensuing guidelines.

(a) The distorted element geometry is mapped into $\xi\eta\zeta$ natural coordinate space into a 2 unit cube (Figure 3.2(a) and (b)). The master element consists of eight corner nodes (nodes 1, 3, 5, 7, 13, 15, 17, 19), twelve mid-side nodes (nodes 2, 4, 6, 8, 9, 10, 11, 12, 14, 16, 18, 20), six face nodes (21, 22, 23, 24, 25, 26) and one center node (node 27). The mid-side nodes are hierarchical in one direction whereas face nodes are hierarchical in two directions. The center node is hierarchical along all three coordinate axes ξ, η and ζ. The origin of the ξ, η, ζ coordinate system is located at the center node of the cube and we have the following for the mapping of points,

$$\left\{ \begin{array}{c} x \\ y \\ z \end{array} \right\} = \sum_{i=1}^{n} \hat{N}_i(\xi, \eta, \zeta) \left\{ \begin{array}{c} x_i \\ y_i \\ z_i \end{array} \right\} \tag{3.1}$$

In which, (x_i, y_i, z_i) are the cartesian coordinates of the nodes and $\hat{N}_i(\xi, \eta, \zeta)$ are the shape functions. We could use twenty node configuration with serendipity functions [49] for this purpose.

(b) If possible, we would like to consider C^{000} p-version hierarchical local approximation as a starting point in the derivation of 3-D HGDA. Figure 3.2(c) shows nodal degrees of freedom for a standard C^{000} p-version hierarchic element in which φ is the field variable being interpolated. The degrees of freedom at the corner nodes of this element consists of only function values.

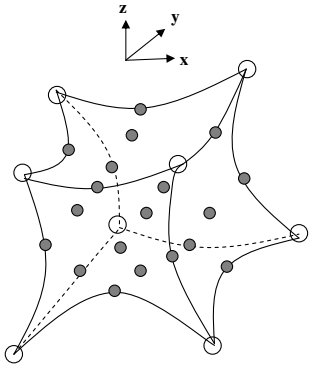

(a) A 27-node distorted element in xyz space

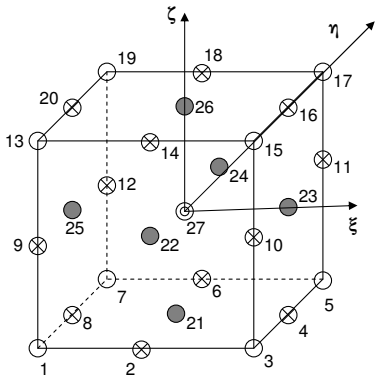

(b) Map of the 27-node distorted element in $\xi\eta\zeta$ space

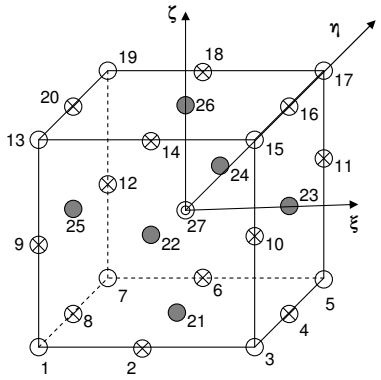

φ : Nodes 1, 3, 5, 7, 13, 15, 17, 19

$\partial^i\varphi/\partial\xi^i$: Nodes 2, 6, 14, 18 $\quad$ $\partial^j\varphi/\partial\eta^j$: Nodes 4, 8, 16, 20 $\quad$ $\partial^k\varphi/\partial\zeta^k$: Nodes 9, 10, 11, 12

$\partial^{i+j}\varphi/\partial\xi^i\partial\eta^j$: Nodes 21, 26 $\quad$ $\partial^{j+k}\varphi/\partial\eta^j\partial\zeta^j$: Nodes 23, 25 $\quad$ $\partial^{i+k}\varphi/\partial\xi^i\partial\zeta^j$: Nodes 22, 24

$\partial^{i+j+k}\varphi/\partial\xi^i\partial\eta^j\partial\zeta^k$: Node 27

$i = 2, 3, \ldots p_\xi$; $j = 2, 3, \ldots p_\eta$; $k = 2, 3, \ldots p_\zeta$

(c) Dofs for C^{000} p-version hierarchical element with p - levels p_ξ , p_η and p_ζ in ξ , η and ζ directions

Figure 3.2: 3-D distorted element mapped to natural coordinate space and C^{000} p-version element

(c) Different degrees of freedom are needed at the corner nodes than those for the 3-D HGDA generated using tensor product. This is due to the fact that dofs in tensor product 3-D HGDA do not transform from xyz to $\xi\eta\zeta$ or vice-versa. Obviously the choices of the dofs at the corner nodes are dictated by the transformation between xyz and $\xi\eta\zeta$ spaces.

(d) The degrees of freedom for 3-D HGDA element should be such that they can be transformable using standard jacobians of transformation from natural coordinate space to physical coordinate space. The choices of nodal operators (or dofs) at the corner nodes listed in Table 3.1 for C^{111} and C^{222} HGDA satisfy the requirement. We note that for C^{111}, the derivative operators are a complete set of first order operators. For C^{222} HGDA, the set of C^{111} is augmented by a complete second order set and so on.

(e) Since C^{000} p-version hierarchical approximations are used as a starting point and that in these local approximations function value is the only degree of freedom at the corner nodes, we must establish some rules that allow us to borrow some dofs from C^{000} p-version hierarchical approximations to generate the desired dofs at the corner nodes of the 3-D HGDA for the distorted element.

Table 3.1: Choices of dofs at the corner nodes for C^{ijk} 3-D distorted hexahedral elements in xyz space

Type of HGDA	Nodal Operators at the corner nodes
C^{111}	$1\ ,\ \frac{\partial}{\partial x}\ ,\ \frac{\partial}{\partial y},\ \frac{\partial}{\partial z}$
C^{222}	$1\ ,\ \frac{\partial}{\partial x}\ ,\ \frac{\partial}{\partial y}\ ,\ \frac{\partial}{\partial z},\quad \frac{\partial^2}{\partial x^2}\ ,\ \frac{\partial^2}{\partial y^2}\ \frac{\partial^2}{\partial z^2}, \frac{\partial^2}{\partial y \partial x}\ ,\ \frac{\partial^2}{\partial x \partial z},\ \frac{\partial^2}{\partial y \partial z}$

3.3 Transformation matrices

In this section we present details of the transformation matrices essential to derive 3-D HGDA for distorted hexahedral geometries in xyz space. Figure 3.2 (c) shows nodal degrees of freedom for C^{000} p-version hierarchical element in which φ is dependent variable. From Equation (3.1), we obtain the following for mapping of lengths in (ξ, η, ζ) and (x, y, z) spaces,

$$\left\{ \begin{array}{c} dx \\ dy \\ dz \end{array} \right\} = [J] \left\{ \begin{array}{c} d\xi \\ d\eta \\ d\zeta \end{array} \right\} \tag{3.2}$$

Using Murnaghan's notation [48] we can write,

$$[J] = \left[\frac{x \; y \; z}{\xi \; \eta \; \zeta} \right] \tag{3.3}$$

in which the quantities in numerator define a row and those in the denominator define column wise differentiation of the terms in the numerator. Thus,

$$[J] = \left[\frac{x \; y \; z}{\xi \; \eta \; \zeta} \right] = \left[\begin{array}{ccc} x_\xi & x_\eta & x_\zeta \\ y_\xi & y_\eta & y_\zeta \\ z_\xi & z_\eta & z_\zeta \end{array} \right] \tag{3.4}$$

where subscript denotes differentiation, i.e. $x_\xi = \frac{\partial x}{\partial \xi}$, $x_\eta = \frac{\partial x}{\partial \eta}$, $x_\zeta = \frac{\partial x}{\partial \zeta}$ etc.

Using the C^{000} p-version hierarchical approximations for a twenty seven node element (Figure 3.2(c)),the field variable φ can be approximated as [5],

$$\varphi(\xi, \eta, \zeta) = [N(\xi, \eta, \zeta)]\{\delta^e\} \tag{3.5}$$

in which $[N(\xi, \eta, \zeta)]$ is a row matrix of C^{000} p-version hierarchical local approximations and $\{\delta^e\}$ are the corresponding nodal dofs (arranged in some suitable fashion).

We define,

$$\{\varphi\}_1^{\xi\eta\zeta} = \left[\frac{\partial\varphi}{\partial\xi}\ ,\ \frac{\partial\varphi}{\partial\eta}\ ,\ \frac{\partial\varphi}{\partial\zeta}\right]^T \tag{3.6}$$

$$\{\varphi\}_1^{xyz} = \left[\frac{\partial\varphi}{\partial x}\ ,\ \frac{\partial\varphi}{\partial y}\ ,\ \frac{\partial\varphi}{\partial z}\right]^T \tag{3.7}$$

$$\{\varphi\}_2^{\xi\eta\zeta} = \left[\frac{\partial^2\varphi}{\partial\xi^2}\ ,\ \frac{\partial^2\varphi}{\partial\eta^2}\ ,\ \frac{\partial^2\varphi}{\partial\zeta^2}\ ,\ \frac{\partial^2\varphi}{\partial\eta\partial\xi}\ ,\ \frac{\partial^2\varphi}{\partial\zeta\partial\xi}\ ,\ \frac{\partial^2\varphi}{\partial\eta\partial\zeta}\right]^T \tag{3.8}$$

$$\{\varphi\}_2^{xyz} = \left[\frac{\partial^2\varphi}{\partial x^2}\ ,\ \frac{\partial^2\varphi}{\partial y^2}\ ,\ \frac{\partial^2\varphi}{\partial z^2}\ ,\ \frac{\partial^2\varphi}{\partial y\partial x}\ ,\ \frac{\partial^2\varphi}{\partial z\partial x}\ ,\ \frac{\partial^2\varphi}{\partial y\partial z}\right]^T \tag{3.9}$$

where T denotes transpose of a matrix.

We note that Equations (3.6) and (3.7) are complete first order derivative sets, Equations (3.8) and (3.9) are complete second order derivative sets in $\xi\eta\zeta$ and xyz spaces. In this manner, we can define $\{\varphi\}_i^{\xi\eta\zeta}$ and $\{\varphi\}_i^{xyz}$ as complete sets of the derivatives of order i in (ξ,η,ζ) and (x,y,z) spaces. Next we define the rules of transformation between the sets of different order derivatives in (ξ,η,ζ) and (x,y,z) spaces.

$$\{\varphi\}_i^{\xi\eta\zeta} = [J_i]\{\varphi\}_i^{xyz} \tag{3.10}$$

Obviously,

$$[J_1] = \begin{bmatrix} x_\xi & y_\xi & z_\xi \\ x_\eta & y_\eta & z_\eta \\ x_\zeta & y_\zeta & z_\zeta \end{bmatrix} = [J]^T \tag{3.11}$$

Using chain rule of differentiation, we can determine the transformation matrices

for higher order derivatives of the dependent variable.

We will use the following notations for higher order derivatives of x with respect to natural coordinates ξ, η and ζ

$$x_\xi = \frac{\partial x}{\partial \xi} \;\; ; \;\; x_\xi^i = \left(\frac{\partial x}{\partial \xi}\right)^i \;\; ; \;\; x_{\xi^i} = \frac{\partial^i x}{\partial \xi^i} \;\; ; \;\; x_{\xi^i \eta^j} = \frac{\partial^{i+j} x}{\partial \xi^i \partial \eta^j} \tag{3.12}$$

$$x_\eta = \frac{\partial x}{\partial \eta} \;\; ; \;\; x_\eta^i = \left(\frac{\partial x}{\partial \eta}\right)^i \;\; ; \;\; x_{\eta^i} = \frac{\partial^i x}{\partial \eta^i} \;\; ; \;\; x_{\xi^i \zeta^j} = \frac{\partial^{i+j} x}{\partial \xi^i \partial \zeta^j} \tag{3.13}$$

$$x_\zeta = \frac{\partial x}{\partial \zeta} \;\; ; \;\; x_\zeta^i = \left(\frac{\partial x}{\partial \zeta}\right)^i \;\; ; \;\; x_{\zeta^i} = \frac{\partial^i x}{\partial \zeta^i} \;\; ; \;\; x_{\eta^i \zeta^j} = \frac{\partial^{i+j} x}{\partial \eta^i \partial \zeta^j} \tag{3.14}$$

Similar notations hold true for the derivatives of y and z with respect to ξ, η and ζ Following these notations, the transformation matrices for the second order derivatives are as follows:

$$\{\varphi\}_2^{xyz} = [J_2]^{-1} \left[\{\varphi\}_2^{\xi\eta\zeta} - [J_2^1]\{\varphi\}_1^{xyz}\right] \tag{3.15}$$

$$[J_2] = \begin{bmatrix} {x_\xi}^2 & {y_\xi}^2 & {z_\xi}^2 & 2x_\xi y_\xi & 2x_\xi z_\xi & 2y_\xi z_\xi \\ {x_\eta}^2 & {y_\eta}^2 & {z_\eta}^2 & 2x_\eta y_\eta & 2x_\eta z_\eta & 2y_\eta z_\eta \\ {x_\zeta}^2 & {y_\zeta}^2 & {z_\zeta}^2 & 2x_\zeta y_\zeta & 2x_\zeta z_\zeta & 2y_\zeta z_\zeta \\ x_\eta x_\xi & y_\eta y_\xi & z_\eta z_\xi & x_\xi y_\eta + x_\eta y_\xi & x_\xi z_\eta + x_\eta z_\xi & y_\xi z_\eta + y_\eta z_\xi \\ x_\xi x_\zeta & y_\zeta y_\xi & z_\zeta z_\xi & x_\zeta y_\xi + x_\xi y_\zeta & x_\zeta z_\xi + x_\xi z_\zeta & y_\zeta z_\xi + y_\xi z_\zeta \\ x_\eta x_\zeta & y_\eta y_\zeta & z_\eta z_\zeta & x_\zeta y_\eta + x_\eta y_\zeta & x_\zeta z_\eta + x_\eta z_\zeta & y_\zeta z_\eta + y_\eta z_\zeta \end{bmatrix} \tag{3.16}$$

$$[J_2^1] = \begin{bmatrix} x_{\xi^2} & y_{\xi^2} & z_{\xi^2} \\ x_{\eta^2} & y_{\eta^2} & z_{\eta^2} \\ x_{\zeta^2} & y_{\zeta^2} & z_{\zeta^2} \\ x_{\xi\eta} & y_{\xi\eta} & z_{\xi\eta} \\ x_{\xi\zeta} & y_{\xi\zeta} & z_{\xi\zeta} \\ x_{\eta\zeta} & y_{\eta\zeta} & z_{\eta\zeta} \end{bmatrix} \tag{3.17}$$

From Equation (3.10) we can write

$$\{\varphi\}_i^{xyz} = [J_i]^{-1}\{\varphi\}_i^{\xi\eta\zeta} \tag{3.18}$$

3.4 C^{111} HGDA for 3-D distorted quadrilateral elements in xyz space

In order to show specific details of the development, we consider C^{111} HGDA. Figure 3.3(a) shows the dofs at the corner nodes of C^{111} HGDA element (subscript indicates differentiation). Comparing Figure 3.3(a) with C^{000} p-version element of Figure 3.2(c), we note that the element of Figure 3.3(a) requires φ_x, φ_y and φ_z as additional dofs at each of the eight corner nodes i.e. a total of twenty four dofs for the eight corner nodes. We borrow twenty four dofs and the corresponding C^{000} p-version approximation functions to generate these dofs and the corresponding approximation functions for the 3-D C^{111} HGDA element. This would obviously result in reduction of dofs at the hierarchical nodes of the 3-D HGDA element. For this case, the choice of dofs from C^{000} element is rather straightforward. We borrow two dofs which are associated with the lowest p-levels (i.e. p = 2 and 3)and their corresponding approximation functions from each of the twelve mid-side nodes which would give us the required twenty four dofs and corresponding approximation functions. These dofs must be eliminated from C^{000} p-version element to generate the derivative dofs at the corner nodes of C^{111} HGDA element as shown in Figure 3.3(a). Figure 3.3(b) shows the dofs at the hierarchical nodes of the 3-D C^{111} HGDA element.

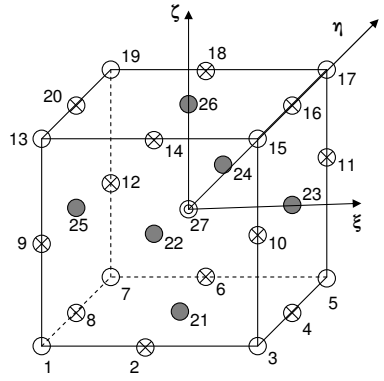

$\varphi, \varphi_x, \varphi_y, \varphi_z$: Nodes 1, 3, 5, 7, 13, 15, 17, 19

(a) Nodal Dofs at the corner nodes of a C^{111} HGDA element

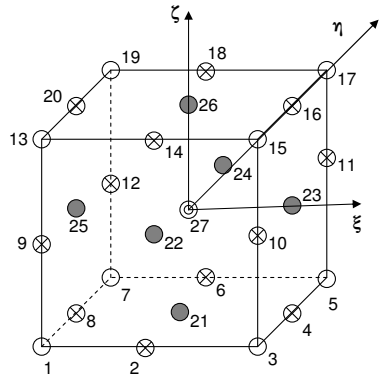

$\partial^i\varphi/\partial\xi^i$: Nodes 2, 6, 14, 18 $\partial^j\varphi/\partial\eta^j$: Nodes 4, 8, 16, 20 $\partial^k\varphi/\partial\zeta^k$: Nodes 9,10,11,12

$\partial^{l+m}\varphi/\partial\xi^l\partial\eta^m$: Nodes 21, 26 $\partial^{m+n}\varphi/\partial\eta^m\partial\zeta^n$: Nodes 23, 25 $\partial^{l+n}\varphi/\partial\xi^l\partial\zeta^n$: Nodes 22, 24

$\partial^{l+m+n}\varphi/\partial\xi^l\partial\eta^m\partial\zeta^n$: Node 27

$i = 4, 5, \ldots p_\xi$; $j = 4, 5, \ldots p_\eta$; $k = 4, 5, \ldots p_\zeta$

$l = 2, 3, \ldots p_\xi$; $m = 2, 3, \ldots p_\eta$; $k = 2, 3, \ldots p_\zeta$

(b) Dofs at the hierarchical nodes for C^{111} HGDA element

Figure 3.3: Nodal dofs for 2-D C^{111} HGDA distorted hexahedral element

We note that the dofs removed from the mid side nodes of the C^{000} p-version element correspond to p-levels 2 and 3 and hence consistent with the tensor product C^{111} element. The first degree of freedom at the mid side nodes of the C^{111} HGDA element correspond to p-level of 4. For C^{111} HGDA element, we do not need to borrow any dofs from the face nodes or center node of C^{000} p-version element.

3.5 C^{222} HGDA for 3-D distorted hexahedral elements in xyz space

Here we consider 3-D C^{222} HGDA for distorted quadrilateral elements in xyz space. Figure 3.4(a) shows dofs at the corner nodes of the element. Comparing this with C^{000} HGDA of Figure 3.2(c), we note that φ_x, φ_y, φ_z, φ_{x^2}, φ_{y^2}, φ_{z^2}, φ_{xy}, φ_{xz} and φ_{yz} are additional dofs at each of the eight corner nodes, a total of seventy two. Hence, we need to borrow seventy two dofs from the hierarchical nodes of C^{000} HGDA element shown in Figure 3.4(b), keeping in mind that the remaining dofs at the mid side nodes of Figure 3.2(c) element must begin with p-level of six. This is to ensure that C^{222} HGDA is in conformity with C^{222} tensor product element. This allows us to borrow four dofs (corresponding to p-levels of 2, 3, 4 and 5) from each of the mid side nodes of Figure 3.2(c), making a total of forty eight. The remaining twenty four dofs needed to generate the derivative dofs at the corner nodes of C^{222} HGDA element must come from the six face nodes.

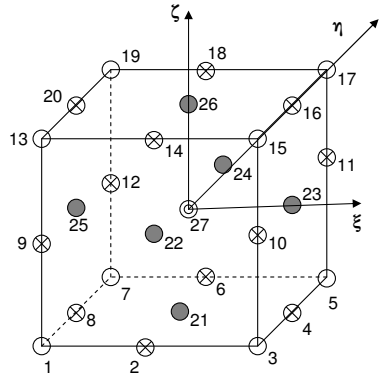

φ , $\varphi_x, \varphi_y, \varphi_z$, $\varphi_{xy}, \varphi_{yz}, \varphi_{xz}$, $\varphi_{x^2}, \varphi_{y^2}, \varphi_{z^2}$: Nodes 1, 3, 5, 7, 13, 15, 17, 19

(a) Nodal Dofs at the corner nodes of a C^{222} HGDA element

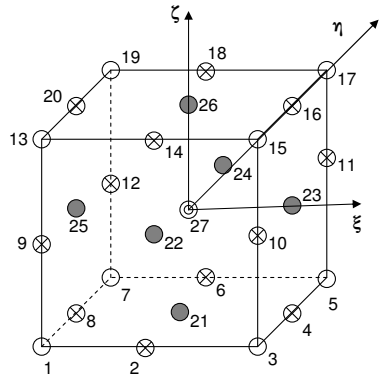

$\partial^i\varphi/\partial\xi^i$: Nodes 2, 6, 14, 18 $\partial^j\varphi/\partial\eta^j$: Nodes 4, 8, 16, 20 $\partial^k\varphi/\partial\zeta^k$: Nodes 9,10,11,12

$\partial^6\varphi/\partial\xi^2\partial\eta^4$; $\partial^6\varphi/\partial\xi^4\partial\eta^2$; $\partial^{l+m}\varphi/\partial\xi^l\partial\eta^m$: Nodes 21, 26 $\partial^{a+b+c}\varphi/\partial\xi^a\partial\eta^b\partial\zeta^c$: Node 27

$\partial^6\varphi/\partial\eta^2\partial\zeta^4$; $\partial^6\varphi/\partial\eta^4\partial\zeta^2$; $\partial^{m+n}\varphi/\partial\eta^m\partial\zeta^n$: Nodes 23, 25

$\partial^6\varphi/\partial\xi^4\partial\zeta^2$; $\partial^6\varphi/\partial\xi^2\partial\zeta^4$; $\partial^{l+n}\varphi/\partial\xi^l\partial\zeta^n$: Nodes 22, 24

$i = 6, 7, ...p_\xi$; $j = 6, 7, ...p_\eta$; $k = 6, 7, ...p_\zeta$ $a = 2, 3, ...p_\xi$; $b = 2, 3, ...p_\eta$; $c = 2, 3, ...p_\zeta$

$l = 2, 3, ...p_\xi$; $m = 2, 3, ...p_\eta$; $k = 2, 3, ...p_\zeta$ where $l + m \geq 7$; $m + n \geq 7$; $l + n \geq 7$

(b) Dofs at the hierarchical nodes for C^{222} HGDA element

Figure 3.4: Nodal dofs for 3-D C^{222} HGDA distorted hexahedral element

The degrees of freedom are borrowed from face nodes of the C^{000} tensor product element in such a way that the dofs corresponding to a lower p-level are selected before those corresponding to higher p-levels. Figure 3.5 shows the dofs generated at two of the face nodes which are hierarchical along ξ and η directions (nodes 21 and 26 from Figure 3.2(c)). Similar figures can be produced for face nodes 22 and 24 (hierarchical along ξ and ζ directions) and face nodes 23 and 25 (hierarchical along η and ζ directions). The dofs illustrated with a circle are the four dofs selected from face nodes 21 and 26 in deriving a C^{222} HGDA element. They correspond to (p_ξ, p_η) pairs of $(2,2)$, $(3,2)$, $(2,3)$ and $(3,3)$. Degree of freedom corresponding to p-level pair of $(3,3)$ is chosen over $(4,2)$ or $(2,4)$ to ensure symmetry with respect to p_ξ and p_η. Similarly four nodes need to be selected from face nodes 22, 24, 23 and 25. Symmetry in the degrees of freedom pairs is maintained to preserve the symmetry of finite element solutions for symmetric discretizations.

With the discussion of the concepts relating to the transformation of the matrices, selection of the dofs and appropriate guidelines, we now proceed to the derivation of the C^{ijk} approximations for distorted hexahedral elements.

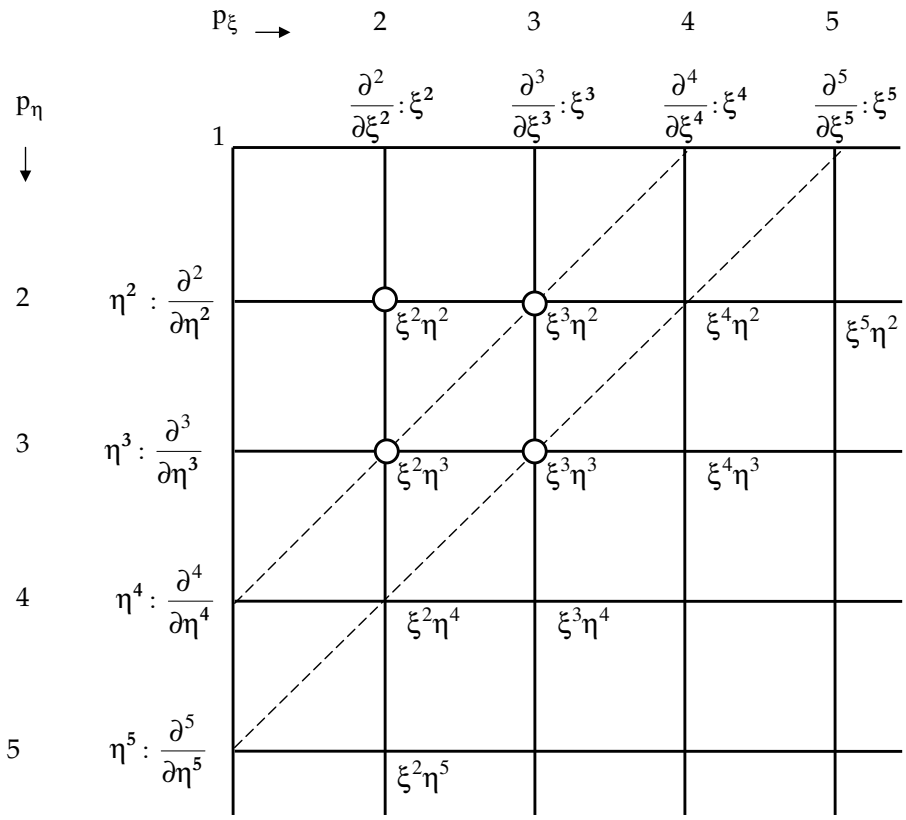

○ Additional dofs from the face nodes numbered 21, 26 (hierarchical in ξ and η) of C^{000} *p*-version element for C^{222} HGDA element

Similar dof selections are made at face nodes 22, 24 (ξ and ζ directions) and 23, 25 (η and ζ directions) of C^{000} p-version element for C^{222} HGDA element

Figure 3.5: Dofs at the face nodes of a C^{000} p-version hierarchical element

3.6 Derivation of C^{ijk} approximations for distorted hexahedral elements

We propose a new methodology which utilizes C^{000} p-version hierarchical interpolation functions as a starting point and generates desired order global differentiability approximations for distorted hexahedral elements. Since the approximation functions are functions of natural coordinates ξ, η, ζ, i.e. $N_i = N_i(\xi, \eta, \zeta)$, the desired derivative degrees of freedom need to be generated first in $\xi\eta\zeta$ space and then transformed into xyz space. The matrices described in Section 3.2.2 assist us in transforming the desired derivative degrees of freedom.

The dofs in $\{\delta^e\}$ of a twenty seven node C^{000} p-version hierarchical element from Equation(3.5) are separated into those corresponding to corner nodes (denoted by co), mid-side nodes (denoted by m), face nodes (denoted by f), center node (denoted by c) as follows:

$$\varphi(\xi, \eta, \zeta) = [a]\{\delta^e_{co}\}_{r_1} + [b]\{\delta^e_{mf}\}_{el} + [c]\{\delta^e_{mf}\}_{r_2} + [d]\{\delta^e_{c}\}_{r_3} \tag{3.19}$$

where a subscript 'r_1' denotes the degrees of freedom retained from corner nodes, 'r_2' denotes the degrees of freedom remaining from mid-side nodes and face nodes (after borrowing the required degrees of freedom), 'r_3' denotes the degrees of freedom retained from center node. Subscript 'el' corresponds to the degrees of freedom borrowed from the mid-side nodes and the face node to derive the new derivative degrees of freedom at the corner nodes of a C^{ijk} HGDA element. $[a]$, $[b]$,$[c]$ and $[d]$ are vectors containing C^{000} p-version local approximations corresponding to the dofs in the r_1, el and r_2, r_3 sets respectively.

For a C^{111} HGDA element, $\{\delta^e_{mf}\}_{el}$ consists of dofs from mid-side nodes only, since we do not need any from the face node, i.e. $\{\delta^e_{mf}\}_{el}$=$\{\delta^e_{m}\}_{el}$. For classes higher than C^{111}, $\{\delta^e_{mf}\}_{el}$ will consist of dofs from mid-side nodes as well as face nodes.

Let the desired new derivative dofs at the corner nodes of a C^{ijk} HGDA element

be denoted by $\{\delta^e\}_n^{xyz}$. In case of a C^{111} HGDA element, these dofs will consist of complete set of first order derivatives of the dependent variable evaluated at the eight corner nodes, i.e.

$$\{\delta^e\}_n^{\xi\eta\zeta} = \left\{ \{\delta_1^e\}^{\xi\eta\zeta}, \{\delta_3^e\}^{\xi\eta\zeta}, \{\delta_5^e\}^{\xi\eta\zeta}, \{\delta_7^e\}^{\xi\eta\zeta}, \{\delta_{13}^e\}^{\xi\eta\zeta}, \{\delta_{15}^e\}^{\xi\eta\zeta}, \{\delta_{17}^e\}^{\xi\eta\zeta}, \{\delta_{19}^e\}^{\xi\eta\zeta} \right\}^T \tag{3.20}$$

with

$$\{\delta_1^e\}^{\xi\eta\zeta} = \left\{ \frac{\partial\varphi}{\partial\xi} \, , \, \frac{\partial\varphi}{\partial\eta} \, , \, \frac{\partial\varphi}{\partial\zeta} \right\}^T_{\text{at node 1}} \tag{3.21}$$

where subscript denotes differentiation i.e. $\frac{\partial\varphi}{\partial\xi}|_{\text{node 1}} = \frac{\partial\varphi}{\partial\xi}|_{(\xi=-1\ ,\ \eta=-1\ ,\ \zeta=-1)}$

For classes higher than C^{111}, the new derivative dofs at the corner nodes will be augmented with the complete sets of derivatives up to the class being derived.

Differentiating Equation (3.19) with respect to ξ , η and ζ and evaluating the resulting expression at each of the eight corner nodes, we get

$$\{\delta^e\}_n^{\xi\eta\zeta} = [A]\{\delta_{co}^e\}_{r_1} + [B]\{\delta_{mf}^e\}_{el} + [C]\{\delta_{mf}^e\}_{r_2} + [D]\{\delta_c^e\}_{r_3} \tag{3.22}$$

Solving for $\{\delta_{mf}^e\}_{el}$ in Equation (3.22), we get

$$\{\delta_{mf}^e\}_{el} = [B]^{-1}\{\delta^e\}_n^{\xi\eta\zeta} - [B]^{-1}[A]\{\delta_{co}^e\}_{r_1} - [B]^{-1}[C]\{\delta_{mf}^e\}_{r_2} - [B]^{-1}[D]\{\delta_c^e\}_{r_3} \tag{3.23}$$

Substituting Jacobian of transformation from Equation (3.18) into the above equation, we can transform the new derivative dofs from $\xi\eta\zeta$ space to xyz space. Equation (3.23) can thus be rewritten as

$$\{\delta_{mf}^e\}_{el} = [B]^{-1}[J_i]\{\delta^e\}_n^{xyz} - [B]^{-1}[A]\{\delta_{co}^e\}_{r_1} - [B]^{-1}[C]\{\delta_{mf}^e\}_{r_2} - [B]^{-1}[D]\{\delta_c^e\}_{r_3} \tag{3.24}$$

Now, substituting $\{\delta^e_{mf}\}_{el}$ from Equation (3.24) into Equation (3.19) and collecting terms, we get the final form of the C^{ijk} HGDA local approximations as follows:

$$\begin{aligned}\varphi(\xi,\eta,\zeta) = \big([a]-[b][B]^{-1}[A]\big)\{\delta^e_{co}\}_{r_1} + [b][B]^{-1}[J_i]\{\delta^e\}^{xyz}_n \\ + \big([c]-[b][B]^{-1}[C]\big)\{\delta^e_{mc}\}_{r_2} + \big([d]-[b][B]^{-1}[D]\big)\{\delta^e_c\}_{r_3}\end{aligned} \tag{3.25}$$

3.6.1 Limitations of 3-D C^{111} and C^{222} global differentiability local approximations for distorted hexahedral elements

In the proposed framework, 3-D C^{ijk} global differentiability local approximations are derived by borrowing appropriate degrees of freedom and the corresponding approximation functions from the hierarchical nodes of C^{000} element. In Equation 3.25, $[a]$ and $[d]$ contain C^{000} local approximations which are retained at corner, and center nodes. $[b]$ contains C^{000} local approximation functions which are borrowed from mid-side and face nodes whereas $[c]$ contains the C^{000} local approximations functions retained from mid-side and face nodes. $[A]$, $[B]$, $[C]$ and $[D]$ are matrices containing derivatives of C^{00} approximations collected in $[a]$, $[b]$, $[c]$ and $[d]$ with respect to ξ, η and ζ evaluated at the corner nodes. The approximation functions for the higher order distorted elements at the corner, mid-side, face and center nodes (which are retained) are obtained by modifying the corresponding functions for the C^{000} element by $[b][B]^{-1}[A]$, $[b][B]^{-1}[C]$ and $[b][B]^{-1}[D]$ respectively.

In case of 3-D C^{111} and C^{222} HGDA elements, the new derivative degrees of freedom introduced at the corner nodes are first and second order derivatives (with respect to x, y and z) respectively. The nature of the C^{000} local approximation functions and the coordinates of the corner nodes (ξ , η and ζ coordinates are either $+1$ or -1) always result in all the coefficients of $[D]$ matrix to be zeros regardless of the p-level. The coefficients of matrices $[A]$, $[B]$, $[C]$ however are not all zero. This results in the approximation functions at the center node of C^{111} and C^{222} distorted elements to coincide with those corresponding to C^{000} element (since $[b][B]^{-1}[D]$ is a row matrix containing all zeros). As a consequence, we have incomplete C^{111} and C^{222} HGDA distorted elements, which are prone to yield inaccurate results for coarser discretizations. When

we derive approximation functions for C^{333} and higher order elements, the derivative degree of freedoms introduced at the corner nodes include mixed derivatives of third order or higher with respect to ξ, η and ζ. The third and higher order mixed derivatives of the C^{000} approximation functions in $[d]$ (center node) evaluated at the corner nodes are not all zero and hence we do have some non-zero coefficients in $[D]$ matrix. For the current work, we only consider 3-D C^{ijk} ; $i,\ j,\ k, \geq 3$ HGDA elements and alternative ways to generate C^{111} and C^{222} HGDA elements are under investigation.

3.7 Summary

In this chapter, a framework to derive higher order global differentiability local approximations for C^{ijk} elements of hexahedral type is presented. The distorted element in physical coordinate space xyz is mapped into a 2 unit cube in natural coordinate space $\xi\eta\zeta$. The higher order global differentiability approximations are first generated in $\xi\eta\zeta$ space and then transformed into xyz space using Jacobian of transformation matrices. 3-D C^{000} hierarchical approximations are used as a starting point and the basis for the developments of C^{ijk} local approximations. New degrees of freedom are introduced at the corner nodes (inter-element nodes) which enforce the higher order inter element continuity. The degrees of freedom chosen in developing the framework consists of a complete set of derivatives of order $i(= j = k)$ in deriving C^{ijk} global differentiability approximations. The derivation presented is general and is independent of the nature of the C^{000} interpolation functions. The type of C^{000} approximation functions (for example, Lagrange, Legendre or Chebyshev functions) chosen would determine the nature of the interpolation functions for the resulting 3-D C^{ijk} HGDA element. The approximation functions being borrowed from the mid-side nodes and face nodes should be such that: (i) lowest degree admissible functions (corresponding to a lower p-level) should be selected first (ii) and a symmetric pattern maintained in selecting the approximation functions.

Chapter 4

Assessment of accuracy and convergence rates of higher order continuity 2-D elements with distorted geometries

4.1 Introduction

A finite element discretization consists of (1) finite subdomains (or finite elements) that are interconnected with each other at their boundaries and (2) interpolation of the quantities of interest over each element (local approximation). The precise approximation of the quantities of interest over entire domain is controlled by (a) the nature of subdivision (i.e. number and type of elements (uniform or graded mesh)) (b) nature of local approximation (linear, parabolic etc.), (c) inter-element behavior of the local approximations of the discretization and (d) the nature of the differential operator appearing in the governing equations.

Surana et al. [1-3] classified the boundary value problems based upon the strict mathematical nature of the differential operators into three categories: (1) those described by self-adjoint differential operators (2) those described by non self-adjoint differential operators and (3) those described by non-linear differential operators.

In chapters 2 and 3, a general framework is presented for deriving desired order global differentiability local approximations for 2-D and 3-D distorted element geometries. 2-D C^{00} or 3-D C^{000} p-version hierarchical approximations are used as a basis and appropriate degrees of freedom and corresponding approximation functions are borrowed to generate the higher order global differentiability approximations (HGDA) in two or three dimensions.

In this chapter we consider Galerkin method with weak form (GAL) and Least squares processes (LSP) for self-adjoint operators whereas only Least squares processes for non self-adjoint and non-linear operators [1–3] to present various numerical studies using standard model problems. The numerical studies are intended to assess performance of the developed HGDA elements of distorted geometries as well as those based on tensor product.

In all the numerical studies presented here, various of interest are computed for model problems defined by self-adjoint, non self-adjoint and non-linear differential operators [6–10]:

(1) **Least squares error or residual functional (*I*)** : If an approximation φ_h of φ in $\bar{\Omega}^T$ is substituted in boundary value problem $A\varphi - f = 0$, we get the residuals (or errors) E. Least squares error functional is constructed by taking the sum of squares of E over the whole domain $\bar{\Omega}^T$, i.e. I is an inner product of E with itself, defined as,

$$I(\varphi_h) = (E, E) = \int_{\Omega} E^T E d\Omega \tag{4.1}$$

(2) **Functional corresponding to Galerkin method with weak form (*I*)** : If the operator A is self-adjoint,using integration by parts in Galerkin method, we obtain weak form $B(\varphi, v) = l(v)$ of the boundary value problem (where $v = \delta\varphi$). In this case, we can construct functional I as follows,

$$I(\varphi_h) = \frac{1}{2} B(\varphi, \varphi) - l(\varphi) \tag{4.2}$$

(3) $\boldsymbol{L_2}$ **- norm of error in solution** : If φ and φ_h are square integrable functions defined over $\bar{\Omega}^T$, then L_2 - norm of error can be written as (Consider 1-D case) :

$$\| e \|_0 = \|\varphi - \varphi_h\|_0 = \left(\int_{\bar{\Omega}^T} |\varphi - \varphi_h|^2 \, d\Omega \right)^{\frac{1}{2}} \tag{4.3}$$

(4) $\boldsymbol{H_1}$ **- norm of error in solution** : If φ and φ_h are square integrable functions defined over $\bar{\Omega}^T$, then H_1 - norm of error can be written as

$$\| e \|_{H^1(\bar{\Omega}^T)} = \left(\int_{\bar{\Omega}^T} \left(|\varphi - \varphi_h|^2 \; + \; |\varphi' - \varphi'_h|^2 \right) d\Omega \right)^{\frac{1}{2}} \tag{4.4}$$

where ′ denotes all first order derivatives

(5) $\boldsymbol{H_2}$ **- norm of error in solution** : If φ and φ_h are square integrable functions defined over $\bar{\Omega}^T$, then H_2 - norm of error in the solution can be written as

$$\| e \|_{H^2(\bar{\Omega}^T)} = \left(\int_{\bar{\Omega}^T} \left(|\varphi - \varphi_h|^2 \; + \; |\varphi' - \varphi'_h|^2 \; + \; |\varphi'' - \varphi''_h|^2 \right) d\Omega \right)^{\frac{1}{2}} \tag{4.5}$$

where ′ and ″ denote all first and second order derivatives

All the computed quantities of interest ($\sqrt{I}$, L_2 - norm of error, H^1 - norm of error, H^2 - norm of error) are always plotted on a logarithmic scale against logarithmic values of the characteristic length of discretization (h_e) or logarithmic values of the degrees of freedom ($dofs$). The slopes of such plots enable us to determine the convergence rates of the corresponding quantities of interest.

Numerical studies

The numerical studies for all the model problems considered in this chapter can be broadly divided into the following groups:

(1) **Undistorted discretizations:** The domains of definition of the model problems are discretized with rectangular meshes. For these discretizations, tensor product elements have the best performance and hence can be considered as benchmark

results. When higher order global differentiability distorted elements are used, they are provided with all the benefits. The results obtained would indeed be their best performance hence, their comparison with tensor product elements will be meaningful.

(a) ***h*-convergence study:** For the rectangular domains, a study is performed with fixed p-level and varying characteristic length of discretization. The quantities of interest and their convergence rates are computed for both tensor product and HGDA elements (plotted against (i) discretization length (h_e) and (ii) total number of degrees of freedom).

(b) ***p*-convergence study:** For the same rectangular domains, another study is conducted with a fixed characteristic length of discretization and progressively increasing p levels. The quantities of interest and their convergence rates are computed for both tensor product and HGDA elements (plotted against the degrees of freedom).

(2) **Distorted discretizations:** The domains in (1) are now discretized with quadrilateral elements of irregular or distorted shapes. The higher order global differentiability distorted elements are used for these discretizations and the results are compared with the undistorted discretizations.

(a) ***h*-convergence study:** For these distorted discretizations, a study is performed with a fixed p-level and varying characteristic length of discretization. The quantities of interest and their convergence rates are computed for distorted discretizations and compared with the solutions obtained using rectangular meshes.

(b) ***p*-convergence study:** Another study is conducted with a fixed characteristic length of discretization and progressively increasing p levels. The quantities of interest and their convergence rates are computed for distorted discretizations and compared with the solutions obtained using rectangular meshes.

4.2 Model Problem # 1 : 2-D steady state Poisson's equation

The governing differential equation (GDE) for 2-D steady state Poisson's equation is given by:

$$\frac{\partial^2 u}{\partial x^2} + \frac{\partial^2 u}{\partial y^2} = -f(x,y) \quad \text{over } \Omega = (-a,a) \times (-b,b) \tag{4.6}$$

with boundary conditions

$$u(x,-b) \;=\; u(a,y) \;=\; u(x,b) \;=\; u(-a,y) \;=\; 0 \tag{4.7}$$

where $f(x,y)$ is such that the theoretical solution is given by

$$u(x,y) = (a^n \;-\; x^n)(b^m \;-\; y^m) \tag{4.8}$$

For computations, $a \;=\; b \;=\; 1$ and $m \;=\; n \;=\; 8$ are considered.

The differential operator describing the governing differential equation is self-adjoint and hence both Galerkin method with weak form and Least squares processes are variationally consistent [1–3]. When an approximation $u_h(x,y)$ of $u(x,y)$ is considered, the local approximations need to be at least of class $C^{2,2}(\bar{\Omega}^e)$ since the governing differential equation contains second order derivatives of dependent variable. However, if we permit weak convergence of second order derivatives of u_h, the requirement can be lowered to $C^{1,1}(\bar{\Omega}^e)$. Local approximations of class $C^{0,0}(\bar{\Omega}^e)$ are not admissible in case of least squares process using strong form of the GDE (i.e. Equation (4.6)). Figure 4.1(a) shows a schematic of the domain Ω used in the computations.

4.2.1 Undistorted discretizations

The domain of definition Ω ($(-1,1) \times (-1,1)$) is discretized uniformly with rectangular elements. The following uniform discretizations for h-convergence are considered:

(1) 4 element uniform discretization (2 x 2) : characteristic length : h_e = 1

(2) 16 element uniform discretization (4 x 4) : characteristic length : h_e = 0.5

(3) 64 element uniform discretization (8 x 8) : characteristic length : h_e = 0.25

(4) 256 element uniform discretization (16 x 16) : characteristic length : h_e = 0.125

(5) 1024 element uniform discretization (32 x 32) : characteristic length : h_e = 0.0625

The first and second uniform discretizations are shown in Figure 4.1(b) and (c).

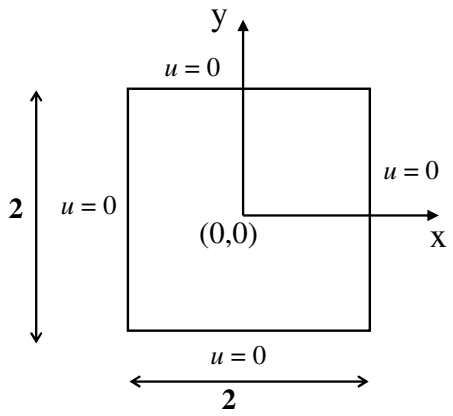

(a) Schematic of Ω

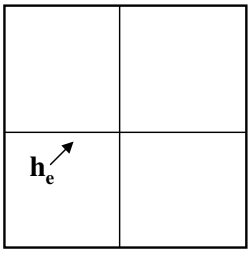

(b) 2 x 2 uniform discretization (h_e =1)

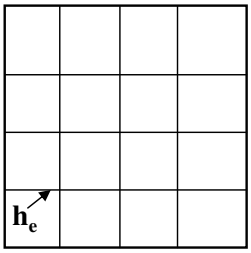

(c) 4 x 4 uniform discretization (h_e = 0.5)

Figure 4.1: Schematic, uniform discretizations for 2-D steady state Poisson's equation

4.2.2 Numerical studies for Undistorted discretizations : h-convergence

The numerical solutions are obtained using C^{11}, C^{22} and C^{33} HGDA elements employing the minimum p-level required by the corresponding HGDA elements. The minimum p-levels required for C^{11}, C^{22} and C^{33} HGDA elements are 3, 5 and 7 respectively. The numerical studies are obtained by progressively refining the discretization (adding more elements) thereby reducing the characteristic length of discretization. Since the differential operator is self-adjoint, solutions are computed using both Galerkin method with weak form and Least squares processes.

(i) Figures 4.2 (a)-(d) show the C^{11} (p=3) solutions computed for both tensor product and HGDA elements plotted against the characteristic length of discretization. Figures 4.3 (a)-(d) and 4.4 (a)-(d) show similar plots computed with C^{22} (p=5) and C^{33} (p=7) HGDA elements. The convergence rates of all the solutions in Figures 4.2-4.4 are listed in Table 4.1.

(ii) Figures 4.5 (a)-(d) show the C^{11} (p=3) solutions computed for both tensor product and HGDA elements plotted against the total number of degrees of freedom. Figures 4.6 (a)-(d) and 4.7 (a)-(d) show similar plots for C^{22} (p=5) and C^{33} (p=7) HGDA elements. The convergence rates of all the solutions in Figures 4.5-4.7 are listed in Table 4.2

(iii) Figures 4.8(a)-(d) and 4.9(a)-(d) show comparison of numerical solutions obtained using C^{22} and C^{33} HGDA elements for a p level of 7 plotted against characteristic length and degrees of freedom respectively. The convergence rates of all the solutions in Figures 4.8-4.9 are listed in Table 4.3.

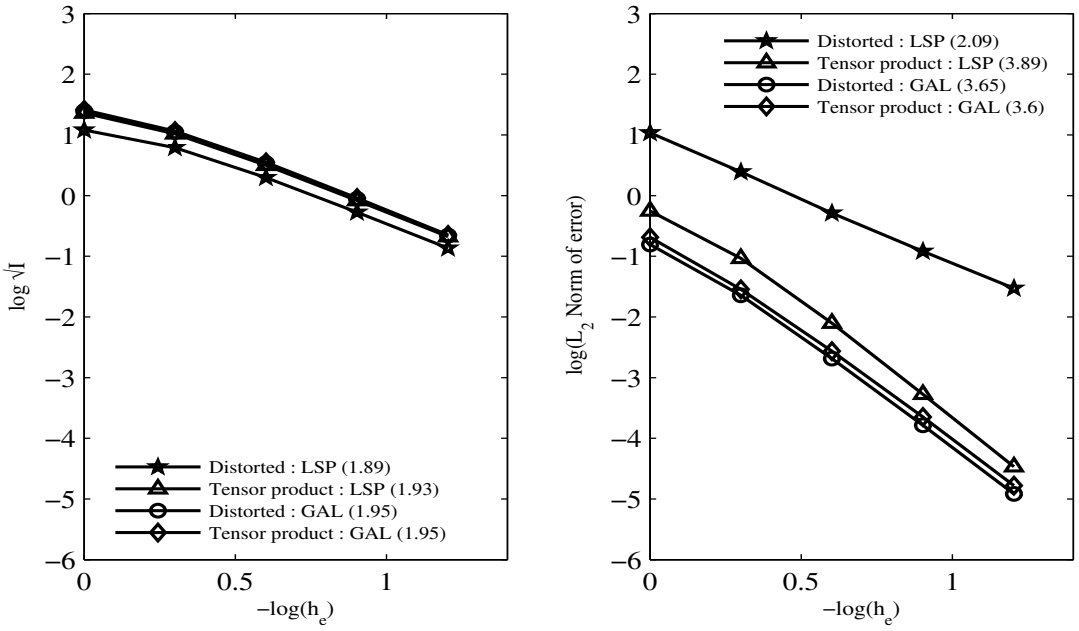

(a) $\sqrt{I}$ versus h_e

(b) L_2 norm of error in u versus h_e

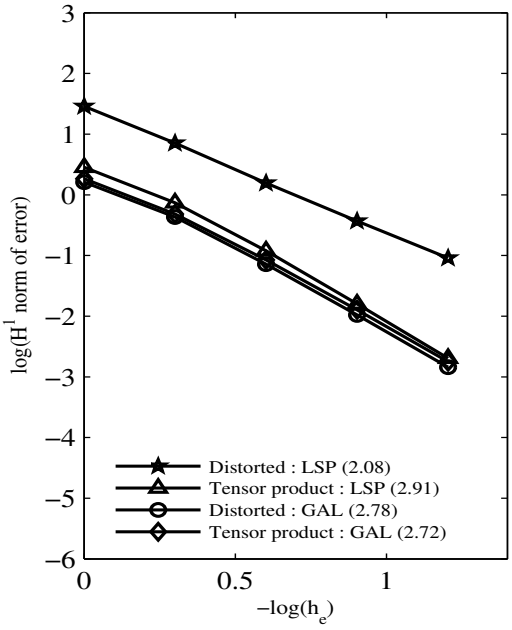

(c) H^1 norm of error in u versus h_e

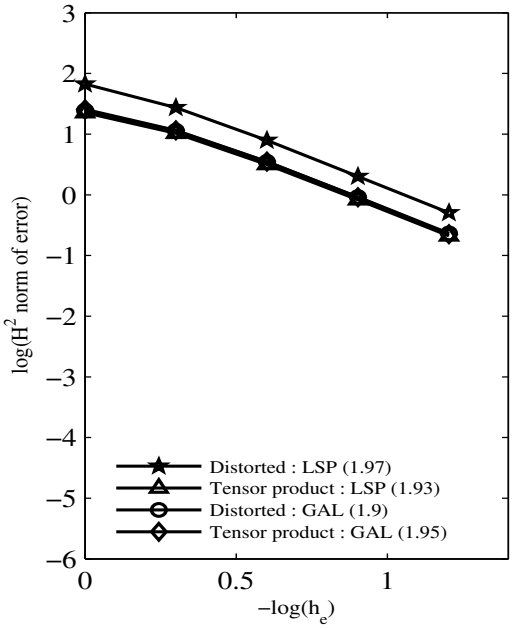

(d) H^2 norm of error in u versus h_e

Figure 4.2: Comparison of Distorted HGDA and Tensor product elements versus discretization length for 2-D Poisson's equation : C^{11}, $p_\xi = p_\eta = 3$, **Undistorted discretizations**

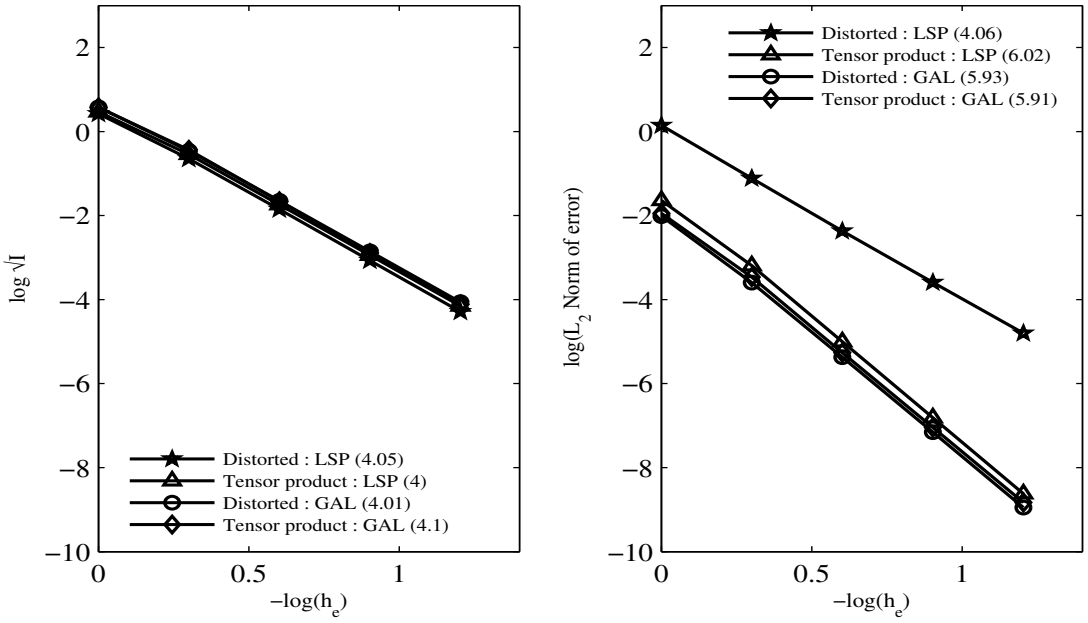

(a) $\sqrt{I}$ versus h_e

(b) L_2 norm of error in u versus h_e

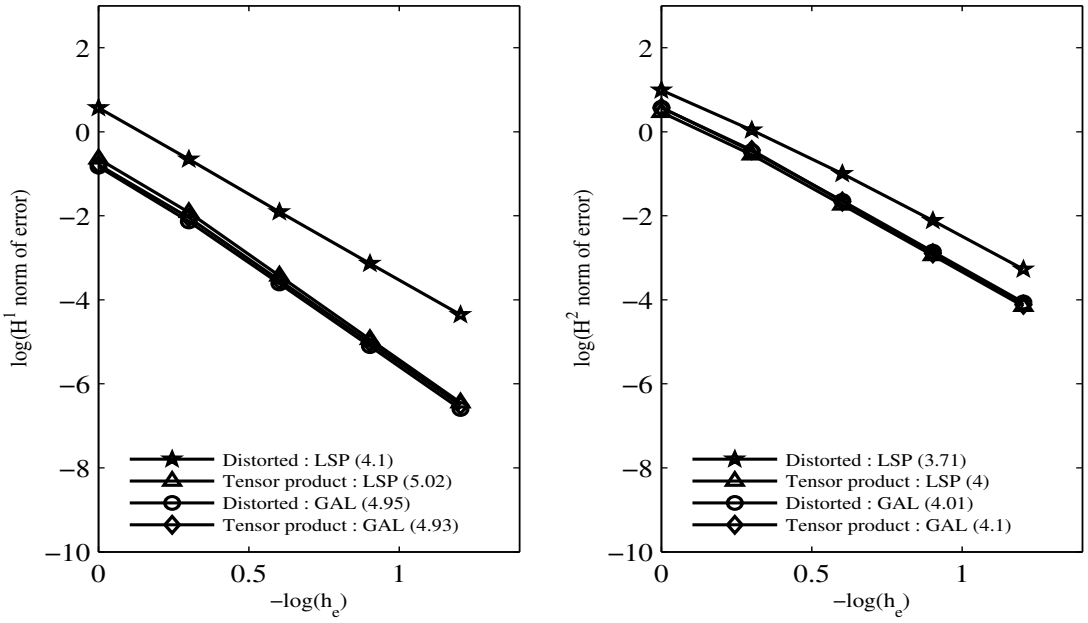

(c) H^1 norm of error in u versus h_e

(d) H^2 norm of error in u versus h_e

Figure 4.3: Comparison of Distorted HGDA and Tensor product elements versus discretization length for 2-D Poisson's equation : C^{22}, $p_\xi = p_\eta = 5$, **Undistorted discretizations**

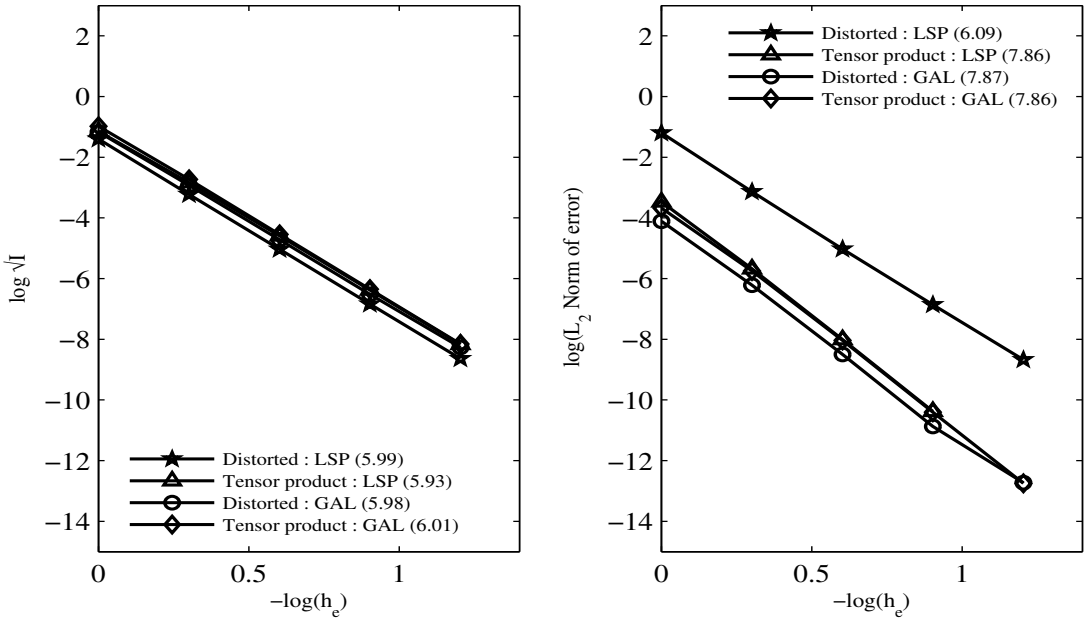

(a) $\sqrt{I}$ versus h_e

(b) L_2 norm of error in u versus h_e

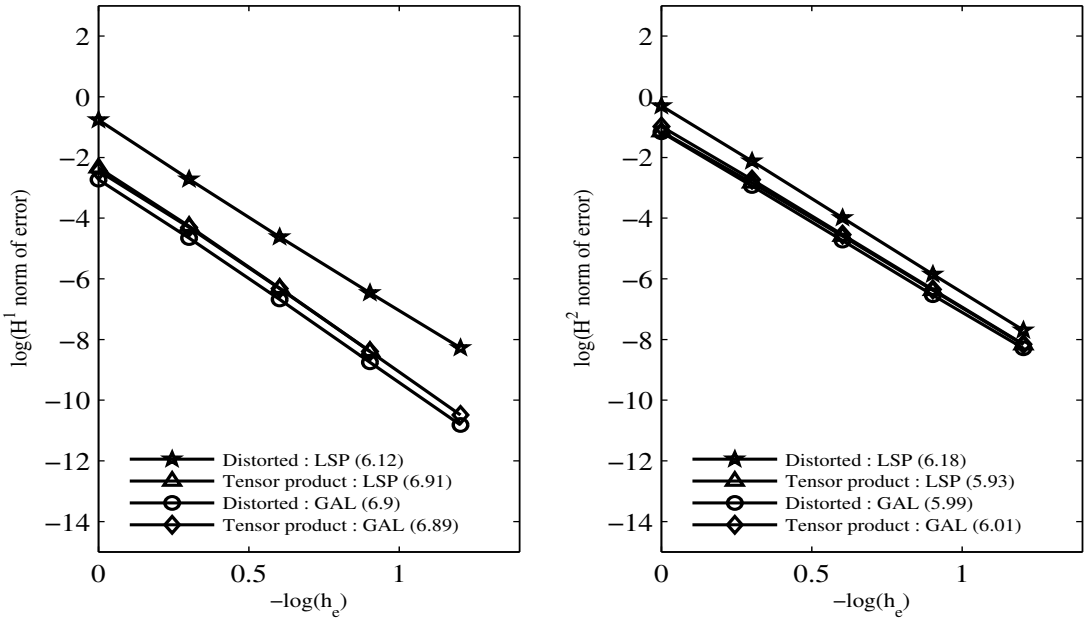

(c) H^1 norm of error in u versus h_e

(d) H^2 norm of error in u versus h_e

Figure 4.4: Comparison of Distorted HGDA and Tensor product elements versus discretization length for 2-D Poisson's equation : C^{33}, $p_\xi = p_\eta = 7$, **Undistorted discretizations**

Table 4.1: Convergence rates for 2-D Poisson's equation : h-convergence, Undistorted discretizations using Distorted HGDA and Tensor product elements

(a) $\sqrt{I}$ versus h_e

C^{ij}	LSP		GAL	
	Distorted	Tensor Product	Distorted	Tensor Product
C^{11} ; p=3	1.89	1.93	1.95	1.95
C^{22} : p=5	4.05	4	4.01	4.1
C^{33} : p=7	5.99	5.93	5.98	6.01

(b) L_2 - norm of error versus h_e

C^{ij}	LSP		GAL	
	Distorted	Tensor Product	Distorted	Tensor Product
C^{11} ; p=3	2.09	3.89	3.65	3.6
C^{22} : p=5	4.06	6.02	5.93	5.91
C^{33} : p=7	6.09	7.86	7.87	7.86

(c) H^1 - norm of error versus h_e

C^{ij}	LSP		GAL	
	Distorted	Tensor Product	Distorted	Tensor Product
C^{11} ; p=3	2.08	2.91	2.78	2.72
C^{22} : p=5	4.1	5.02	4.95	4.93
C^{33} : p=7	6.12	6.91	6.9	6.89

(d) H^2 - norm of error versus h_e

C^{ij}	LSP		GAL	
	Distorted	Tensor Product	Distorted	Tensor Product
C^{11} ; p=3	1.97	1.93	1.9	1.95
C^{22} : p=5	3.71	4	4.01	4.1
C^{33} : p=7	6.18	5.93	5.99	6.01

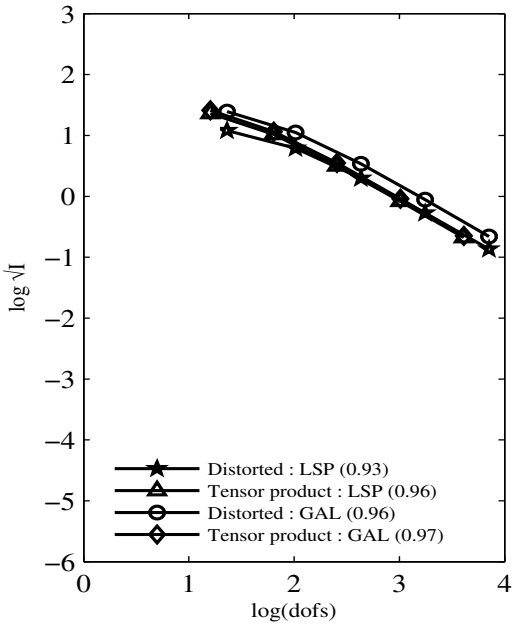

(a) √I versus dofs

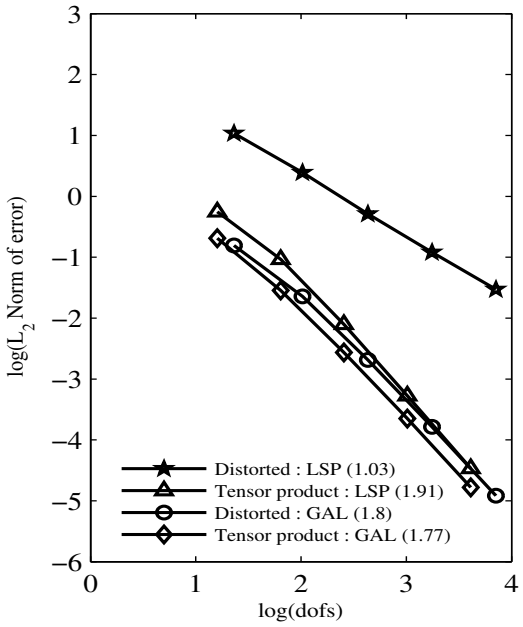

(b) L_2 norm of error in u versus dofs

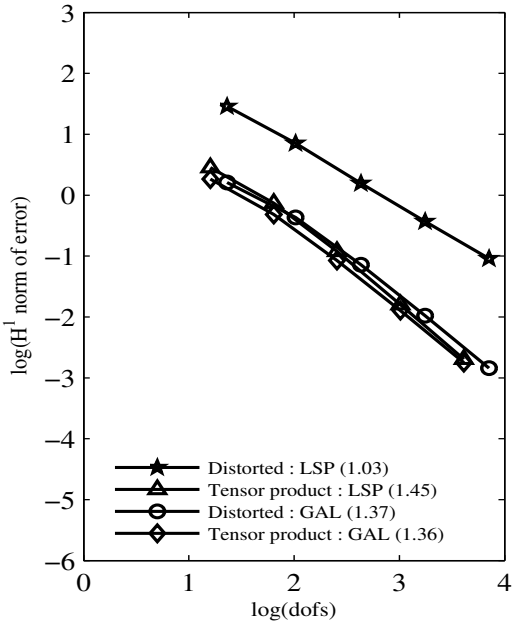

(c) H^1 norm of error in u versus dofs

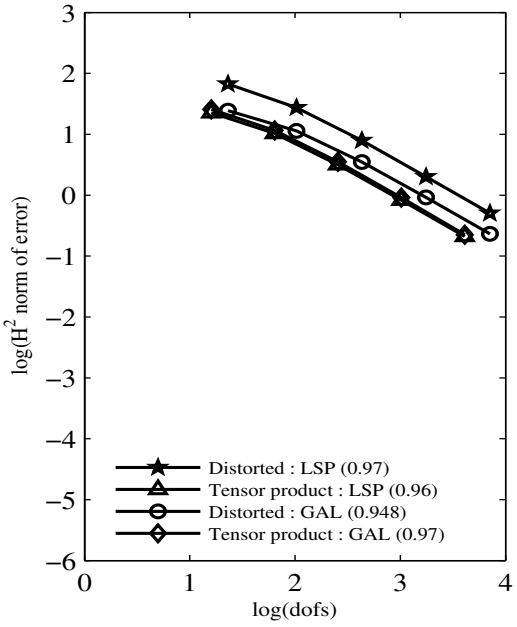

(d) H^2 norm of error in u versus dofs

Figure 4.5: Comparison of Distorted HGDA and Tensor product elements versus degrees of freedom for 2-D Poisson's equation : C^{11}, $p_\xi = p_\eta = 3$, **Undistorted discretizations**

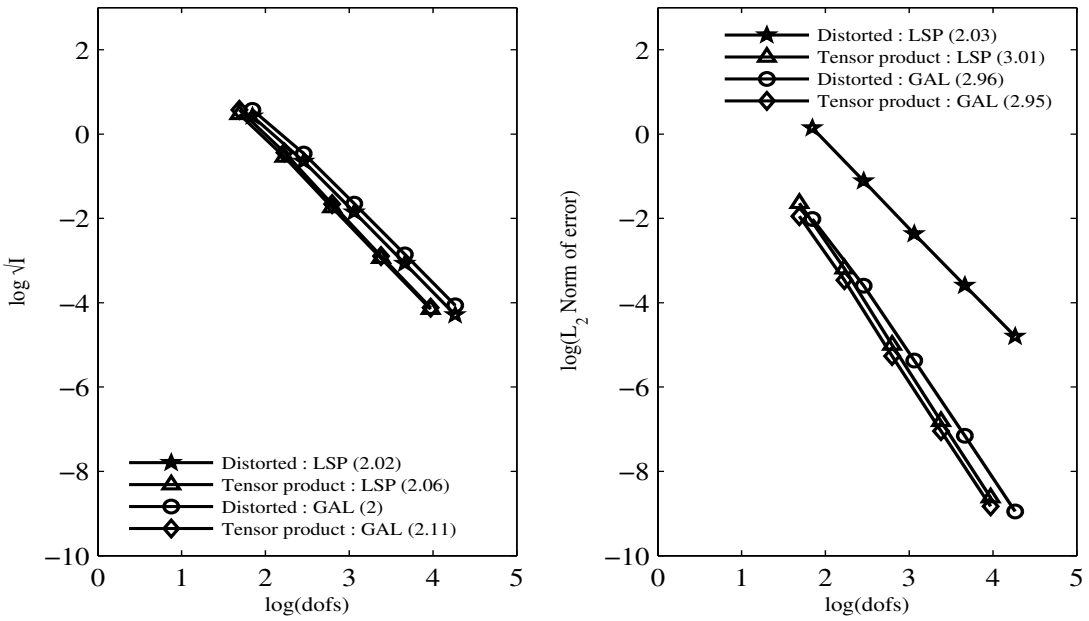

(a) √I versus dofs

(b) L_2 norm of error in u versus dofs

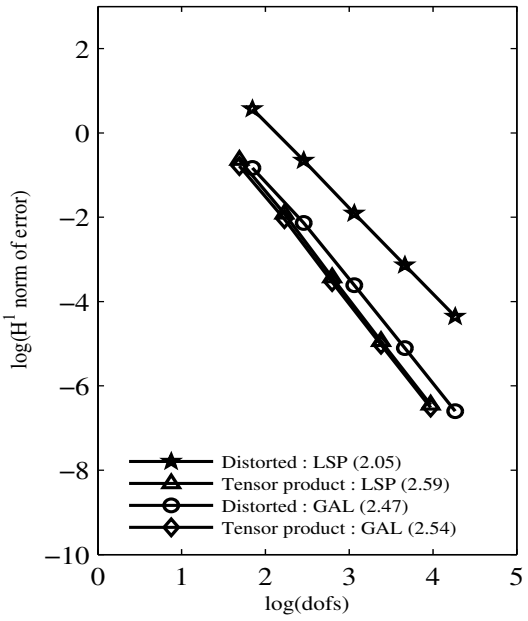

(c) H^1 norm of error in u versus dofs

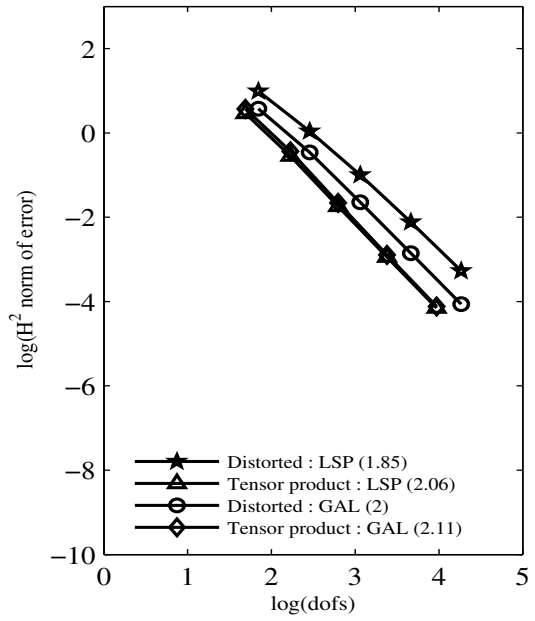

(d) H^2 norm of error in u versus dofs

Figure 4.6: Comparison of Distorted HGDA and Tensor product elements versus degrees of freedom for 2-D Poisson's equation : C^{22}, $p_\xi = p_\eta = 5$, **Undistorted discretizations**

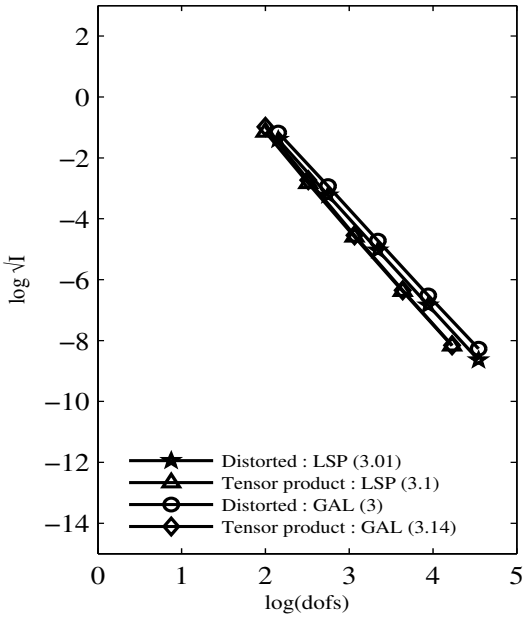

(a) √I versus dofs

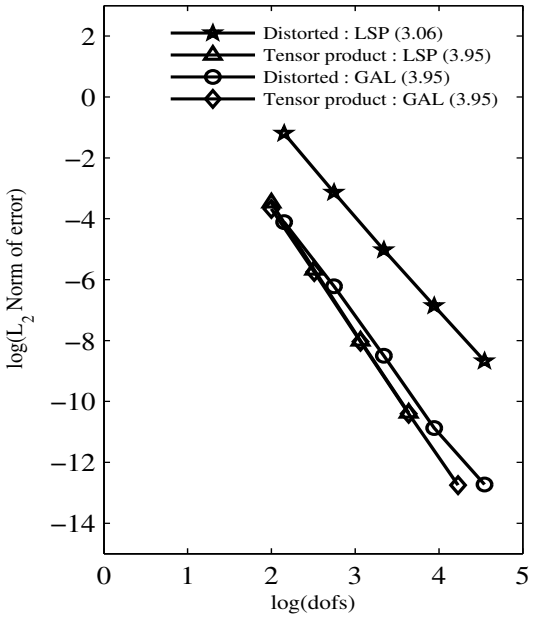

(b) L_2 norm of error in u versus dofs

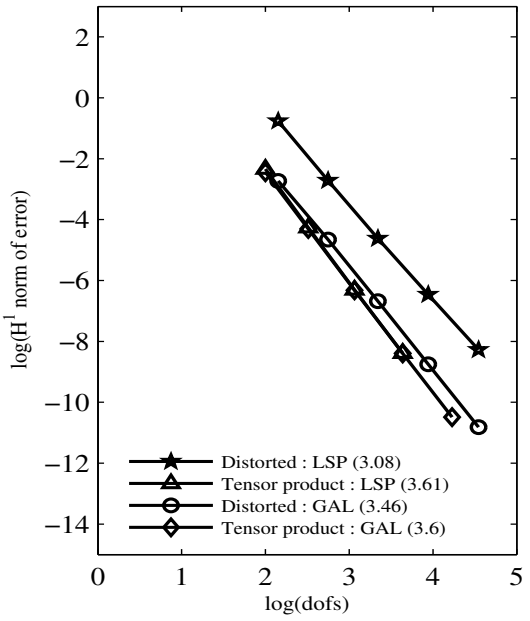

(c) H^1 norm of error in u versus dofs

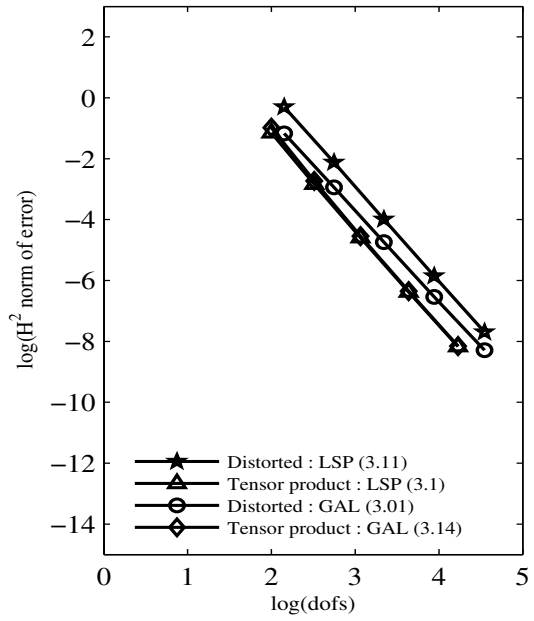

(d) H^2 norm of error in u versus dofs

Figure 4.7: Comparison of Distorted HGDA and Tensor product elements versus degrees of freedom for 2-D Poisson's equation : C^{33}, $p_\xi = p_\eta = 7$, **Undistorted discretizations**

Table 4.2: Convergence rates for 2-D Poisson's equation : h-convergence, Undistorted discretizations using Distorted HGDA and Tensor product elements

(a) $\sqrt{I}$ versus dofs

C^{ij}	LSP		GAL	
	Distorted	Tensor Product	Distorted	Tensor Product
C^{11} ; p=3	0.93	0.96	0.96	0.97
C^{22} : p=5	2.0	2.06	2	2.11
C^{33} : p=7	3.01	3.1	3	3.14

(b) L_2 - norm of error versus dofs

C^{ij}	LSP		GAL	
	Distorted	Tensor Product	Distorted	Tensor Product
C^{11} ; p=3	1.03	1.91	1.8	1.77
C^{22} : p=5	2.03	3.01	2.96	2.95
C^{33} : p=7	3.06	3.95	3.95	3.95

(c) H^1 - norm of error versus dofs

C^{ij}	LSP		GAL	
	Distorted	Tensor Product	Distorted	Tensor Product
C^{11} ; p=3	1.03	1.45	1.37	1.36
C^{22} : p=5	2.05	2.59	2.47	2.54
C^{33} : p=7	3.08	3.61	3.46	3.6

(d) H^2 - norm of error versus dofs

C^{ij}	LSP		GAL	
	Distorted	Tensor Product	Distorted	Tensor Product
C^{11} ; p=3	0.97	0.96	0.95	0.97
C^{22} : p=5	1.85	2.06	2	2.11
C^{33} : p=7	3.11	3.1	3.01	3.14

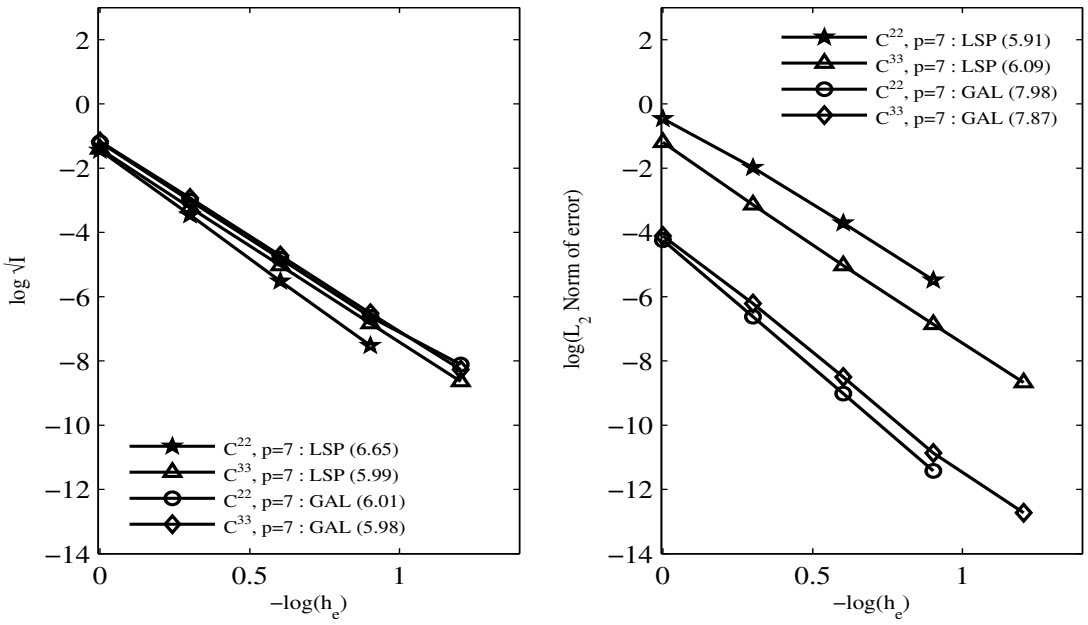

(a) $\sqrt{I}$ versus h_e

(b) L_2 norm of error in u versus h_e

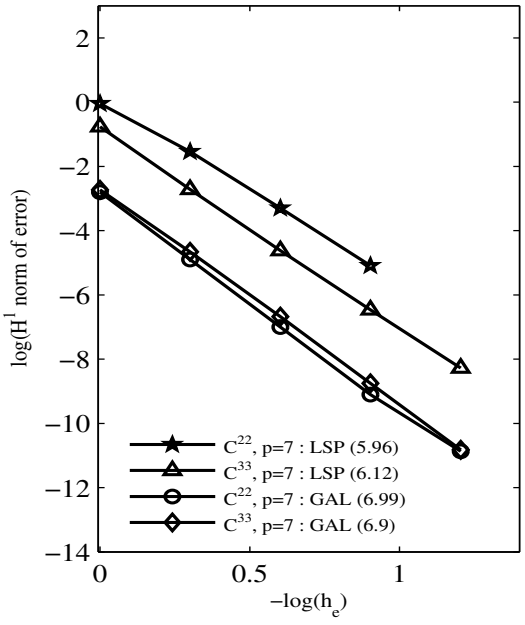

(c) H^1 norm of error in u versus h_e

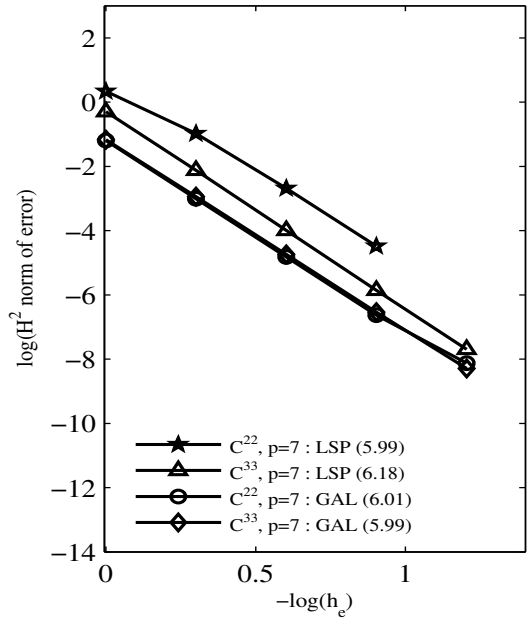

(d) H^2 norm of error in u versus h_e

Figure 4.8: Comparison of C^{ij} Distorted HGDA elements versus discretization length for 2-D Poisson's equation : $\boldsymbol{C^{22}}$ ($\boldsymbol{k}$ = 3), $\boldsymbol{C^{33}}$ ($\boldsymbol{k}$ = 4), $\boldsymbol{p_\xi = p_\eta = 7}$, **Undistorted discretizations**

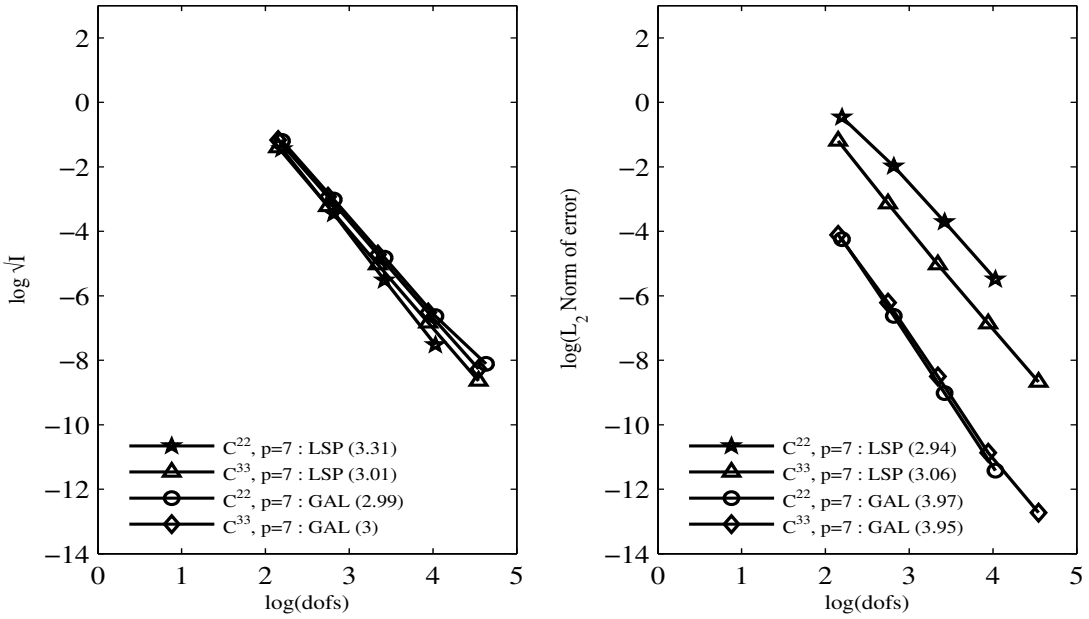

(a) √I versus dofs

(b) L_2 norm of error in u versus dofs

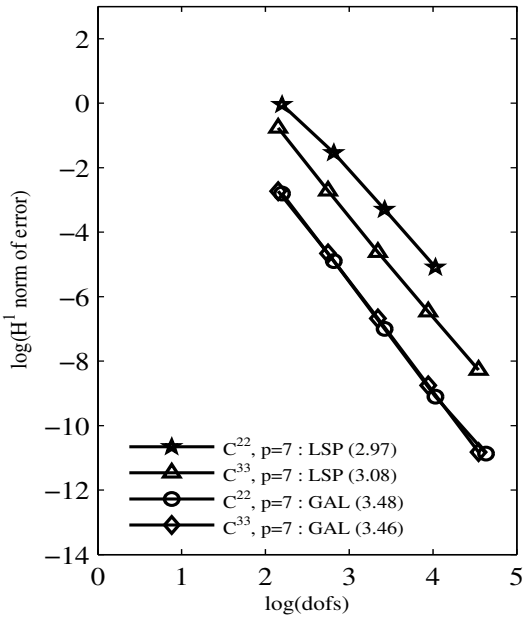

(c) H^1 norm of error in u versus dofs

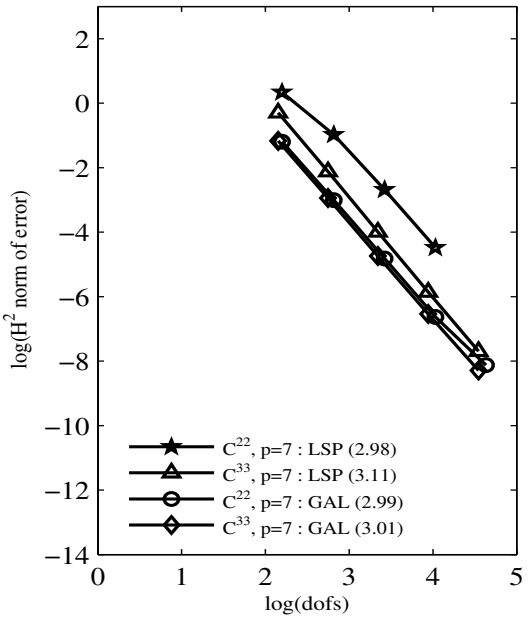

(d) H^2 norm of error in u versus dofs

Figure 4.9: Comparison of C^{ij} Distorted HGDA elements versus degrees of freedom for 2-D Poisson's equation : $\boldsymbol{C^{22}}$ ($\boldsymbol{k}$ = 3), $\boldsymbol{C^{33}}$ ($\boldsymbol{k}$ = 4), $\boldsymbol{p_\xi = p_\eta = 7}$, **Undistorted discretizations**

Table 4.3: Convergence rates for 2-D Poisson's equation : k-convergence, Undistorted discretizations using C^{22} (k = 3) and C^{33} (k = 4) Distorted HGDA elements

(a) √I

C^{ij}	**√I versus he**		**√I versus dofs**	
	LSP	GAL	LSP	GAL
C^{22} : p=7	6.65	6.01	3.31	2.99
C^{33} : p=7	5.99	5.98	3.01	3

(b) L_2 - norm of error

C^{ij}	**L_2 - norm vs he**		**L_2 - norm vs dofs**	
	LSP	GAL	LSP	GAL
C^{22} : p=7	5.91	7.98	2.94	3.97
C^{33} : p=7	6.09	7.87	3.06	3.95

(c) H^1 - norm of error

C^{ij}	**H^1 - norm vs he**		**H^1 - norm vs dofs**	
	LSP	GAL	LSP	GAL
C^{22} : p=7	5.96	6.99	2.97	3.48
C^{33} : p=7	6.12	6.9	3.08	3.46

(d) H^2 - norm of error

C^{ij}	**H^2 - norm vs he**		**H^2 - norm vs dofs**	
	LSP	GAL	LSP	GAL
C^{22} : p=7	5.99	6.01	2.98	2.99
C^{33} : p=7	6.18	5.99	3.11	3.01

Discussion of results

(1) From Figures 4.2-4.9, the error or residual functional values for Galerkin method with weak form and Least squares processes for both distorted and HGDA elements are approximately same (for a given h_e or $dofs$). However, for a given characteristic length of discretization or given number of degrees of freedom, Galerkin method with weak form (using HGDA elements) has lower values of errors in L_2, H_1 and H_2 - norms) compared to Least squares processes (using HGDA elements). This is also true when comparing Galerkin method with weak form and Least squares processes using tensor product elements.

(2) From Table 4.1, the convergence rates depend on the p-level used in the computations. The convergence rates for the computed norms using tensor product approximations (for both Galerkin method with weak form and Least squares processes) are in the vicinity of $(p-1)$ for residual or error functional and error in the H_2-norm (i.e. $\approx$ 2 for C^{11} (p=3), $\approx$ 4 for C^{22} (p=5) and $\approx$ 6 for C^{33} (p=7)). However, the convergence rates for L_2 - norm of error in solution is close to $(p+1)$ (i.e. $\approx$ 4 for C^{11} (p=3), $\approx$ 6 for C^{22} (p=5) and $\approx$ 8 for C^{33} (p=7)). The convergence rates for error in H_2-norm is p (i.e. $\approx$ 3 for C^{11} (p=3), $\approx$ 5 for C^{22} (p=5) and $\approx$ 7 for C^{33} (p=7)). For Galerkin method with weak form the convergence rates for computed quantities are close to the values observed in case of tensor product elements. However, with HGDA elements using Least squares processes the convergence rate for all the computed quantities is approximately $(p-1)$ (i.e. $\approx$ 2 for C^{11} (p=3), C^{22} (p=5) and C^{33} (p=7)).

(3) From Table 4.2, the convergence rates of the computed quantities do not have an explicit relation to the p-level used in the computations as observed in (2). The convergence rates seem to be dependent on both the p-level and order of approximation k.

(4) From Figures 4.8-4.9, the error or residual functional values from all four formulations (Galerkin method with weak form and Least squares processes with C^{22} and C^{33} HGDA elements) are approximately the same. From Table 4.3, in

case of Galerkin method with weak form, the convergence rates and the values of all quantities of interest computed using both C^{22} and C^{33} HGDA elements are almost same. In Least squares formulation, the convergence rates as shown in Table 4.3 for C^{22} and C^{33} HGDA elements are approximately the same. From Figures 4.5-4.7, we observe that for a given value of characteristic length or given number of degrees of freedom, C^{33} HGDA element gives a lower value of the quantity of interest compared to C^{22} HGDA element, thus illustrating the benefit of higher order global differentiability.

4.2.3 Numerical studies for Undistorted mesh : p-convergence

The numerical solutions are obtained using C^{22} and C^{33} HGDA elements with progressively increasing p-levels beginning with the minimum p-level required by the corresponding HGDA element. The minimum p-levels required for C^{22} and C^{33} HGDA elements are 5 and 7 respectively. The values in parenthesis indicate the convergence rate corresponding to the computed quantity for each HGDA element. The numerical studies are conducted using both Galerkin method with weak form and Least squares processes.

(i) Figures 4.10(a)-(d) show the numerical solutions computed for two different undistorted discretizations (4 and 16 elements) with C^{22} HGDA element. Figures 4.11(a)-(d) show similar plots for C^{33} HGDA element. In both cases, we observe for a given accuracy, coarser discretization is beneficial.

(ii) Figures 4.12(a)-(d) show the numerical solutions computed for HGDA elements and tensor product elements for a 4 element undistorted discretization with C^{22} HGDA element. Figures 4.13(a)-(d) show similar plots for C^{33} HGDA element. From Figures 4.12 and 4.13, the tensor product element has lower values of computed quantities of interest for a given number of degrees of freedom hence meritorious.

(iii) Figures 4.14(a)-(d) show comparison of numerical solutions calculated using C^{22} and C^{33} HGDA elements for a 4 element undistorted discretization. For a given

formulation (Galerkin method with weak form or Least squares processes), the computed quantities of interest for C^{33} HGDA element have a lower value compared to those corresponding to C^{22} HGDA (for a given number of degrees of freedom), thus illustrating the benefit of higher order global differentiability.

Remarks

(1) From Figures 4.10 - 4.13, for a given number of degrees of freedom, HGDA element using Least squares processes has a lower value of error or residual functional compared to the value obtained using Galerkin method with weak form. For all other error norms, Galerkin method with weak form has lower error norms in computed quantities of interest compared to Least squares process.

(2) When the domain of definition is rectangular, tensor product elements are expected to have the best performance. This is evident from the plots of all quantities of interest for any order of approximations.

(3) The convergence rates of the computed quantities of interest in Figures 4.11, 4.13 and 4.14 are very high due to the numerical solution at p-level of 8 being in the close vicinity of the theoretical solution.

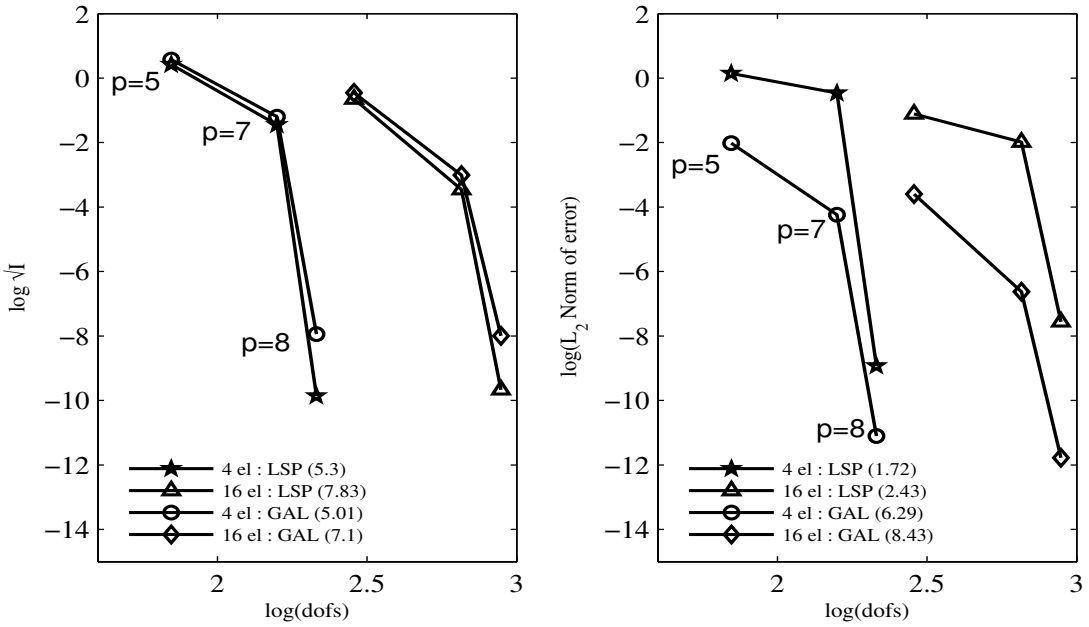

(a) √I versus dofs

(b) L_2 norm of error in u versus dofs

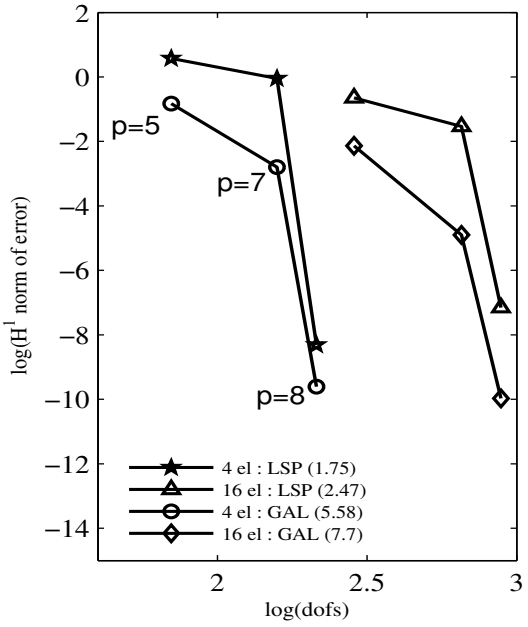

(c) H^1 norm of error in u versus dofs

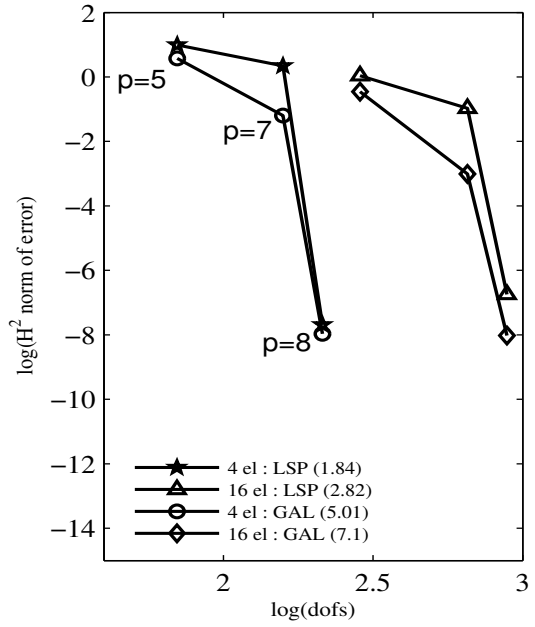

(d) H^2 norm of error in u versus dofs

Figure 4.10: Comparison of 4 element and 16 element discretizations using Distorted HGDA elements for 2-D Poisson's equation : C^{22}, **Undistorted discretizations**

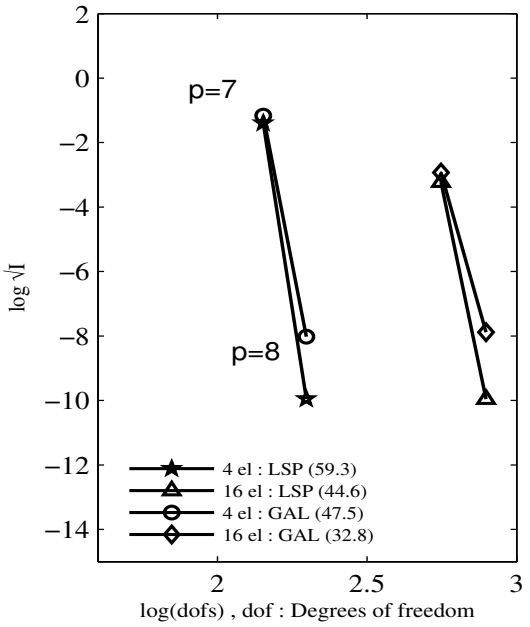

(a) √I versus dofs

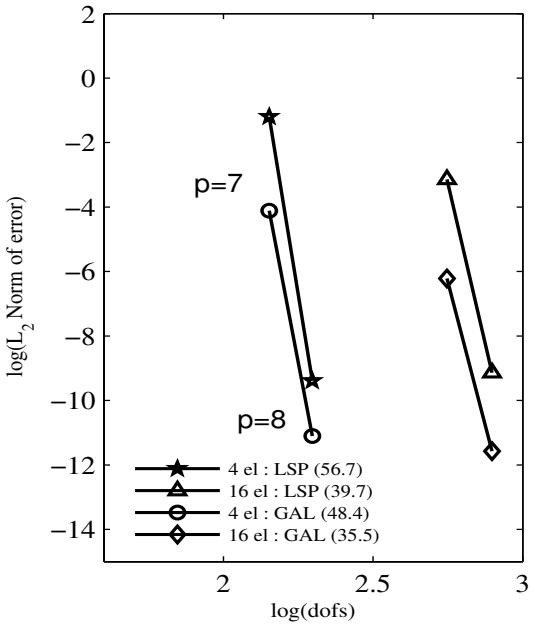

(b) L_2 norm of error in u versus dofs

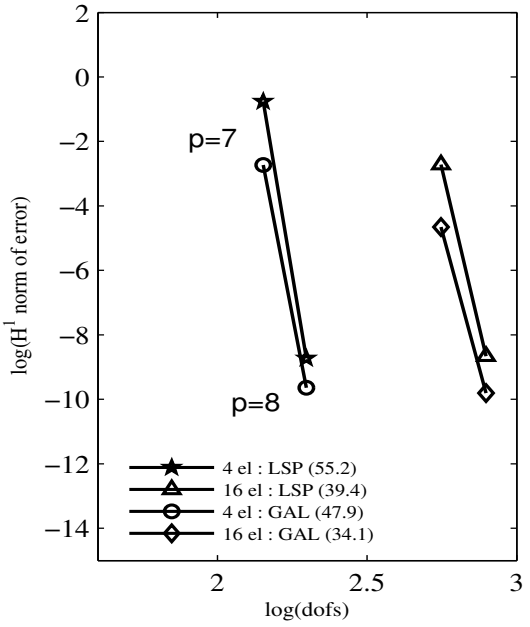

(c) H^1 norm of error in u versus dofs

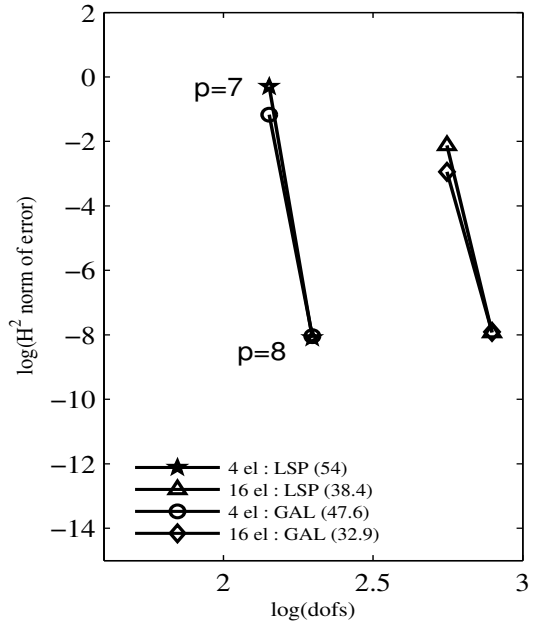

(d) H^2 norm of error in u versus dofs

Figure 4.11: Comparison of 4 element and 16 element discretizations using Distorted HGDA elements for 2-D Poisson's equation : C^{33}, **Undistorted discretizations**

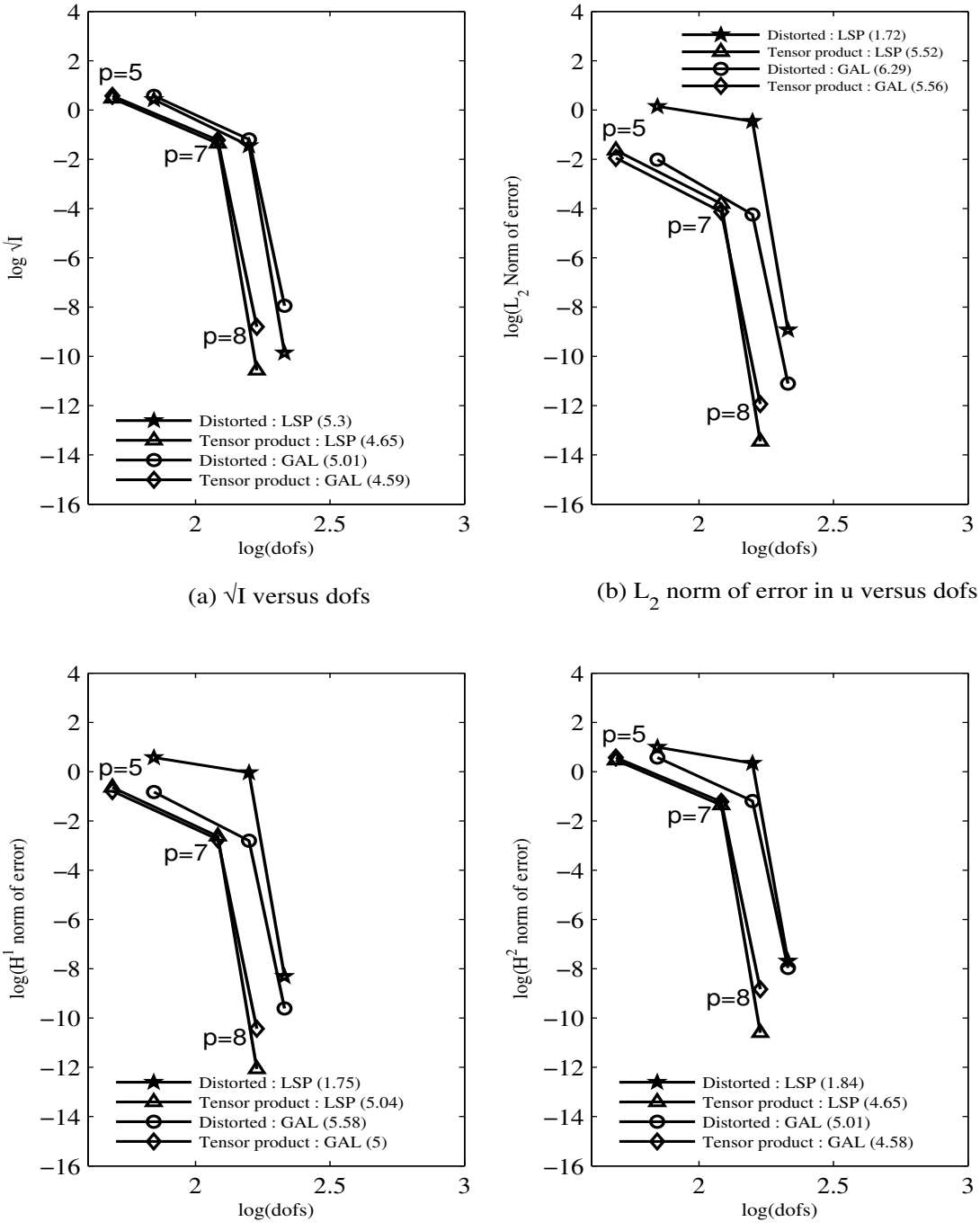

(a) √I versus dofs

(b) L_2 norm of error in u versus dofs

(c) H^1 norm of error in u versus dofs

(d) H^2 norm of error in u versus dofs

Figure 4.12: Comparison of Distorted HGDA and Tensor product elements for 2-D Poisson's equation : C^{22}, **4 element Undistorted discretization**

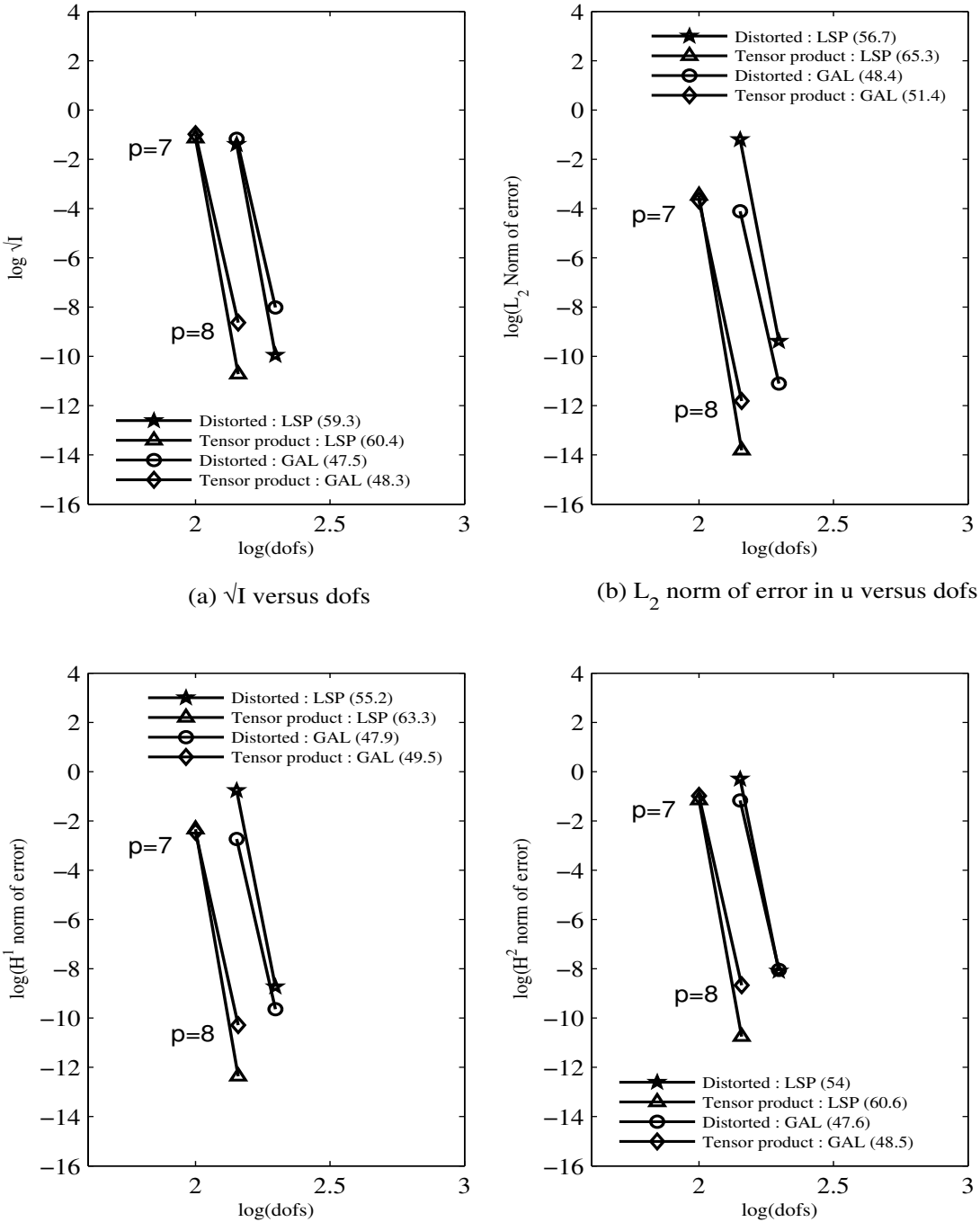

(a) √I versus dofs

(b) L_2 norm of error in u versus dofs

(c) H^1 norm of error in u versus dofs

(d) H^2 norm of error in u versus dofs

Figure 4.13: Comparison of Distorted HGDA and Tensor product elements for 2-D Poisson's equation : C^{33}, **4 element Undistorted discretization**

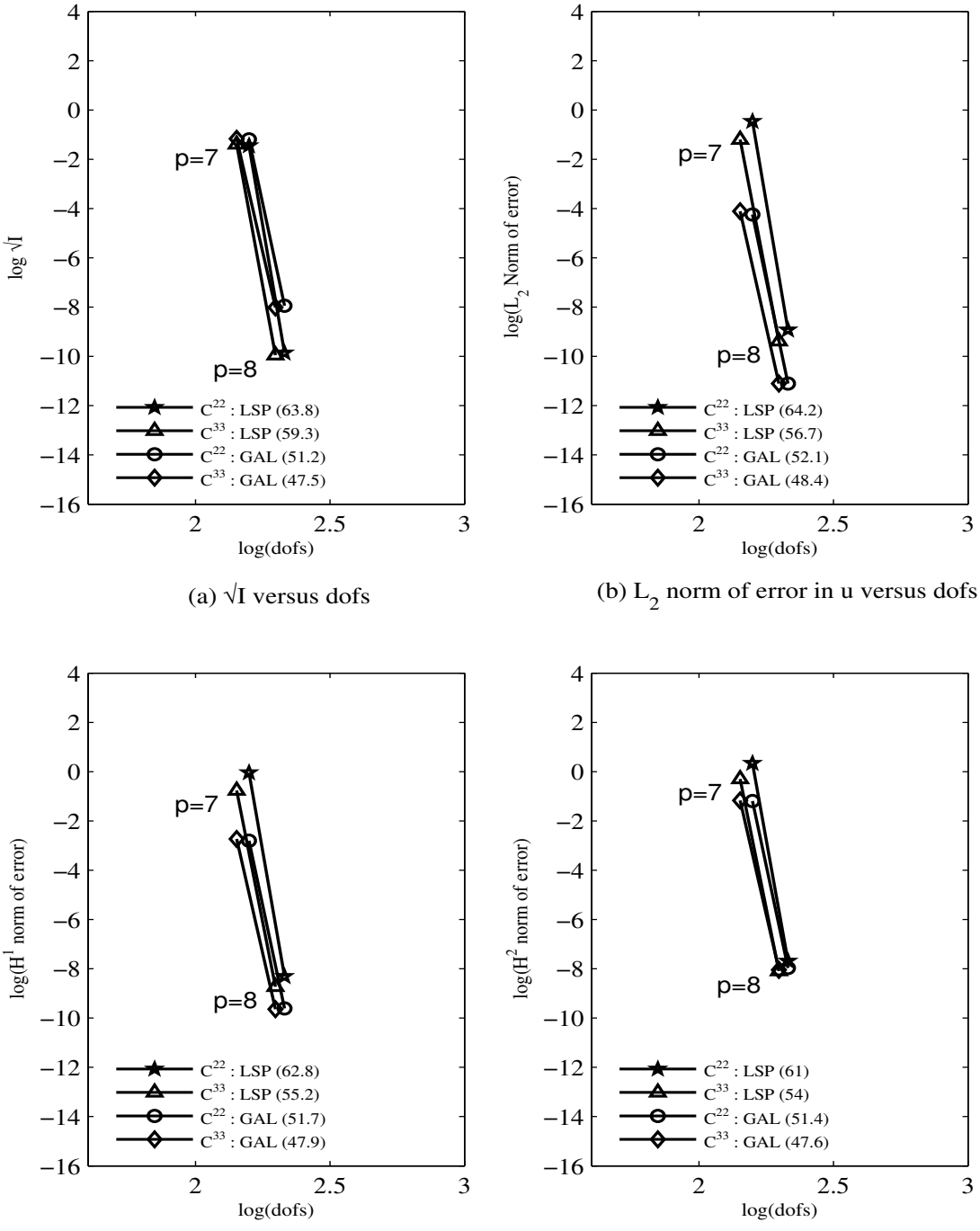

(a) √I versus dofs

(b) L_2 norm of error in u versus dofs

(c) H^1 norm of error in u versus dofs

(d) H^2 norm of error in u versus dofs

Figure 4.14: Comparison of C^{ij} Distorted HGDA elements for 2-D Poisson's equation : $\boldsymbol{C^{22}}$ ($\boldsymbol{k}$ = 3), $\boldsymbol{C^{33}}$ ($\boldsymbol{k}$ = 4), **4 element Undistorted discretization**

4.2.4 Distorted discretizations

In this numerical study, the domain of definition is discretized using elements of non-rectangular shapes. The longest side among all the elements in the entire discretization is chosen as the characteristic length for such a discretization. We consider the following distorted discretizations for h-convergence:

(1) 4 element distorted discretization (2 x 2) : characteristic length : h_e = 1.5

(2) 16 element distorted discretization (4 x 4) : characteristic length : h_e = 0.75

(3) 64 element distorted discretization (8 x 8) : characteristic length : h_e = 0.375

(4) 256 element distorted discretization (16 x 16) : characteristic length : h_e = 0.1875

(5) 1024 element distorted discretization (32 x 32) : characteristic length : h_e = 0.09375

The first and second distorted discretizations are shown in Figure 4.15(a) and (b).

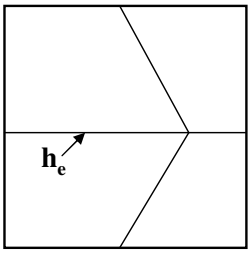

(a) 2 x 2 distorted discretization (h_e =1.5)

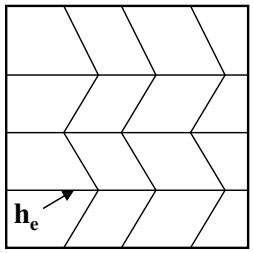

(b) 4 x 4 distorted discretization (h_e = 0.75)

Figure 4.15: Schematic, distorted discretizations for 2-D steady state Poisson's equation

4.2.5 Numerical studies for Distorted mesh : h-convergence

For these studies, tensor product elements are not applicable since the elements are not rectangular. However, since the domain of definition is still rectangular, we can compare the numerical solutions computed with HGDA elements with those using tensor product but rectangular discretizations. The p-level is kept fixed and the characteristic length is progressively reduced. Since the differential operator is self-adjoint, solutions using both Galerkin method with weak form and Least squares processes are computed.

(i) Figures 4.16(a)-(d) show the C^{11} (p=3) HGDA solutions computed for distorted discretizations and compared with the results obtained with undistorted discretizations. The solutions are plotted versus the characteristic length of discretization. Figures 4.17 (a)-(d) and 4.18 (a)-(d) show similar plots for C^{22} (p=5) and C^{33} (p=7) elements. The convergence rates of all the solutions plotted in Figures 4.16-4.18 are listed in Table 4.4.

(ii) Figures 4.19 - 4.21 show numerical solutions obtained in (i) as a function of the total number of degrees of freedom and Table 4.5 lists the convergence rates of all the solutions.

(iii) Figures 4.22(a)-(d) and 4.23(a)-(d) show comparison of solutions computed using C^{22} and C^{33} elements (for a p level of 7) plotted against characteristic length and degrees of freedom respectively. The convergence rates of all the solutions plotted in Figures 4.22-4.23 are listed in Table 4.6.

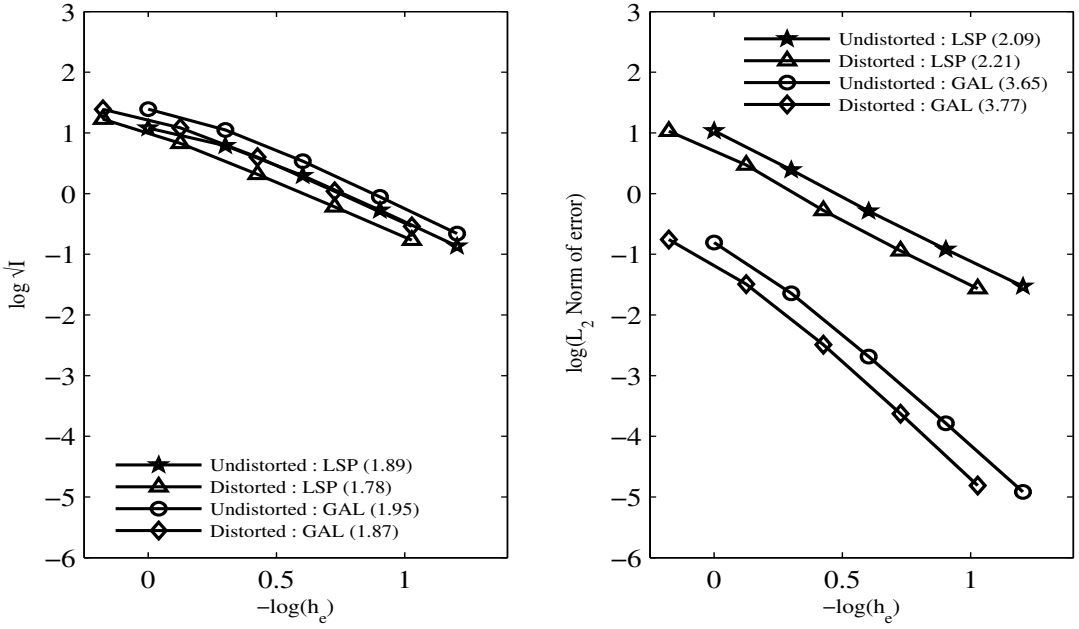

(a) √I versus h_e

(b) L_2 norm of error in u versus h_e

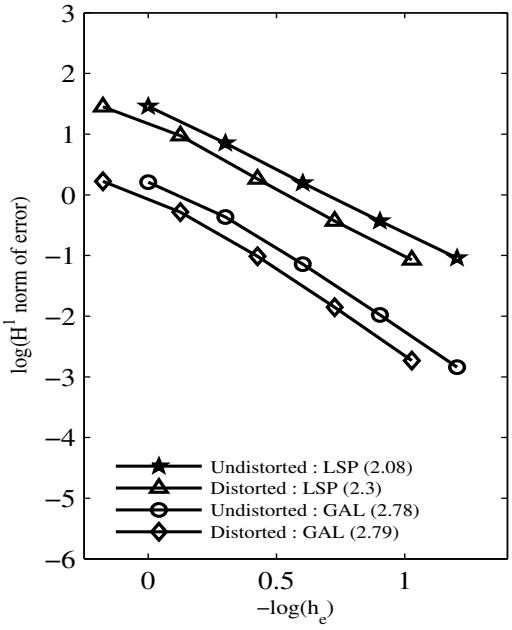

(c) H^1 norm of error in u versus h_e

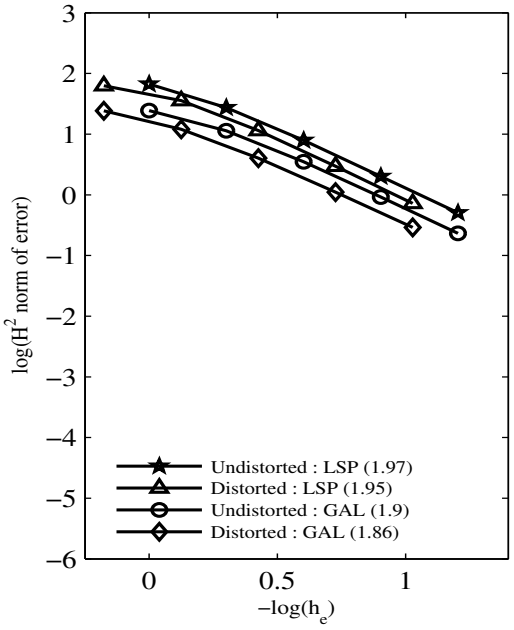

(d) H^2 norm of error in u versus h_e

Figure 4.16: Comparison of Undistorted and Distorted discretizations versus discretization length for 2-D Poisson's equation : C^{11} HGDA element, $p_\xi = p_\eta = 3$

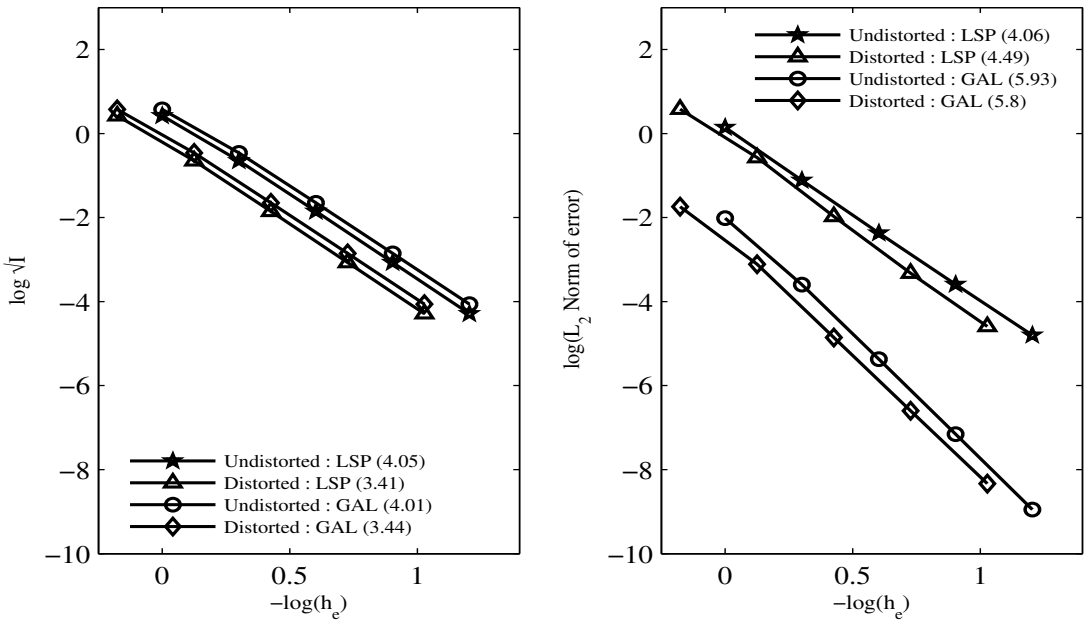

(a) √I versus h_e

(b) L_2 norm of error in u versus h_e

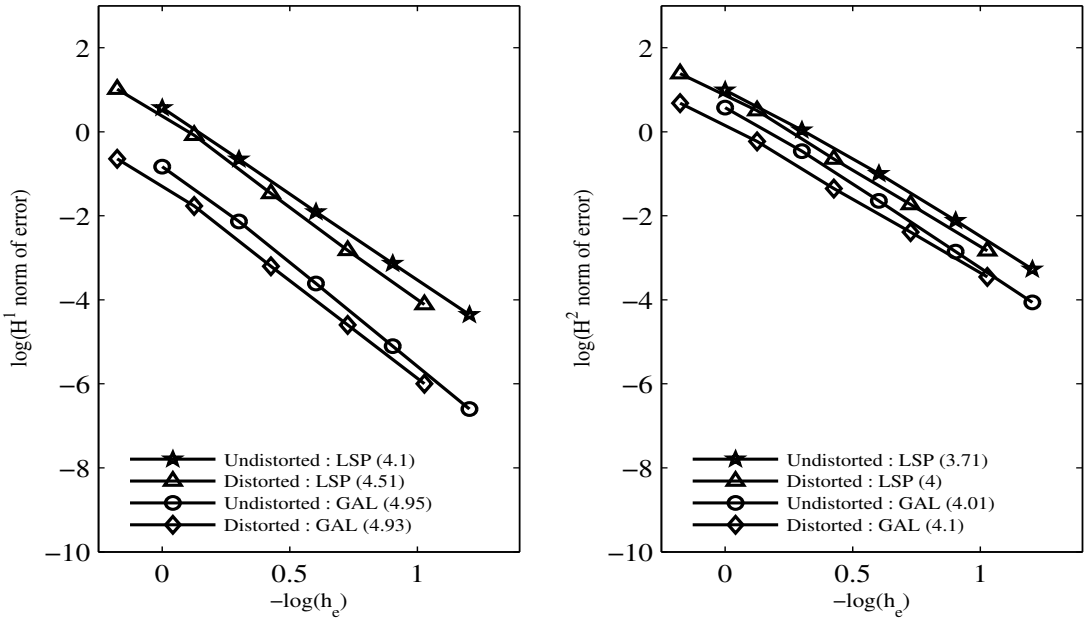

(c) H^1 norm of error in u versus h_e

(d) H^2 norm of error in u versus h_e

Figure 4.17: Comparison of Undistorted and Distorted discretizations versus discretization length for 2-D Poisson's equation : C^{22} HGDA element, $p_\xi = p_\eta = 5$

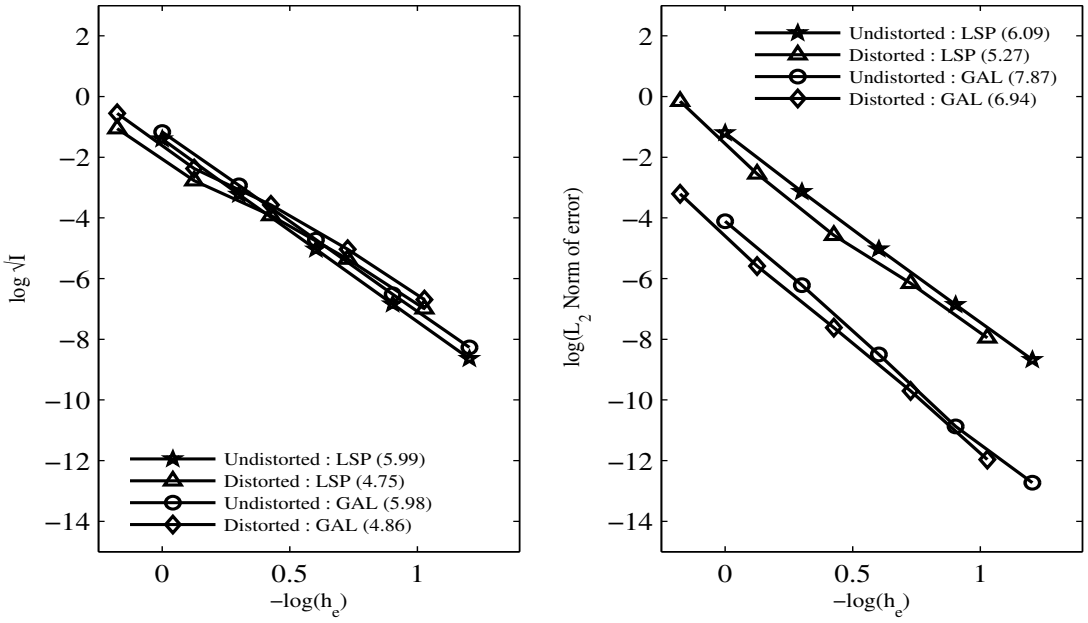

(a) √I versus h_e

(b) L_2 norm of error in u versus h_e

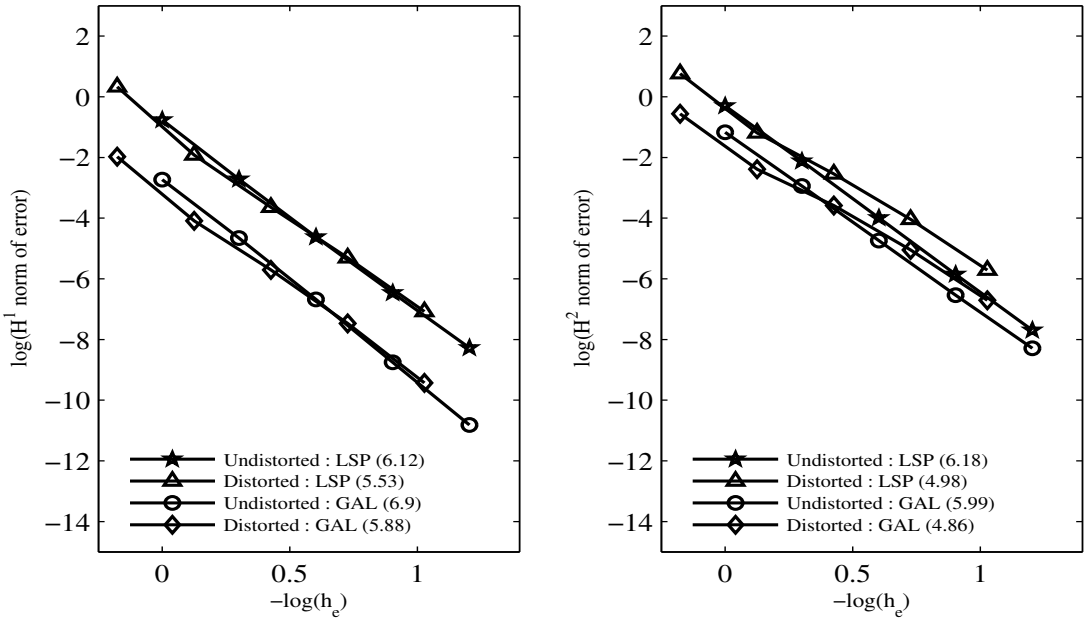

(c) H^1 norm of error in u versus h_e

(d) H^2 norm of error in u versus h_e

Figure 4.18: Comparison of Undistorted and Distorted discretizations versus discretization length for 2-D Poisson's equation : C^{33} HGDA element, $p_\xi = p_\eta = 7$

Table 4.4: Convergence rates for 2-D Poisson's equation : h-convergence, Undistorted and Distorted discretizations using Distorted HGDA elements

(a) $\sqrt{I}$ versus h_e

C^{ij}	LSP		GAL	
	Undistorted mesh	Distorted mesh	Undistorted mesh	Distorted mesh
C^{11} ; p=3	1.89	1.78	1.95	1.87
C^{22} : p=5	4.05	3.41	4.01	3.44
C^{33} : p=7	5.99	4.75	5.98	4.86

(b) L_2 - norm of error versus h_e

C^{ij}	LSP		GAL	
	Undistorted mesh	Distorted mesh	Undistorted mesh	Distorted mesh
C^{11} ; p=3	2.09	2.21	3.65	3.77
C^{22} : p=5	4.06	4.49	5.93	5.8
C^{33} : p=7	6.09	5.27	7.87	6.94

(c) H^1 - norm of error versus h_e

C^{ij}	LSP		GAL	
	Undistorted mesh	Distorted mesh	Undistorted mesh	Distorted mesh
C^{11} ; p=3	2.08	2.3	2.78	2.79
C^{22} : p=5	4.1	4.51	4.95	4.93
C^{33} : p=7	6.12	5.53	6.9	5.88

(d) H^2 - norm of error versus h_e

C^{ij}	LSP		GAL	
	Undistorted mesh	Distorted mesh	Undistorted mesh	Distorted mesh
C^{11} ; p=3	1.97	1.95	1.9	1.86
C^{22} : p=5	3.71	4	4.01	4.1
C^{33} : p=7	6.18	4.98	5.99	4.86

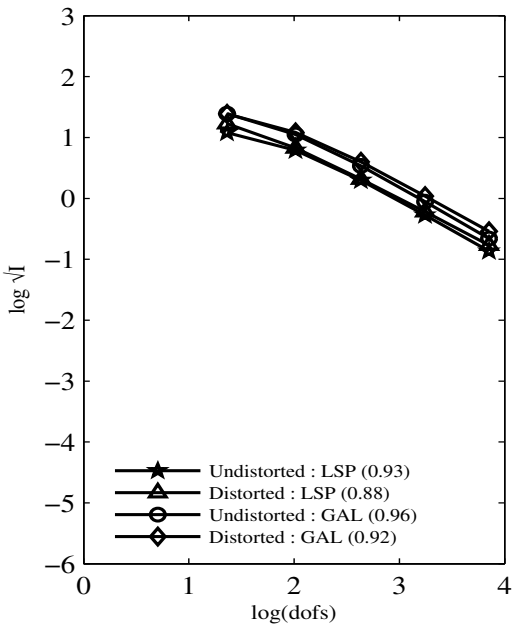

(a) √I versus dofs

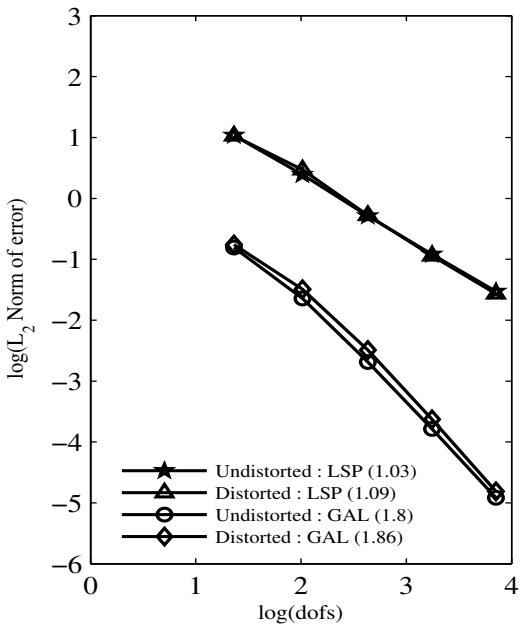

(b) L_2 norm of error in u versus dofs

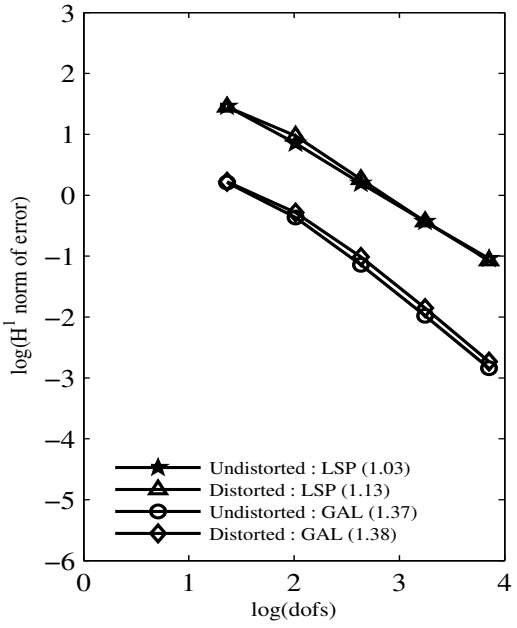

(c) H^1 norm of error in u versus dofs

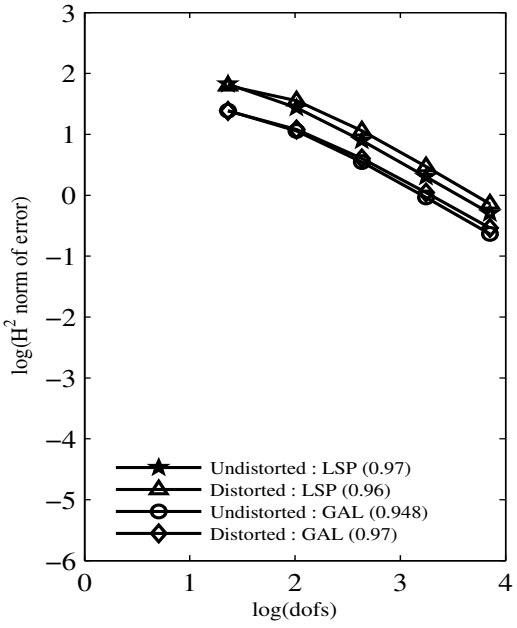

(d) H^2 norm of error in u versus dofs

Figure 4.19: Comparison of Undistorted and Distorted discretizations versus degrees of freedom for 2-D Poisson's equation : C^{11} HGDA element, $p_\xi = p_\eta = 3$

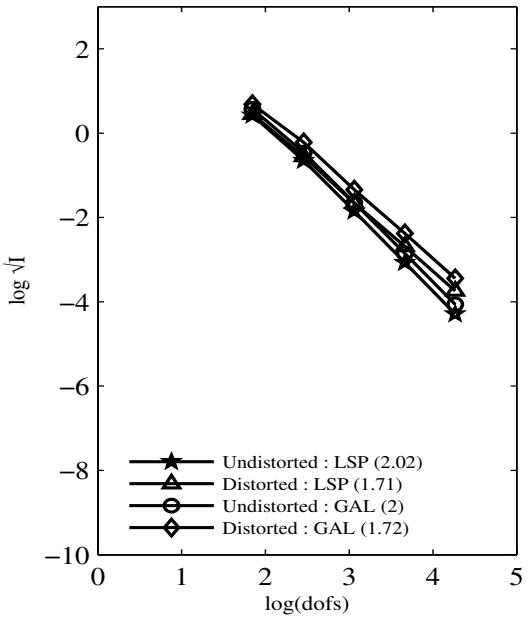

(a) √I versus dofs

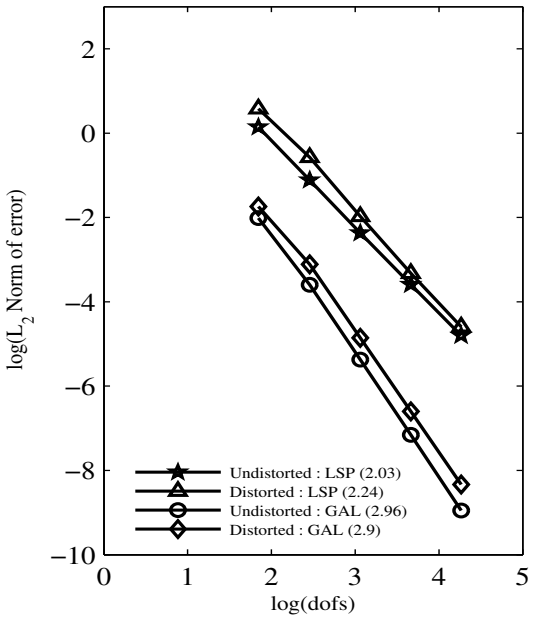

(b) L_2 norm of error in u versus dofs

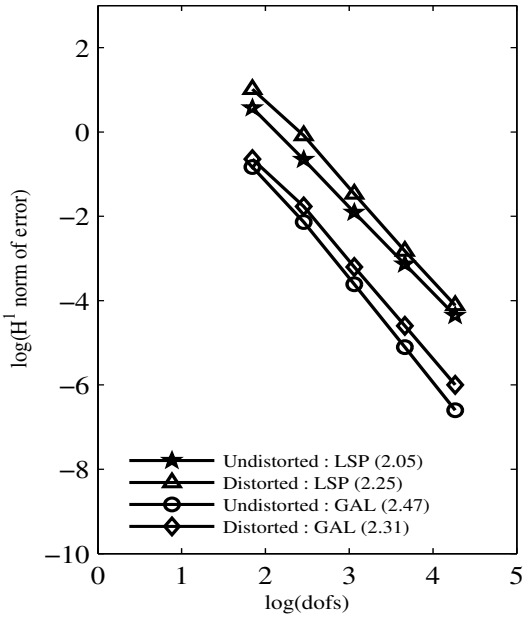

(c) H^1 norm of error in u versus dofs

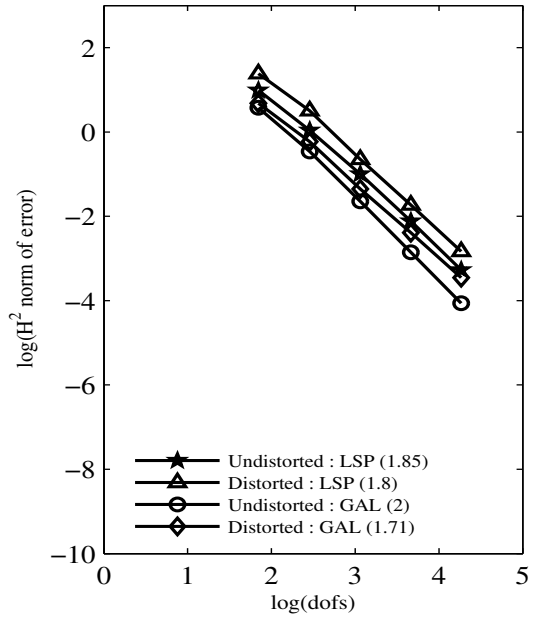

(d) H^2 norm of error in u versus dofs

Figure 4.20: Comparison of Undistorted and Distorted discretizations versus degrees of freedom for 2-D Poisson's equation : C^{22} HGDA element, $p_\xi = p_\eta = 5$

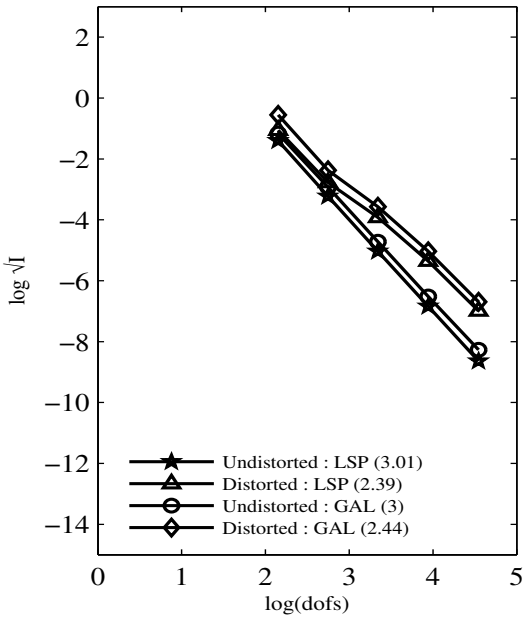

(a) √I versus dofs

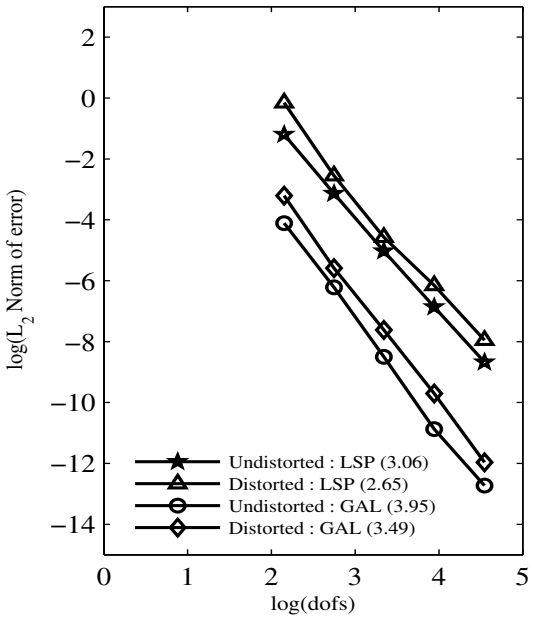

(b) L_2 norm of error in u versus dofs

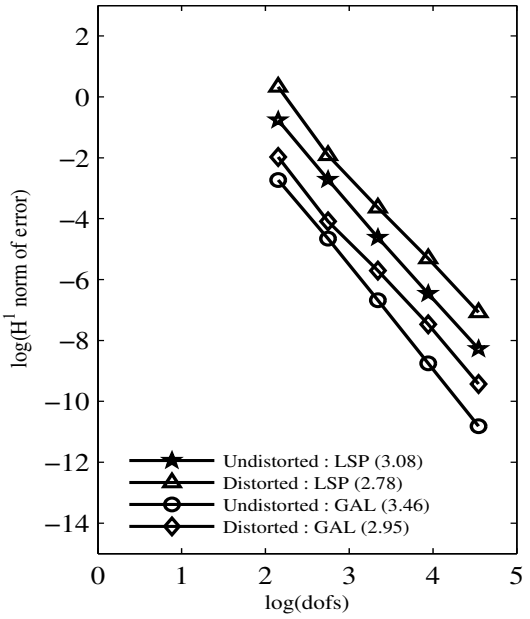

(c) H^1 norm of error in u versus dofs

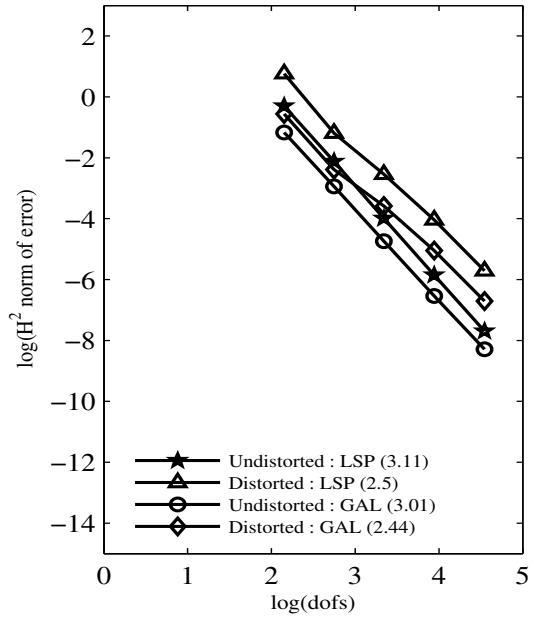

(d) H^2 norm of error in u versus dofs

Figure 4.21: Comparison of Undistorted and Distorted discretizations versus degrees of freedom for 2-D Poisson's equation : C^{33} HGDA element, $p_\xi = p_\eta = 7$

Table 4.5: Convergence rates for 2-D Poisson's equation : h-convergence, Undistorted and Distorted discretizations using Distorted HGDA elements

(a) $\sqrt{I}$ versus dofs

C^{ij}	LSP		GAL	
	Undistorted mesh	Distorted mesh	Undistorted mesh	Distorted mesh
C^{11} ; p=3	0.93	0.88	0.96	0.92
C^{22} : p=5	2.02	1.71	2	1.72
C^{33} : p=7	3.01	2.39	3	2.44

(b) L_2 - norm of error versus dofs

C^{ij}	LSP		GAL	
	Undistorted mesh	Distorted mesh	Undistorted mesh	Distorted mesh
C^{11} ; p=3	1.03	1.09	1.8	1.86
C^{22} : p=5	2.03	2.24	2.96	2.9
C^{33} : p=7	3.06	2.65	3.95	3.49

(c) H^1 - norm of error versus dofs

C^{ij}	LSP		GAL	
	Undistorted mesh	Distorted mesh	Undistorted mesh	Distorted mesh
C^{11} ; p=3	1.03	1.13	1.37	1.38
C^{22} : p=5	2.05	2.25	2.47	2.31
C^{33} : p=7	3.08	2.78	3.46	2.95

(d) H^2 - norm of error versus dofs

C^{ij}	LSP		GAL	
	Undistorted mesh	Distorted mesh	Undistorted mesh	Distorted mesh
C^{11} ; p=3	0.97	0.96	0.95	0.97
C^{22} : p=5	1.85	1.8	2	1.71
C^{33} : p=7	3.11	2.5	3.01	2.44

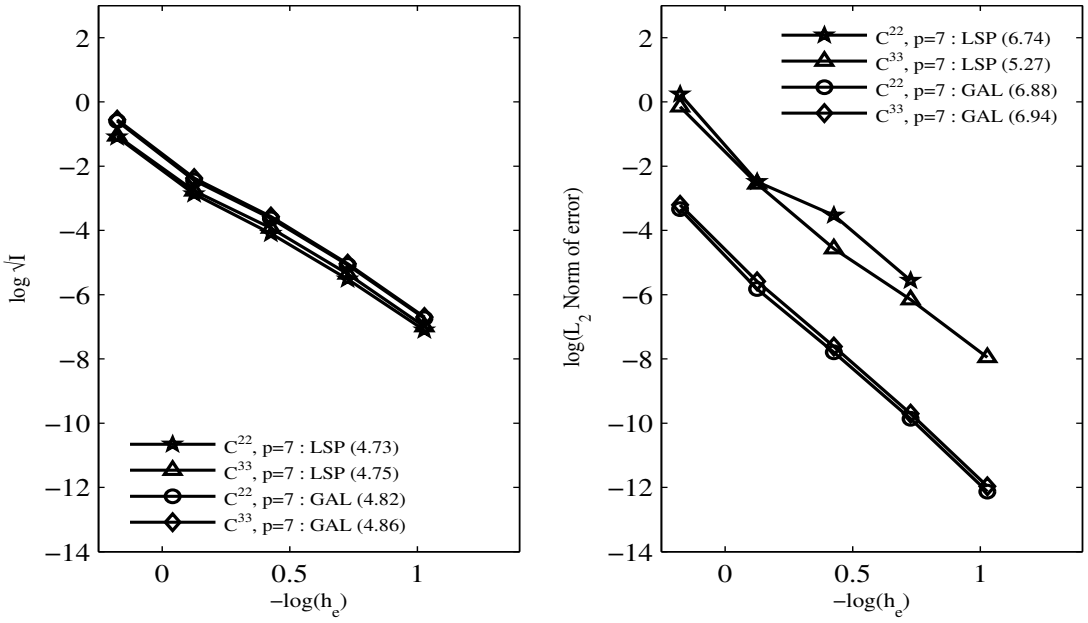

(a) $\sqrt{I}$ versus h_e

(b) L_2 norm of error in u versus h_e

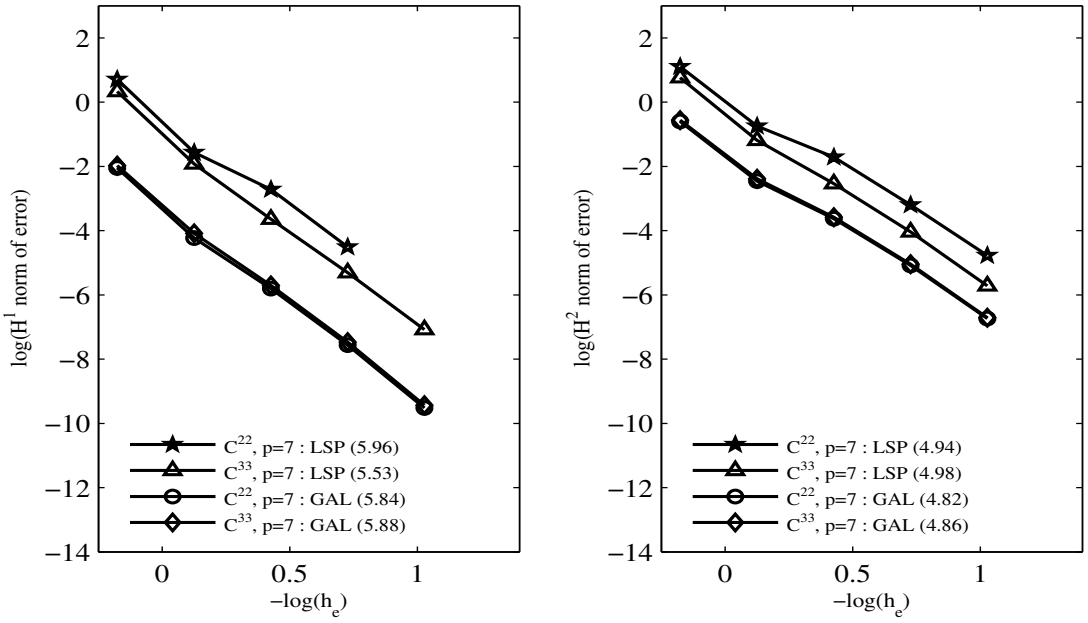

(c) H^1 norm of error in u versus h_e

(d) H^2 norm of error in u versus h_e

Figure 4.22: Comparison of C^{ij} Distorted HGDA elements versus discretization length for 2-D Poisson's equation : $\boldsymbol{C^{22}}$ ($\boldsymbol{k}$ = 3), $\boldsymbol{C^{33}}$ ($\boldsymbol{k}$ = 4), $\boldsymbol{p_\xi = p_\eta = 7}$, **Distorted discretizations**

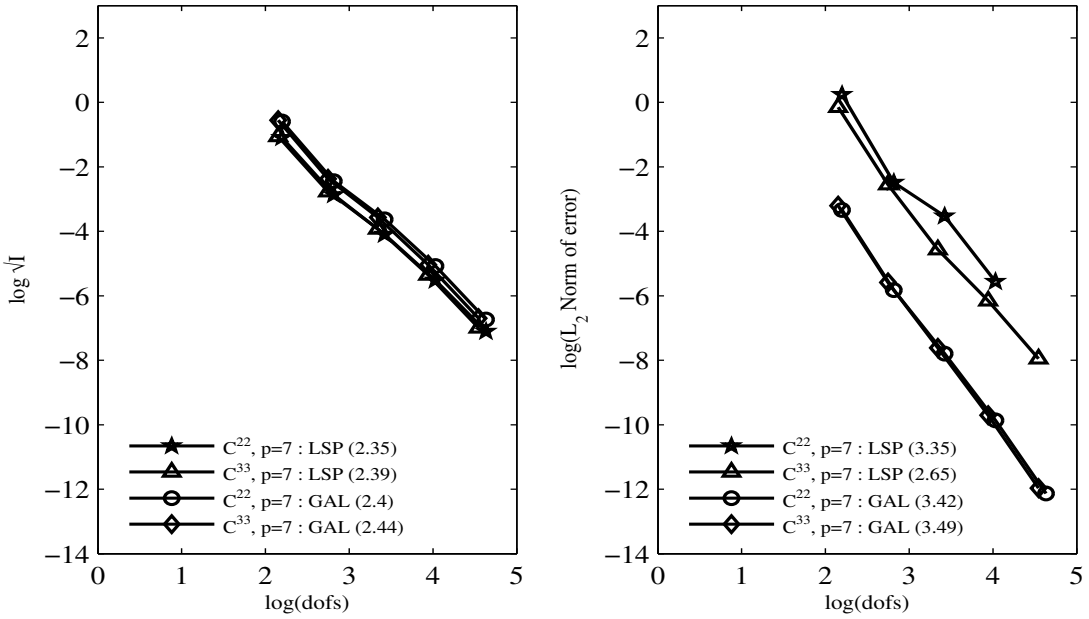

(a) √I versus dofs

(b) L_2 norm of error in u versus dofs

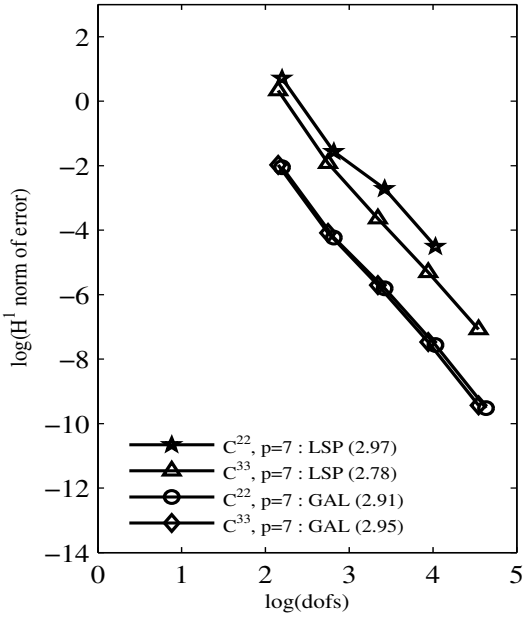

(c) H^1 norm of error in u versus dofs

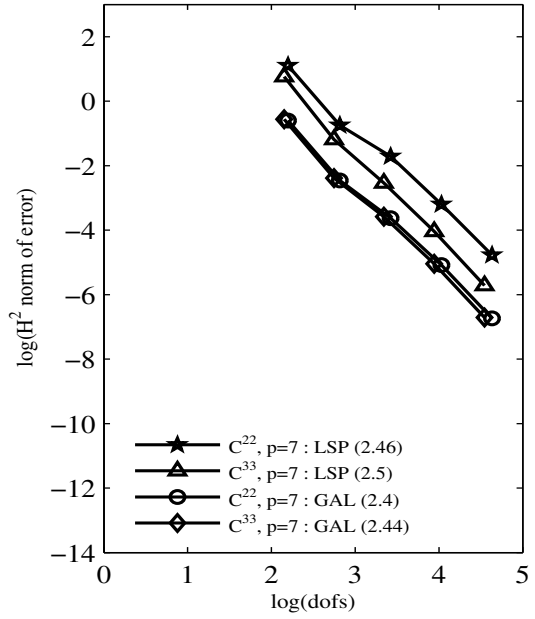

(d) H^2 norm of error in u versus dofs

Figure 4.23: Comparison of C^{ij} Distorted HGDA elements versus degrees of freedom for 2-D Poisson's equation : $\boldsymbol{C^{22}}$ ($\boldsymbol{k}$ = 3), $\boldsymbol{C^{33}}$ ($\boldsymbol{k}$ = 4), $\boldsymbol{p_\xi = p_\eta = 7}$, **Distorted discretizations**

Table 4.6: Convergence rates for 2-D Poisson's equation : k-convergence, Distorted discretizations using C^{22} (k = 3) and C^{33} (k = 4) Distorted HGDA elements

(a) √I

	√I versus he		**√I versus dofs**	
C^{ij}	LSP	GAL	LSP	GAL
C^{22} : p=7	4.73	4.82	2.35	2.4
C^{33} : p=7	4.75	4.86	2.39	2.44

(b) L_2 - norm of error

	L_2 - norm vs he		**L_2 - norm vs dofs**	
C^{ij}	LSP	GAL	LSP	GAL
C^{22} : p=7	6.74	6.88	3.35	3.42
C^{33} : p=7	5.27	6.94	2.65	3.49

(c) H^1 - norm of error

	H^1 - norm vs he		**H^1 - norm vs dofs**	
C^{ij}	LSP	GAL	LSP	GAL
C^{22} : p=7	5.96	5.84	2.97	2.91
C^{33} : p=7	5.53	5.88	2.78	2.95

(d) H^2 - norm of error

	H^2 - norm vs he		**H^2 - norm vs dofs**	
C^{ij}	LSP	GAL	LSP	GAL
C^{22} : p=7	4.94	4.82	2.46	2.4
C^{33} : p=7	4.98	4.86	2.5	2.44

Remarks

(1) The best performance of HGDA elements is obtained when the domain of discretization is rectangular. From Tables 4.4-4.5, the convergence rates utilizing undistorted discretizations are higher than those corresponding to the distorted discretizations.

(2) From Figures 4.16-4.18, for a given formulation (Least squares processes or Galerkin method with weak form), for a given value of discretization length, computed quantities of interest corresponding to distorted discretizations have a slightly lower value compared to those obtained with Undistorted discretization.

(3) In all the numerical studies, Galerkin method with weak form has lower values of computed quantities of interest (except error or residual functional) compared to Least squares processes for a given h_e or $dofs$.

(4) From Table 4.6, for Galerkin method with weak form, the convergence rates and the values of the computed quantities are approximately same for both C^{22} and C^{33} HGDA elements. However, for least squares processes, from Figures 4.22 and 4.23 for a given value of characteristic length or given number of degrees of freedom, C^{33} HGDA element gives a lower value of the quantity of interest compared to C^{22} HGDA element, thus illustrating the benefit of k.

4.2.6 Numerical studies for Distorted mesh : p-convergence

Numerical studies are conducted using C^{22} and C^{33} HGDA elements with progressively increasing p-levels starting from the minimum p-level required by the corresponding HGDA element. The numerical solutions are computed using a fixed characteristic length of discretization. The values in parenthesis indicate the convergence rate. Galerkin method with weak form and Least squares processes are both considered for these numerical studies.

(i) Figures 4.24(a)-(d) show the solutions computed for two different distorted discretizations (4 and 16 elements) with C^{22} HGDA element. Figures 4.25(a)-(d) show similar plots for C^{33} HGDA element. In both cases, to obtain a given value of quantity of interest, we need lesser number of degrees of freedom for four element mesh (coarser of the two meshes) compared to the sixteen element mesh.

(ii) Figures 4.26(a)-(d) show the solutions computed with C^{22} HGDA elements using distorted discretizations compared with solutions obtained using undistorted discretizations. Figures 4.27(a)-(d) show similar plots for C^{33} HGDA element.

(iii) Figures 4.28(a)-(d) show comparison of solutions calculated using C^{22} and C^{33} HGDA elements for a 4 element distorted discretization with progressively increasing p levels.

Remarks

(1) From Figures 4.24 and 4.26, for a given number of degrees of freedom, HGDA element using Least squares processes has a lower value of error or residual functional compared to the value obtained using Galerkin method with weak form. For all other error norms, Galerkin method with weak form has lower computed quantities of interest for a given number of degrees of freedom.

(2) The convergence rates of the computed quantities of interest in Figures 4.25, 4.27 and 4.28 are very high due to the numerical solution at p-level of 8 being in the close vicinity of the theoretical solution.

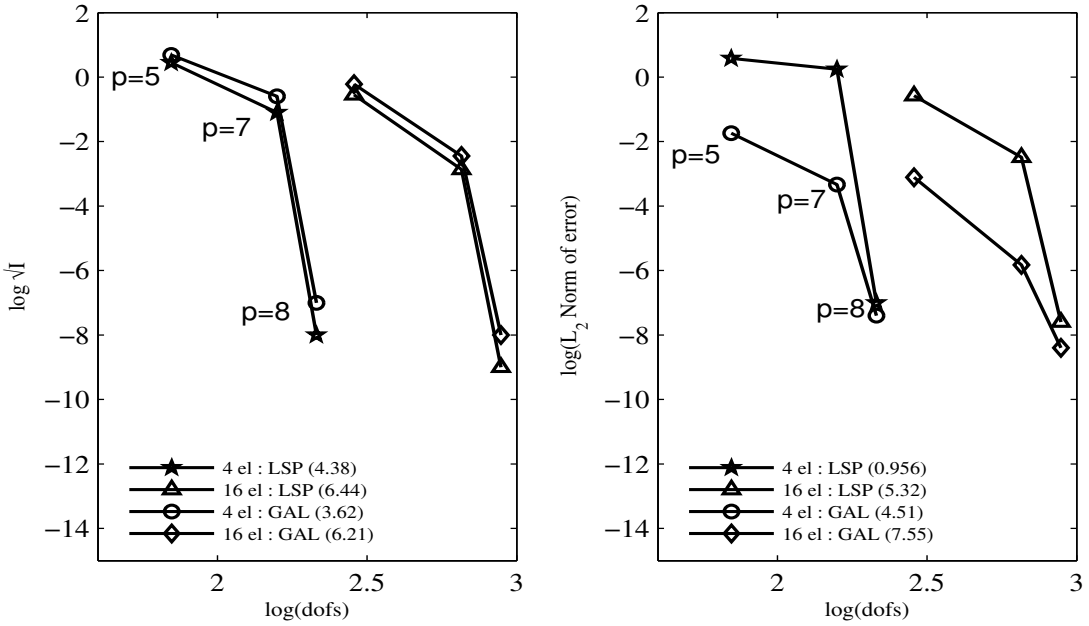

(a) √I versus dofs

(b) L_2 norm of error in u versus dofs

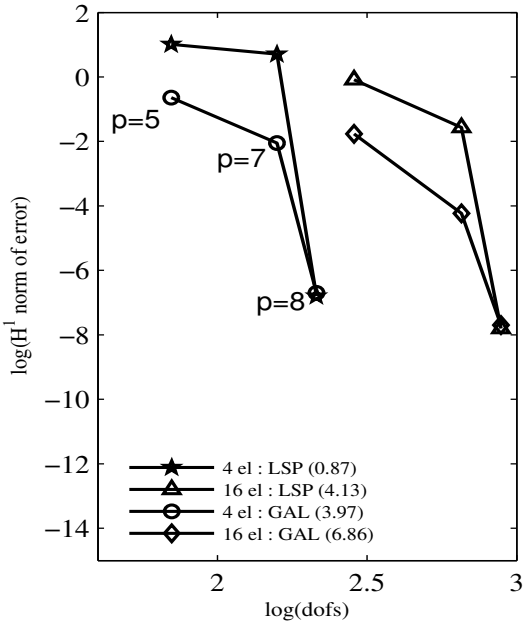

(c) H^1 norm of error in u versus dofs

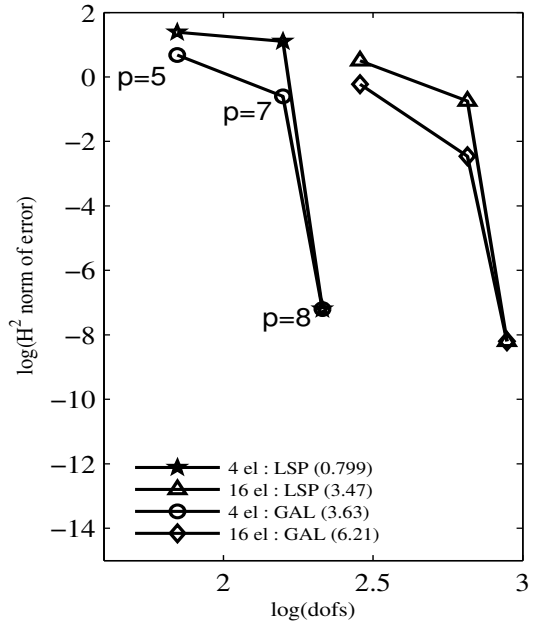

(d) H^2 norm of error in u versus dofs

Figure 4.24: Comparison of 4 element and 16 element discretizations using Distorted HGDA elements for 2-D Poisson's equation : C^{22}, **Distorted discretizations**

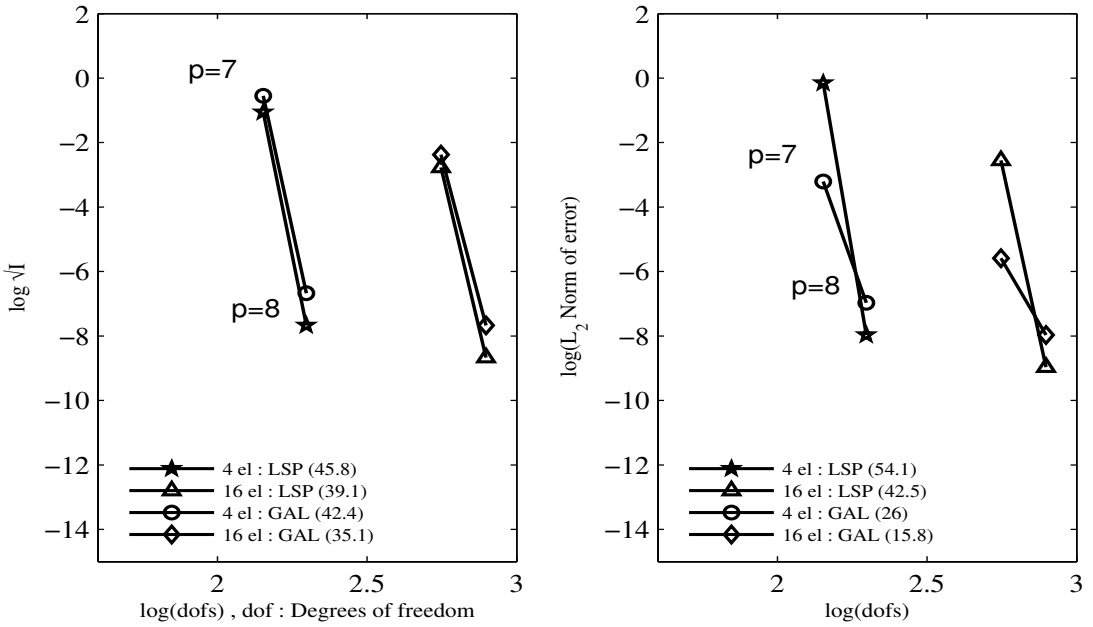

(a) √I versus dofs

(b) L_2 norm of error in u versus dofs

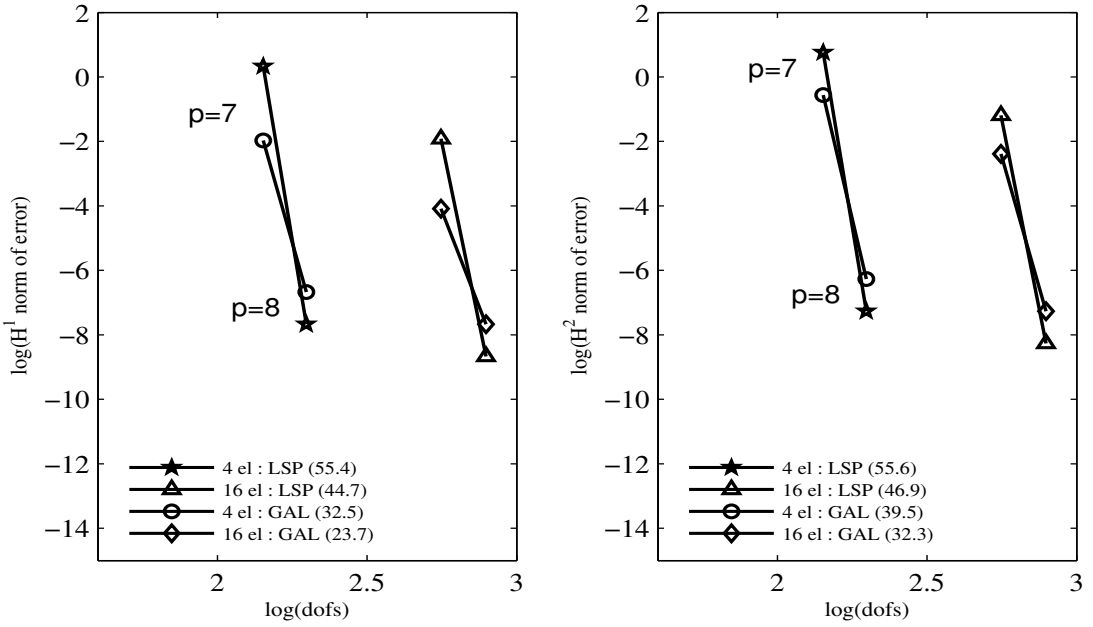

(c) H^1 norm of error in u versus dofs

(d) H^2 norm of error in u versus dofs

Figure 4.25: Comparison of 4 element and 16 element discretizations using Distorted HGDA elements for 2-D Poisson's equation : C^{33}, **Distorted discretizations**

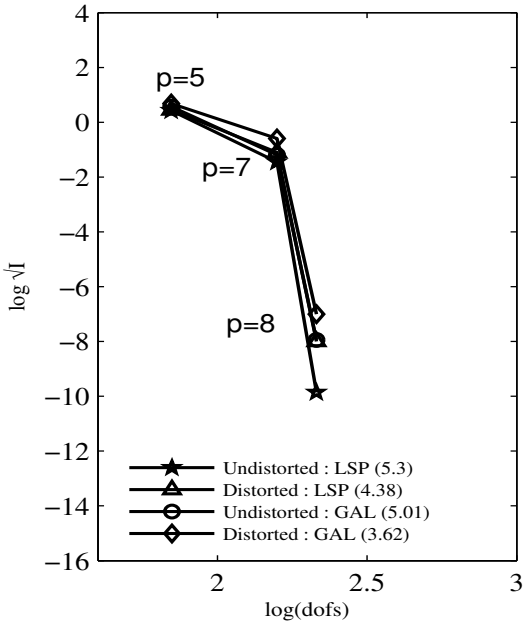

(a) √I versus dofs

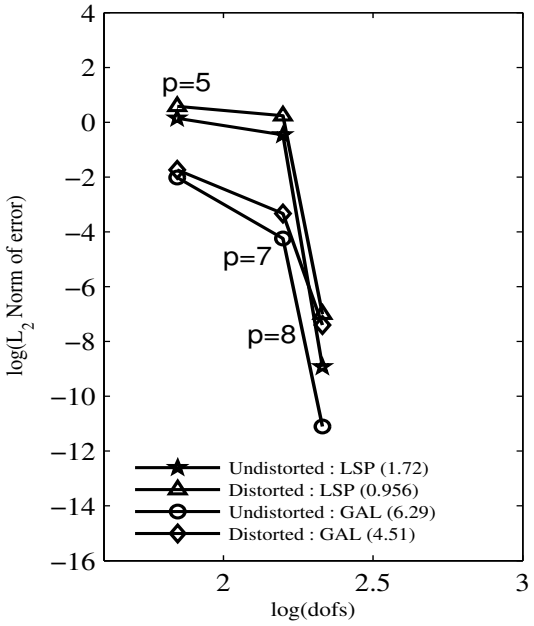

(b) L_2 norm of error in u versus dofs

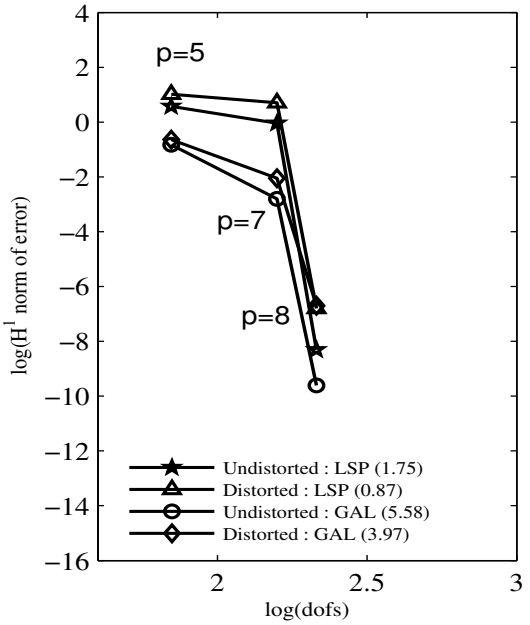

(c) H^1 norm of error in u versus dofs

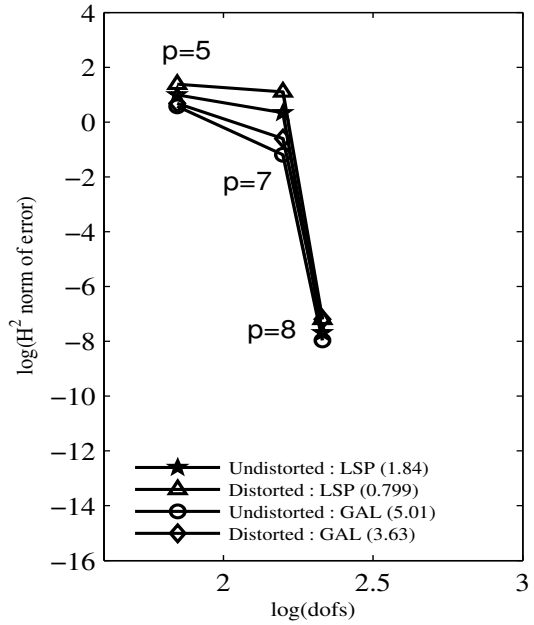

(d) H^2 norm of error in u versus dofs

Figure 4.26: Comparison of Distorted and Undistorted discretizations using Distorted HGDA elements for 2-D Poisson's equation : C^{22}, **4 element discretization**

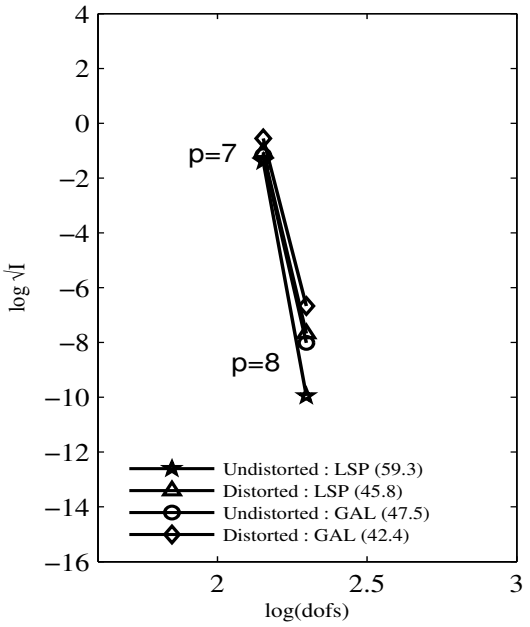

(a) √I versus dofs

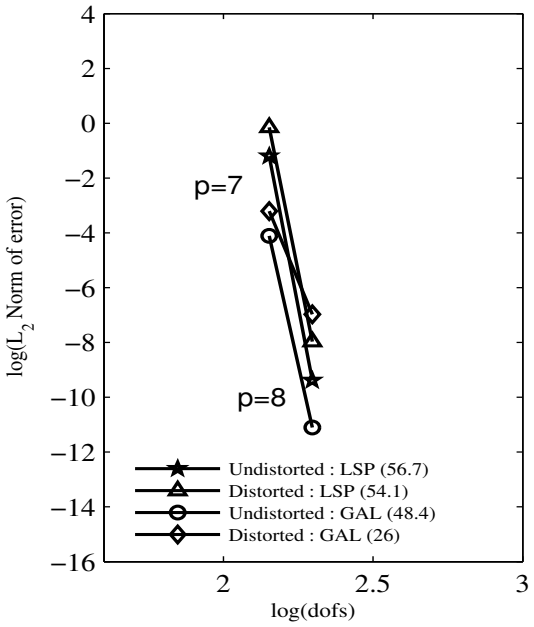

(b) L_2 norm of error in u versus dofs

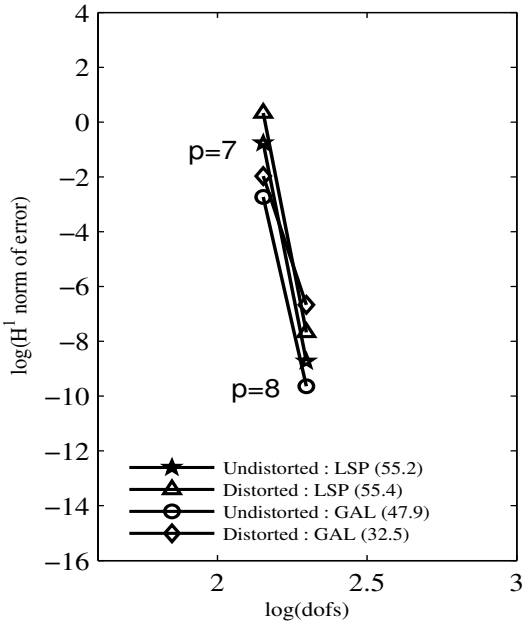

(c) H^1 norm of error in u versus dofs

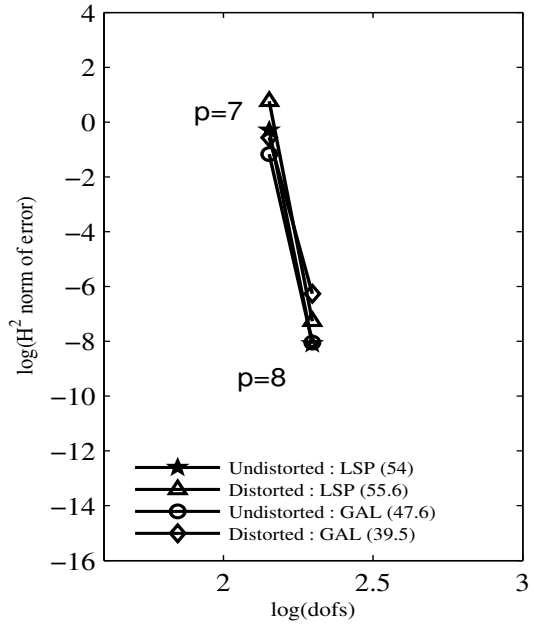

(d) H^2 norm of error in u versus dofs

Figure 4.27: Comparison of Distorted and Undistorted discretizations using Distorted HGDA elements for 2-D Poisson's equation : C^{33}, **4 element discretization**

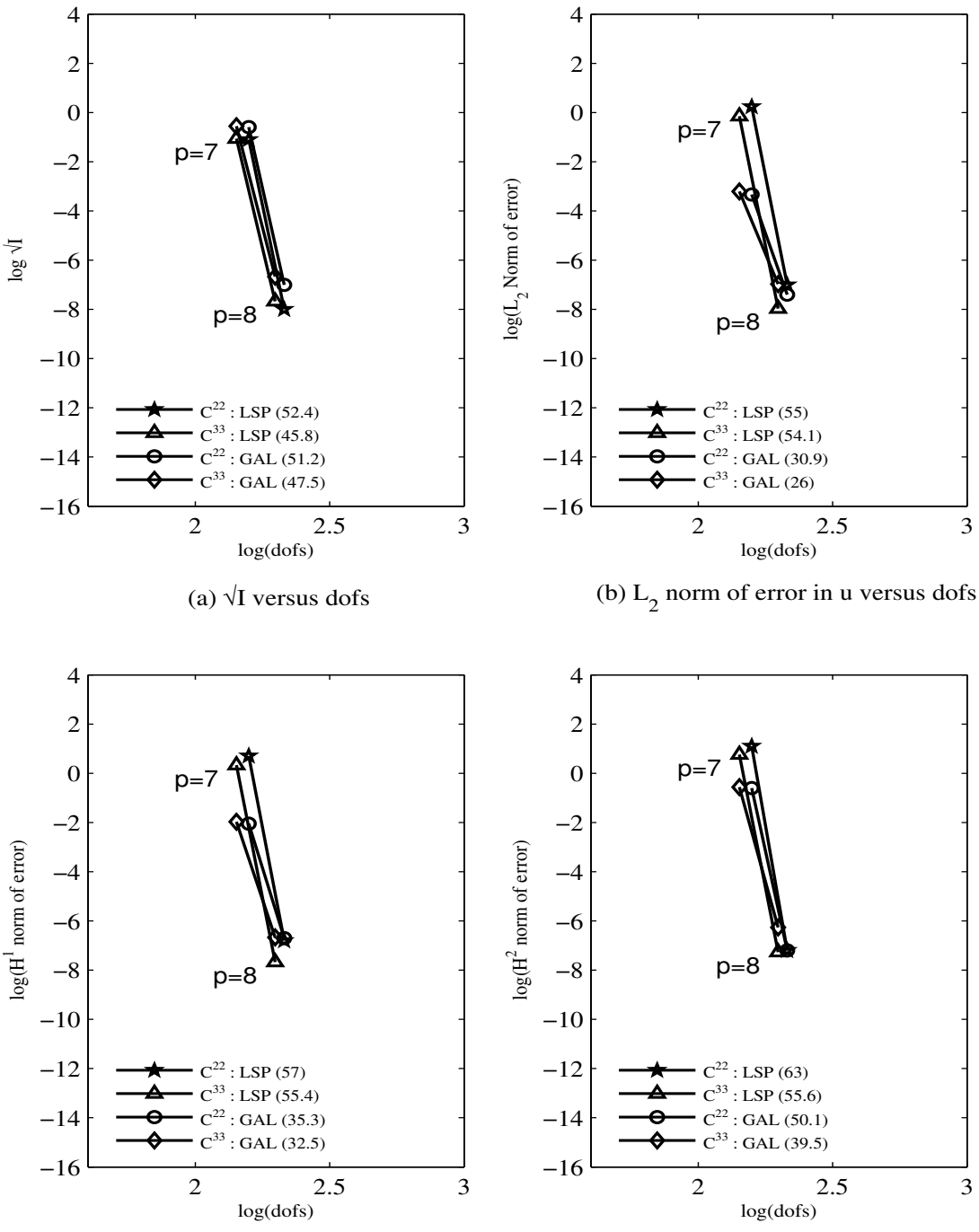

(a) √I versus dofs

(b) L_2 norm of error in u versus dofs

(c) H^1 norm of error in u versus dofs

(d) H^2 norm of error in u versus dofs

Figure 4.28: Comparison of C^{ij} Distorted HGDA elements for 2-D Poisson's equation : $\boldsymbol{C^{22}}$ ($\boldsymbol{k}$ = 3), $\boldsymbol{C^{33}}$ ($\boldsymbol{k}$ = 4), **4 element Distorted discretization**

4.3 Model Problem # 2 : 2-D steady state convection diffusion equation

The governing differential equation for 2-D steady state convection diffusion equation is given by:

$$\frac{\partial u}{\partial x} + \frac{\partial u}{\partial y} - \frac{1}{P_e}\left(\frac{\partial^2 u}{\partial x^2} + \frac{\partial^2 u}{\partial y^2}\right) = 0 \quad \text{over } \Omega = (0,1) \times (0,1) \tag{4.9}$$

with boundary conditions

$$u(x,0) \;=\; \frac{1 - e^{(x-1)P_e}}{1 - e^{-P_e}} \;\;;\;\; u(0,y) \;=\; \frac{1 - e^{(y-1)P_e}}{1 - e^{-P_e}} \tag{4.10}$$

and

$$u(x,1) \;=\; u(1,y) \;=\; 0 \tag{4.11}$$

where P_e is the Peclet number. A theoretical solution is given by

$$u(x,y) = \frac{\left(1 - e^{(x-1)P_e}\right)\left(1 - e^{(y-1)P_e}\right)}{\left(1 - e^{-P_e}\right)\left(1 - e^{-P_e}\right)} \tag{4.12}$$

From the theoretical solution, we observe that $u(x,y)$ is analytic for all values of P_e and is of class $C^{L,L}$, where $L = \infty$.

Since the differential operator is non self-adjoint, only least squares finite element method is variationally consistent. The differential operator contains up to second order derivatives of the dependent variable, hence $C^{2,2}$ local approximations are minimally conforming if the integrals in the LSP are to be Riemann. If we accept Lebesgue integrals in the LSP, then C^{11} local approximations are admissible.

For computations, we consider P_e=10. Figure 4.29(a) shows a schematic of the domain Ω.

4.3.1 Undistorted Discretizations

We consider the following uniform discretizations for h-convergence:

(1) 4 element uniform discretization (2 x 2) : characteristic length : h_e = 0.5

(2) 16 element uniform discretization (4 x 4) : characteristic length : h_e = 0.25

(3) 64 element uniform discretization (8 x 8) : characteristic length : h_e = 0.125

(4) 256 element uniform discretization (16 x 16) : characteristic length : h_e = 0.0625

(5) 1024 element uniform discretization (32 x 32) : characteristic length : h_e = 0.03125

The first and second uniform discretizations are shown in Figure 4.29(b) and (c).

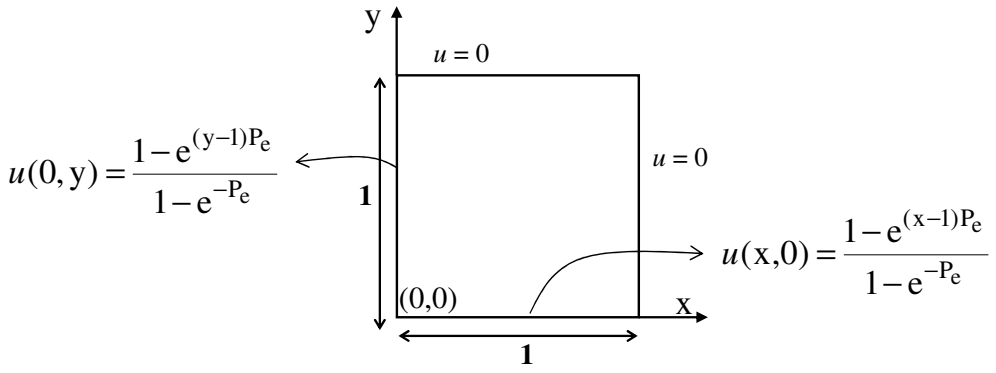

(a) Schematic of Ω

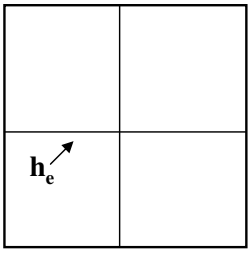

(b) 2 x 2 uniform discretization ($h_e = 0.5$)

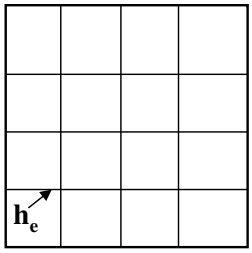

(c) 4 x 4 uniform discretization ($h_e = 0.25$)

Figure 4.29: Schematic, uniform discretizations for Convection-Diffusion equation

4.3.2 Distorted discretizations

The domain of definition is now discretized using non-rectangular quadrilateral elements. The longest side among all the elements in the entire discretization is chosen as the characteristic length for such a discretization. The following distorted discretizations are considered for h-convergence studies:

(1) 4 element distorted discretization (2 x 2) : characteristic length : h_e = 0.75

(2) 16 element distorted discretization (4 x 4) : characteristic length : h_e = 0.375

(3) 64 element distorted discretization (8 x 8) : characteristic length : h_e = 0.1875

(4) 256 element distorted discretization (16 x 16) : characteristic length : h_e = 0.09375

(5) 1024 element distorted discretization (32 x 32) : characteristic length : h_e = 0.046875

The first and second distorted discretizations are shown in Figure 4.30(a) and (b).

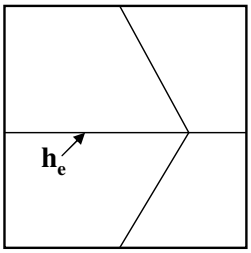

(a) 2 x 2 distorted discretization (h_e =0.75)

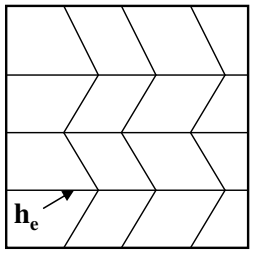

(b) 4 x 4 distorted discretization (h_e = 0.375)

Figure 4.30: Schematic, distorted discretization for 2-D Convection-diffusion equation

4.4 Model Problem # 3 : 2-D steady state non-linear Poisson's equation

The governing differential equation for 2-D steady state non-linear Poisson's equation is given by:

$$u\frac{\partial u}{\partial x} + u\frac{\partial u}{\partial y} - \frac{\partial^2 u}{\partial x^2} - \frac{\partial^2 u}{\partial y^2} = f(x,y) \quad \text{over } \Omega = (-a,a) \times (-b,b) \tag{4.13}$$

with boundary conditions

$$u(x,-b) \;=\; u(a,y) \;=\; u(x,b) \;=\; u(-a,y) \;=\; 0 \tag{4.14}$$

where $f(x,y)$ is such that the theoretical solution is given by

$$u(x,y) = (a^n \;-\; x^n)(b^m \;-\; y^m) \tag{4.15}$$

For computations, we consider $a \;=\; b \;=\; 1$ and $m \;=\; n \;=\; 8$

In this case, the differential operator is non-linear hence all other methods of approximation are variationally inconsistent except least squares method. The remarks regarding minimally conforming approximations made for Model problem # 2 hold here as well due to the fact that in this case also we have up to second order derivatives in Equation (4.13).

Surana et al. [1–4] have shown that when the differential operators in the BVPs are non-linear only least squares processes in which non-linear algebraic equations are solved using Newton's linear method are variationally consistent with the approximation that the term containing the second variation of residual be neglected in the second variation of the least squares functional. Figure 4.31(a) shows a schematic of the computational domain Ω.

4.4.1 Undistorted Discretizations

We consider the following uniform discretizations for h-convergence studies:

(1) 4 element uniform discretization (2 x 2) : characteristic length : h_e = 1

(2) 16 element uniform discretization (4 x 4) : characteristic length : h_e = 0.5

(3) 64 element uniform discretization (8 x 8) : characteristic length : h_e = 0.25

(4) 256 element uniform discretization (16 x 16) : characteristic length : h_e = 0.125

(5) 1024 element uniform discretization (32 x 32) : characteristic length : h_e = 0.0625

The first and second uniform discretizations are shown in Figure 4.31(b) and (c).

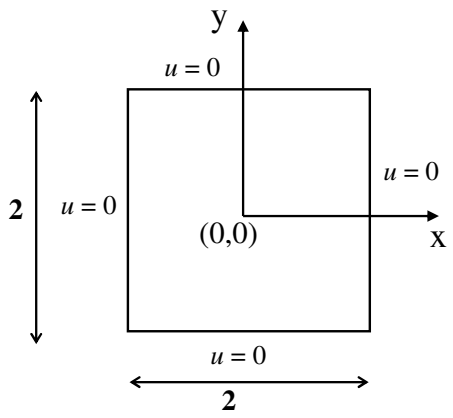

(a) Schematic of Ω

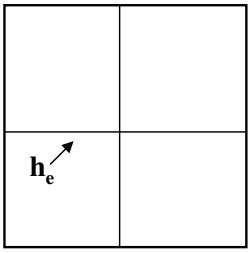

(b) 2 x 2 uniform discretization (h_e =1)

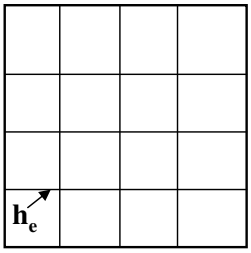

(c) 4 x 4 uniform discretization (h_e = 0.5)

Figure 4.31: Schematic, uniform discretizations for 2-D non-linear Poisson's equation

4.4.2 Distorted Discretizations

The domain of definition is now discretized using non-rectangular distorted elements. The longest side among all the elements in the entire discretization is selected as the characteristic length for such a discretization. We consider the following distorted discretizations for h-convergence:

(1) 4 element distorted discretization (2 x 2) : characteristic length : h_e = 1.5

(2) 16 element distorted discretization (4 x 4) : characteristic length : h_e = 0.75

(3) 64 element distorted discretization (8 x 8) : characteristic length : h_e = 0.375

(4) 256 element distorted discretization (16 x 16) : characteristic length : h_e = 0.1875

(5) 1024 element distorted discretization (32 x 32) : characteristic length : h_e = 0.09375

The first and second distorted discretizations are shown in Figure 4.32(a) and (b).

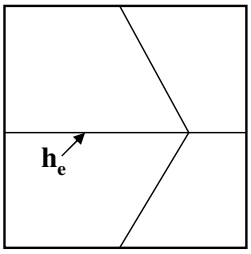

(a) 2 x 2 distorted discretization (h_e =1.5)

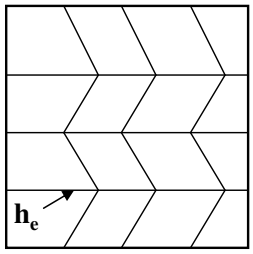

(b) 4 x 4 distorted discretization (h_e = 0.75)

Figure 4.32: Schematic, distorted discretizations for 2-D non-linear Poisson's equation

4.5 Numerical studies for Model Problems # 2 and 3

Numerical studies for the model problems discussed in Sections 4.3 and 4.4 are presented together since it is observed that the behavior of the computed solutions is the same in both cases. Only Least squares finite element formulation is considered in the numerical studies.

4.5.1 Numerical solutions for Undistorted discretizations : h-convergence

The numerical solutions are computed using C^{11}, C^{22} and C^{33} HGDA elements as well as tensor product elements employing the minimum p-level. The minimum p-levels required for C^{11}, C^{22} and C^{33} HGDA elements are 3, 5 and 7 respectively. The progressively refined uniform discretizations are considered in the numerical studies.

(i) Figures 4.33 (a)-(d) show results for C^{11} (p=3) approximation using tensor product and HGDA elements plotted against h_e for 2-D steady state convection-diffusion equation. Figures 4.34 (a)-(d) and 4.35 (a)-(d) show similar plots for C^{22} (p=5) and C^{33}(p=7) HGDA elements and Table 4.7 lists the convergence rates of all the solutions.

(ii) Figures 4.36 - 4.38 show similar plots as in (i) for 2-D non-linear Poisson's equation. The convergence rates for these solutions are listed in Table 4.8.

(iii) Figures 4.39 (a)-(d) show the C^{11} (p=3) numerical solutions computed for both tensor product and HGDA elements plotted against the total number of degrees of freedom for 2-D convection-diffusion equation. Figures 4.40 (a)-(d) and 4.41 (a)-(d) show similar plots for C^{22} (p=5) and C^{33} (p=7) HGDA elements. The convergence rates obtained for each computed quantity are listed in Table 4.9.

(iv) Figures 4.42 - 4.44 show similar plots as in (iii) computed for 2-D non-linear Poisson's equation. The convergence rates obtained for each computed quantity are listed in Table 4.10.

(v) Figures 4.45(a)-(d) and 4.46(a)-(d) show comparison of numerical solutions obtained using C^{22} and C^{33} HGDA elements for a p level of 7 plotted against charac-

teristic length and degrees of freedom respectively for 2-D convection-diffusion equation. The convergence rates for these solutions are listed in Table 4.11.

(vi) Figures 4.47(a)-(d) and 4.48(a)-(d) show similar comparison as in (v) of C^{22} and C^{33} HGDA elements for non-linear Poisson's equation. The convergence rates are listed in Table 4.12.

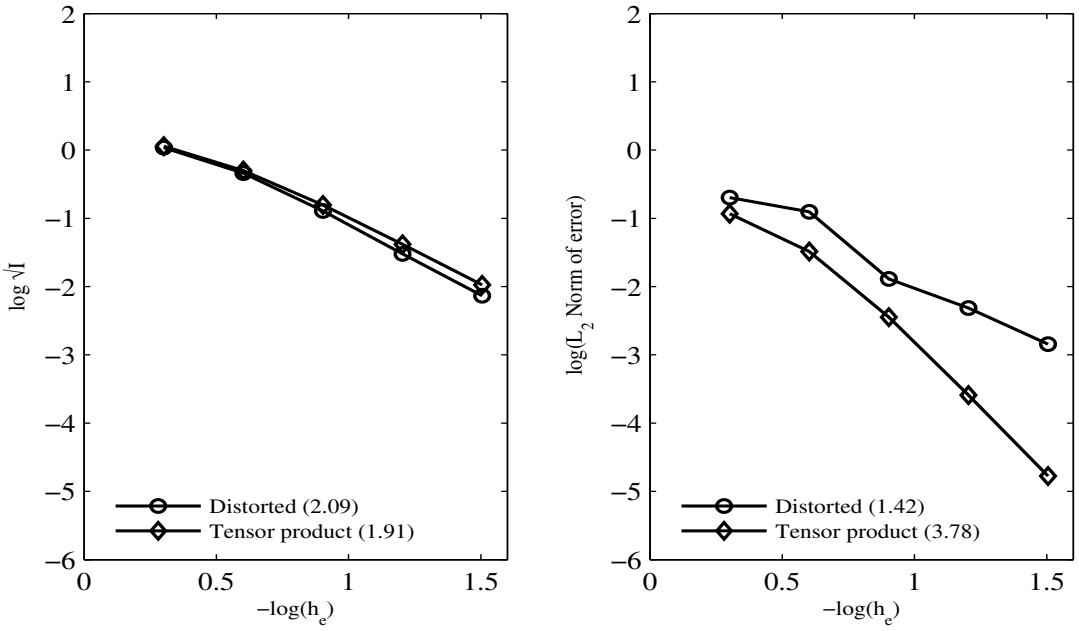

(a) $\sqrt{I}$ versus h_e

(b) L_2 norm of error in u versus h_e

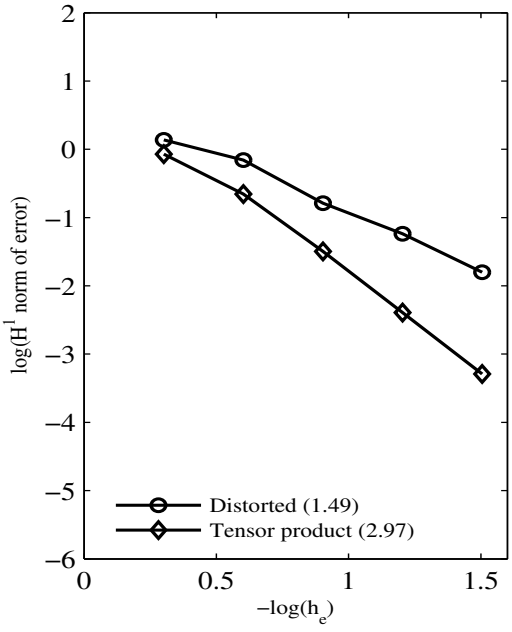

(c) H^1 norm of error in u versus h_e

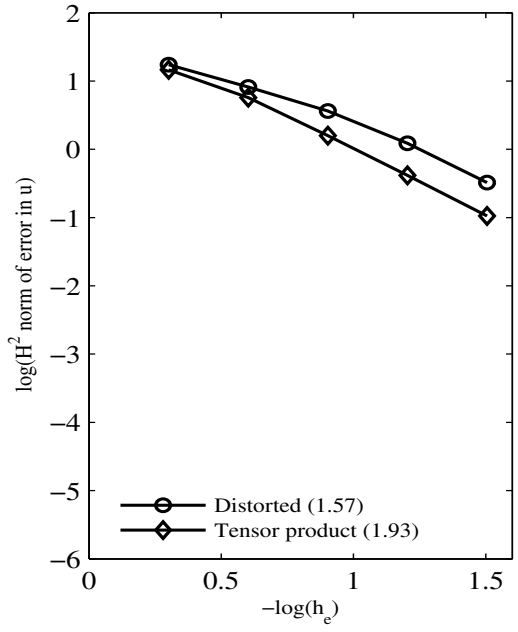

(d) H^2 norm of error in u versus h_e

Figure 4.33: Comparison of Distorted HGDA and Tensor product elements versus discretization length for 2-D Convection-diffusion equation : $\boldsymbol{C^{11}}$, $\boldsymbol{p_\xi = p_\eta = 3}$, **Undistorted discretizations**

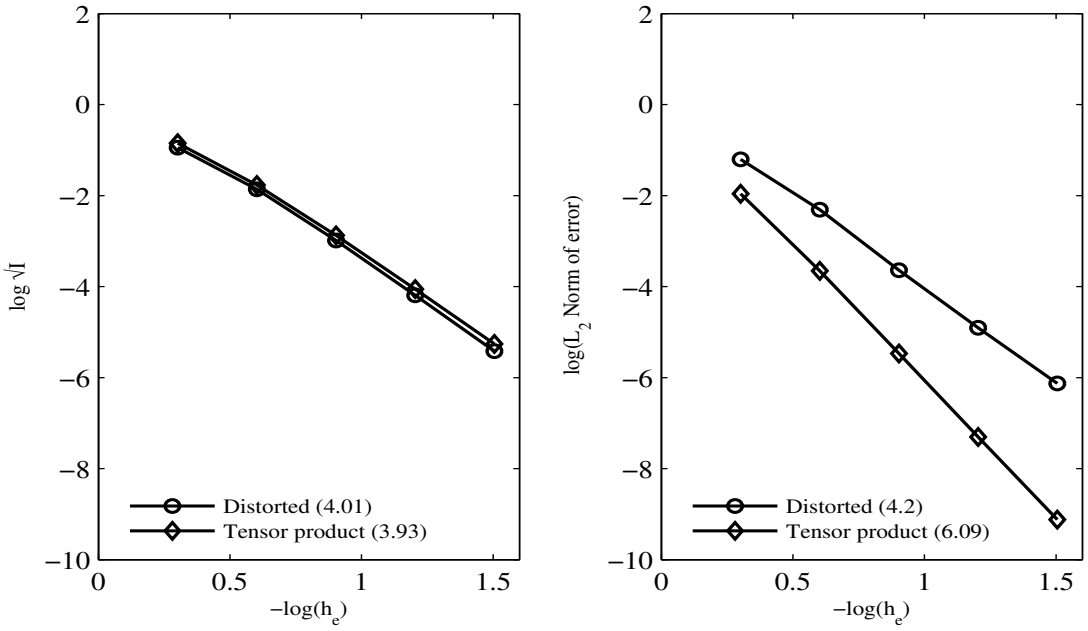

(a) $\sqrt{I}$ versus h_e

(b) L_2 norm of error in u versus h_e

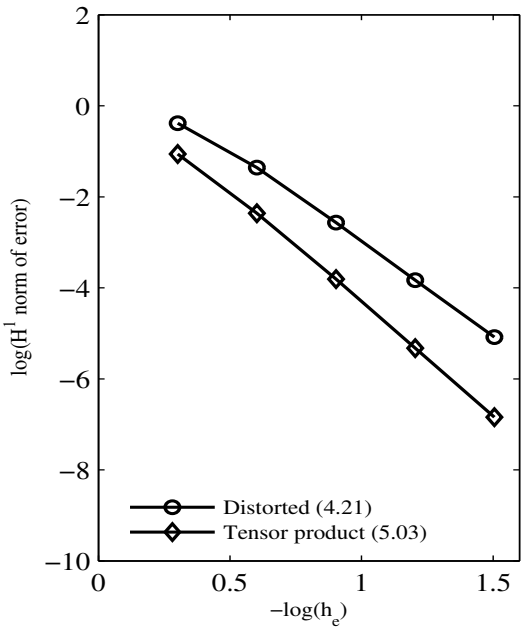

(c) H^1 norm of error in u versus h_e

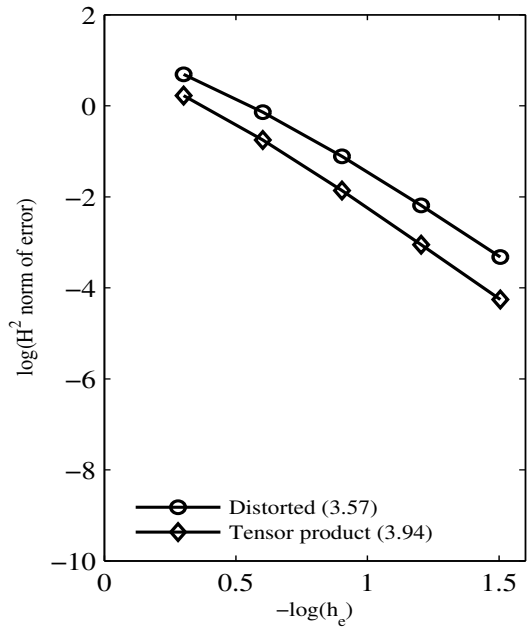

(d) H^2 norm of error in u versus h_e

Figure 4.34: Comparison of Distorted HGDA and Tensor product elements versus discretization length for 2-D Convection-diffusion equation : $\boldsymbol{C^{22}}$, $\boldsymbol{p_\xi = p_\eta = 5}$, **Undistorted discretizations**

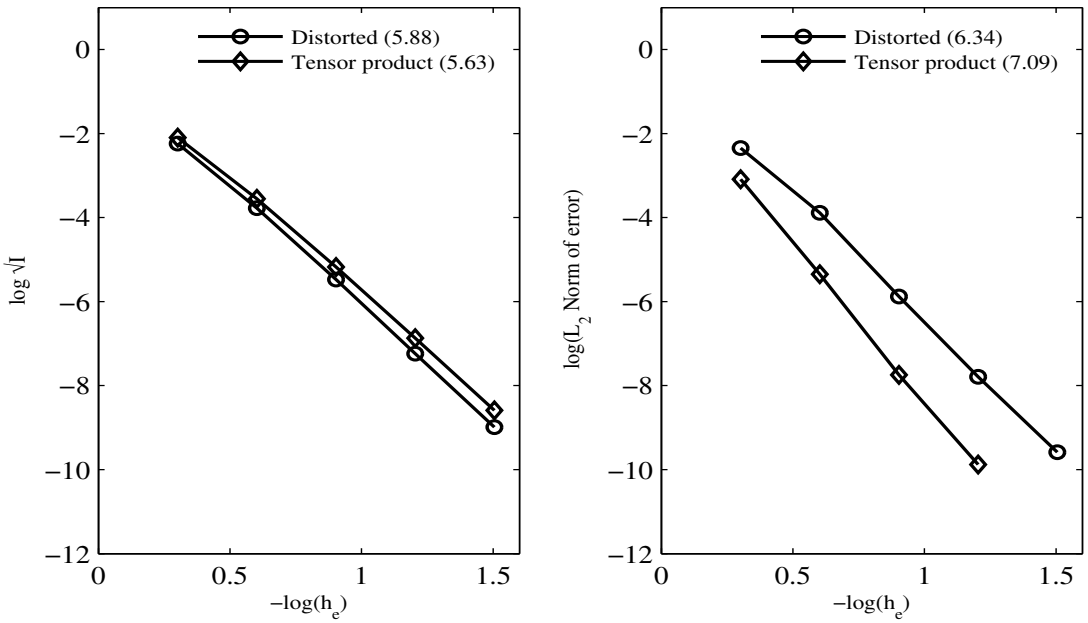

(a) $\sqrt{I}$ versus h_e

(b) L_2 norm of error in u versus h_e

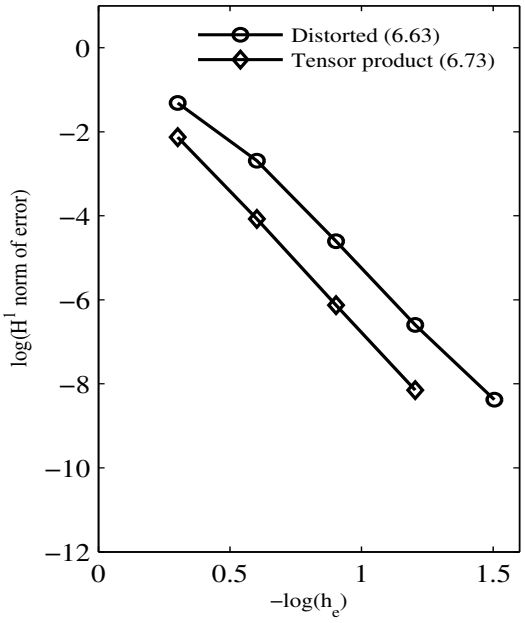

(c) H^1 norm of error in u versus h_e

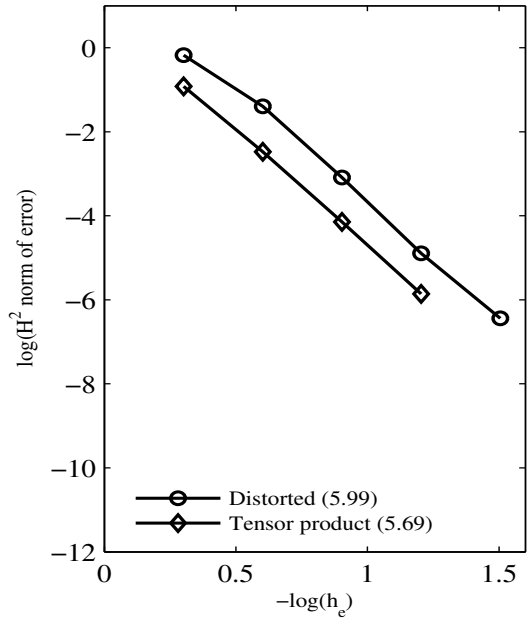

(d) H^2 norm of error in u versus h_e

Figure 4.35: Comparison of Distorted HGDA and Tensor product elements versus discretization length for 2-D Convection-diffusion equation : C^{33}, $p_\xi = p_\eta = 7$, **Undistorted discretizations**

Table 4.7: Convergence rates for 2-D Convection-diffusion equation : h-convergence, Undistorted discretizations using Distorted HGDA and Tensor product elements

(a) $\sqrt{I}$ versus h_e

$\mathbf{C^{ij}}$	Distorted	Tensor Product
C^{11} ; p=3	2.09	1.91
C^{22} : p=5	4.01	3.93
C^{33} : p=7	5.88	5.63

(b) L_2 - norm of error versus h_e

$\mathbf{C^{ij}}$	Distorted	Tensor Product
C^{11} ; p=3	1.42	3.78
C^{22} : p=5	4.2	6.09
C^{33} : p=7	6.34	7.09

(c) H^1 - norm of error versus h_e

$\mathbf{C^{ij}}$	Distorted	Tensor Product
C^{11} ; p=3	1.49	2.97
C^{22} : p=5	4.21	5.03
C^{33} : p=7	6.63	6.73

(d) H^2 - norm of error versus h_e

$\mathbf{C^{ij}}$	Distorted	Tensor Product
C^{11} ; p=3	1.57	1.93
C^{22} : p=5	3.57	3.94
C^{33} : p=7	5.99	5.69

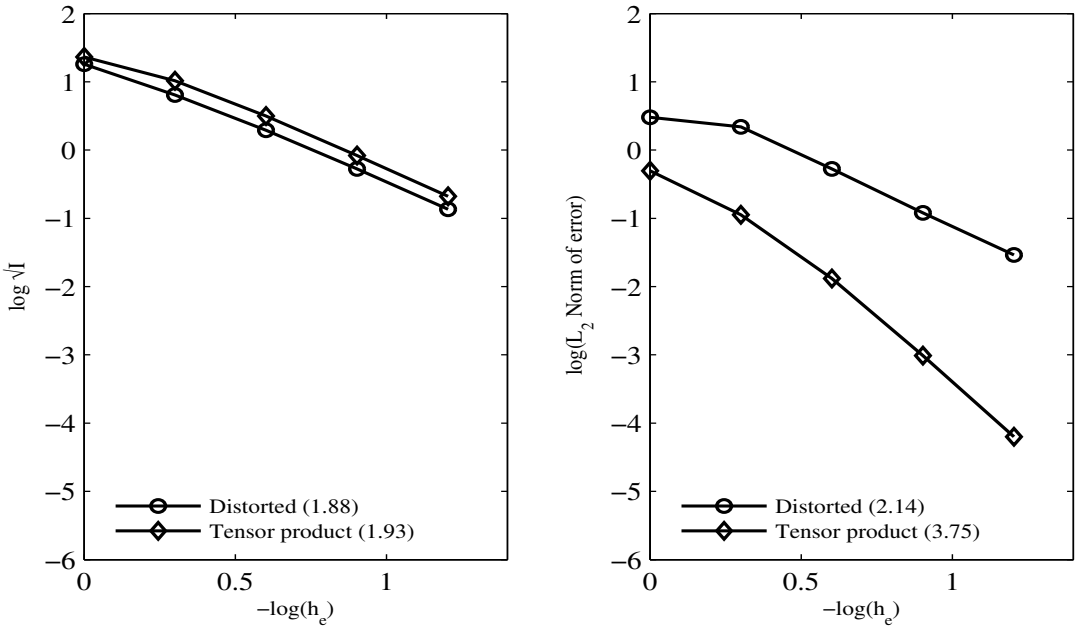

(a) $\sqrt{I}$ versus h_e

(b) L_2 norm of error in u versus h_e

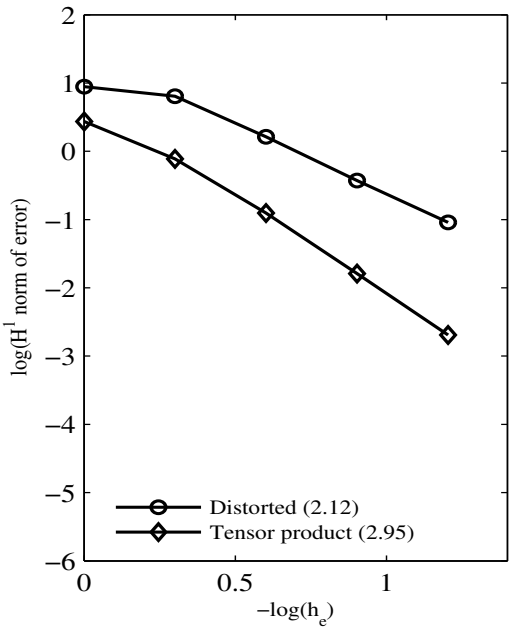

(c) H^1 norm of error in u versus h_e

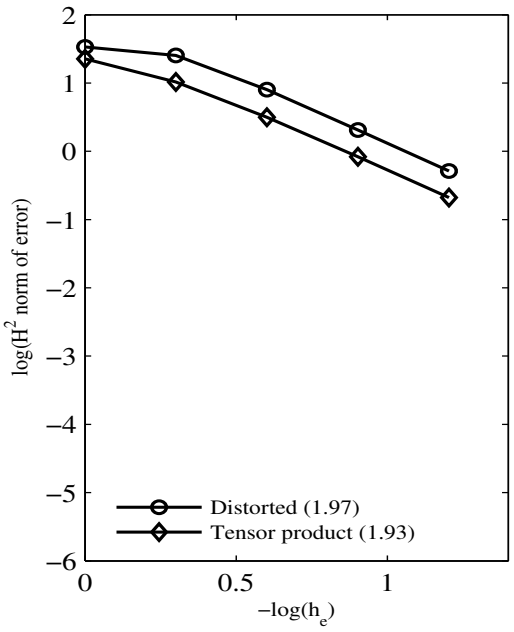

(d) H^2 norm of error in u versus h_e

Figure 4.36: Comparison of Distorted HGDA and Tensor product elements versus discretization length for 2-D non-linear Poisson's equation : C^{11}, $p_\xi = p_\eta = 3$, **Undistorted discretizations**

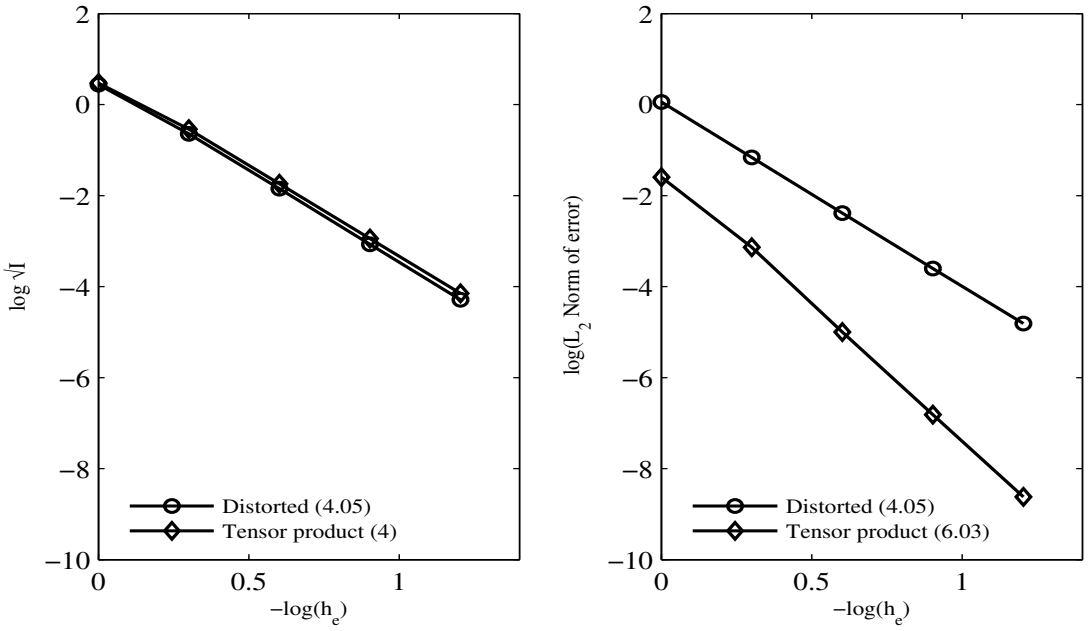

(a) $\sqrt{I}$ versus h_e

(b) L_2 norm of error in u versus h_e

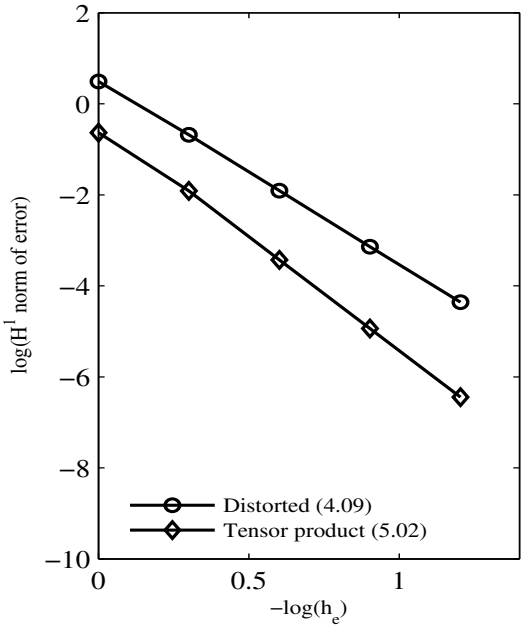

(c) H^1 norm of error in u versus h_e

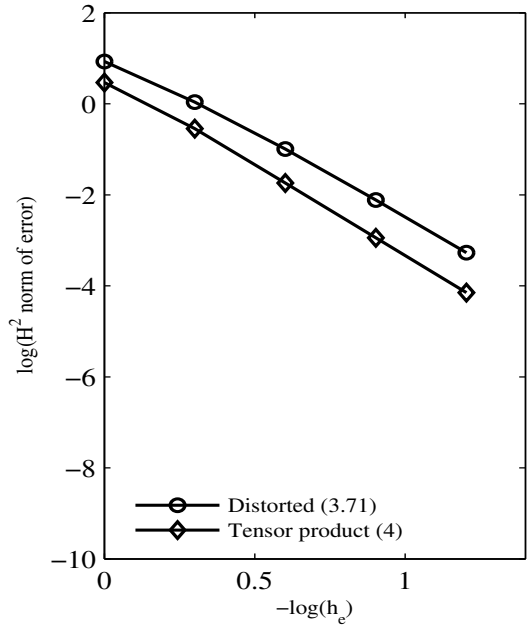

(d) H^2 norm of error in u versus h_e

Figure 4.37: Comparison of Distorted HGDA and Tensor product elements versus discretization length for 2-D non-linear Poisson's equation : C^{22}, $p_\xi = p_\eta = 5$, **Undistorted discretizations**

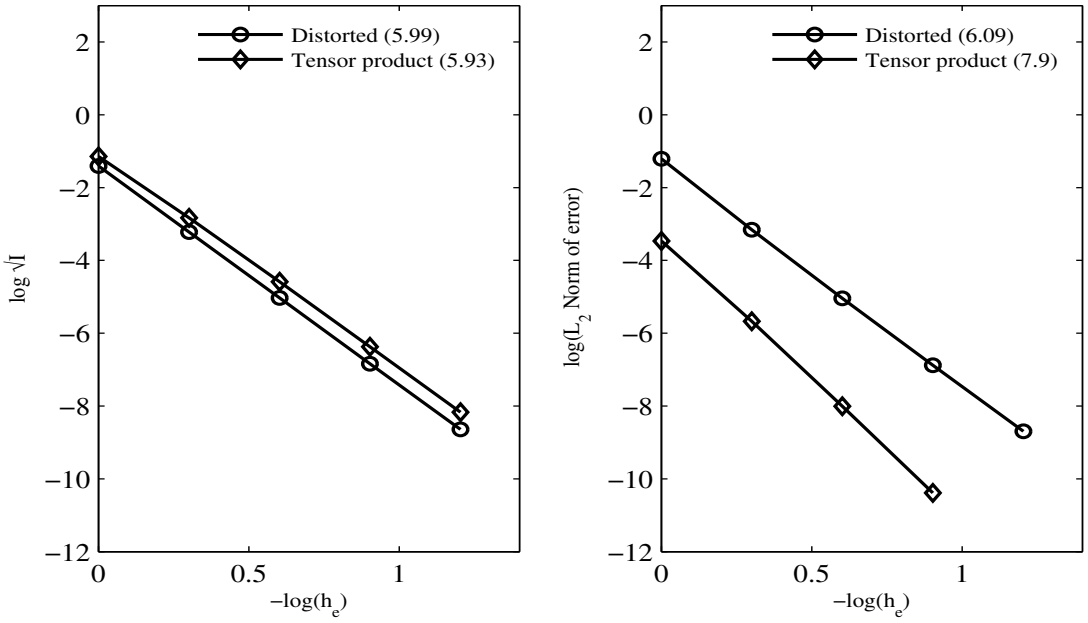

(a) √I versus h_e

(b) L_2 norm of error in u versus h_e

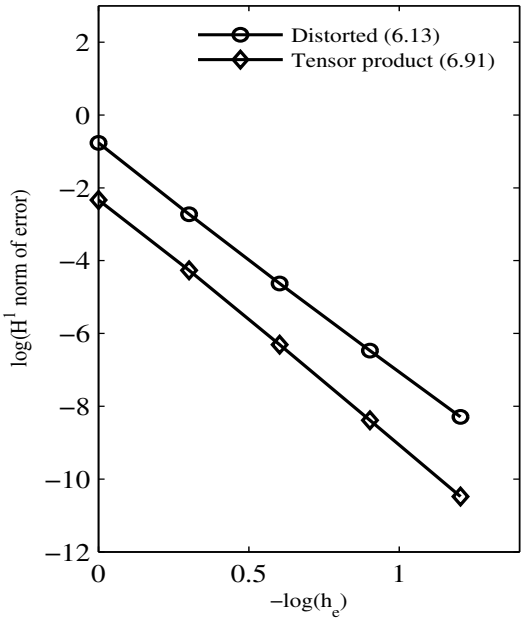

(c) H^1 norm of error in u versus h_e

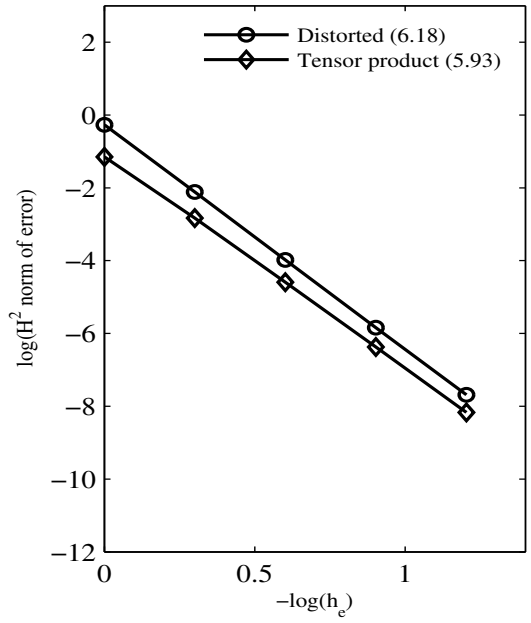

(d) H^2 norm of error in u versus h_e

Figure 4.38: Comparison of Distorted HGDA and Tensor product elements versus discretization length for 2-D non-linear Poisson's equation : $\boldsymbol{C^{33}}$, $\boldsymbol{p_\xi = p_\eta = 7}$, **Undistorted discretizations**

Table 4.8: Convergence rates for 2-D non-linear Poisson's equation : h-convergence, Undistorted discretizations using Distorted HGDA and Tensor product elements

(a) $\sqrt{I}$ versus h_e

$\mathbf{C^{ij}}$	Distorted	Tensor Product
C^{11} ; p=3	1.88	1.93
C^{22} : p=5	4.05	4
C^{33} : p=7	5.99	5.93

(b) L_2 - norm of error versus h_e

$\mathbf{C^{ij}}$	Distorted	Tensor Product
C^{11} ; p=3	2.14	3.75
C^{22} : p=5	4.05	6.03
C^{33} : p=7	6.09	7.9

(c) H^1 - norm of error versus h_e

$\mathbf{C^{ij}}$	Distorted	Tensor Product
C^{11} ; p=3	2.12	2.95
C^{22} : p=5	4.09	5.02
C^{33} : p=7	6.13	6.91

(d) H^2 - norm of error versus h_e

$\mathbf{C^{ij}}$	Distorted	Tensor Product
C^{11} ; p=3	1.97	1.93
C^{22} : p=5	3.71	4
C^{33} : p=7	6.18	5.93

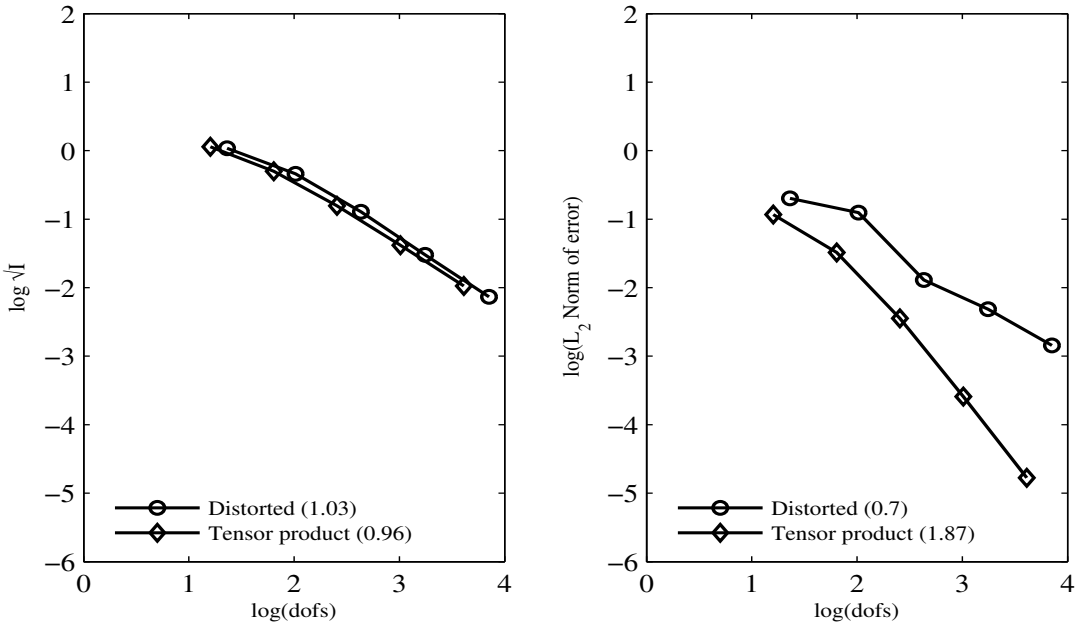

(a) $\sqrt{I}$ versus dofs

(b) L_2 norm of error in u versus dofs

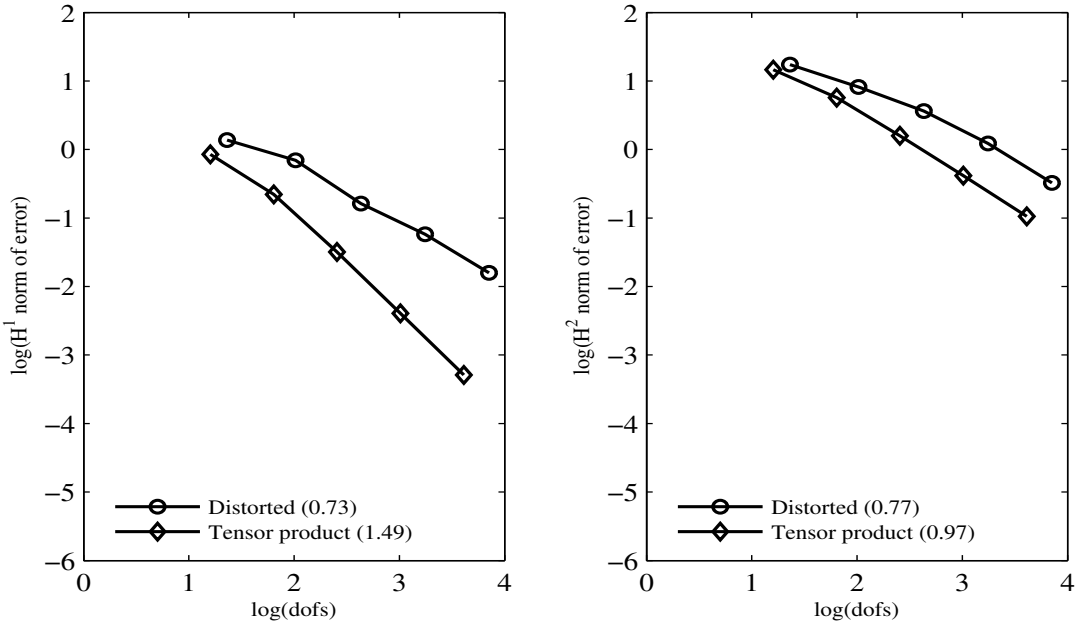

(c) H^1 norm of error in u versus dofs

(d) H^2 norm of error in u versus dofs

Figure 4.39: Comparison of Distorted HGDA and Tensor product elements versus degrees of freedom for 2-D Convection-diffusion equation : C^{11}, $p_\xi = p_\eta = 3$, **Undistorted discretizations**

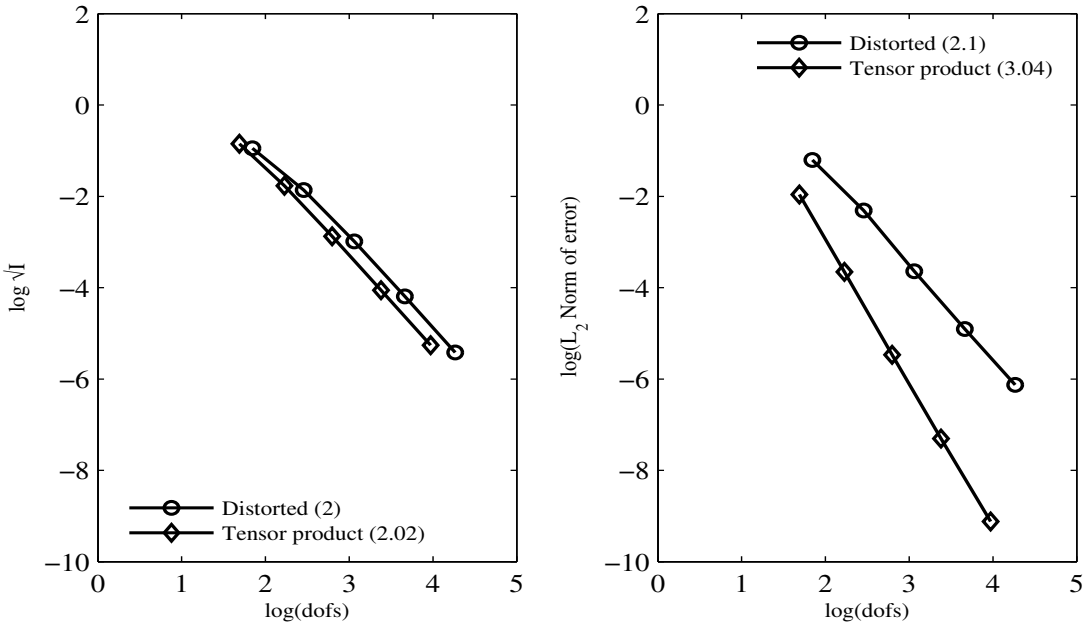

(a) √I versus dofs

(b) L_2 norm of error in u versus dofs

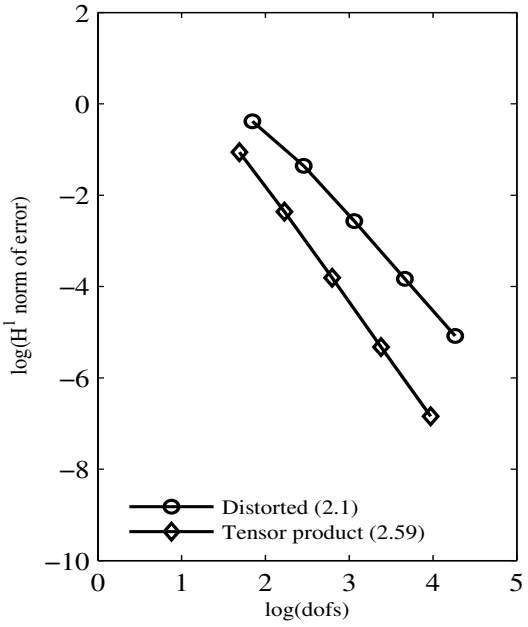

(c) H^1 norm of error in u versus dofs

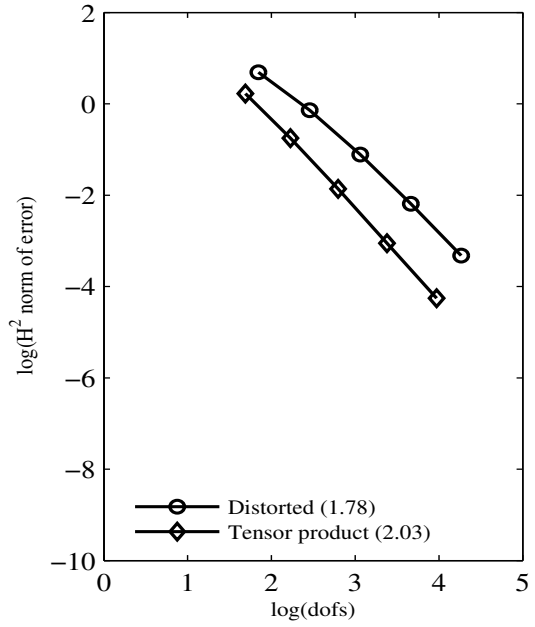

(d) H^2 norm of error in u versus dofs

Figure 4.40: Comparison of Distorted HGDA and Tensor product elements versus degrees of freedom for 2-D Convection-diffusion equation : $\boldsymbol{C^{22}}$, $\boldsymbol{p_\xi = p_\eta = 5}$, **Undistorted discretizations**

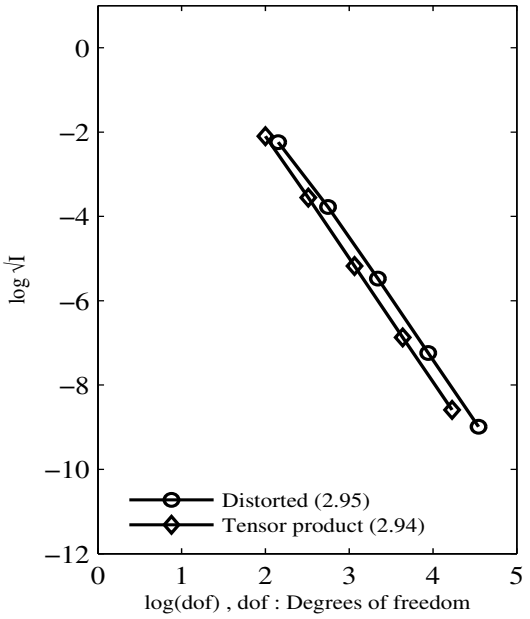

(a) √I versus dofs

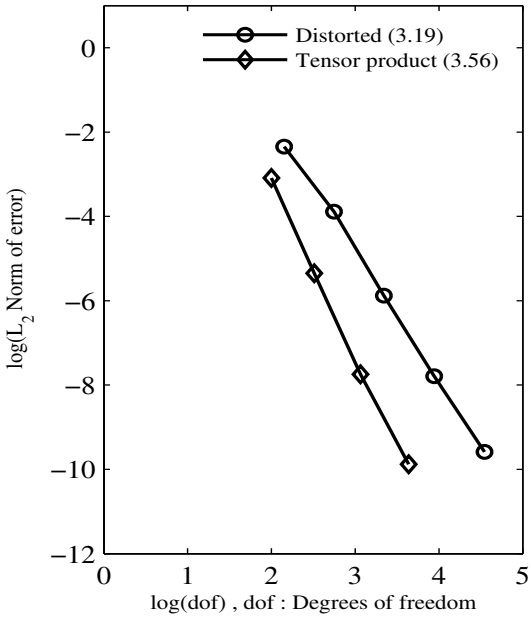

(b) L_2 norm of error in u versus dofs

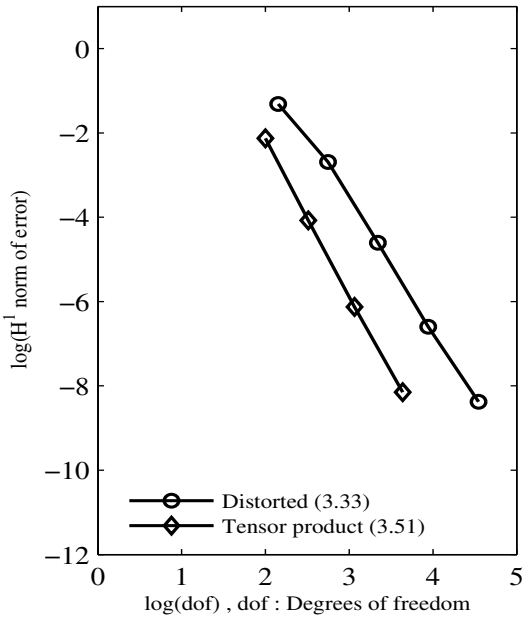

(c) H^1 norm of error in u versus dofs

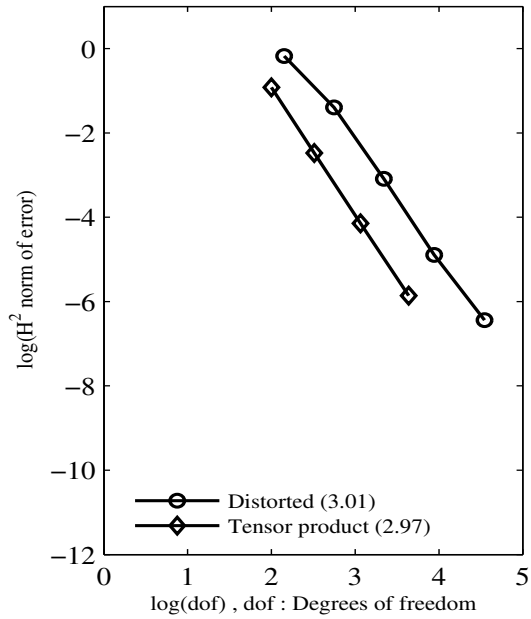

(d) H^2 norm of error in u versus dofs

Figure 4.41: Comparison of Distorted HGDA and Tensor product elements versus degrees of freedom for 2-D Convection-diffusion equation : C^{33}, $p_\xi = p_\eta = 7$, **Undistorted discretizations**

Table 4.9: Convergence rates for 2-D Convection-diffusion equation : h-convergence, Undistorted discretizations using Distorted HGDA and Tensor product elements

(a) $\sqrt{I}$ versus dofs

$\mathbf{C^{ij}}$	Distorted	Tensor Product
C^{11} ; p=3	1.03	0.96
C^{22} : p=5	2	2.02
C^{33} : p=7	2.95	2.94

(b) L_2 - norm of error versus dofs

$\mathbf{C^{ij}}$	Distorted	Tensor Product
C^{11} ; p=3	0.7	1.87
C^{22} : p=5	2.1	3.04
C^{33} : p=7	3.19	3.56

(c) H^1 - norm of error versus dofs

$\mathbf{C^{ij}}$	Distorted	Tensor Product
C^{11} ; p=3	0.73	1.49
C^{22} : p=5	2.1	2.59
C^{33} : p=7	3.33	3.51

(d) H^2 - norm of error versus dofs

$\mathbf{C^{ij}}$	Distorted	Tensor Product
C^{11} ; p=3	0.77	0.97
C^{22} : p=5	1.78	2.03
C^{33} : p=7	3.01	2.97

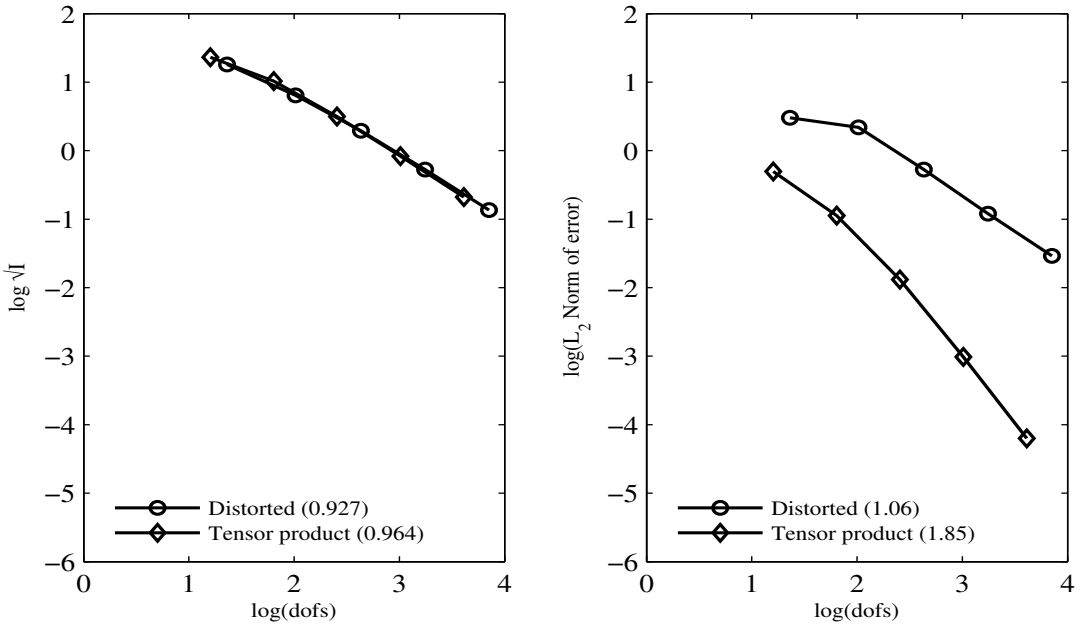

(a) $\sqrt{I}$ versus dofs

(b) L_2 norm of error in u versus dofs

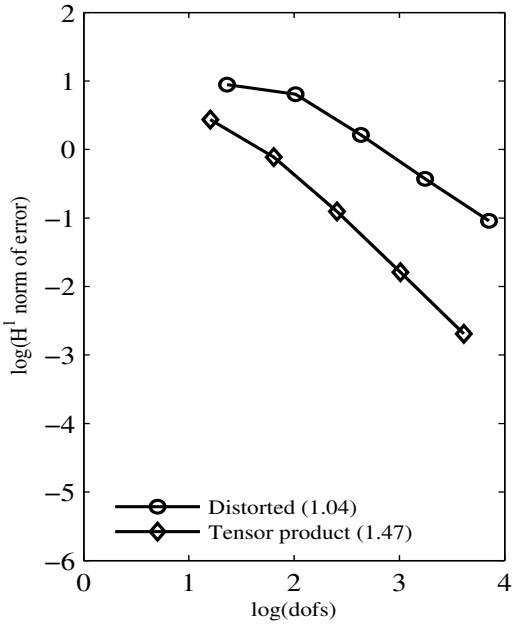

(c) H^1 norm of error in u versus dofs

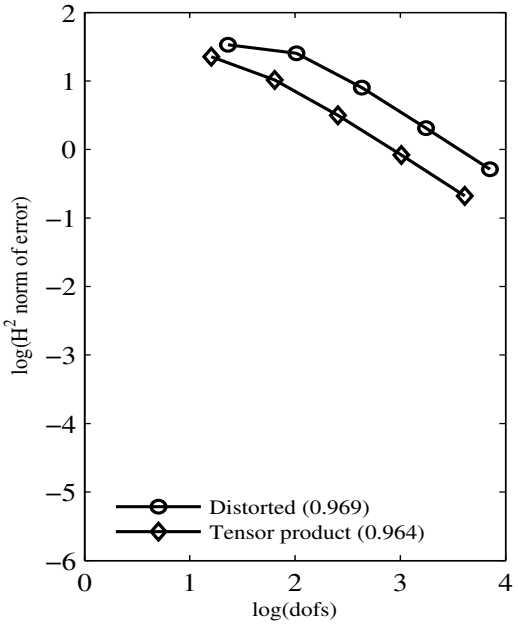

(d) H^2 norm of error in u versus dofs

Figure 4.42: Comparison of Distorted HGDA and Tensor product elements versus degrees of freedom for 2-D non-linear Poisson's equation : C^{11}, $p_\xi = p_\eta = 3$, **Undistorted discretizations**

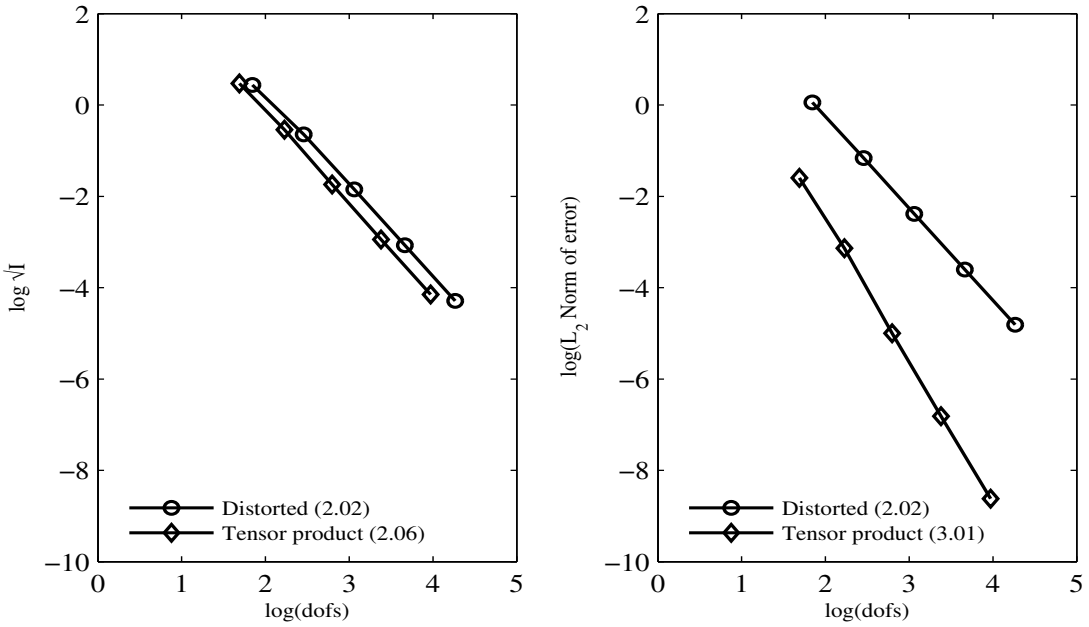

(a) √I versus dofs

(b) L_2 norm of error in u versus dofs

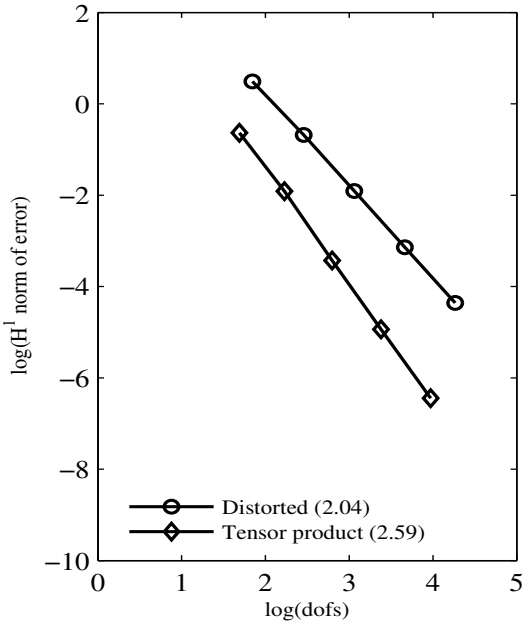

(c) H^1 norm of error in u versus dofs

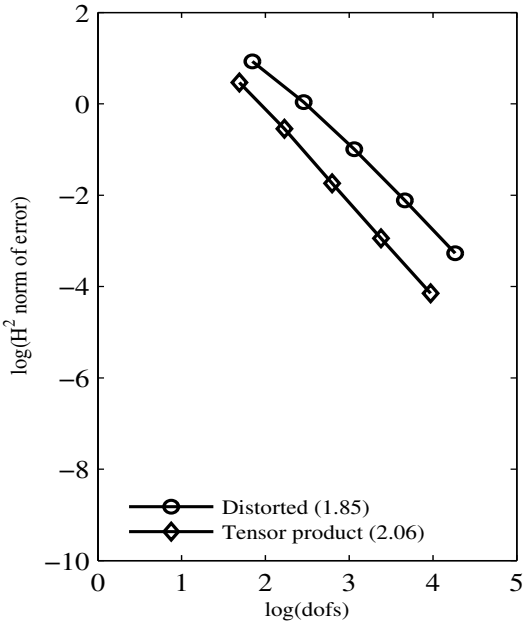

(d) H^2 norm of error in u versus dofs

Figure 4.43: Comparison of Distorted HGDA and Tensor product elements versus degrees of freedom for 2-D non-linear Poisson's equation : $\boldsymbol{C^{22}}$**,** $\boldsymbol{p_\xi = p_\eta = 5}$**, Undistorted discretizations**

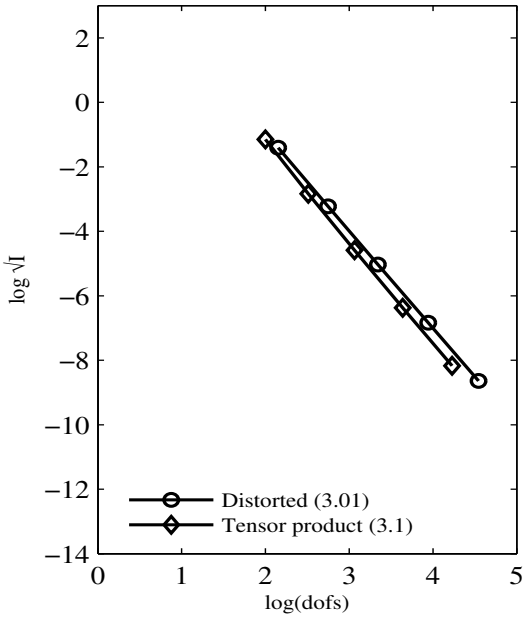

(a) √I versus dofs

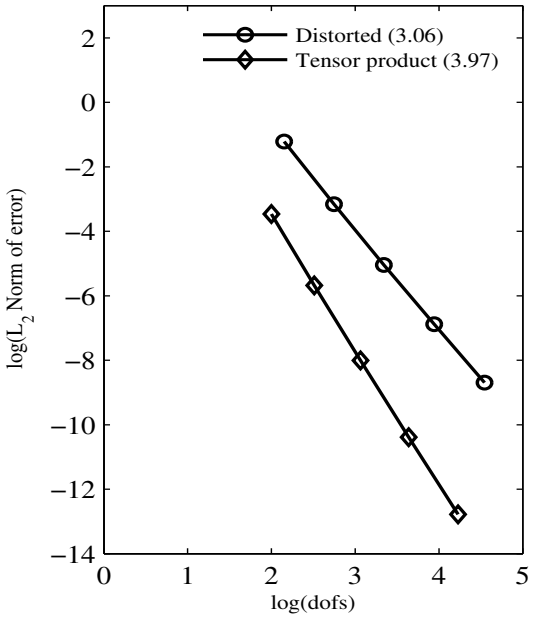

(b) L_2 norm of error in u versus dofs

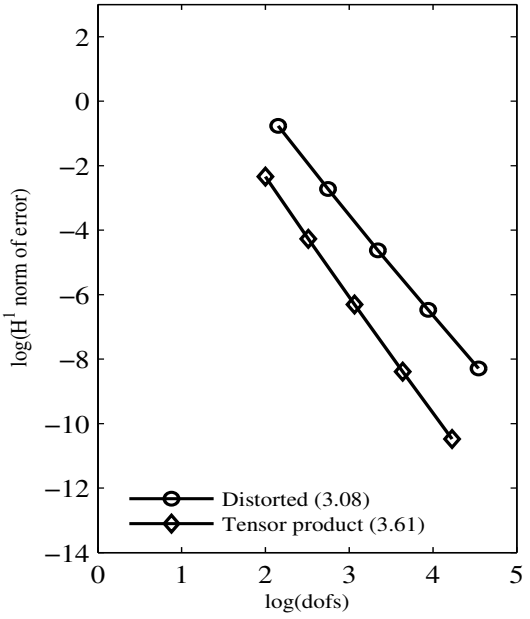

(c) H^1 norm of error in u versus dofs

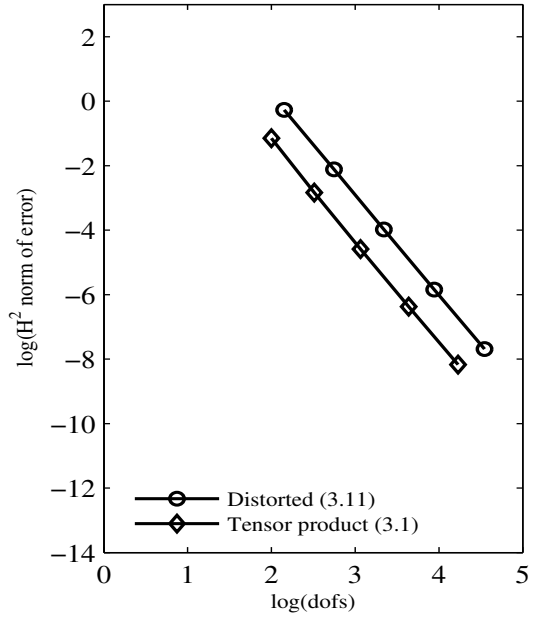

(d) H^2 norm of error in u versus dofs

Figure 4.44: Comparison of Distorted HGDA and Tensor product elements versus degrees of freedom for 2-D non-linear Poisson's equation : $\boldsymbol{C^{33}}$, $\boldsymbol{p_\xi = p_\eta = 7}$, **Undistorted discretizations**

Table 4.10: Convergence rates for 2-D non-linear Poisson's equation : h-convergence, Undistorted discretizations using Distorted HGDA and Tensor product elements

(a) $\sqrt{I}$ versus dofs

$\mathbf{C^{ij}}$	Distorted	Tensor Product
C^{11} ; p=3	0.93	0.96
C^{22} : p=5	2.02	2.06
C^{33} : p=7	3.01	3.1

(b) L_2 - norm of error versus dofs

$\mathbf{C^{ij}}$	Distorted	Tensor Product
C^{11} ; p=3	1.06	1.85
C^{22} : p=5	2.02	3.01
C^{33} : p=7	3.06	3.97

(c) H^1 - norm of error versus dofs

$\mathbf{C^{ij}}$	Distorted	Tensor Product
C^{11} ; p=3	1.04	1.47
C^{22} : p=5	2.04	2.59
C^{33} : p=7	3.08	3.61

(d) H^2 - norm of error versus dofs

$\mathbf{C^{ij}}$	Distorted	Tensor Product
C^{11} ; p=3	0.97	0.97
C^{22} : p=5	1.85	2.06
C^{33} : p=7	3.11	3.1

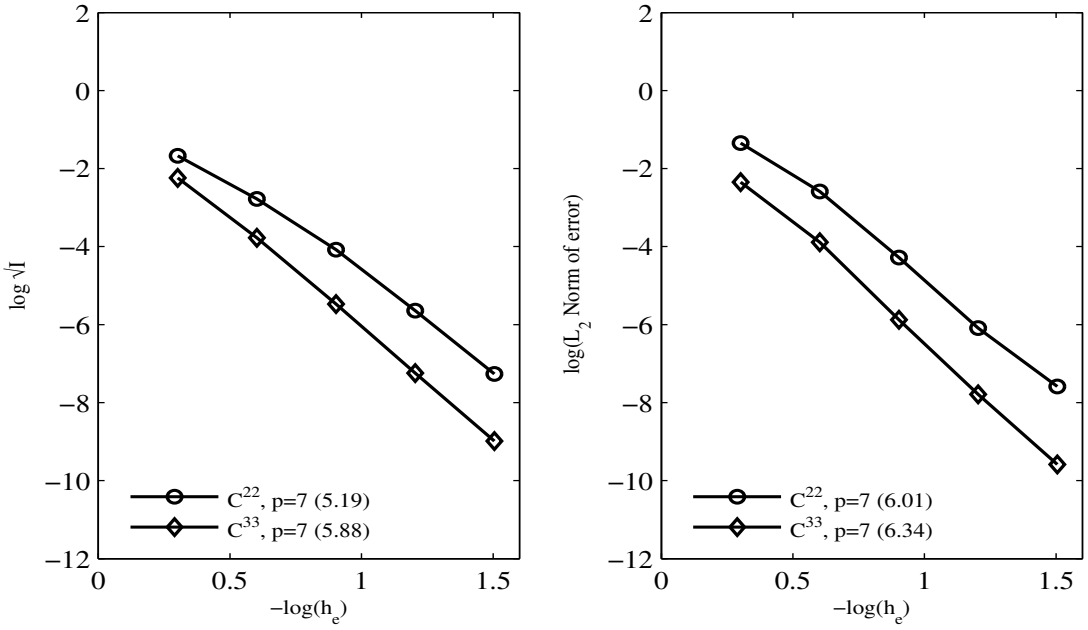

(a) √I versus h_e

(b) L_2 norm of error in u versus h_e

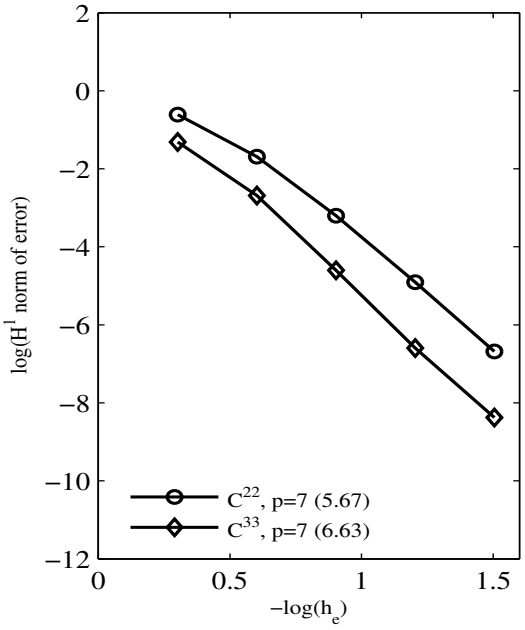

(c) H^1 norm of error in u versus h_e

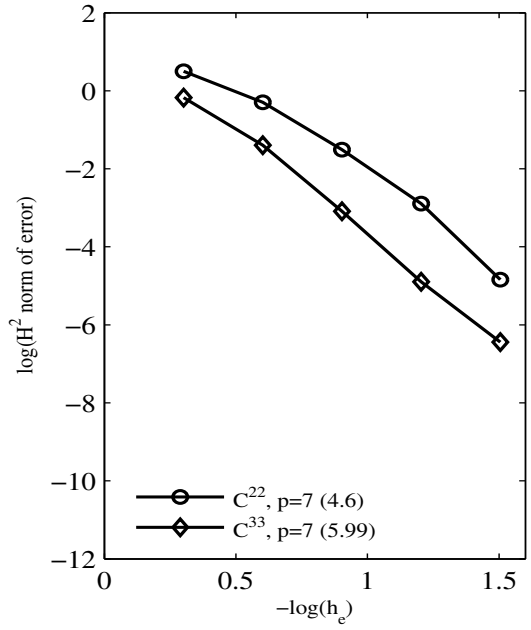

(d) H^2 norm of error in u versus h_e

Figure 4.45: Comparison of C^{ij} Distorted HGDA elements versus discretization length for 2-D Convection-diffusion equation : $\boldsymbol{C^{22}}$ $(\boldsymbol{k = 3})$, $\boldsymbol{C^{33}}$ $(\boldsymbol{k = 4}$, $\boldsymbol{p_\xi = p_\eta = 7}$, **Undistorted discretizations**

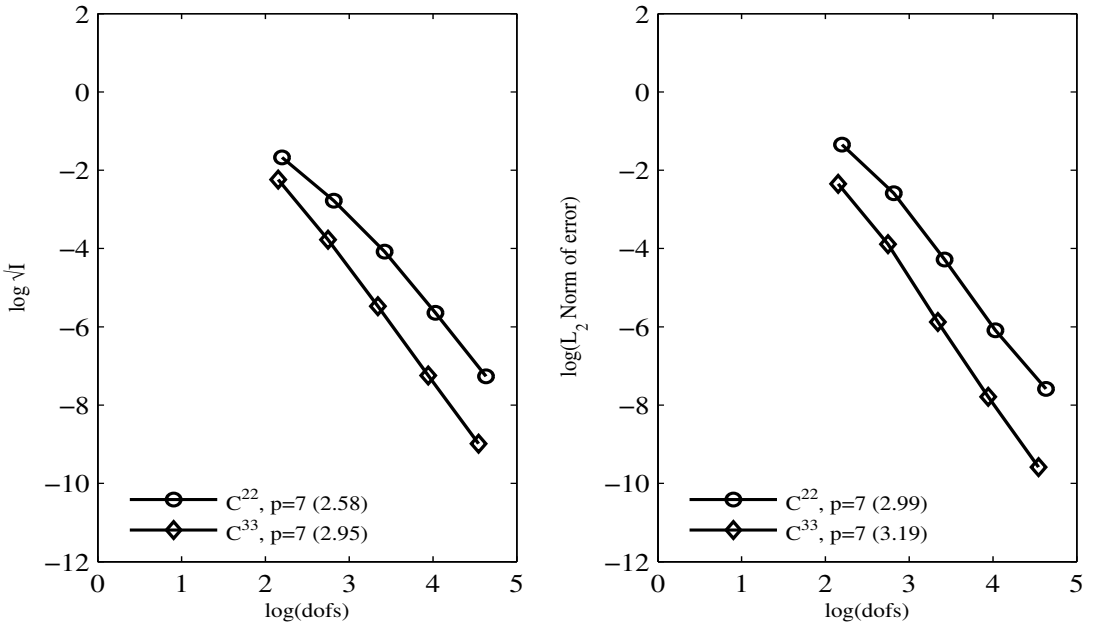

(a) √I versus dofs

(b) L_2 norm of error in u versus dofs

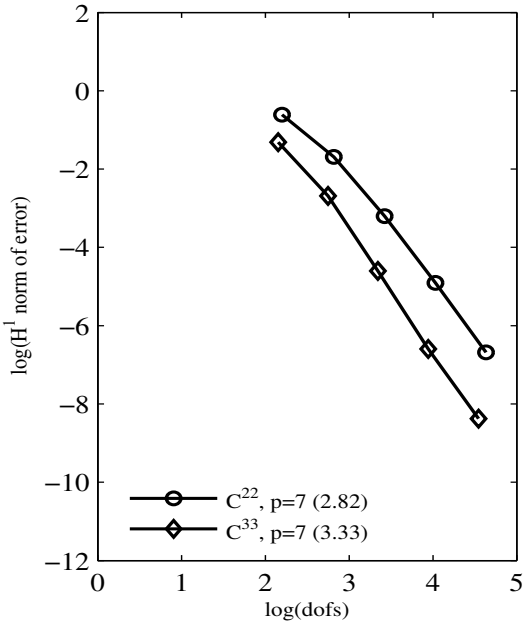

(c) H^1 norm of error in u versus dofs

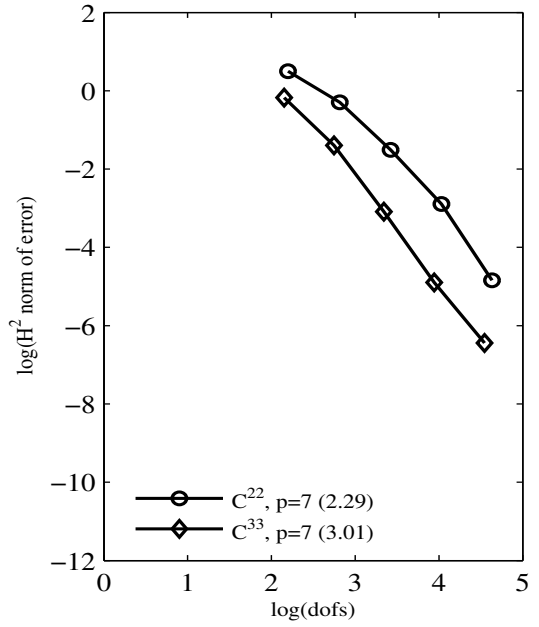

(d) H^2 norm of error in u versus dofs

Figure 4.46: Comparison of C^{ij} Distorted HGDA elements versus degrees of freedom for 2-D Convection-diffusion equation : $\boldsymbol{C^{22}}$ $(\boldsymbol{k = 3})$, $\boldsymbol{C^{33}}$ $(\boldsymbol{k = 4})$, $\boldsymbol{p_\xi = p_\eta = 7}$, **Undistorted discretizations**

Table 4.11: Convergence rates for 2-D Convection-diffusion equation : k-convergence, Undistorted discretizations using C^{22} ($k = 3$) and C^{33} ($k = 4$) Distorted HGDA elements

(a) $\sqrt{I}$

C^{ij}	$\sqrt{I}$ versus he	$\sqrt{I}$ versus dofs
C^{22} : p=7	5.19	2.58
C^{33} : p=7	5.88	2.95

(b) L_2 - norm of error

C^{ij}	L_2 - norm versus he	L_2 - norm versus dofs
C^{22} : p=7	6.01	2.99
C^{33} : p=7	6.34	3.19

(c) H^1 - norm of error

C^{ij}	H^1 - norm versus he	H^1 - norm versus dofs
C^{22} : p=7	5.67	2.82
C^{33} : p=7	6.63	3.33

(d) H^2 - norm of error

C^{ij}	H^2 - norm versus he	H^2 - norm versus dofs
C^{22} : p=7	4.6	2.29
C^{33} : p=7	5.99	3.01

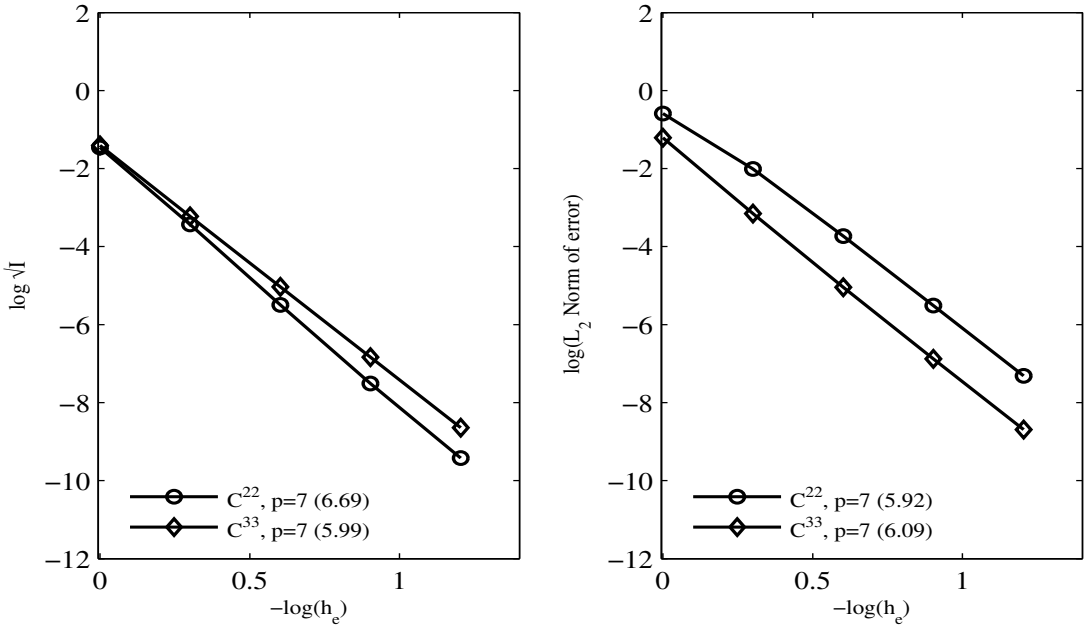

(a) √I versus h_e

(b) L_2 norm of error in u versus h_e

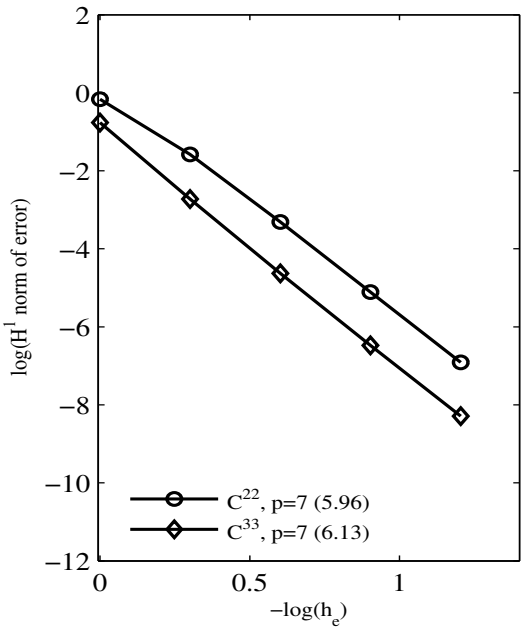

(c) H^1 norm of error in u versus h_e

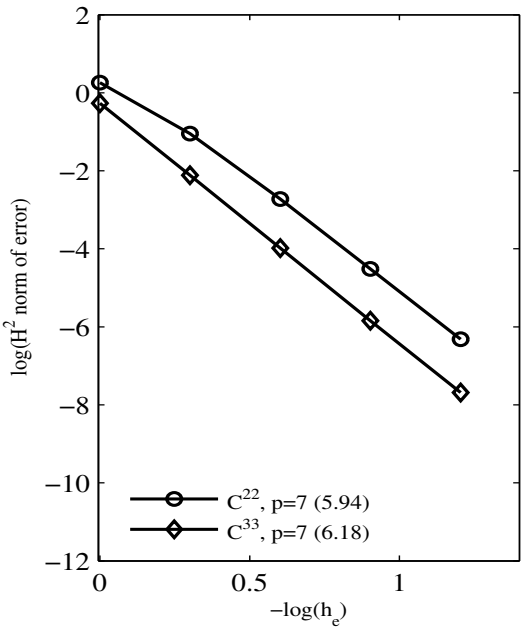

(d) H^2 norm of error in u versus h_e

Figure 4.47: Comparison of C^{ij} Distorted HGDA elements versus discretization length for 2-D non-linear Poisson's equation : $\boldsymbol{C^{22}}$ **(**$\boldsymbol{k = 3}$**)**, $\boldsymbol{C^{33}}$ **(**$\boldsymbol{k = 4}$**,** $\boldsymbol{p_\xi = p_\eta = 7}$**, Undistorted discretizations**

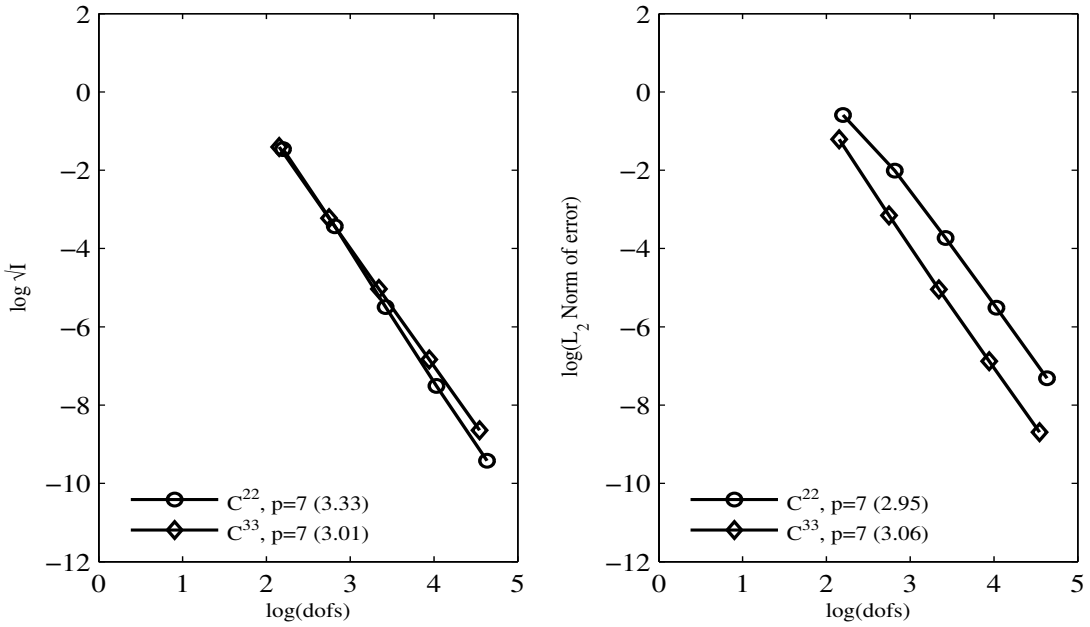

(a) √I versus dofs

(b) L_2 norm of error in u versus dofs

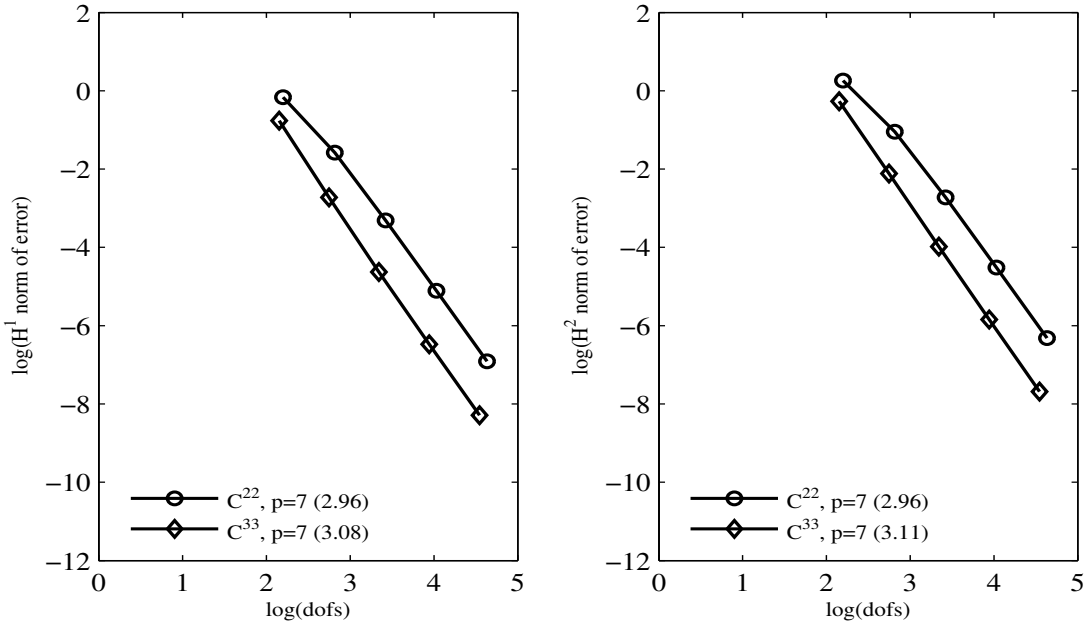

(c) H^1 norm of error in u versus dofs

(d) H^2 norm of error in u versus dofs

Figure 4.48: Comparison of C^{ij} Distorted HGDA elements versus degrees of freedom for 2-D non-linear Poisson's equation : $\boldsymbol{C^{22}}$ $\boldsymbol{(k=3)}$, $\boldsymbol{C^{33}}$ $\boldsymbol{(k=4)}$, $\boldsymbol{p_\xi = p_\eta = 7}$, **Undistorted discretizations**

Table 4.12: Convergence rates for 2-D non-linear Poisson's equation : k-convergence, Undistorted discretizations using C^{22} ($k = 3$) and C^{33} ($k = 4$) Distorted HGDA elements

(a) √I

C^{ij}	**√I versus he**	**√I versus dofs**
C^{22} : p=7	6.69	3.33
C^{33} : p=7	5.99	3.01

(b) L_2 - norm of error

C^{ij}	**L_2 - norm versus he**	**L_2 - norm versus dofs**
C^{22} : p=7	5.92	2.95
C^{33} : p=7	6.09	3.06

(c) H^1 - norm of error

C^{ij}	**H^1 - norm versus he**	**H^1 - norm versus dofs**
C^{22} : p=7	5.96	2.96
C^{33} : p=7	6.13	3.08

(d) H^2 - norm of error

C^{ij}	**H^2 - norm versus he**	**H^2 - norm versus dofs**
C^{22} : p=7	5.94	2.96
C^{33} : p=7	6.18	3.11

Discussion of results

(1) From Figures 4.33-4.44, the tensor product elements have higher convergence rates compared to distorted elements. In all cases a lower value of computed quantity of interest for tensor product elements is observed compared to the distorted elements for a given value of characteristic length or number of degrees of freedom.

(2) From Tables 4.7 and 4.8, we observe that the convergence rates depend on the p-level used in the computations. The convergence rates for the computed norms using tensor product approximations are in the vicinity of $(p-1)$ for residual or error functional and error in the H_2-norm (i.e. $\approx$ 2 for C^{11} (p=3), $\approx$ 4 for C^{22} (p=5) and $\approx$ 6 for C^{33} (p=7)). However, the convergence rates for L_2 - norm of error in solution is close to $(p+1)$ (i.e. $\approx$ 4 for C^{11} (p=3), $\approx$ 6 for C^{22} (p=5) and $\approx$ 8 for C^{33} (p=7)). The convergence rates for H_2 - norm of error in solution is p (i.e. $\approx$ 3 for C^{11} (p=3), $\approx$ 5 for C^{22} (p=5) and $\approx$ 7 for C^{33} (p=7)). When we use HGDA elements using Least squares processes we observe that the convergence rate for all the computed quantities is approximately $(p-1)$ (i.e. $\approx$ 2 for C^{11} (p=3), C^{22} (p=5) and C^{33} (p=7)).

(2) From Tables 4.9 and 4.10, the convergence rates of the computed quantities do not have an explicit relation to the p-level used in the computations as observed in (2).

(3) From Tables 4.11 and 4.12, the convergence rates for C^{22} and C^{33} HGDA elements are approximately same, but from Figures 4.45 - 4.48, for a given value of characteristic length or given number of degrees of freedom, C^{33} HGDA elements give a lower value of the quantity of interest compared to C^{22} HGDA element.

4.5.2 Numerical solutions for Undistorted mesh : p-convergence

The numerical solutions are computed using C^{22} and C^{33} HGDA elements as well as tensor product elements with progressively increasing p-levels beginning from the minimum p-level. The minimum p-levels required for C^{22} and C^{33} elements are 5 and

7 respectively. Since the operators are non self-adjoint and non-linear, we only consider Least squares processes for these numerical studies.

(i) Figures 4.49(a)-(d) show the solutions computed for two different undistorted discretizations (4 and 16 elements) with C^{22} HGDA element for 2-D convection-diffusion equation. Figures 4.50(a)-(d) show similar plots for C^{33} HGDA element. In both cases, we observe that to obtain a given value of quantity of interest, we need lesser number of degrees of freedom for four element mesh

(ii) Figures 4.51 and 4.52 show plots similar to (i) for 2-D non-linear Poisson's equation.

(iii) Figures 4.53(a)-(d) show the solutions computed for HGDA elements and tensor product elements for a 16 element undistorted discretization with C^{22} HGDA element for 2-D convection-diffusion equation. Figures 4.54(a)-(d) show similar plots for C^{33} HGDA element. From Figures 4.53 and 4.54, we observe that tensor product element has lower values of computed quantities of interest for a given number of degrees of freedom hence superior performance compared to the distorted element.

(iv) Figures 4.55 and 4.56 show plots explained in (iii) for 2-D non-linear Poisson's equation computed using a 4 element uniform discretization.

(v) Figures 4.57(a)-(d) show comparison of numerical solutions calculated using C^{22} and C^{33} HGDA elements for 2-D convection-diffusion equation with a 16 element undistorted discretization. The computed quantities of interest for C^{33} HGDA element have a lower value compared to those corresponding to C^{22} HGDA (for a given number of degrees of freedom)

(vi) Figure 4.58 shows the behavior explained in (v) for 2-D non-linear Poisson's equation computed using a 4-element uniform discretization

Remarks

(1) When the domain of definition is rectangular, tensor product elements are expected to have the best performance. This is evident from the plots of all quantities of interest for any order of approximation.

(3) The convergence rates of the computed quantities of interest in plots containing C^{33} HGDA element for both model problems are very high due to the numerical solution at p-level of 8 being in the close vicinity of the theoretical solution.

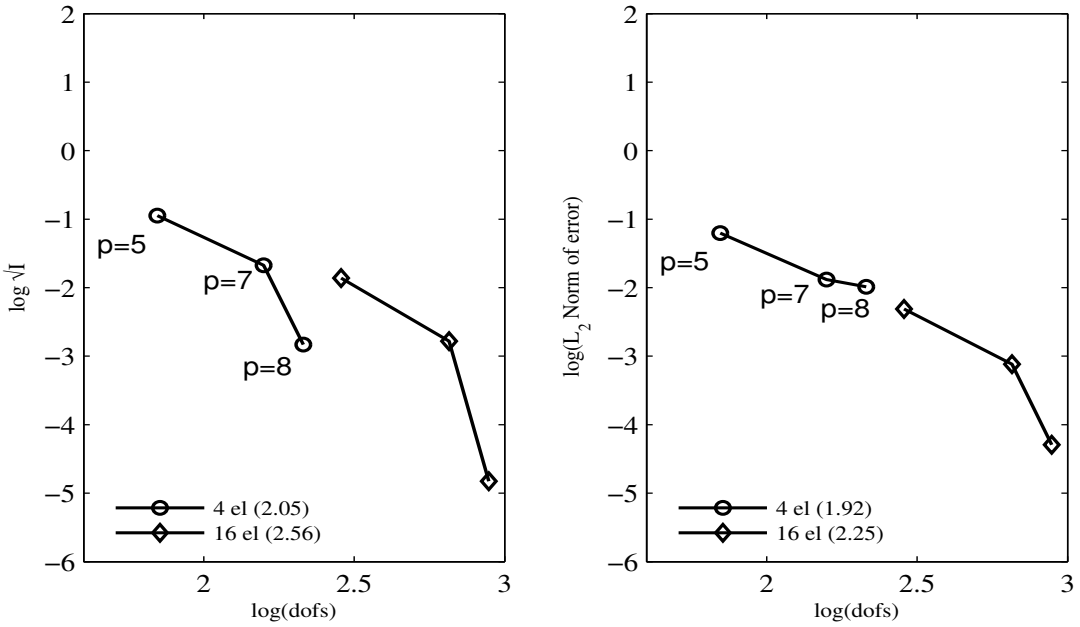

(a) √I versus dofs

(b) L_2 norm of error in u versus dofs

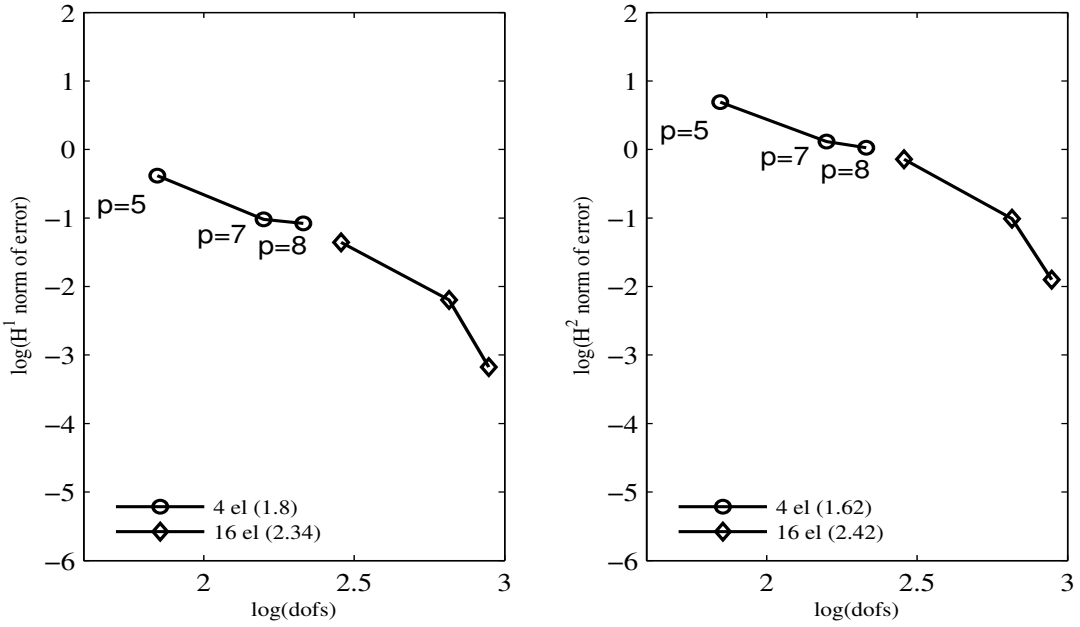

(c) H^1 norm of error in u versus dofs

(d) H^2 norm of error in u versus dofs

Figure 4.49: Comparison of 4 element and 16 element discretizations using Distorted HGDA elements for 2-D Convection-diffusion equation : C^{22}, **Undistorted discretizations**

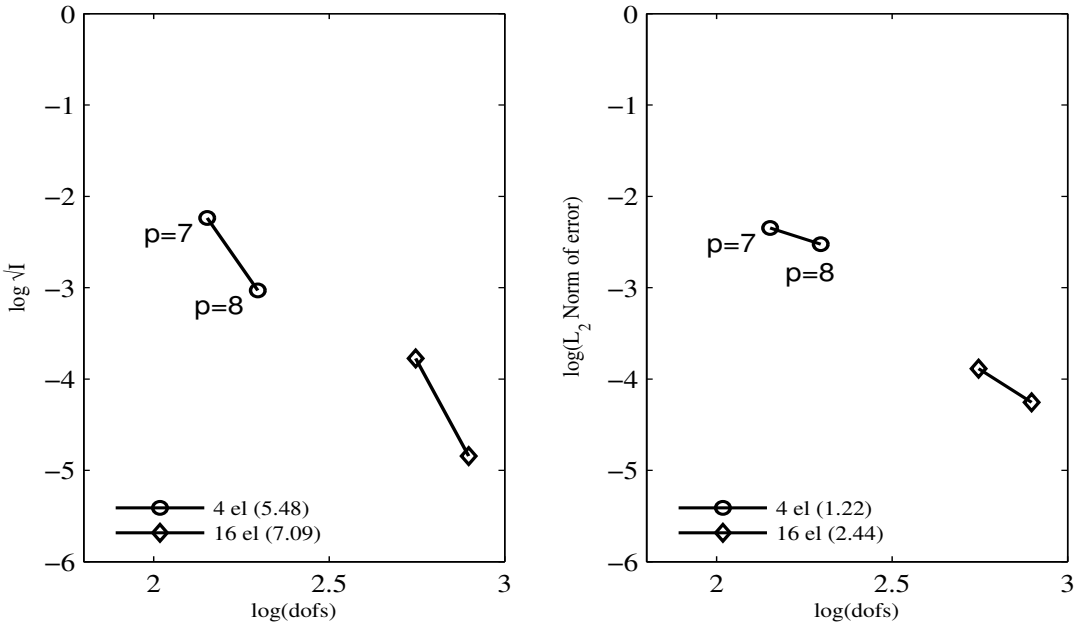

(a) √I versus dofs

(b) L_2 norm of error in u versus dofs

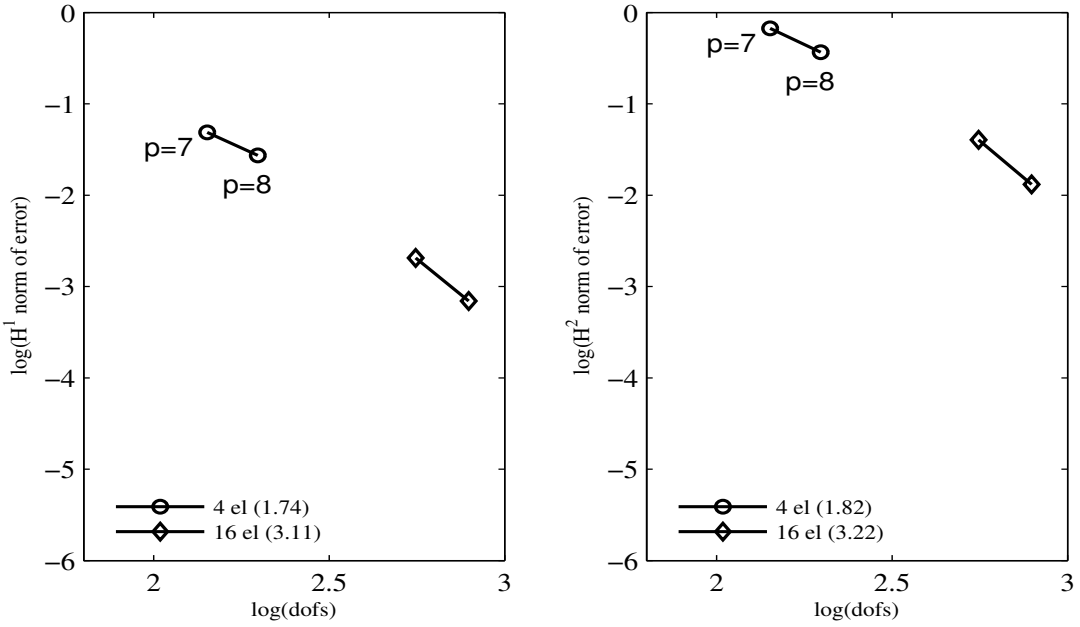

(c) H^1 norm of error in u versus dofs

(d) H^2 norm of error in u versus dofs

Figure 4.50: Comparison of 4 element and 16 element discretizations using Distorted HGDA elements for 2-D Convection-diffusion equation : C^{33}, **Undistorted discretizations**

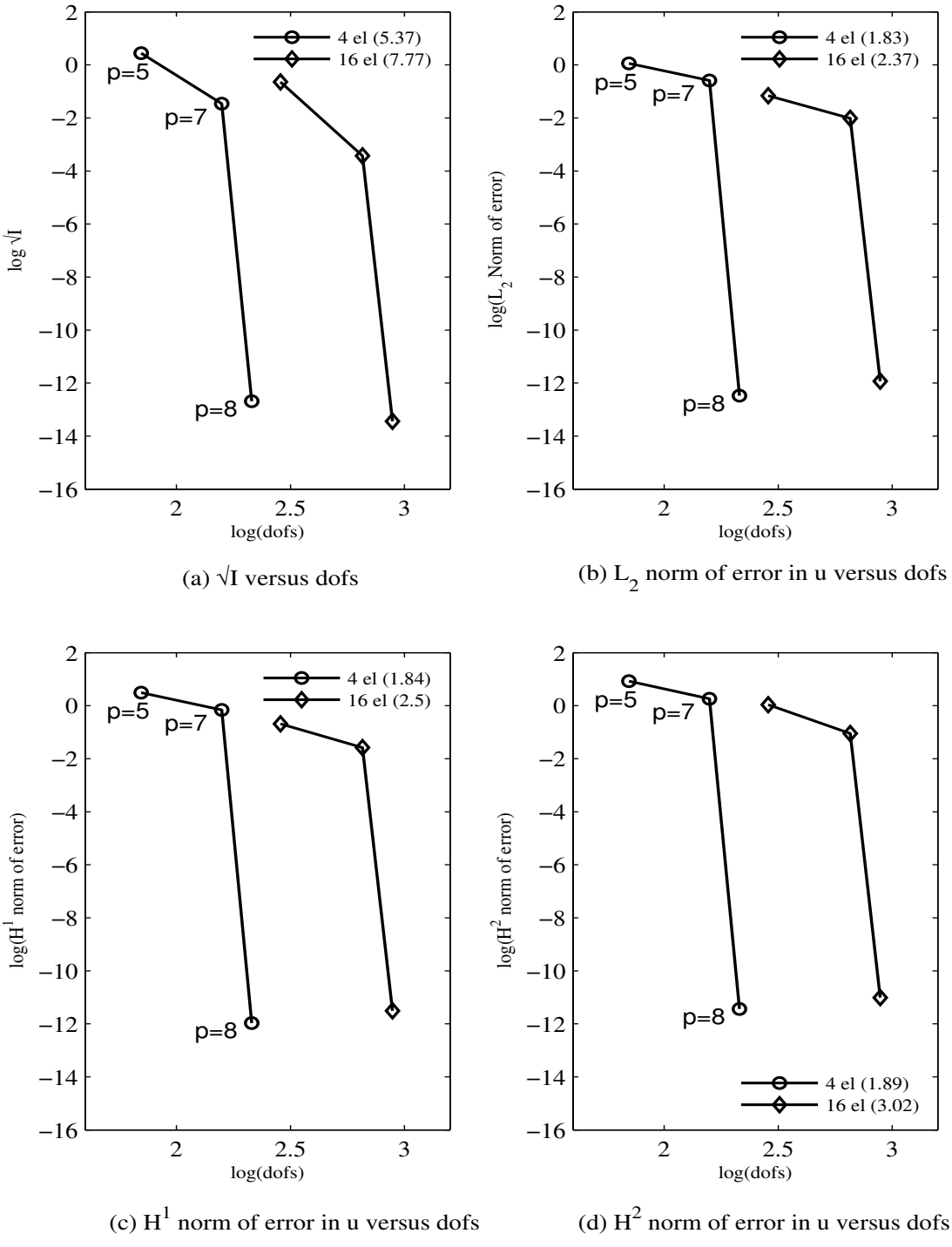

(a) √I versus dofs

(b) L_2 norm of error in u versus dofs

(c) H^1 norm of error in u versus dofs

(d) H^2 norm of error in u versus dofs

Figure 4.51: Comparison of 4 element and 16 element discretizations using Distorted HGDA elements for 2-D non-linear Poisson's equation : C^{22}, **Undistorted discretizations**

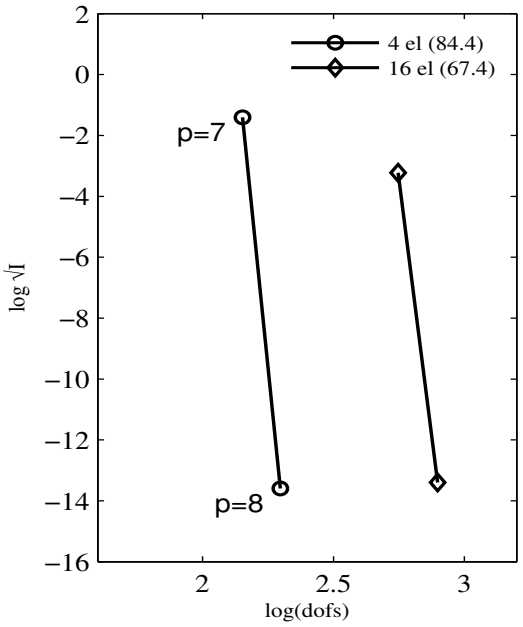

(a) √I versus dofs

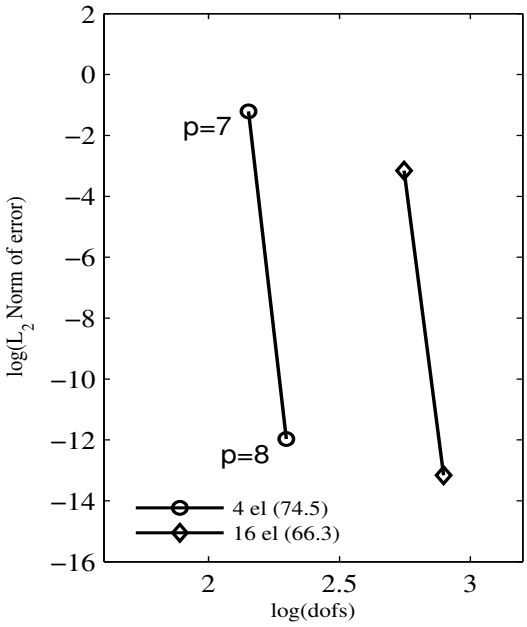

(b) L_2 norm of error in u versus dofs

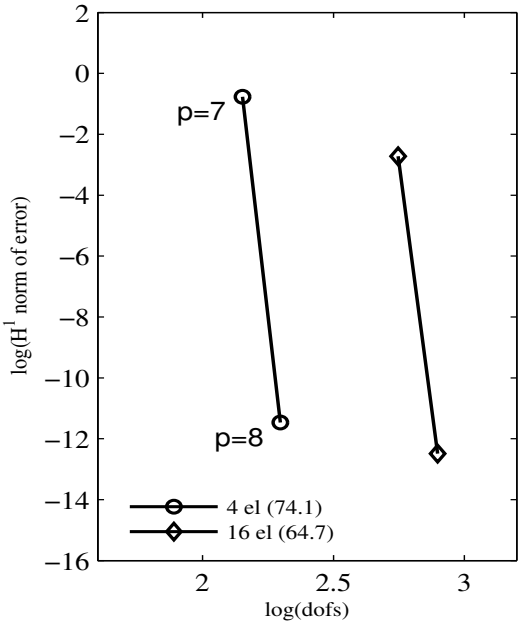

(c) H^1 norm of error in u versus dofs

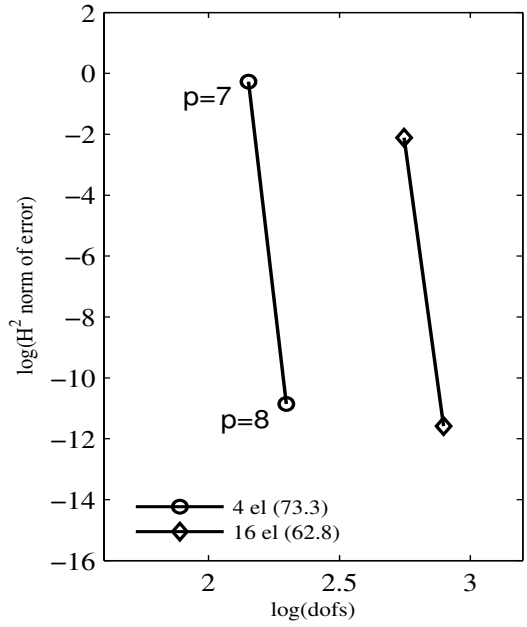

(d) H^2 norm of error in u versus dofs

Figure 4.52: Comparison of 4 element and 16 element discretizations using Distorted HGDA elements for 2-D non-linear Poisson's equation : C^{33}, **Undistorted discretizations**

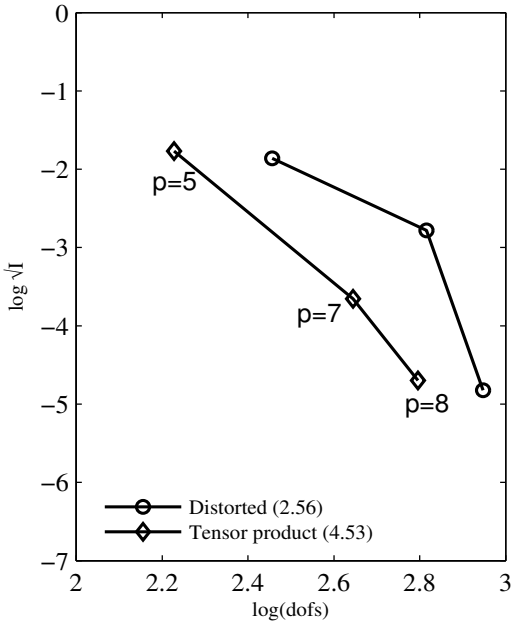

(a) √I versus dofs

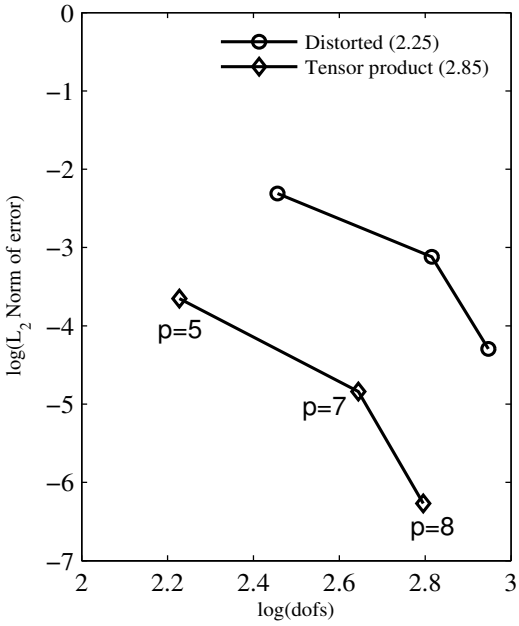

(b) L_2 norm of error in u versus dofs

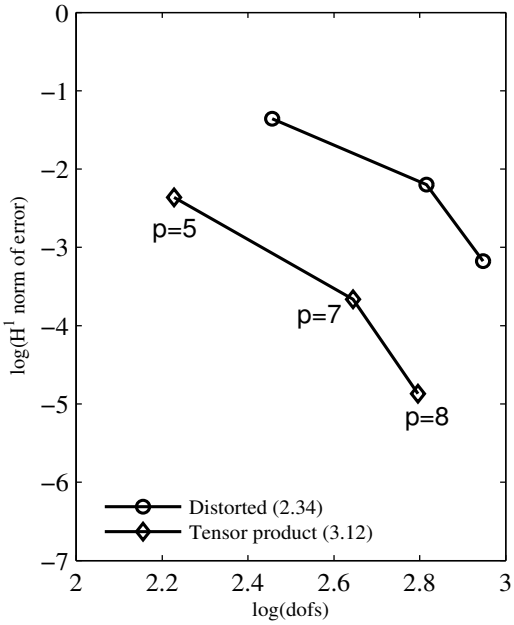

(c) H^1 norm of error in u versus dofs

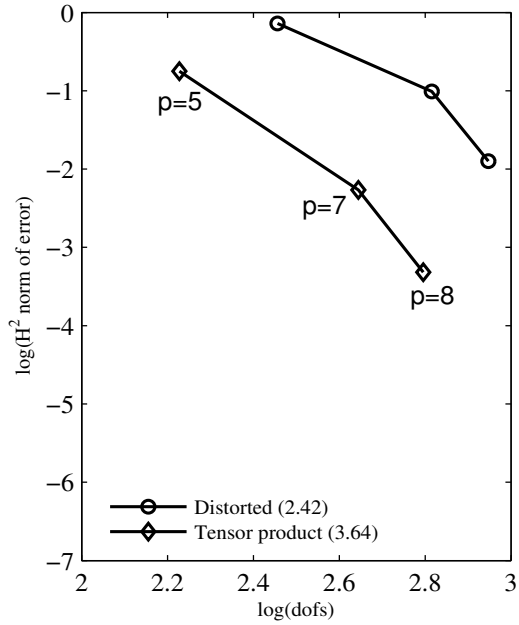

(d) H^2 norm of error in u versus dofs

Figure 4.53: Comparison of Distorted HGDA and Tensor product elements for 2-D Convection-diffusion equation : C^{22}**, 16 element Undistorted discretization**

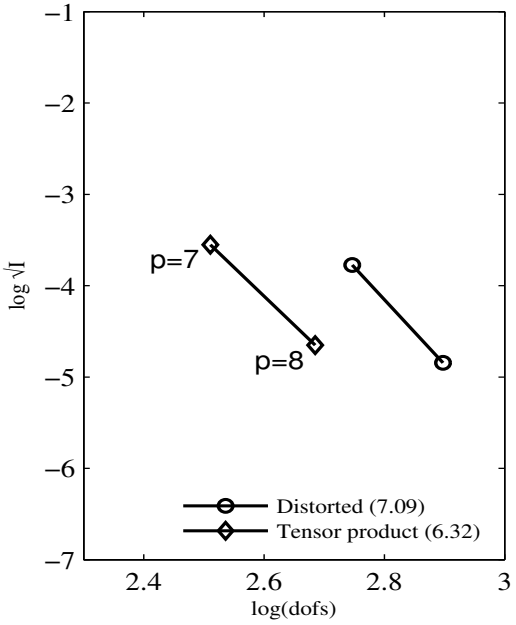

(a) $\sqrt{I}$ versus dofs

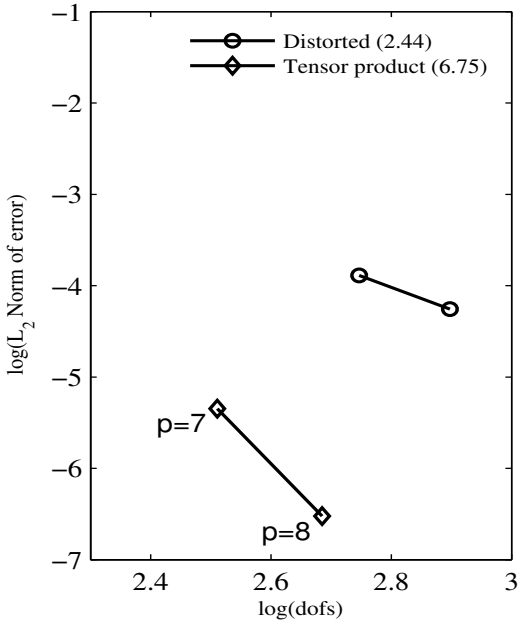

(b) L_2 norm of error in u versus dofs

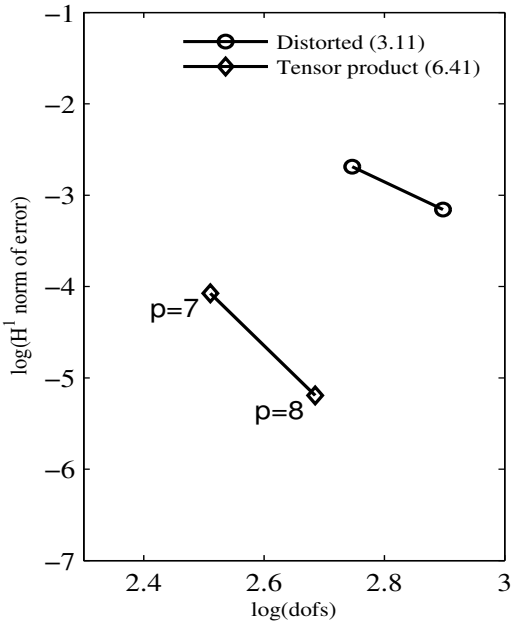

(c) H^1 norm of error in u versus dofs

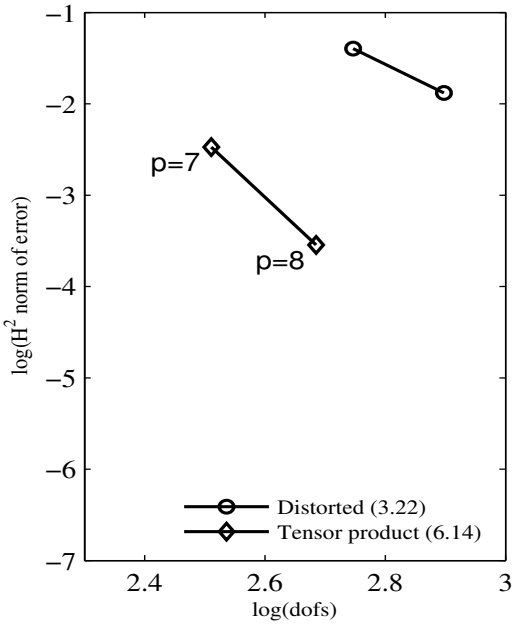

(d) H^2 norm of error in u versus dofs

Figure 4.54: Comparison of Distorted HGDA and Tensor product elements for 2-D Convection-diffusion equation : C^{33}, **16 element Undistorted discretization**

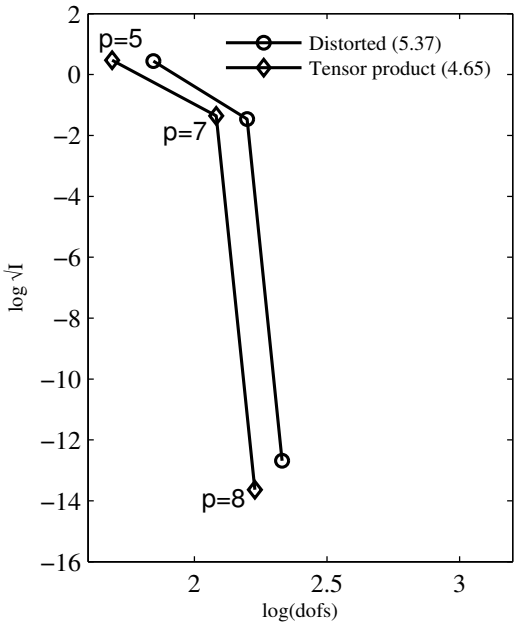

(a) √I versus dofs

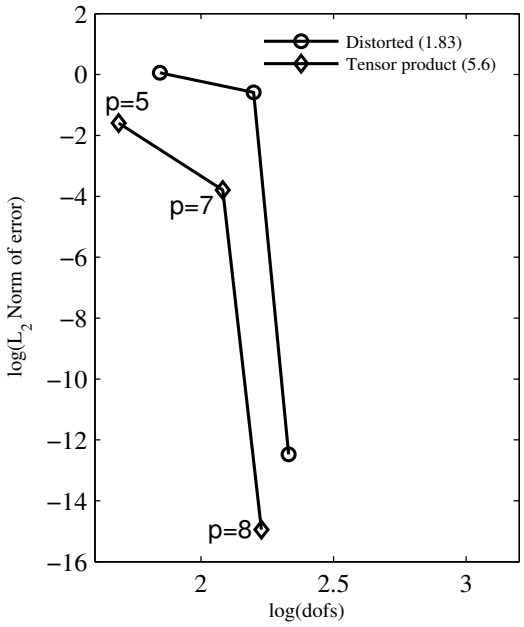

(b) L_2 norm of error in u versus dofs

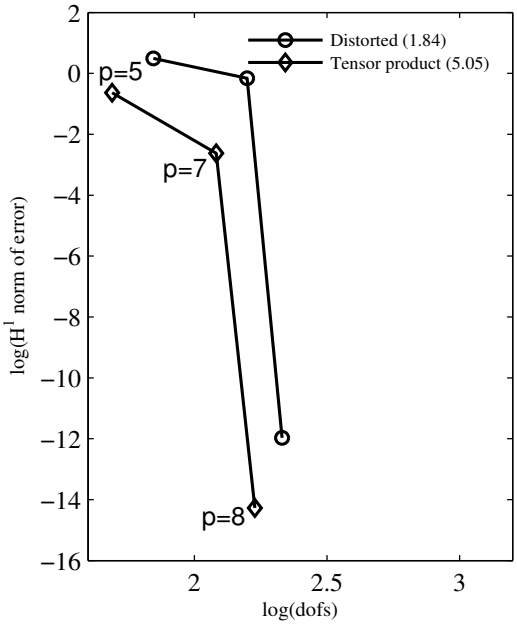

(c) H^1 norm of error in u versus dofs

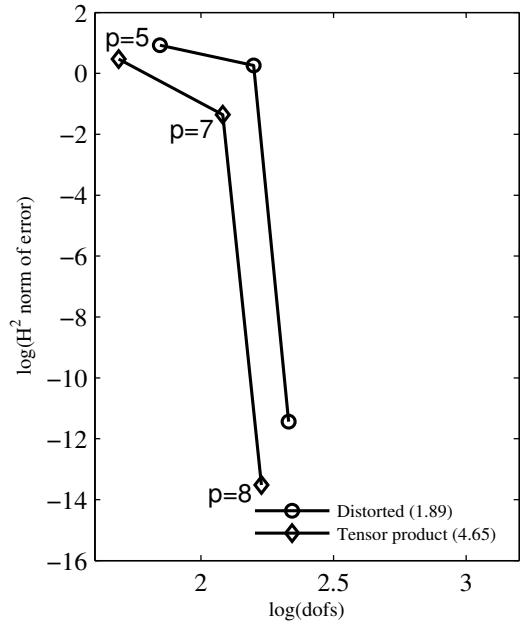

(d) H^2 norm of error in u versus dofs

Figure 4.55: Comparison of Distorted HGDA and Tensor product elements for 2-D non-linear Poisson's equation : C^{22}, **4 element Undistorted discretization**

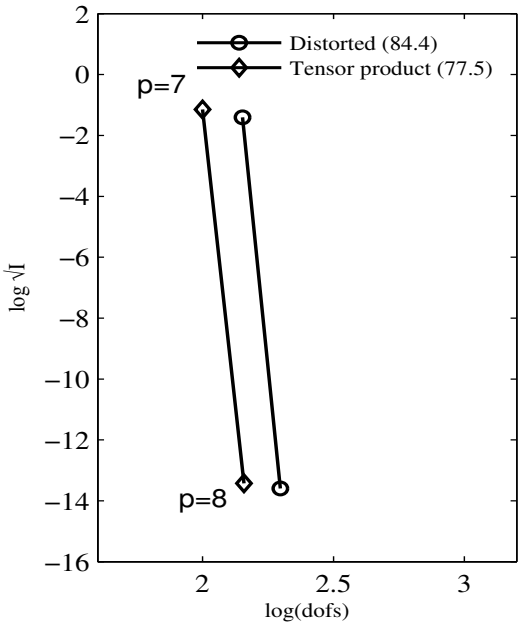

(a) √I versus dofs

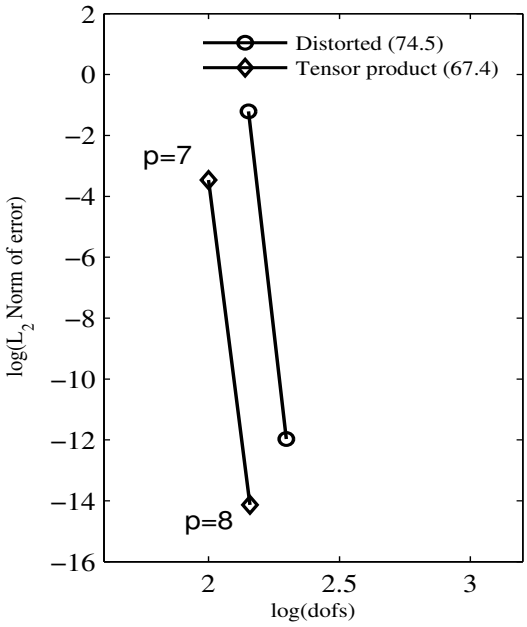

(b) L_2 norm of error in u versus dofs

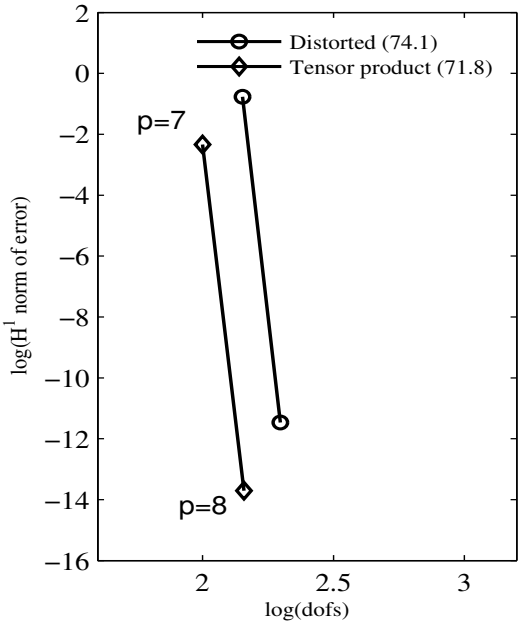

(c) H^1 norm of error in u versus dofs

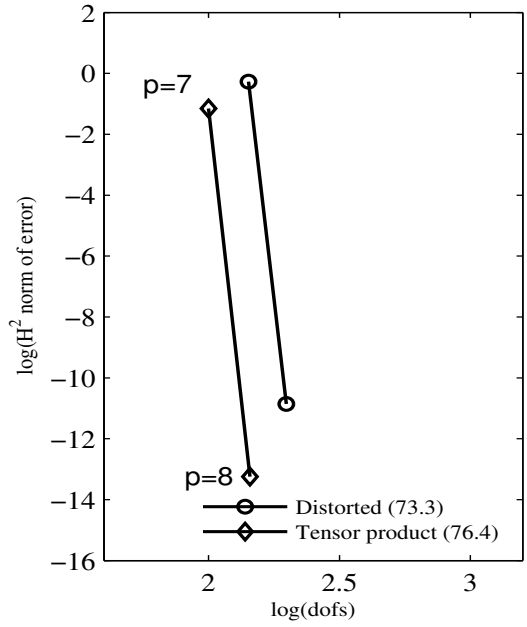

(d) H^2 norm of error in u versus dofs

Figure 4.56: Comparison of Distorted HGDA and Tensor product elements for 2-D non-linear Poisson's equation : C^{33}, **4 element Undistorted discretization**

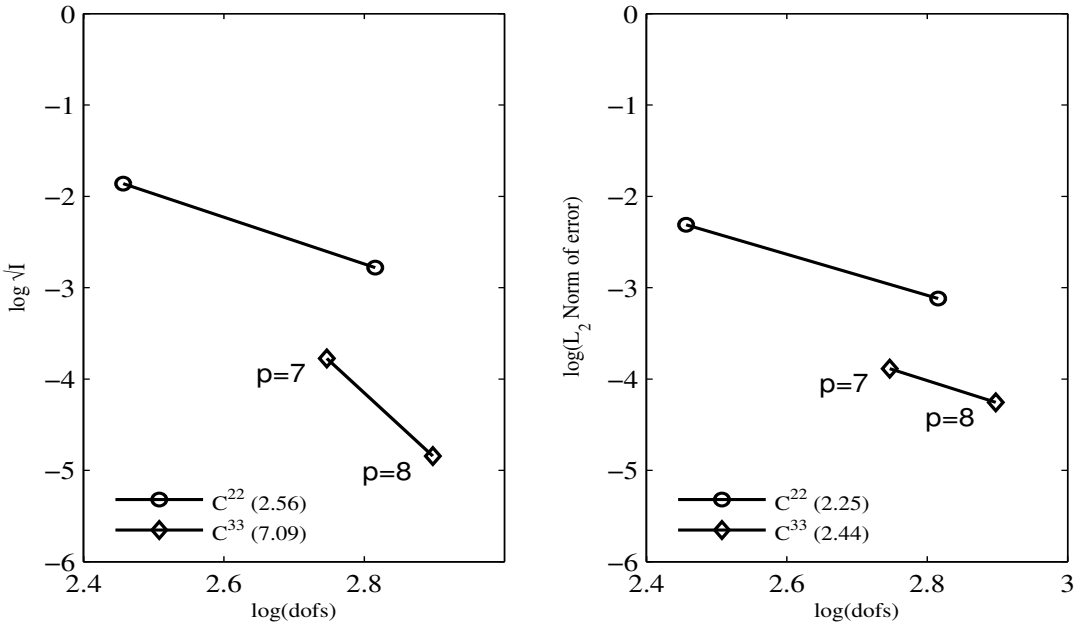

(a) $\sqrt{I}$ versus dofs

(b) L_2 norm of error in u versus dofs

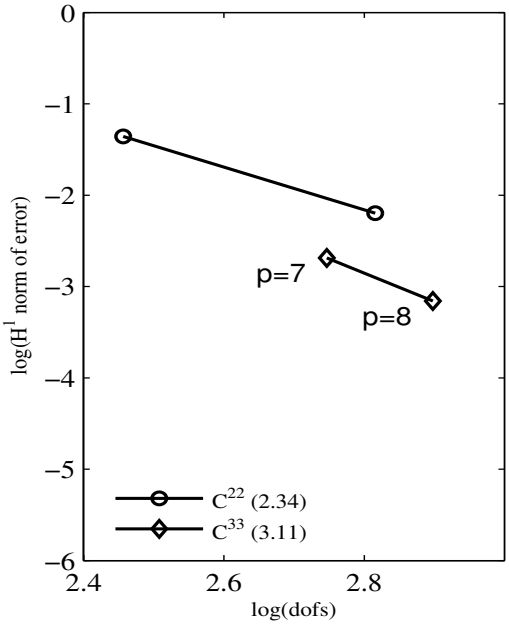

(c) H^1 norm of error in u versus dofs

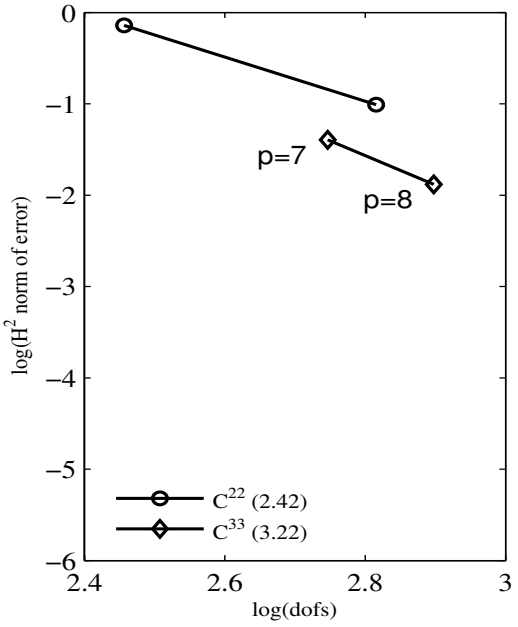

(d) H^2 norm of error in u versus dofs

Figure 4.57: Comparison of C^{ij} Distorted HGDA elements for 2-D Convection-diffusion equation : $\boldsymbol{C^{22}}$ **(**$\boldsymbol{k = 3}$**)**, $\boldsymbol{C^{33}}$ $(k = 4)$, **16 element Undistorted discretization**

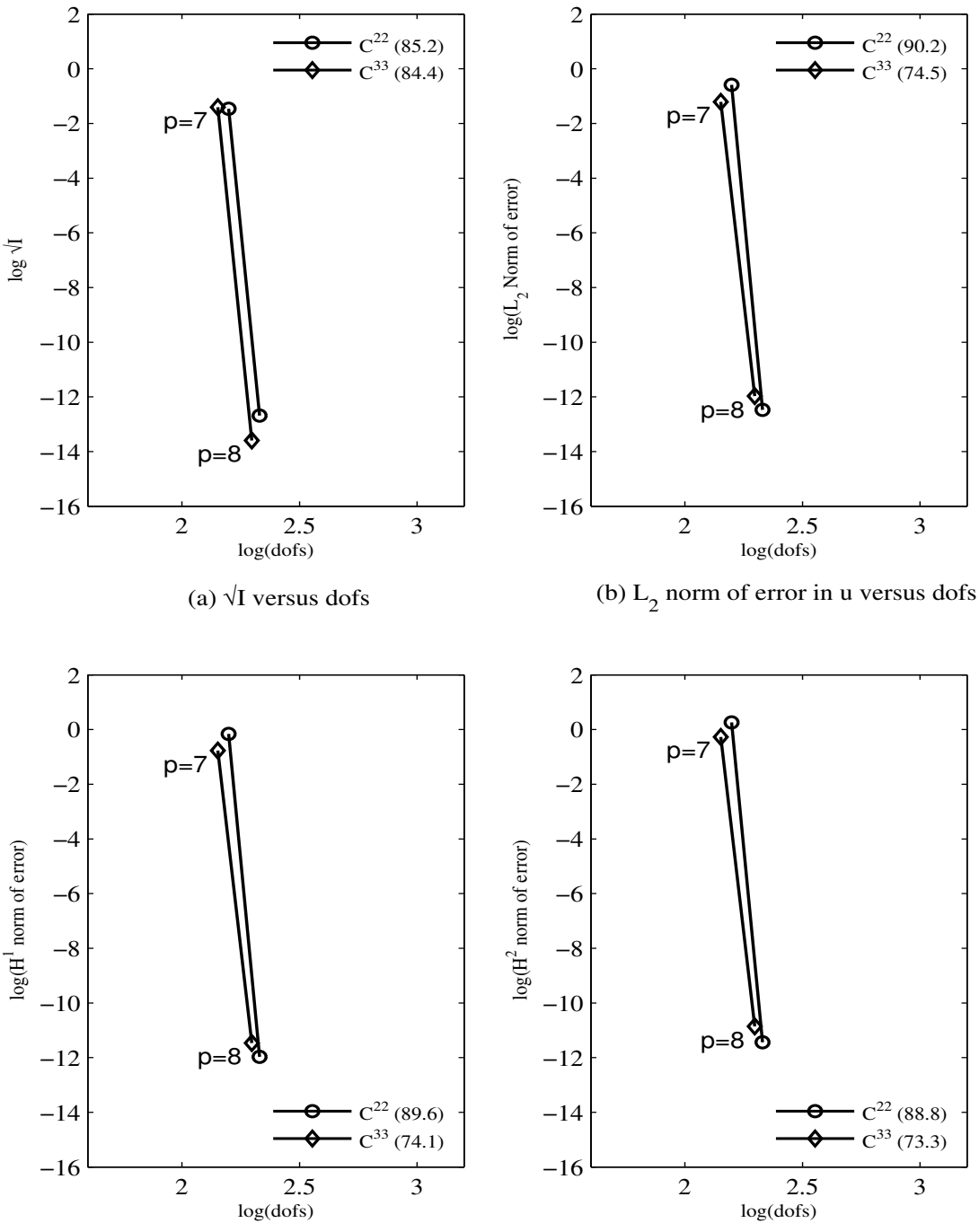

(a) √I versus dofs

(b) L_2 norm of error in u versus dofs

(c) H^1 norm of error in u versus dofs

(d) H^2 norm of error in u versus dofs

Figure 4.58: Comparison of C^{ij} Distorted HGDA elements for 2-D non-linear Poisson's equation : $\boldsymbol{C^{22}}$ **(**$\boldsymbol{k=3}$**)**, $\boldsymbol{C^{33}}$ ($k=4$)**, 4 element Undistorted discretization**

4.5.3 Numerical studies for Distorted discretizations: h-convergence

Since the domain of definition is still a square, the numerical solutions can be computed with HGDA elements utilizing distorted discretizations and compared with the solutions obtained with undistorted discretizations. The p-level of the approximations used is kept fixed and the characteristic length progressively reduced.

(i) Figures 4.59(a)-(d) show the C^{11} (p=3) HGDA solutions for 2-D Convection-diffusion equation computed for distorted discretizations and compared with the solutions obtained with undistorted discretizations. The solutions are plotted against the characteristic length of discretization. Figures 4.60 (a)-(d) and 4.61 (a)-(d) show similar plots for C^{22} (p=5) and C^{33} (p=7) HGDA elements. The convergence rates of all the solutions are listed in Table 4.13.

(ii) Figures 4.62 - 4.64 show similar plots as in (i) for 2-D non-linear Poisson's equation. The convergence rates for these solutions are listed in Table 4.14.

(iii) Figures 4.65 - 4.67 show solutions obtained in (i) as a function of the total number of degrees of freedom for 2-D convection diffusion equation. The convergence rates are listed in Table 4.15.

(iv) Figures 4.68 - 4.70 show solutions obtained in (ii) as a function of the total number of degrees of freedom for 2-D non-linear Poisson's equation. The convergence rates are listed in Table 4.16.

(v) Figures 4.71(a)-(d) and 4.72(a)-(d) show comparison of solutions for C^{22} and C^{33} HGDA elements for a p level of 7 plotted against characteristic length and degrees of freedom respectively. The convergence rates for these solutions are listed in Table 4.17.

(vi) Figures 4.73 and Figures 4.74 show similar plots as in (v) for 2-D non-linear Poisson's equation. The convergence rates are listed in Figure 4.18.

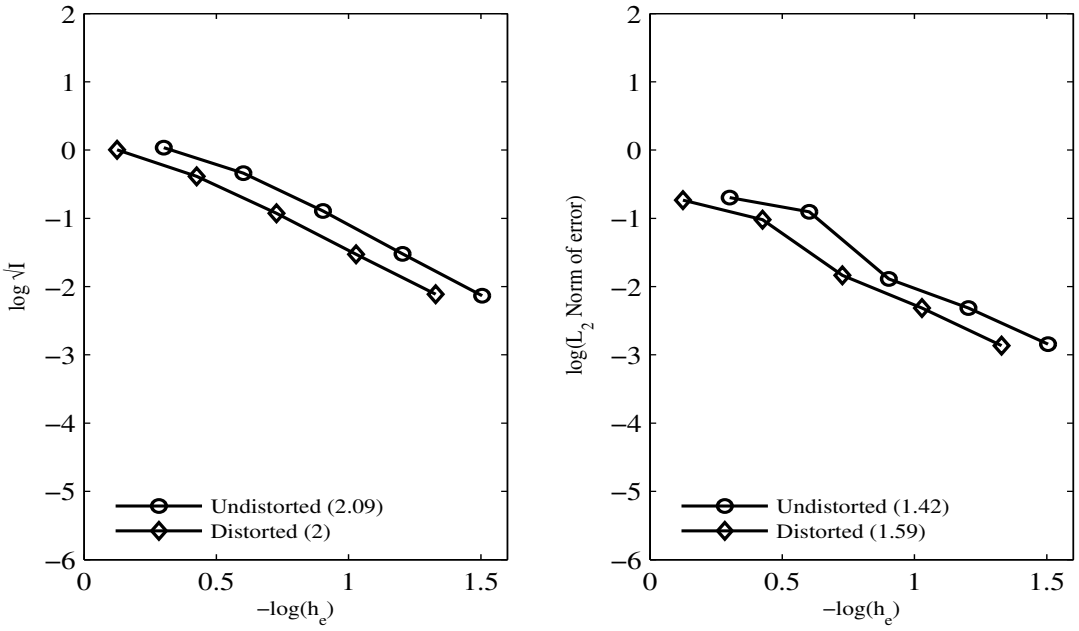

(a) $\sqrt{I}$ versus h_e

(b) L_2 norm of error in u versus h_e

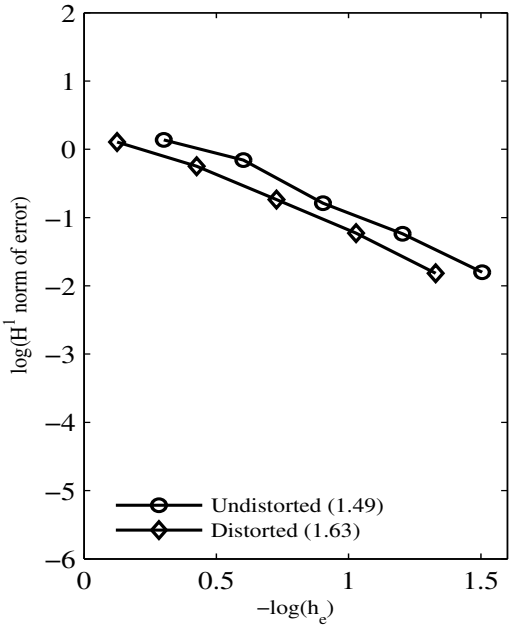

(c) H^1 norm of error in u versus h_e

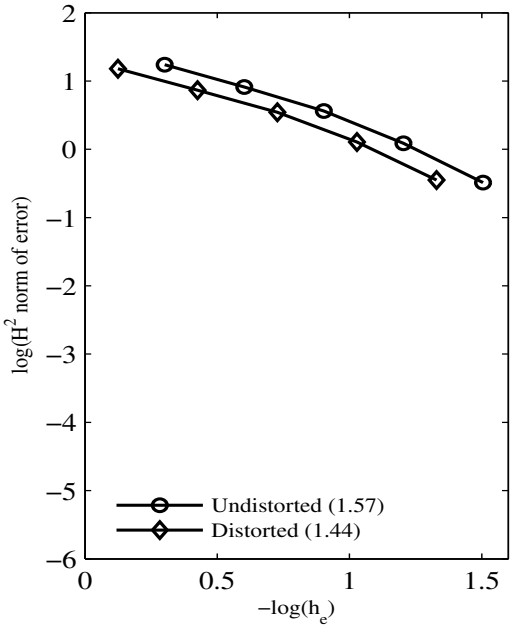

(d) H^2 norm of error in u versus h_e

Figure 4.59: Comparison of Undistorted and distorted discretizations versus discretization length for 2-D Convection-diffusion equation : C^{11} HGDA element, $p_\xi = p_\eta = 3$

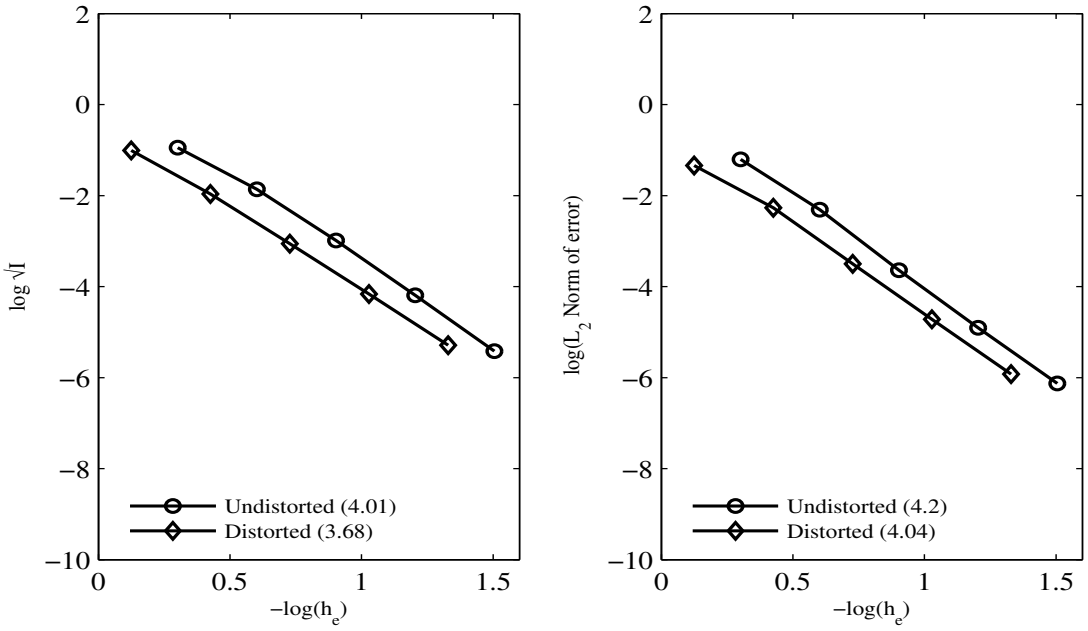

(a) √I versus h_e

(b) L_2 norm of error in u versus h_e

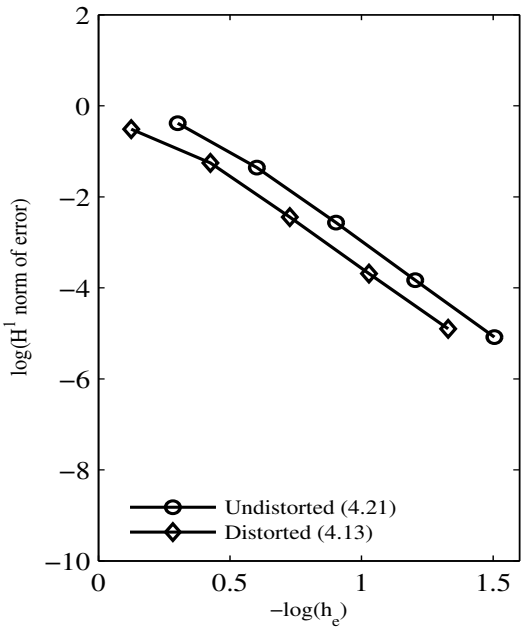

(c) H^1 norm of error in u versus h_e

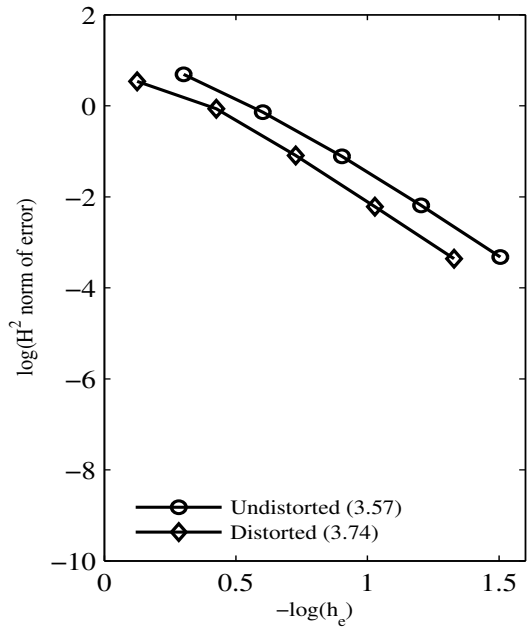

(d) H^2 norm of error in u versus h_e

Figure 4.60: Comparison of Undistorted and distorted discretizations versus discretization length for 2-D Convection-diffusion equation : C^{22} HGDA element, $p_\xi = p_\eta = 5$

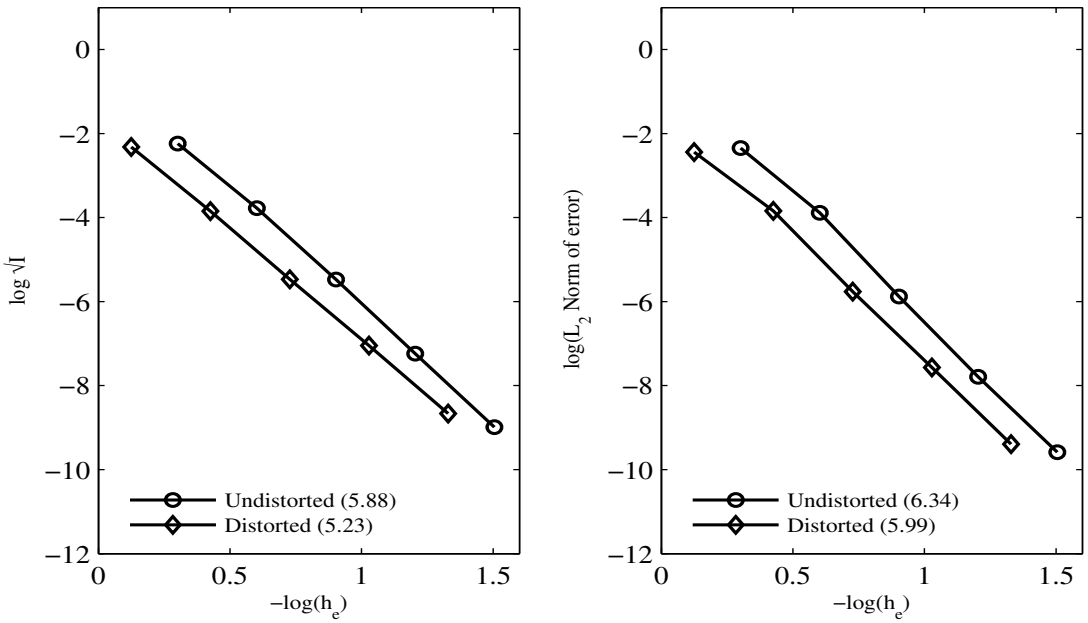

(a) √I versus h_e

(b) L_2 norm of error in u versus h_e

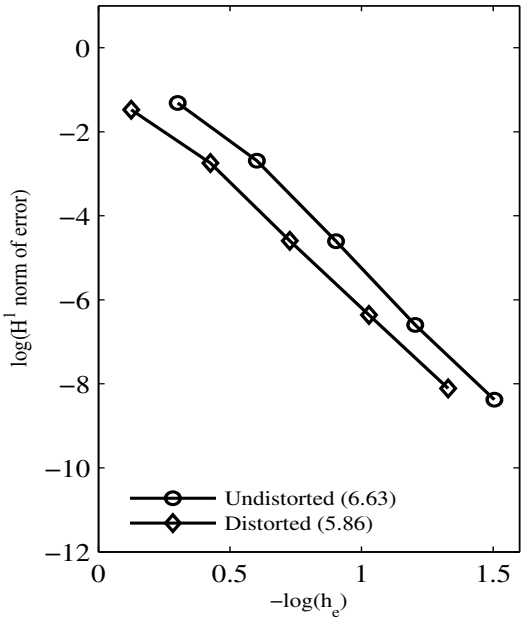

(c) H^1 norm of error in u versus h_e

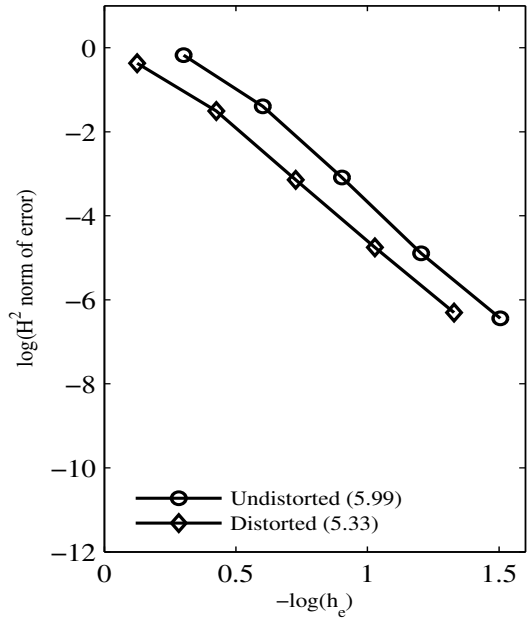

(d) H^2 norm of error in u versus h_e

Figure 4.61: Comparison of Undistorted and distorted discretizations versus discretization length for 2-D Convection-diffusion equation : C^{33} HGDA element, $p_\xi = p_\eta = 7$

Table 4.13: Convergence rates for 2-D Convection-diffusion equation : h-convergence, Undistorted and Distorted discretizations using Distorted HGDA elements

(a) $\sqrt{I}$ versus h_e

$\mathbf{C^{ij}}$	Undistorted mesh	Distorted mesh
C^{11} ; p=3	2.09	2
C^{22} : p=5	4.01	3.68
C^{33} : p=7	5.88	5.23

(b) L_2 - norm of error versus h_e

$\mathbf{C^{ij}}$	Undistorted mesh	Distorted mesh
C^{11} ; p=3	1.42	1.59
C^{22} : p=5	4.2	4.04
C^{33} : p=7	6.34	5.99

(c) H^1 - norm of error versus h_e

$\mathbf{C^{ij}}$	Undistorted mesh	Distorted mesh
C^{11} ; p=3	1.49	1.63
C^{22} : p=5	4.21	4.13
C^{33} : p=7	6.63	5.86

(d) H^2 - norm of error versus h_e

$\mathbf{C^{ij}}$	Undistorted mesh	Distorted mesh
C^{11} ; p=3	1.57	1.44
C^{22} : p=5	3.57	3.74
C^{33} : p=7	5.99	5.33

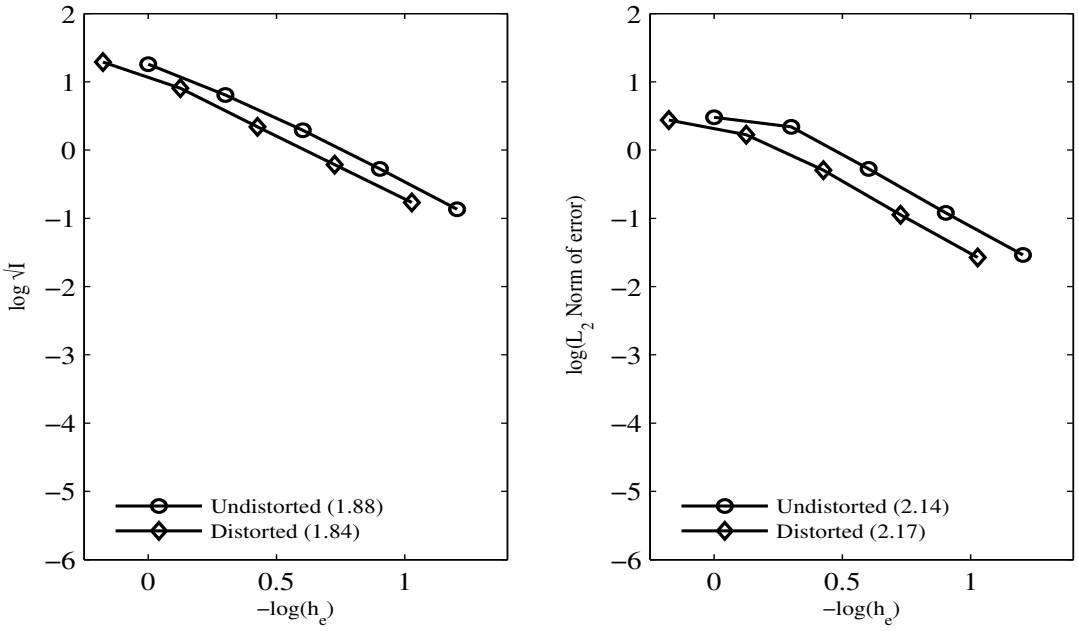

(a) $\sqrt{I}$ versus h_e

(b) L_2 norm of error in u versus h_e

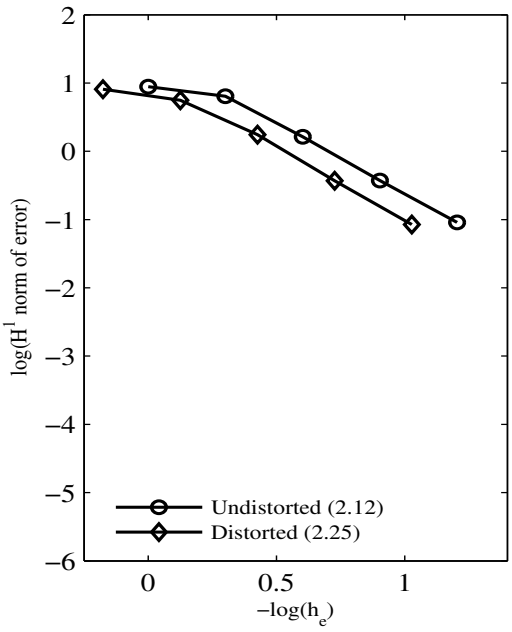

(c) H^1 norm of error in u versus h_e

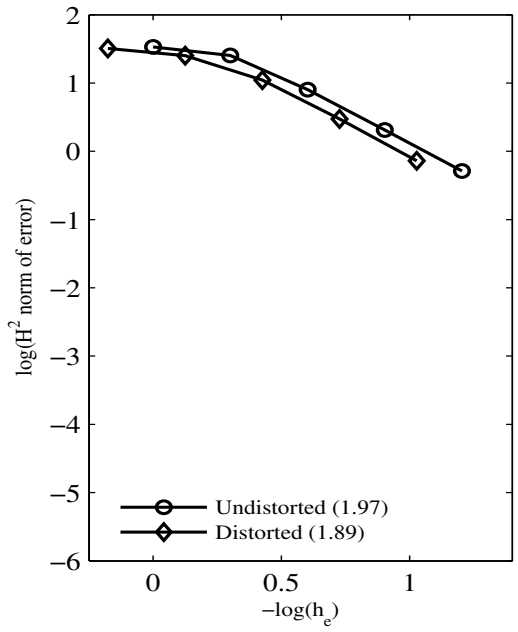

(d) H^2 norm of error in u versus h_e

Figure 4.62: Comparison of Undistorted and distorted discretizations versus discretization length for 2-D non-linear Poisson's equation : C^{11} HGDA element, $p_\xi = p_\eta = 3$

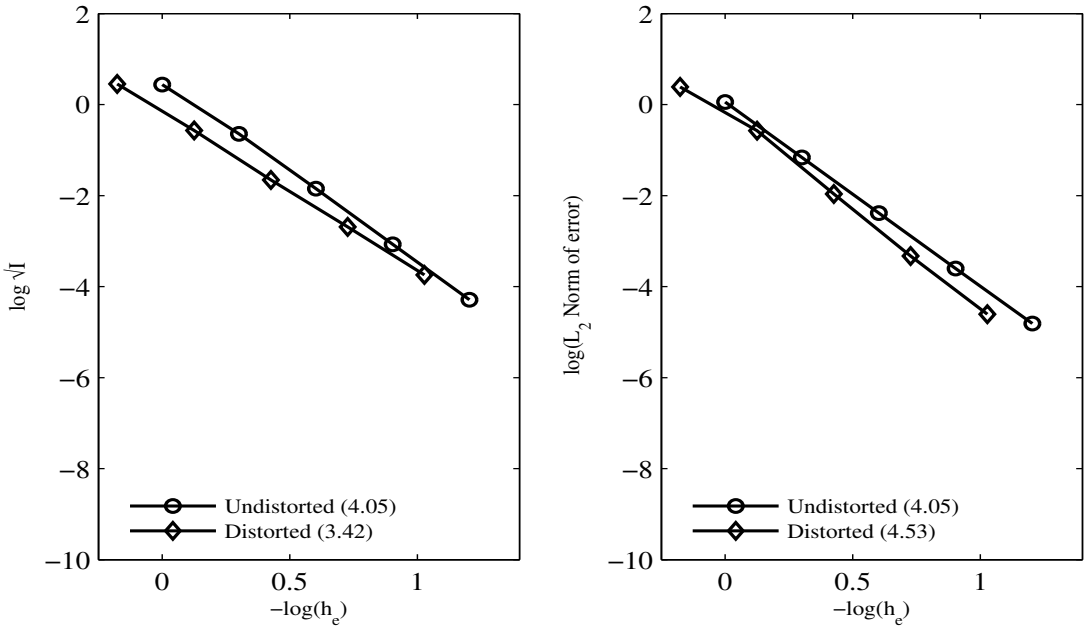

(a) $\sqrt{I}$ versus h_e

(b) L_2 norm of error in u versus h_e

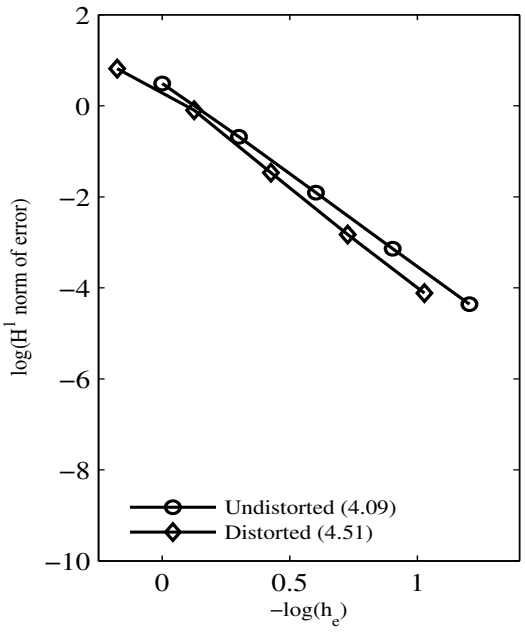

(c) H^1 norm of error in u versus h_e

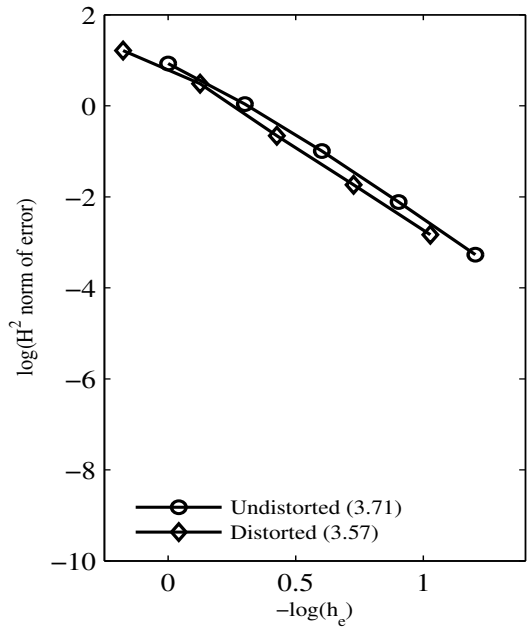

(d) H^2 norm of error in u versus h_e

Figure 4.63: Comparison of Undistorted and distorted discretizations versus discretization length for 2-D non-linear Poisson's equation : C^{22} HGDA element, $p_\xi = p_\eta = 5$

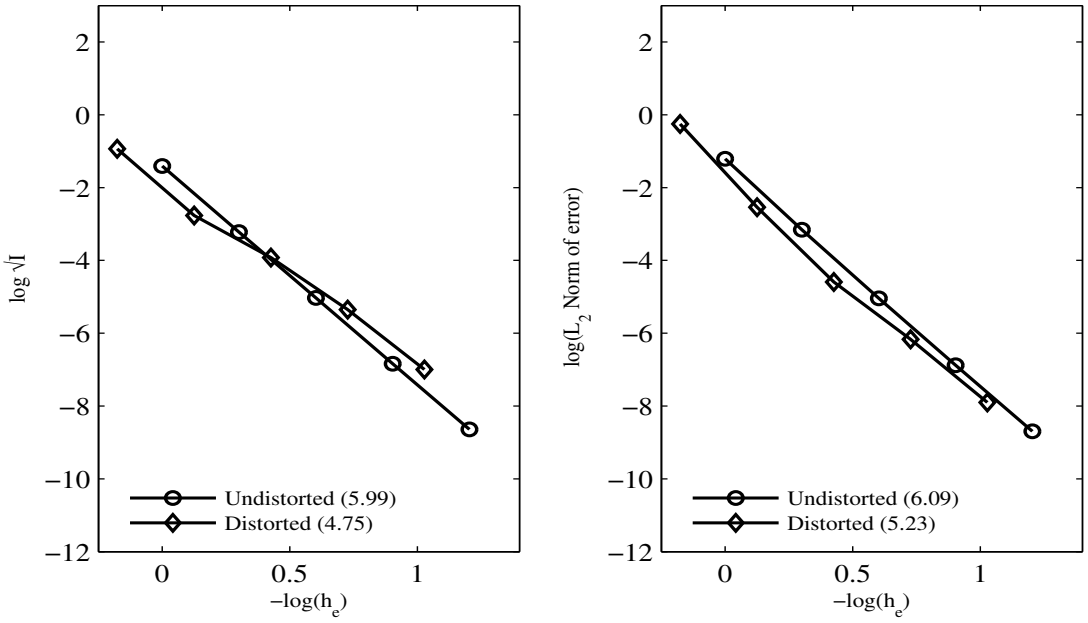

(a) √I versus h_e

(b) L_2 norm of error in u versus h_e

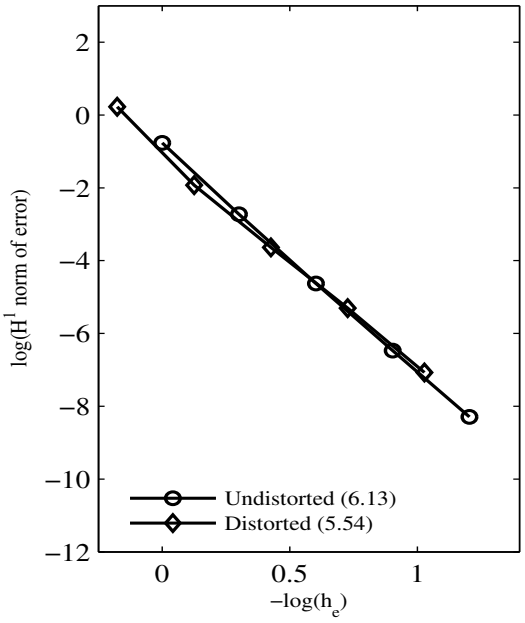

(c) H^1 norm of error in u versus h_e

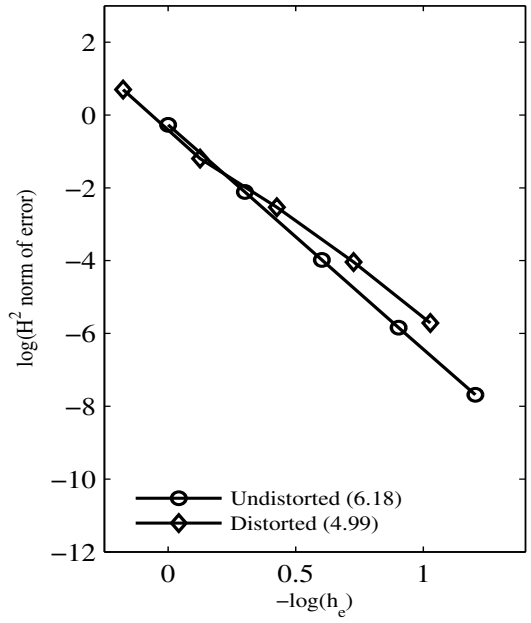

(d) H^2 norm of error in u versus h_e

Figure 4.64: Comparison of Undistorted and distorted discretizations versus discretization length for 2-D non-linear Poisson's equation : C^{33} HGDA element, $p_\xi = p_\eta = 7$

Table 4.14: Convergence rates for 2-D non-linear Poisson's equation : h-convergence, Undistorted and Distorted discretizations using Distorted HGDA elements

(a) $\sqrt{I}$ versus h_e

$\mathbf{C^{ij}}$	Undistorted mesh	Distorted mesh
C^{11} ; p=3	1.88	1.84
C^{22} : p=5	4.05	3.42
C^{33} : p=7	5.99	4.75

(b) L_2 - norm of error versus h_e

$\mathbf{C^{ij}}$	Undistorted mesh	Distorted mesh
C^{11} ; p=3	2.14	2.17
C^{22} : p=5	4.05	4.53
C^{33} : p=7	6.09	5.23

(c) H^1 - norm of error versus h_e

$\mathbf{C^{ij}}$	Undistorted mesh	Distorted mesh
C^{11} ; p=3	2.12	2.25
C^{22} : p=5	4.09	4.51
C^{33} : p=7	6.13	5.54

(d) H^2 - norm of error versus h_e

$\mathbf{C^{ij}}$	Undistorted mesh	Distorted mesh
C^{11} ; p=3	1.97	1.89
C^{22} : p=5	3.71	3.57
C^{33} : p=7	6.18	4.99

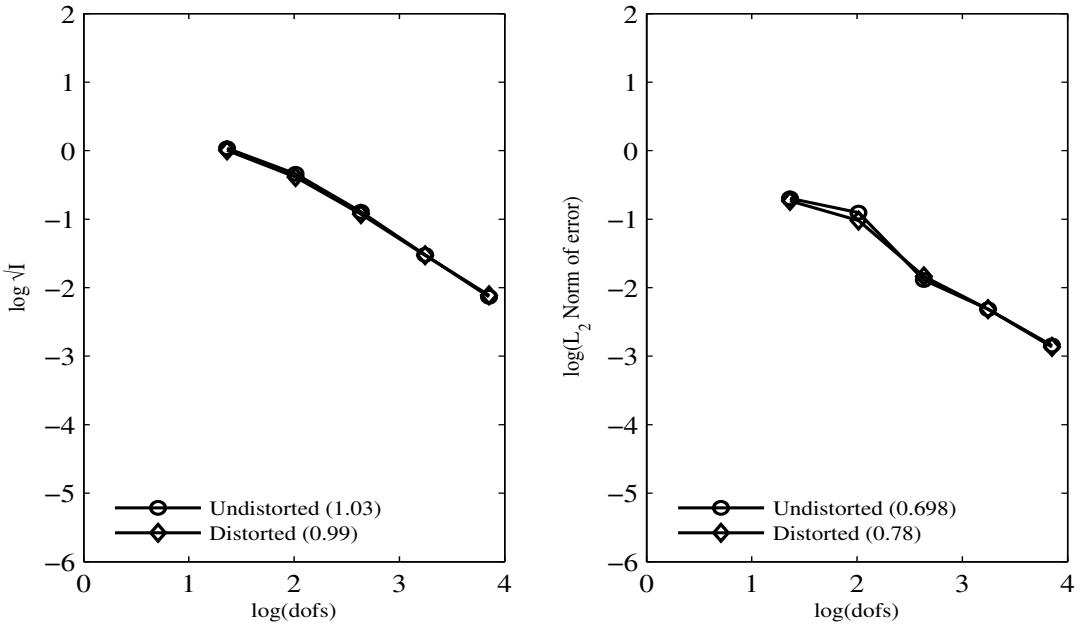

(a) $\sqrt{I}$ versus dofs

(b) L_2 norm of error in u versus dofs

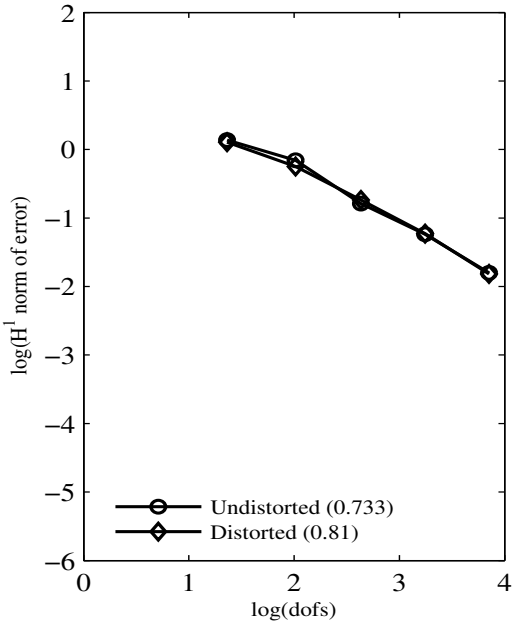

(c) H^1 norm of error in u versus dofs

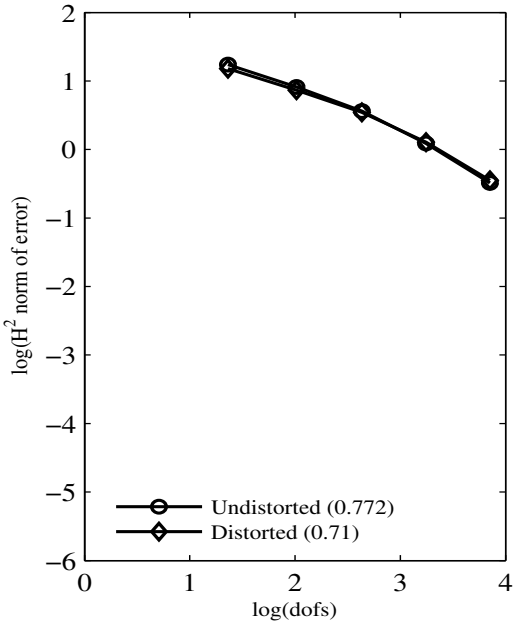

(d) H^2 norm of error in u versus dofs

Figure 4.65: Comparison of Undistorted and distorted discretizations versus degrees of freedom for 2-D Convection-diffusion equation : C^{11} HGDA element, $p_\xi = p_\eta = 3$

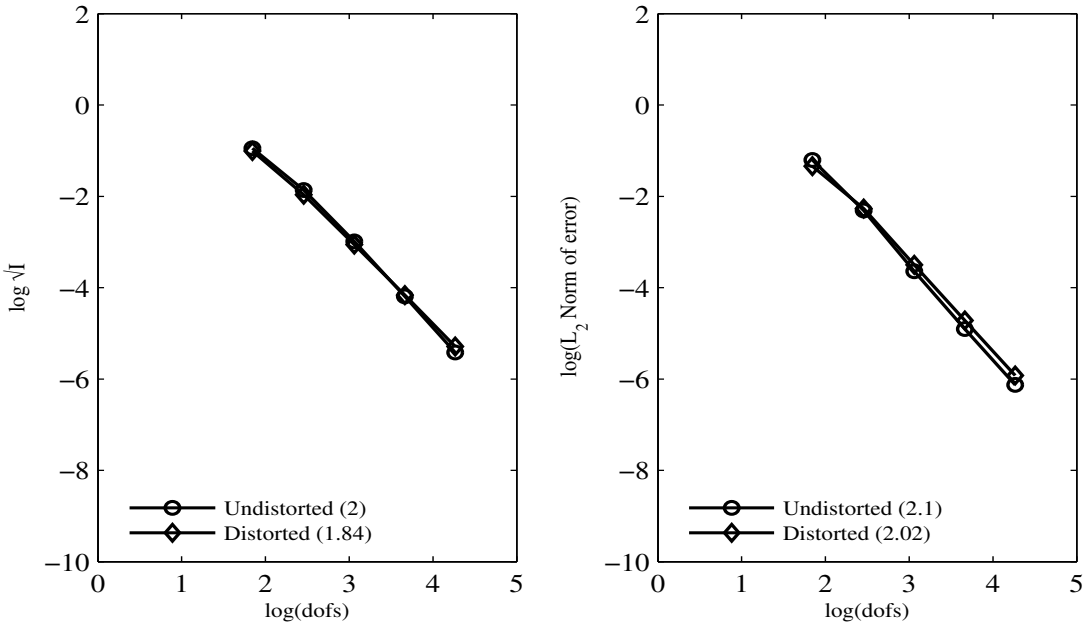

(a) √I versus dofs

(b) L_2 norm of error in u versus dofs

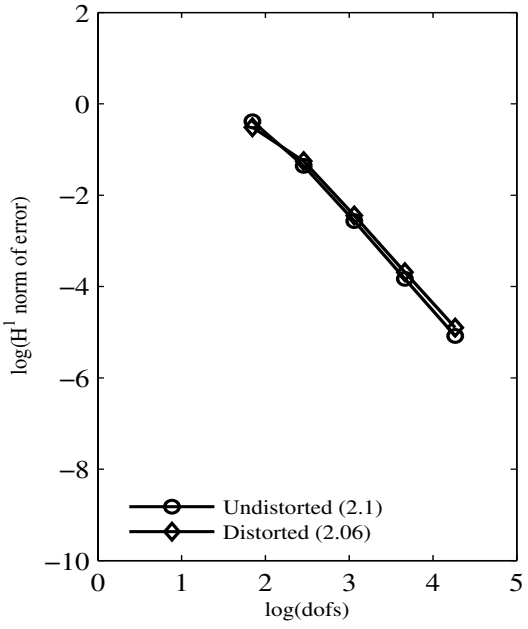

(c) H^1 norm of error in u versus dofs

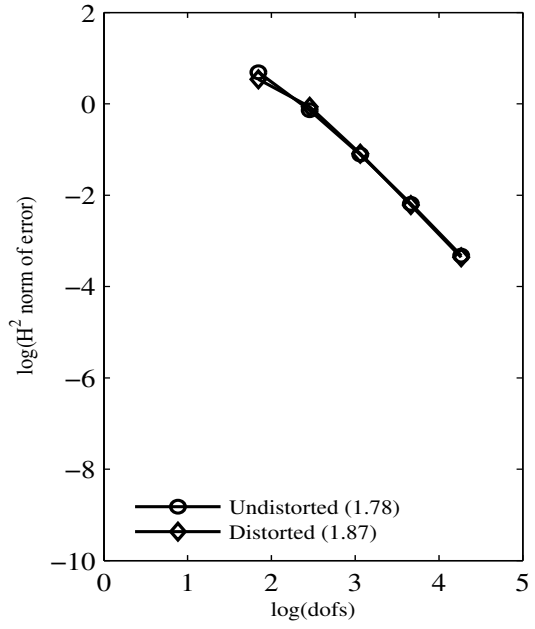

(d) H^2 norm of error in u versus dofs

Figure 4.66: Comparison of Undistorted and distorted discretizations versus degrees of freedom for 2-D Convection-diffusion equation : C^{22} HGDA element, $p_\xi = p_\eta = 5$

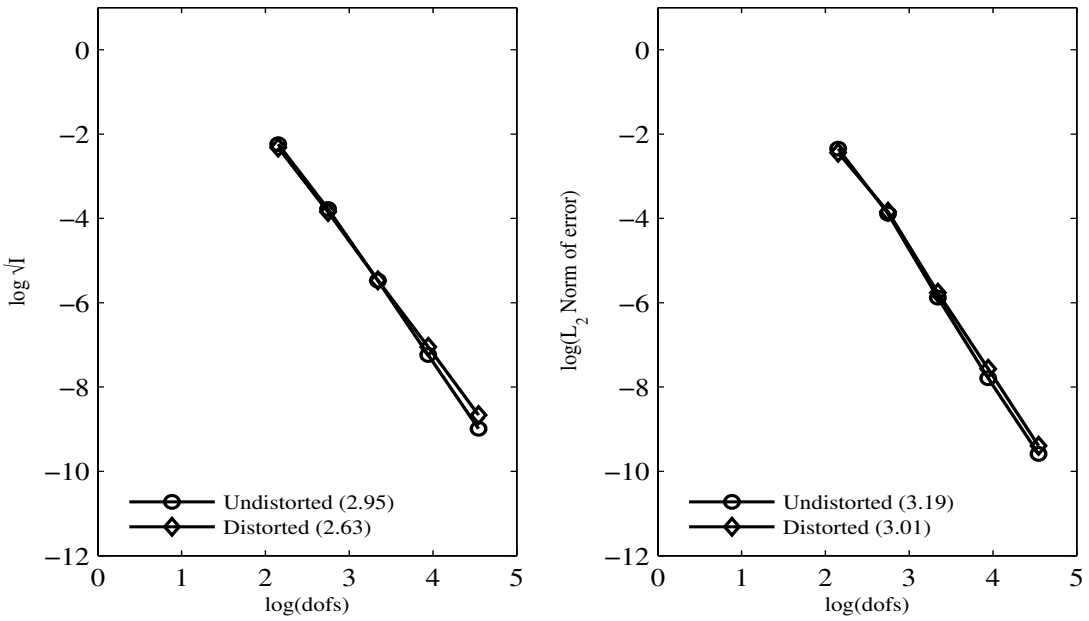

(a) √I versus dofs

(b) L_2 norm of error in u versus dofs

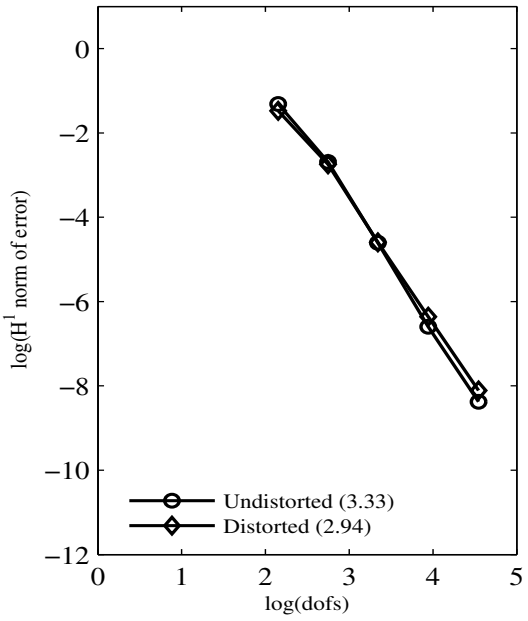

(c) H^1 norm of error in u versus dofs

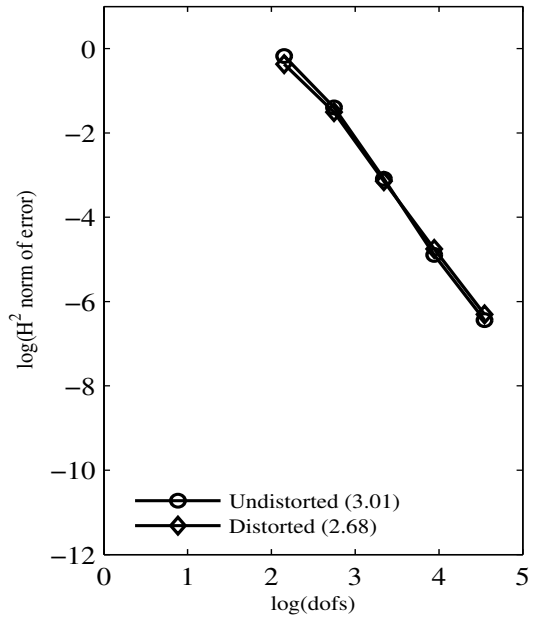

(d) H^2 norm of error in u versus dofs

Figure 4.67: Comparison of Undistorted and distorted discretizations versus degrees of freedom for 2-D Convection-diffusion equation : C^{33} HGDA element, $p_\xi = p_\eta = 7$

Table 4.15: Convergence rates for 2-D Convection-diffusion equation : h-convergence, Undistorted and Distorted discretizations using Distorted HGDA elements

(a) $\sqrt{I}$ versus dofs

$\mathbf{C^{ij}}$	Undistorted mesh	Distorted mesh
C^{11} ; p=3	1.03	0.99
C^{22} : p=5	2	1.84
C^{33} : p=7	2.95	2.63

(b) L_2 - norm of error versus dofs

$\mathbf{C^{ij}}$	Undistorted mesh	Distorted mesh
C^{11} ; p=3	0.7	0.78
C^{22} : p=5	2.1	2.02
C^{33} : p=7	3.19	3.01

(c) H^1 - norm of error versus dofs

$\mathbf{C^{ij}}$	Undistorted mesh	Distorted mesh
C^{11} ; p=3	0.73	0.81
C^{22} : p=5	2.1	2.06
C^{33} : p=7	3.33	2.94

(d) H^2 - norm of error versus dofs

$\mathbf{C^{ij}}$	Undistorted mesh	Distorted mesh
C^{11} ; p=3	0.77	0.71
C^{22} : p=5	1.78	1.87
C^{33} : p=7	3.01	2.68

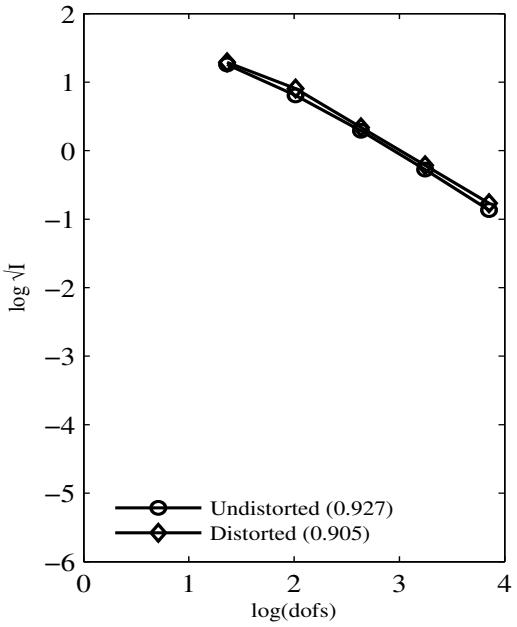

(a) $\sqrt{I}$ versus dofs

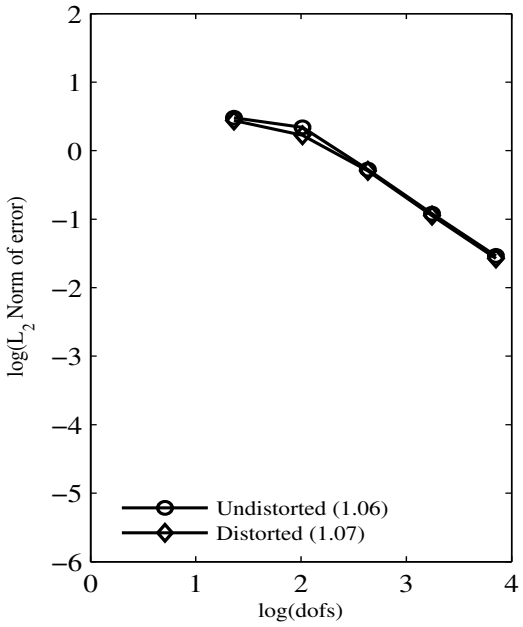

(b) L_2 norm of error in u versus dofs

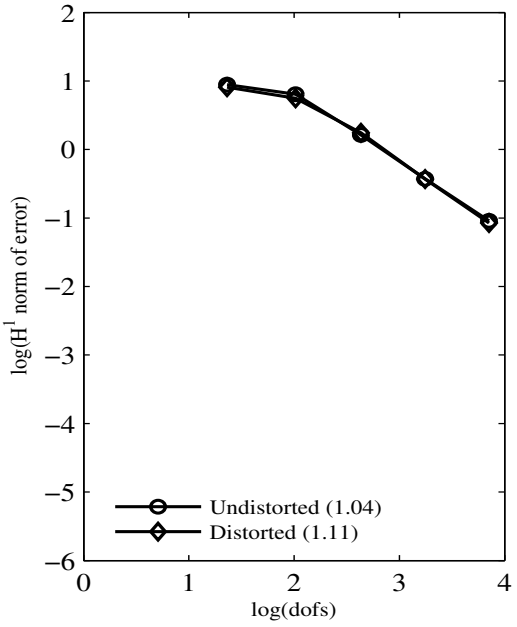

(c) H^1 norm of error in u versus dofs

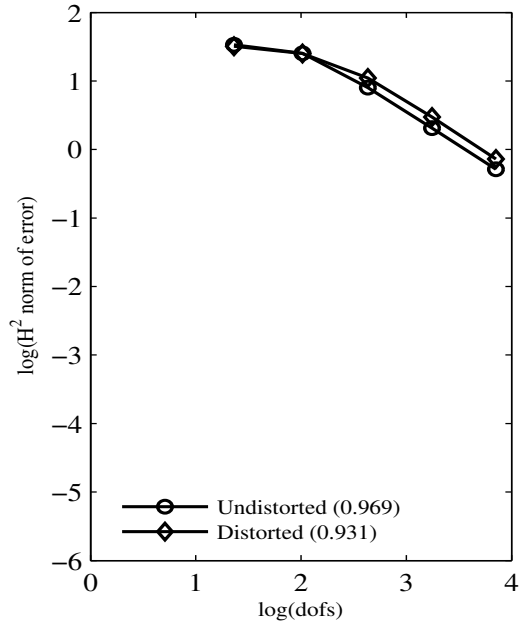

(d) H^2 norm of error in u versus dofs

Figure 4.68: Comparison of Undistorted and distorted discretizations versus degrees of freedom for 2-D non-linear Poisson's equation : C^{11} HGDA element, $p_\xi = p_\eta = 3$

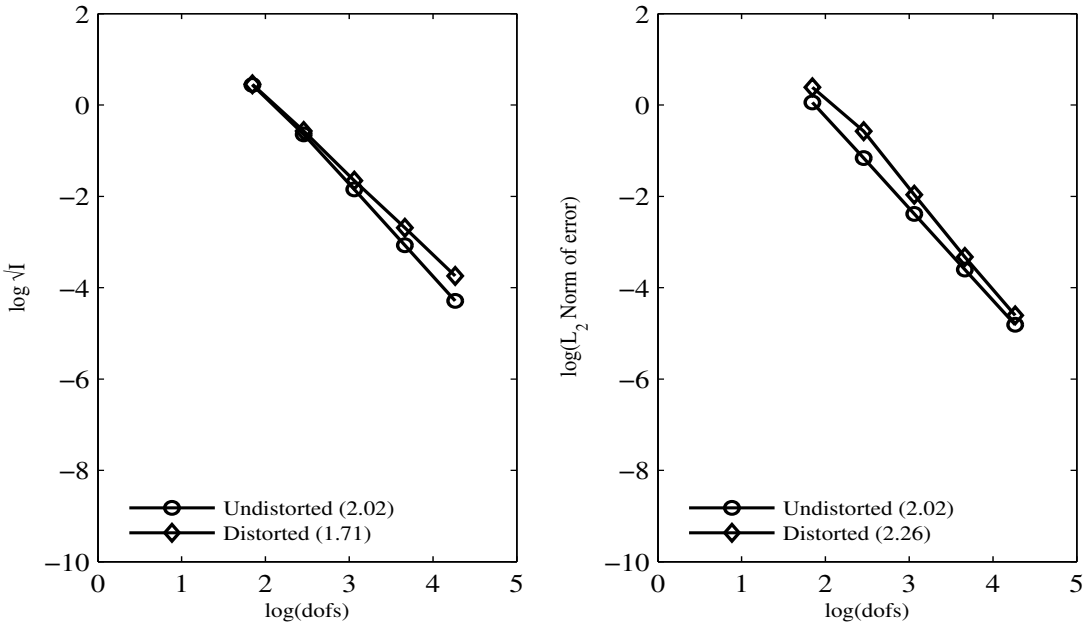

(a) √I versus dofs

(b) L_2 norm of error in u versus dofs

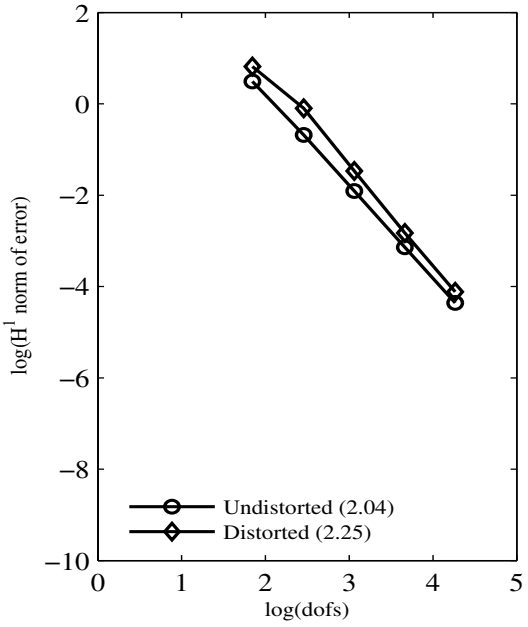

(c) H^1 norm of error in u versus dofs

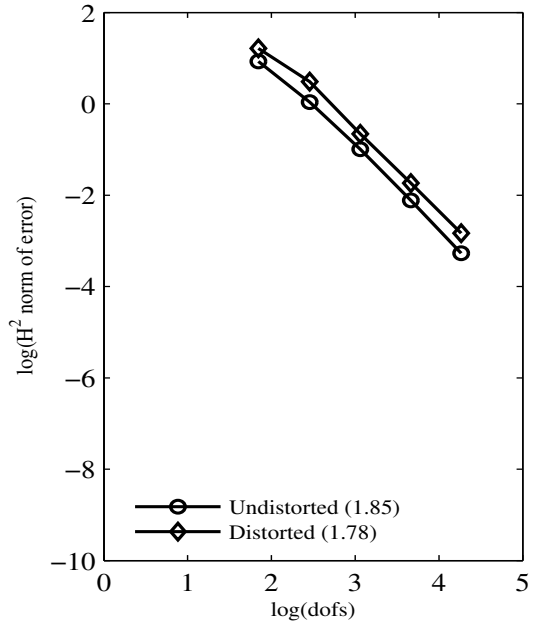

(d) H^2 norm of error in u versus dofs

Figure 4.69: Comparison of Undistorted and distorted discretizations versus degrees of freedom for 2-D non-linear Poisson's equation : $\boldsymbol{C^{22}}$ HGDA element, $\boldsymbol{p_\xi = p_\eta = 5}$

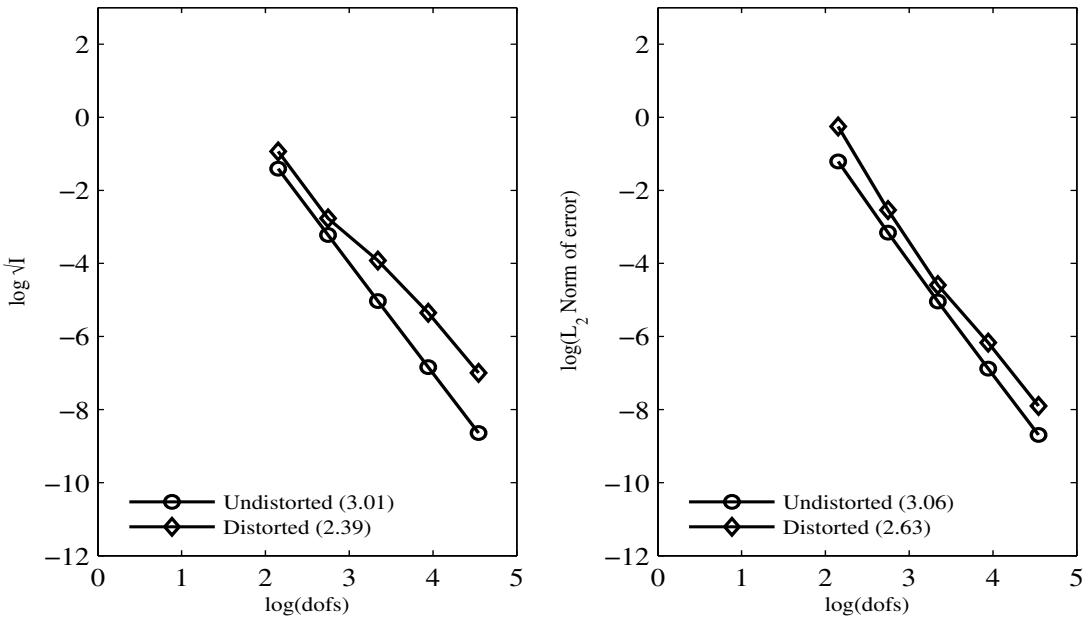

(a) √I versus dofs

(b) L_2 norm of error in u versus dofs

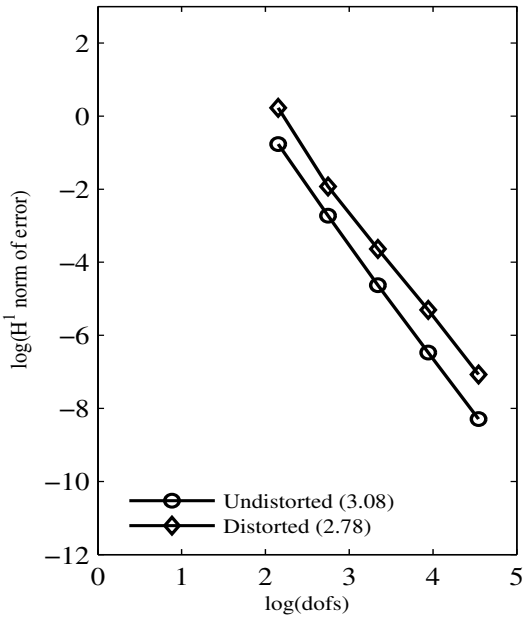

(c) H^1 norm of error in u versus dofs

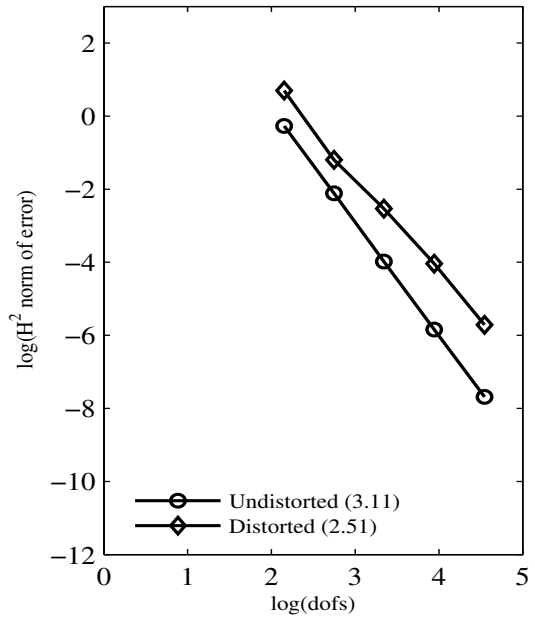

(d) H^2 norm of error in u versus dofs

Figure 4.70: Comparison of Undistorted and distorted discretizations versus degrees of freedom for 2-D non-linear Poisson's equation : C^{33} HGDA element, $p_\xi = p_\eta = 7$

Table 4.16: Convergence rates for 2-D non-linear Poisson's equation : h-convergence, Undistorted and Distorted discretizations using Distorted HGDA elements

(a) $\sqrt{I}$ versus dofs

$\mathbf{C^{ij}}$	Undistorted mesh	Distorted mesh
C^{11} ; p=3	0.93	0.90
C^{22} : p=5	2.02	1.71
C^{33} : p=7	3.01	2.39

(b) L_2 - norm of error versus dofs

$\mathbf{C^{ij}}$	Undistorted mesh	Distorted mesh
C^{11} ; p=3	1.06	1.07
C^{22} : p=5	2.02	2.26
C^{33} : p=7	3.06	2.63

(c) H^1 - norm of error versus dofs

$\mathbf{C^{ij}}$	Undistorted mesh	Distorted mesh
C^{11} ; p=3	1.04	1.11
C^{22} : p=5	2.04	2.25
C^{33} : p=7	3.08	2.78

(d) H^2 - norm of error versus dofs

$\mathbf{C^{ij}}$	Undistorted mesh	Distorted mesh
C^{11} ; p=3	0.97	0.93
C^{22} : p=5	1.85	1.78
C^{33} : p=7	3.11	2.51

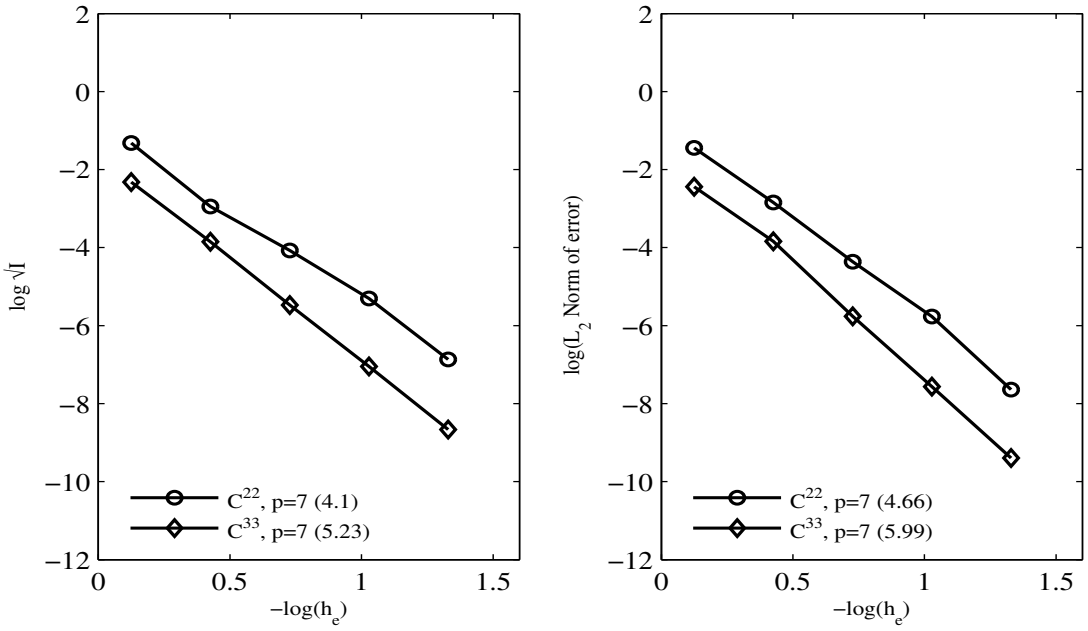

(a) √I versus h_e

(b) L_2 norm of error in u versus h_e

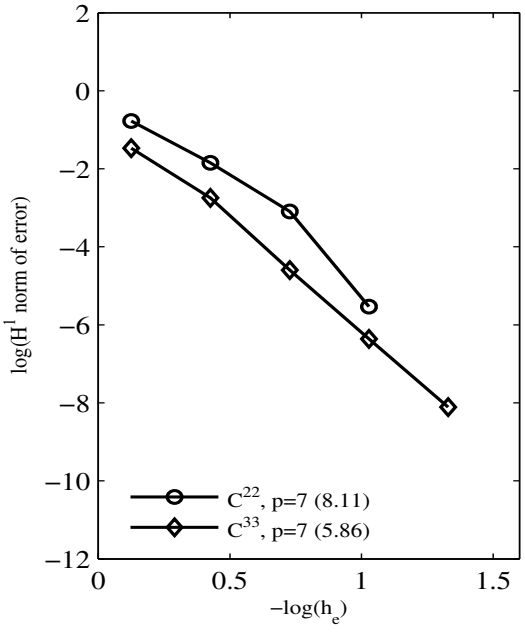

(c) H^1 norm of error in u versus h_e

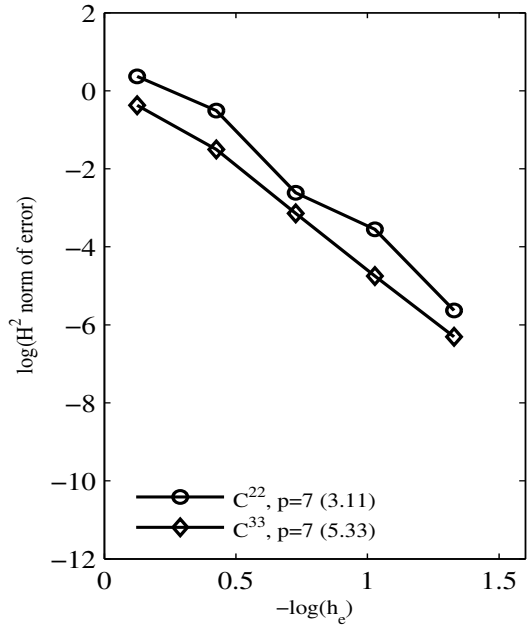

(d) H^2 norm of error in u versus h_e

Figure 4.71: Comparison of C^{ij} Distorted HGDA elements versus discretization length for 2-D Convection-diffusion equation : $\boldsymbol{C^{22}}$ $(\boldsymbol{k = 3})$, $\boldsymbol{C^{33}}$ $(\boldsymbol{k = 4})$, $\boldsymbol{p_\xi = p_\eta = 7}$, **Distorted discretizations**

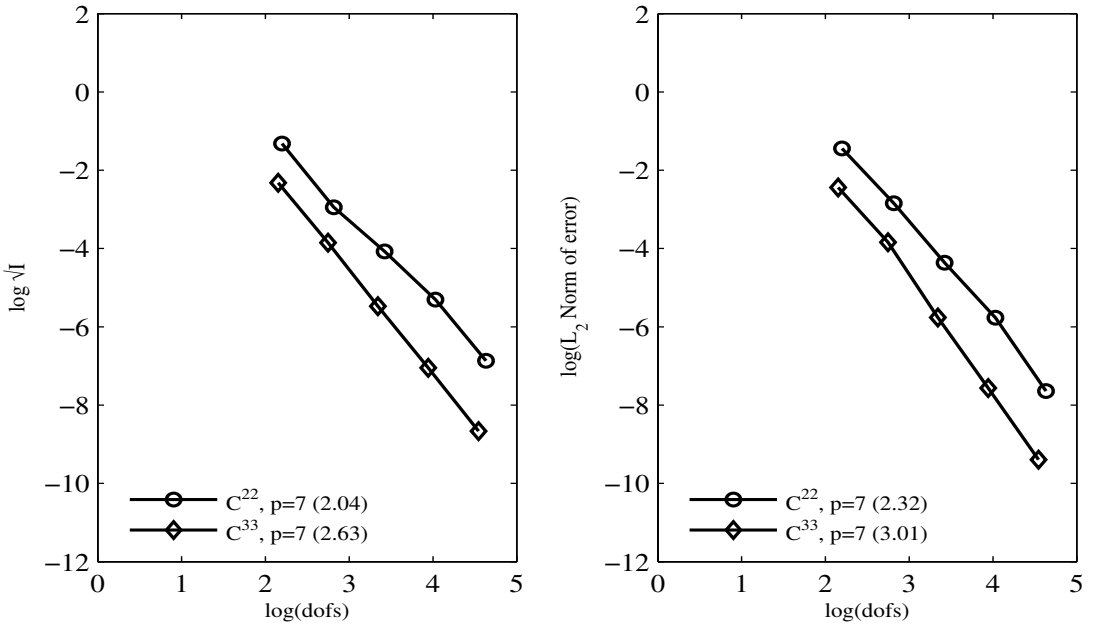

(a) √I versus dofs

(b) L_2 norm of error in u versus dofs

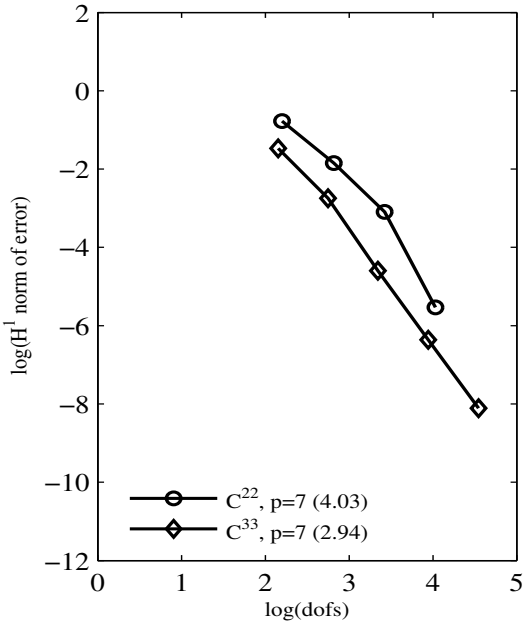

(c) H^1 norm of error in u versus dofs

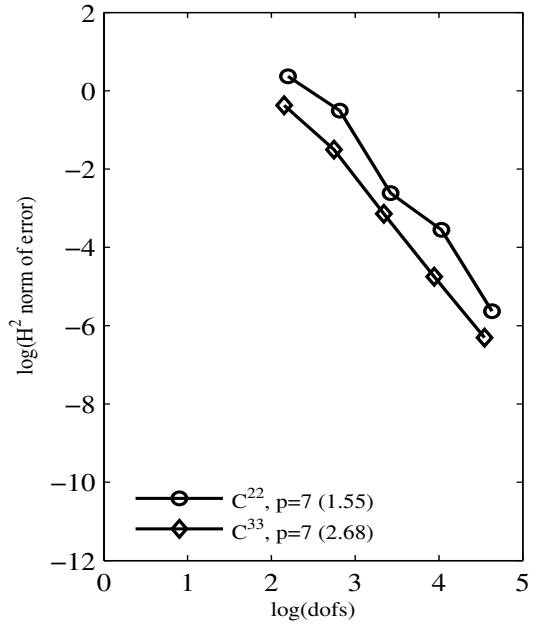

(d) H^2 norm of error in u versus dofs

Figure 4.72: Comparison of C^{ij} Distorted HGDA elements versus degrees of freedom for 2-D Convection-diffusion equation : $\boldsymbol{C^{22}}$ $(\boldsymbol{k = 3})$, $\boldsymbol{C^{33}}$ $(\boldsymbol{k = 4})$, $\boldsymbol{p_\xi = p_\eta = 7}$, **Distorted discretizations**

Table 4.17: Convergence rates for 2-D Convection-diffusion equation : k-convergence, Distorted discretizations using C^{22}, ($k = 3$) and C^{33}, ($k = 4$) Distorted HGDA elements

(a) $\sqrt{I}$

C^{ij}	$\sqrt{I}$ versus he	$\sqrt{I}$ versus dofs
C^{22} : p=7	4.1	2.04
C^{33} : p=7	5.23	2.63

(b) L_2 - norm of error

C^{ij}	L_2 - norm versus he	L_2 - norm versus dofs
C^{22} : p=7	4.66	2.32
C^{33} : p=7	5.99	3.01

(c) H^1 - norm of error

C^{ij}	H^1 - norm versus he	H^1 - norm versus dofs
C^{22} : p=7	8.11	4.03
C^{33} : p=7	5.86	2.94

(d) H^2 - norm of error

C^{ij}	H^2 - norm versus he	H^2 - norm versus dofs
C^{22} : p=7	3.11	1.55
C^{33} : p=7	5.33	2.68

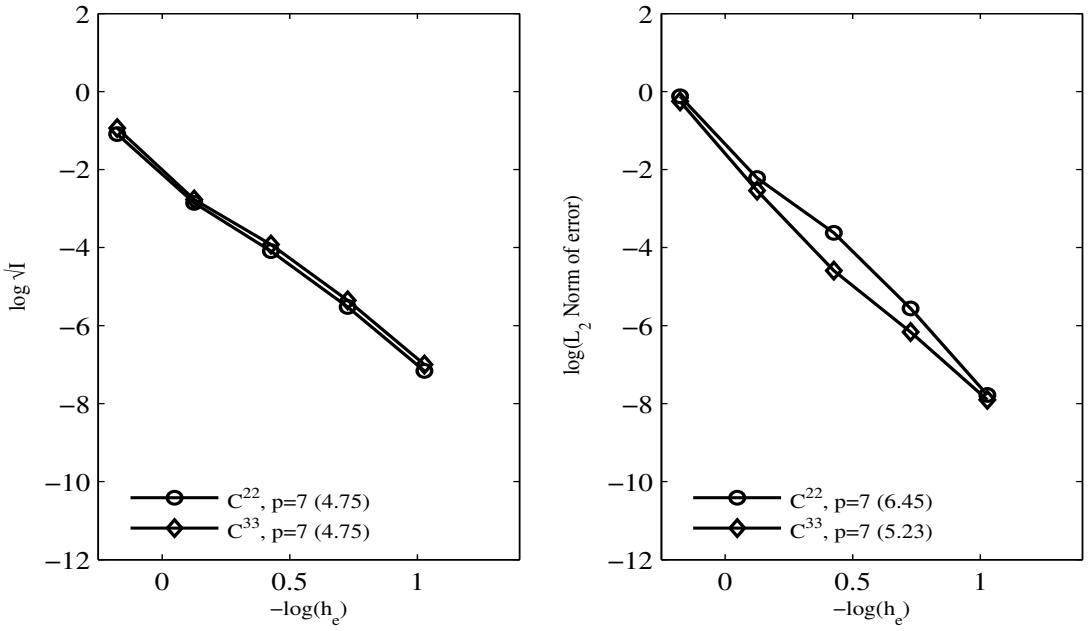

(a) √I versus h_e

(b) L_2 norm of error in u versus h_e

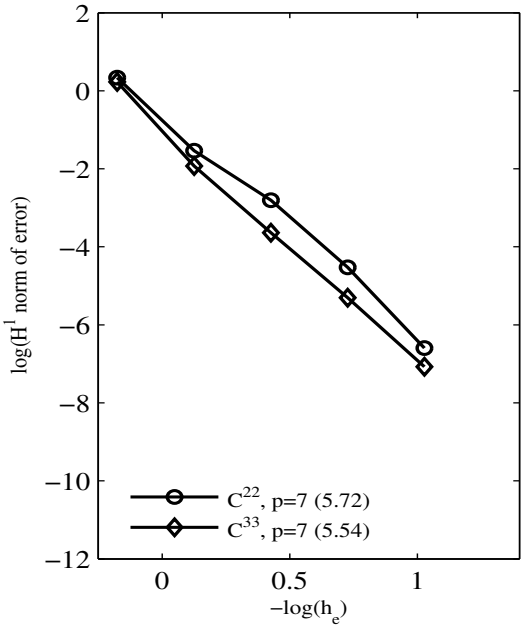

(c) H^1 norm of error in u versus h_e

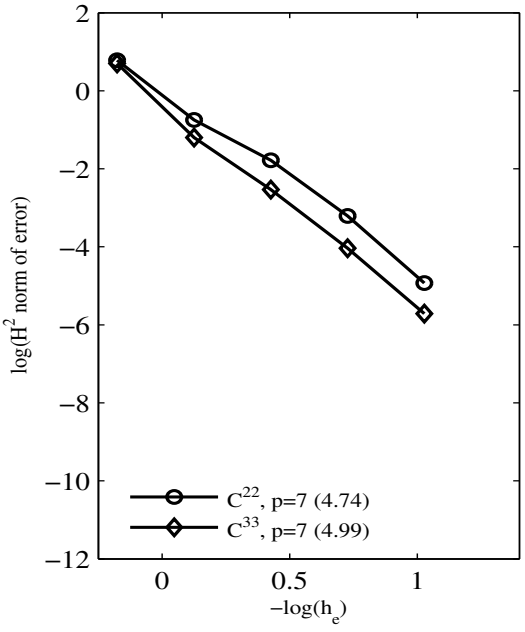

(d) H^2 norm of error in u versus h_e

Figure 4.73: Comparison of C^{ij} Distorted HGDA elements versus discretization length for 2-D non-linear Poisson's equation : $\boldsymbol{C^{22}}$ $(\boldsymbol{k = 3})$, $\boldsymbol{C^{33}}$ $(\boldsymbol{k = 4})$, $\boldsymbol{p_\xi = p_\eta = 7}$, **Distorted discretizations**

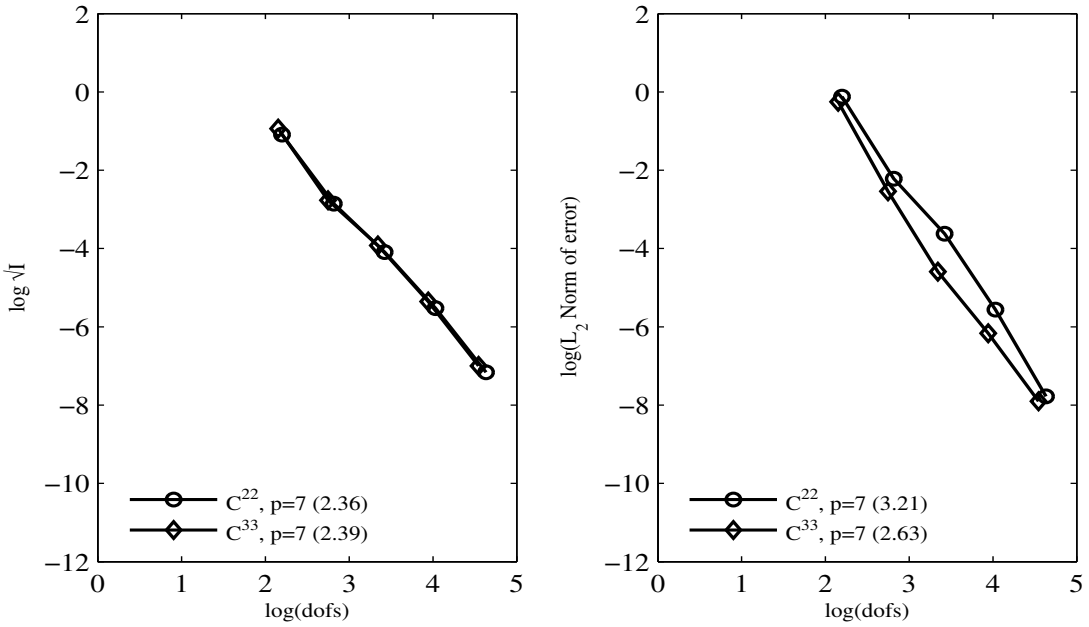

(a) √I versus dofs

(b) L_2 norm of error in u versus dofs

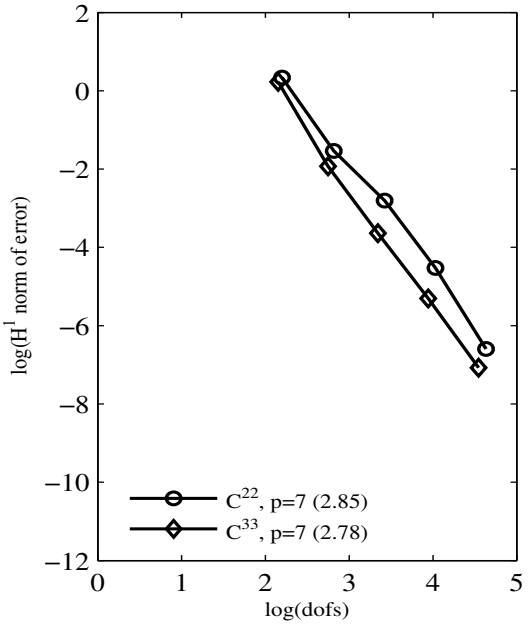

(c) H^1 norm of error in u versus dofs

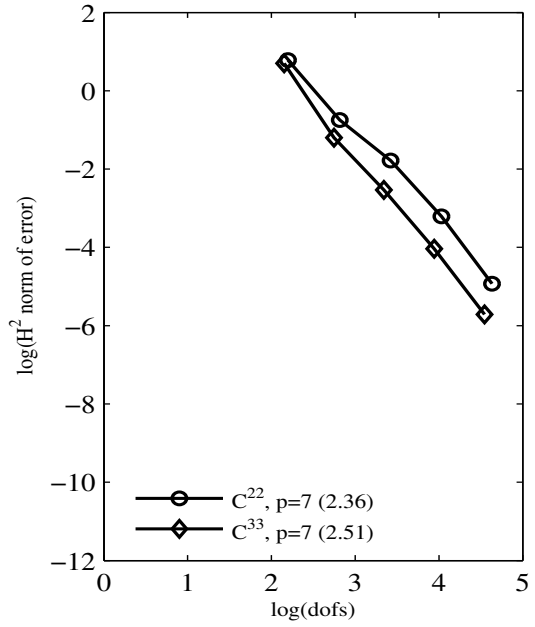

(d) H^2 norm of error in u versus dofs

Figure 4.74: Comparison of C^{ij} Distorted HGDA elements versus degrees of freedom for 2-D non-linear Poisson's equation : $\boldsymbol{C^{22}}$ $(\boldsymbol{k = 3})$, $\boldsymbol{C^{33}}$ $(\boldsymbol{k = 4})$, $\boldsymbol{p_\xi = p_\eta = 7}$, **Distorted discretizations**

Table 4.18: Convergence rates for 2-D non-linear Poisson's equation : k-convergence, Distorted discretizations using C^{22}, ($k = 3$) and C^{33}, ($k = 4$) Distorted HGDA elements

(a) √I

C^{ij}	**√I versus he**	**√I versus dofs**
C^{22} : p=7	4.75	2.36
C^{33} : p=7	4.75	2.39

(b) L_2 - norm of error

C^{ij}	**L_2 - norm versus he**	**L_2 - norm versus dofs**
C^{22} : p=7	6.45	3.21
C^{33} : p=7	5.23	2.63

(c) H^1 - norm of error

C^{ij}	**H^1 - norm versus he**	**H^1 - norm versus dofs**
C^{22} : p=7	5.72	2.85
C^{33} : p=7	5.54	2.78

(d) H^2 - norm of error

C^{ij}	**H^2 - norm versus he**	**H^2 - norm versus dofs**
C^{22} : p=7	4.74	2.36
C^{33} : p=7	4.99	2.51

Remarks

(1) The HGDA elements have best performance when discretizations contain undistorted elements. From Tables 4.13-4.16, we observe that the convergence rates for formulations utilizing Undistorted discretizations are higher than those corresponding to the distorted discretizations.

(2) From Figures 4.71 and 4.74, for a given value of characteristic length or given number of degrees of freedom, C^{33} HGDA element gives a lower value of the quantity of interest compared to C^{22} HGDA element as seen in earlier studies.

4.5.4 Numerical studies for Distorted mesh : p-convergence

Numerical studies are presented using C^{22} and C^{33} HGDA elements with progressively increasing p-levels starting with the minimum p-level required by the corresponding HGDA element. Least squares formulation is used to compute the solutions.

(i) Figures 4.75(a)-(d) show the solutions for 2-D convection-diffusion equation computed for two different distorted discretizations (4 and 16 elements) with C^{22} HGDA element. Figures 4.76(a)-(d) show similar plots for C^{33} HGDA element. In both cases, to obtain a given value of quantity of interest, we need lesser number of degrees of freedom for four element mesh

(ii) Figures 4.77 and 4.78 show similar plots as in (i) for non-linear Poisson's equation.

(iii) Figures 4.79(a)-(d) show the numerical solutions computed with C^{22} HGDA element using distorted and undistorted discretizations. Figures 4.80(a)-(d) show similar plots for C^{33} HGDA element.

(iv) Figures 4.81 and 4.82 show similar numerical solutions as in (iii) for non-linear Poisson's equation.

(v) Figures 4.83(a)-(d) show comparison of numerical solutions for 2-D convection-diffusion equation obtained using C^{22} and C^{33} HGDA elements for a 16 element distorted discretization with progressively increasing p levels.

(vi) Figure 4.84 shows comparison of C^{22} and C^{33} HGDA elements for 2-D non-linear Poisson's equation.

(vii) The convergence rates of the computed quantities of interest for both model problems calculated using C^{33} HGDA element are very high due to the numerical solution at p-level of 8 being in the close vicinity of the theoretical solution.

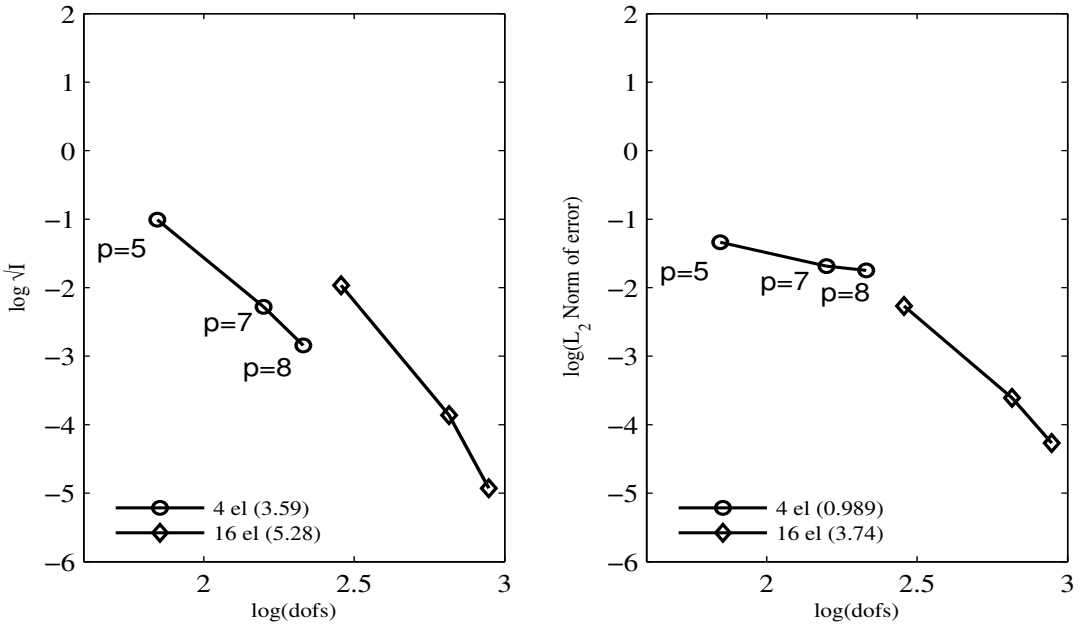

(a) $\sqrt{I}$ versus dofs

(b) L_2 norm of error in u versus dofs

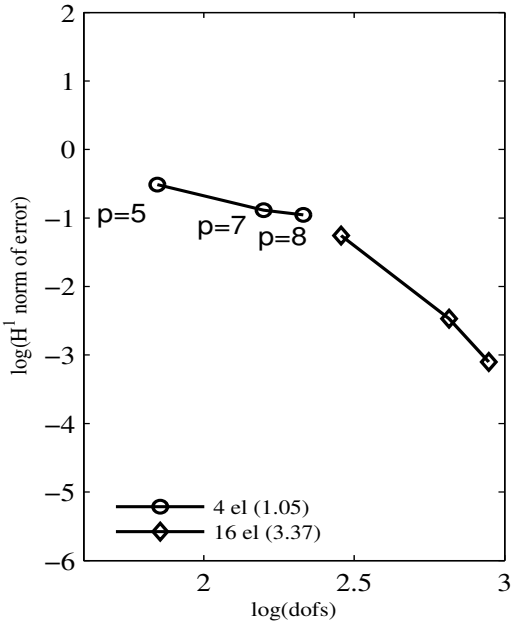

(c) H^1 norm of error in u versus dofs

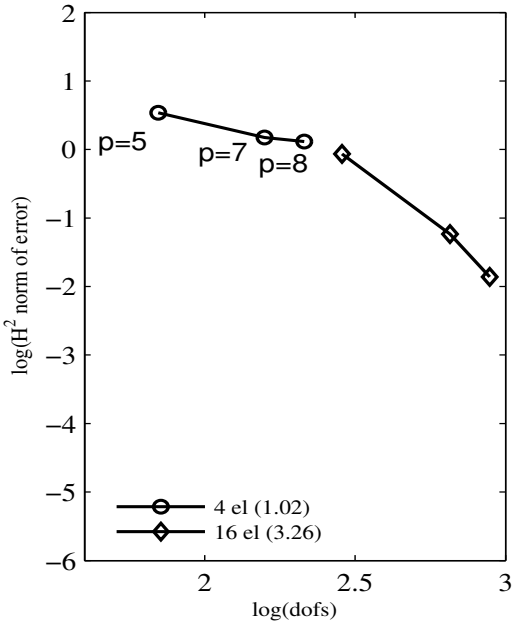

(d) H^2 norm of error in u versus dofs

Figure 4.75: Comparison of 4 element and 16 element discretizations using Distorted HGDA elements for 2-D Convection-diffusion equation : C^{22}, **Distorted discretizations**

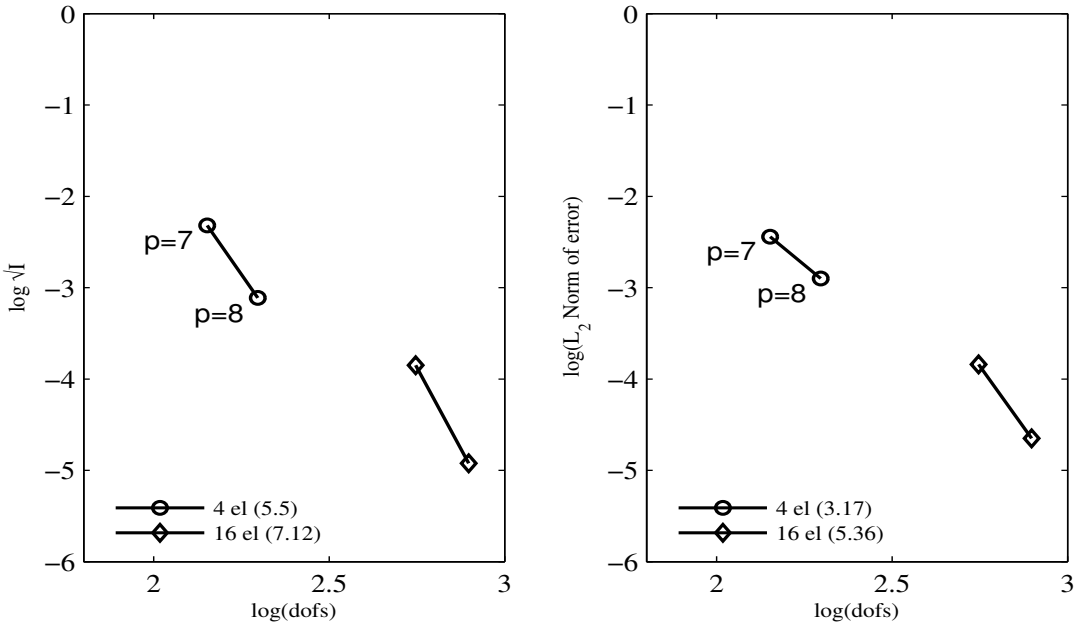

(a) $\sqrt{I}$ versus dofs

(b) L_2 norm of error in u versus dofs

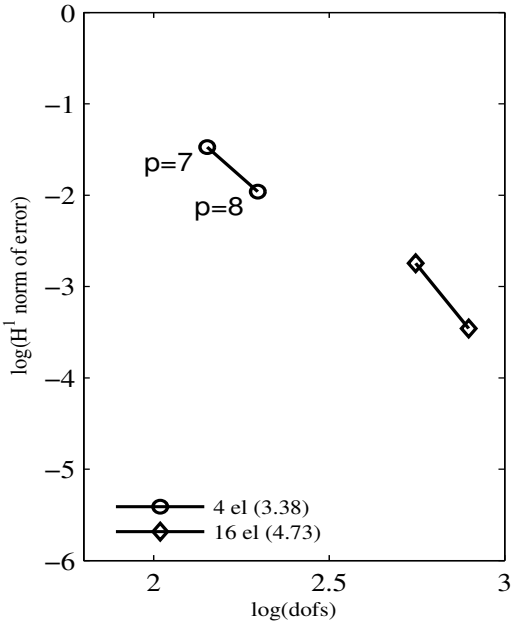

(c) H^1 norm of error in u versus dofs

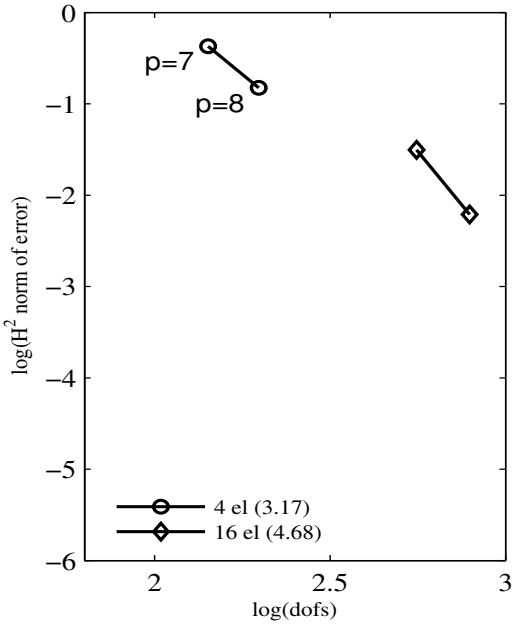

(d) H^2 norm of error in u versus dofs

Figure 4.76: Comparison of 4 element and 16 element discretizations using Distorted HGDA elements for 2-D Convection-diffusion equation : C^{33}, **Distorted discretizations**

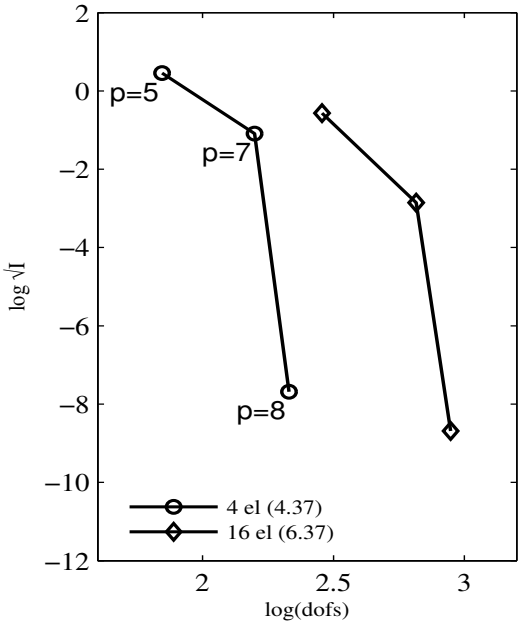

(a) √I versus dofs

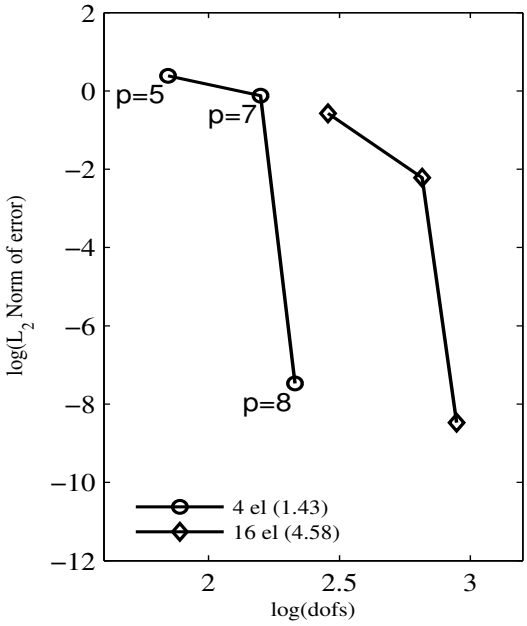

(b) L_2 norm of error in u versus dofs

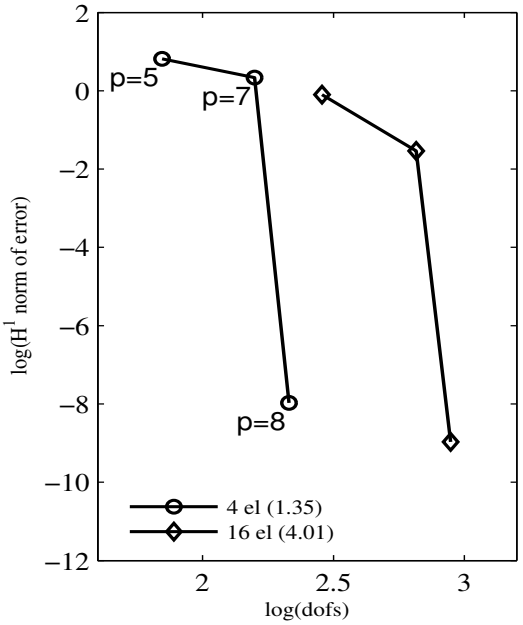

(c) H^1 norm of error in u versus dofs

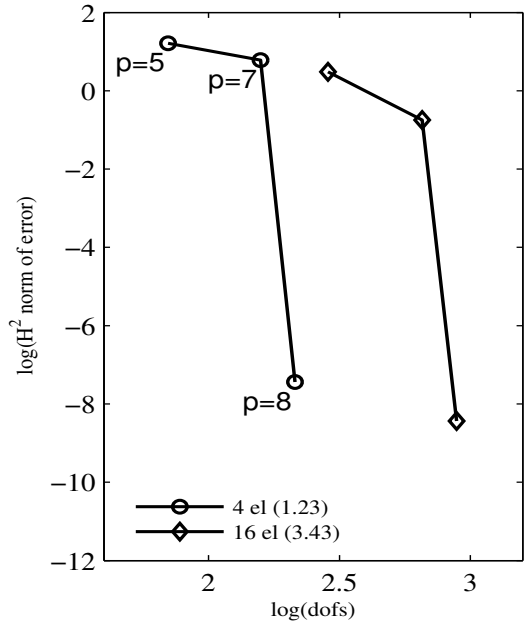

(d) H^2 norm of error in u versus dofs

Figure 4.77: Comparison of 4 element and 16 element discretizations using Distorted HGDA elements for 2-D non-linear Poisson's equation : C^{22}, **Distorted discretizations**

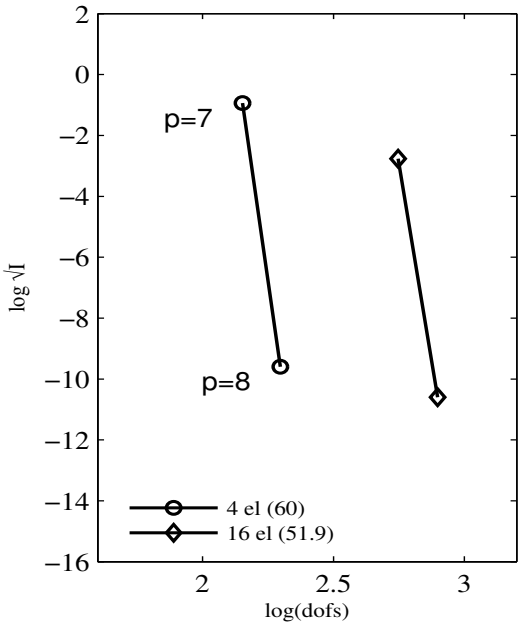

(a) √I versus dofs

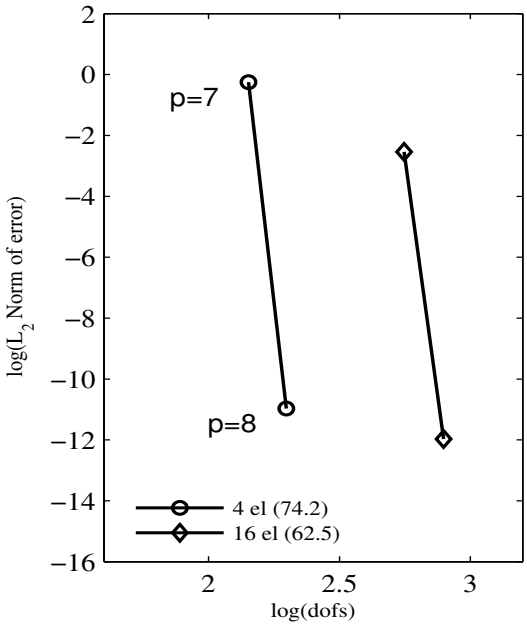

(b) L_2 norm of error in u versus dofs

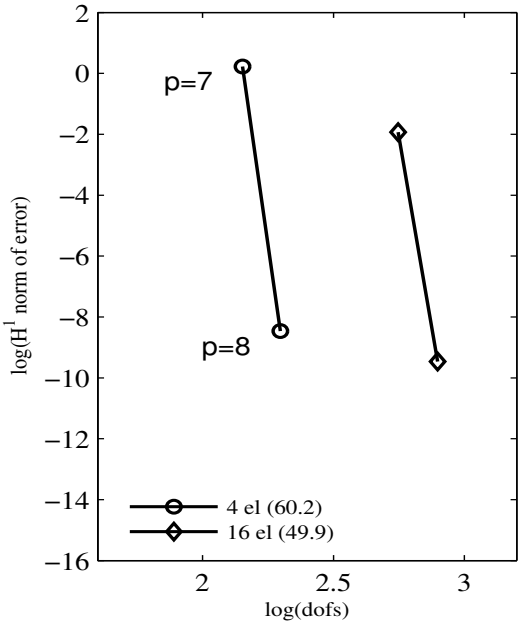

(c) H^1 norm of error in u versus dofs

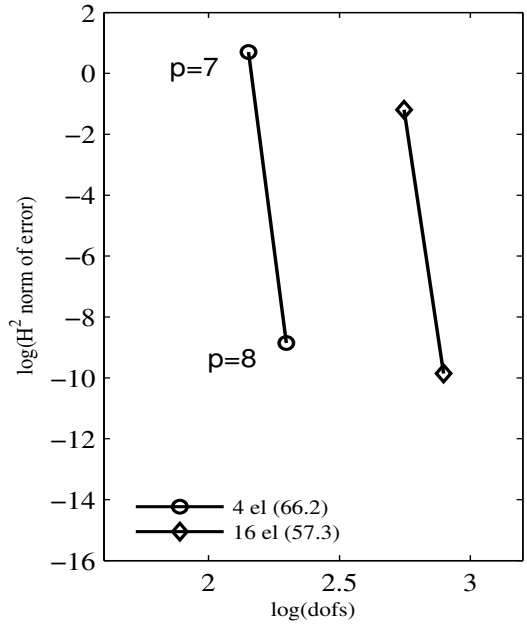

(d) H^2 norm of error in u versus dofs

Figure 4.78: Comparison of 4 element and 16 element discretizations using Distorted HGDA elements for 2-D non-linear Poisson's equation : C^{33}, **Distorted discretizations**

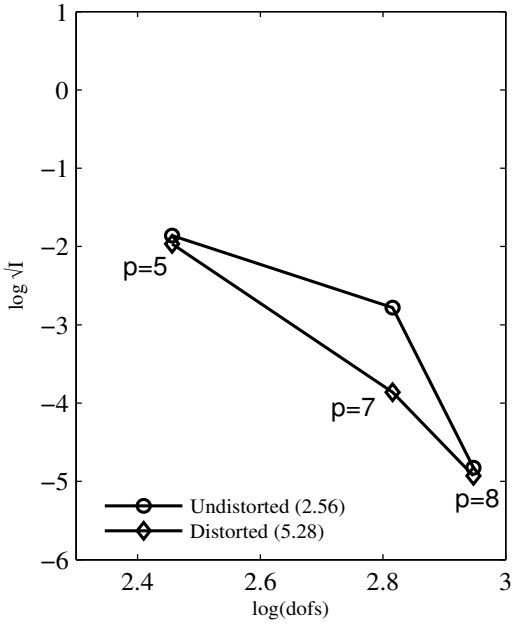

(a) √I versus dofs

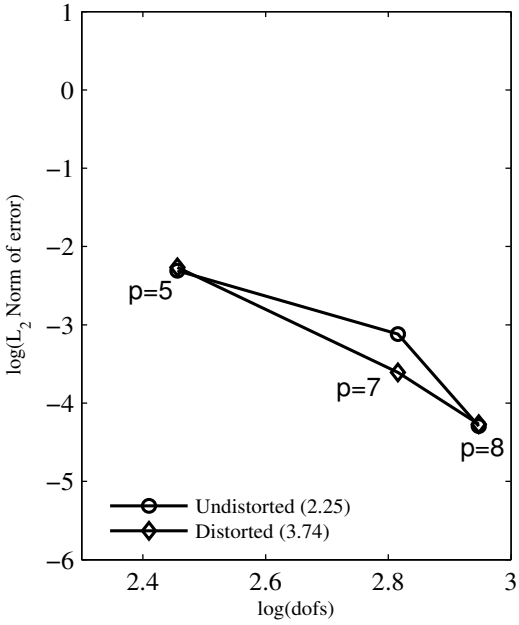

(b) L_2 norm of error in u versus dofs

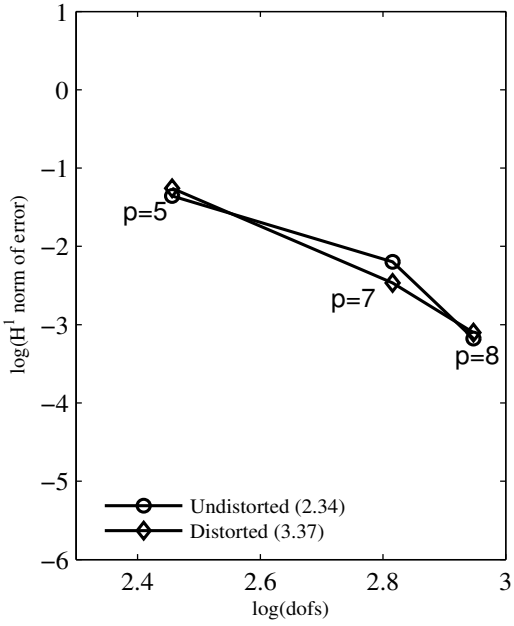

(c) H^1 norm of error in u versus dofs

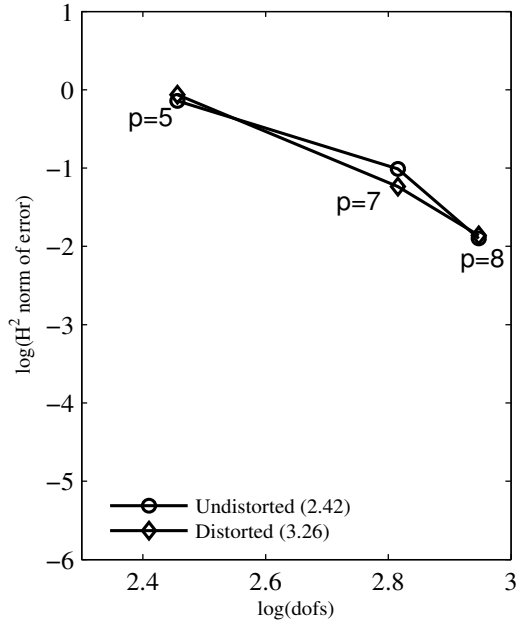

(d) H^2 norm of error in u versus dofs

Figure 4.79: Comparison of Distorted and Undistorted discretizations using Distorted HGDA elements for for 2-D Convection-diffusion equation : C^{22}, **16 element discretization**

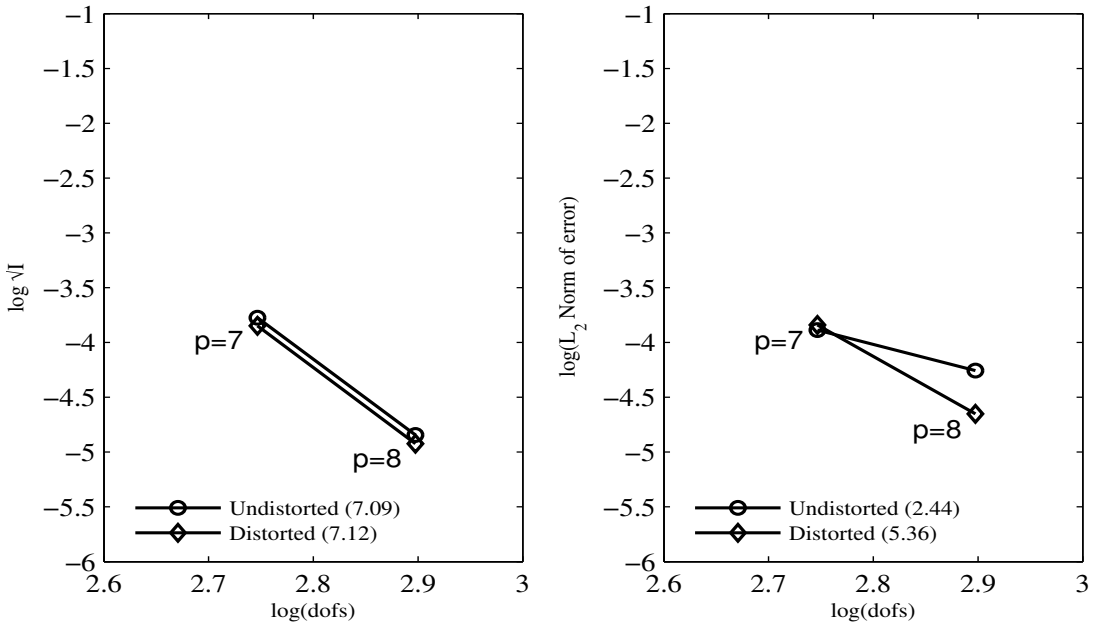

(a) √I versus dofs

(b) L_2 norm of error in u versus dofs

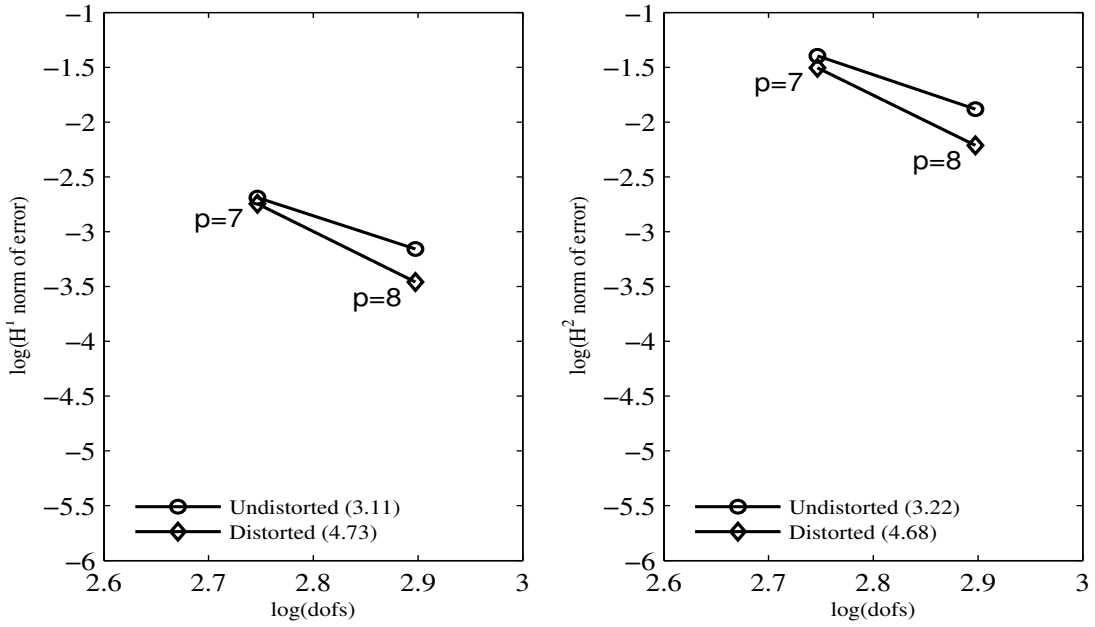

(c) H^1 norm of error in u versus dofs

(d) H^2 norm of error in u versus dofs

Figure 4.80: Comparison of Distorted and Undistorted discretizations using Distorted HGDA elements for for 2-D Convection-diffusion equation : C^{33}, **16 element discretization**

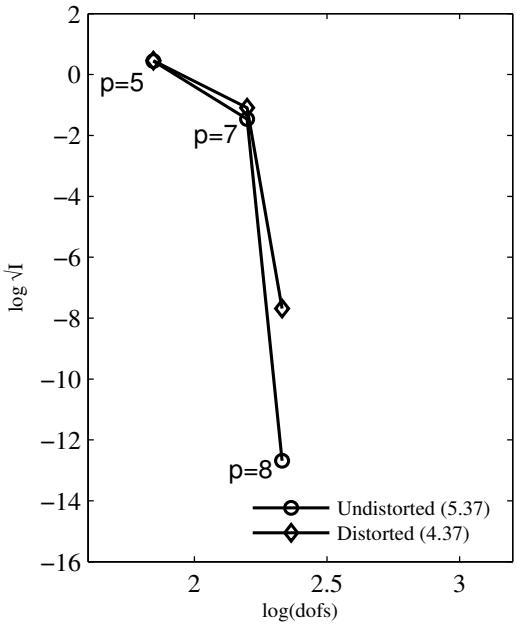

(a) √I versus dofs

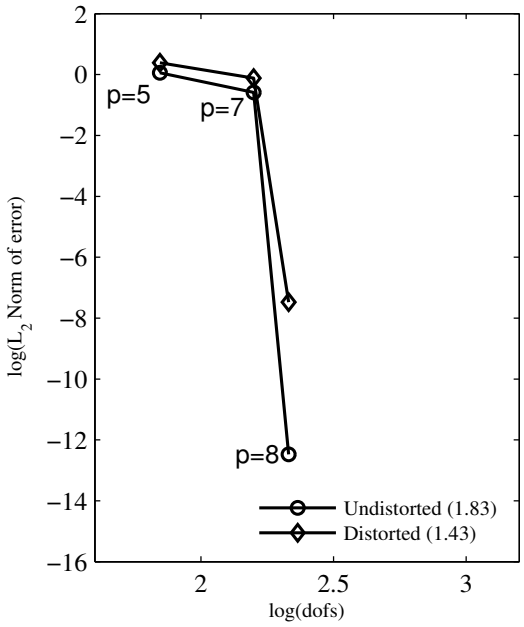

(b) L_2 norm of error in u versus dofs

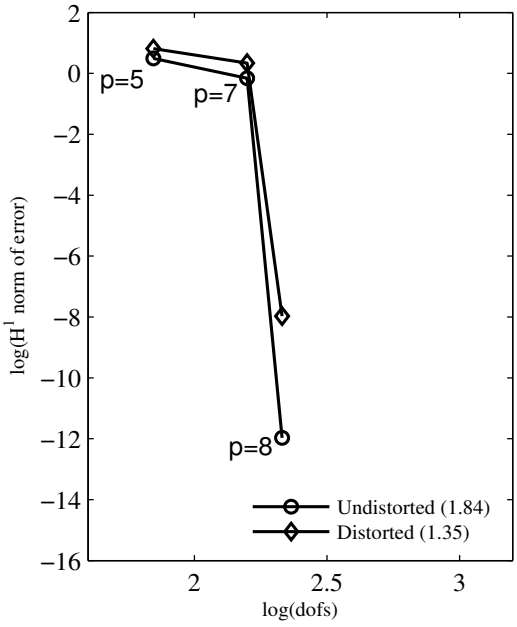

(c) H^1 norm of error in u versus dofs

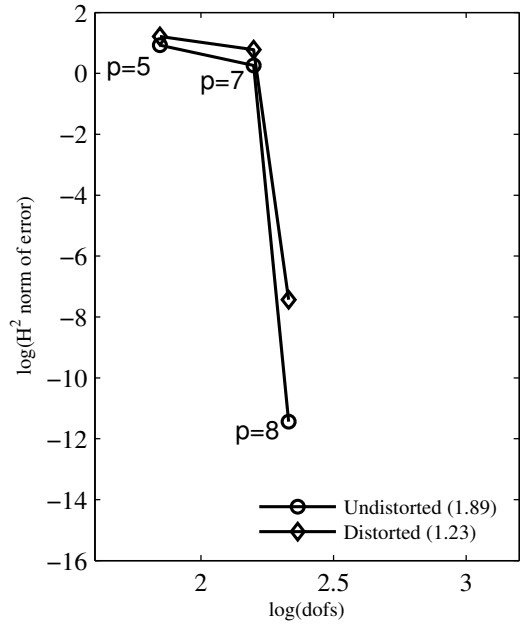

(d) H^2 norm of error in u versus dofs

Figure 4.81: Comparison of Distorted and Undistorted discretizations using Distorted HGDA elements for for 2-D non-linear Poisson's equation : C^{22}, **4 element discretization**

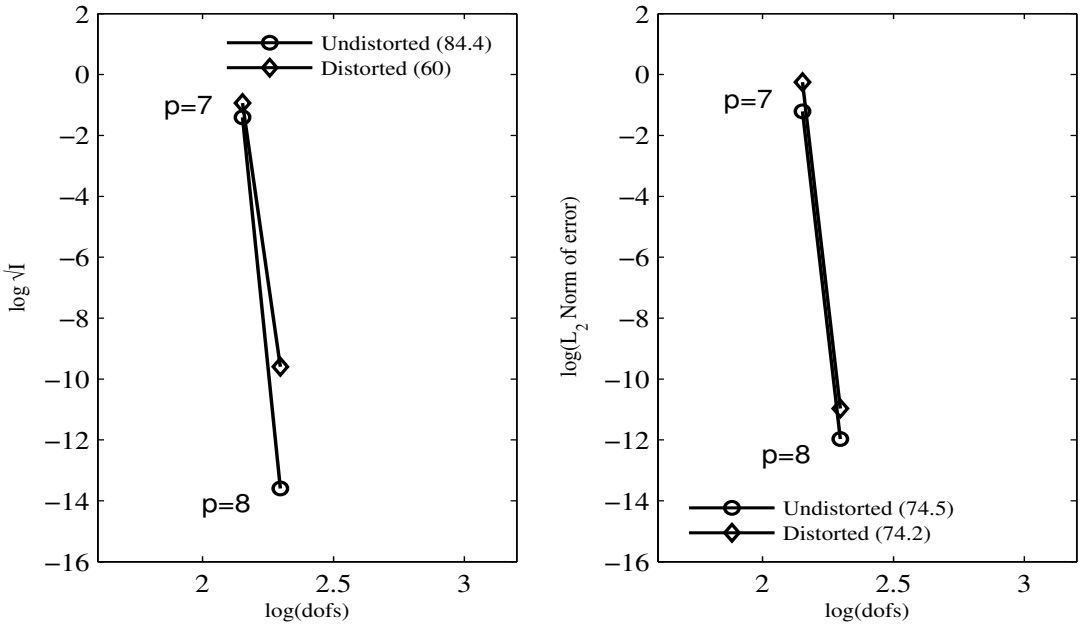

(a) √I versus dofs

(b) L_2 norm of error in u versus dofs

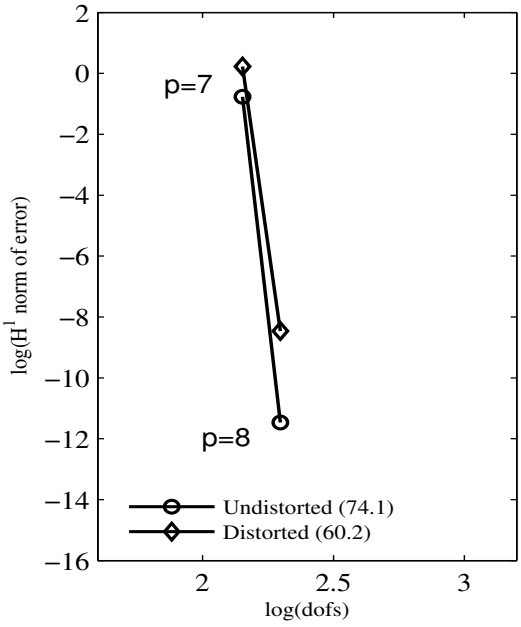

(c) H^1 norm of error in u versus dofs

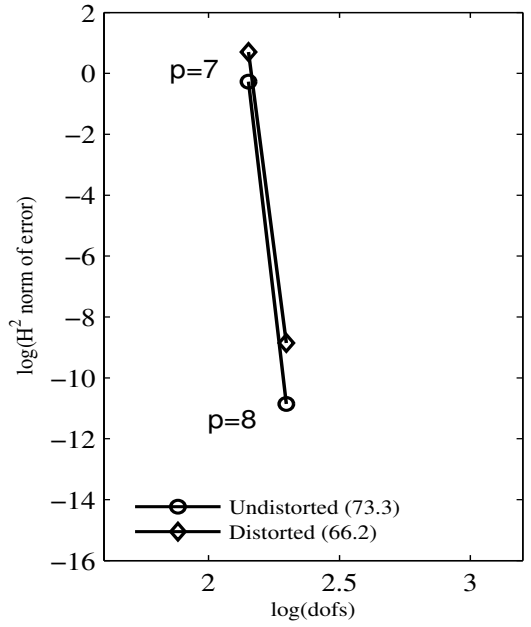

(d) H^2 norm of error in u versus dofs

Figure 4.82: Comparison of Distorted and Undistorted discretizations using Distorted HGDA elements for for 2-D non-linear Poisson's equation : C^{33}, **4 element discretization**

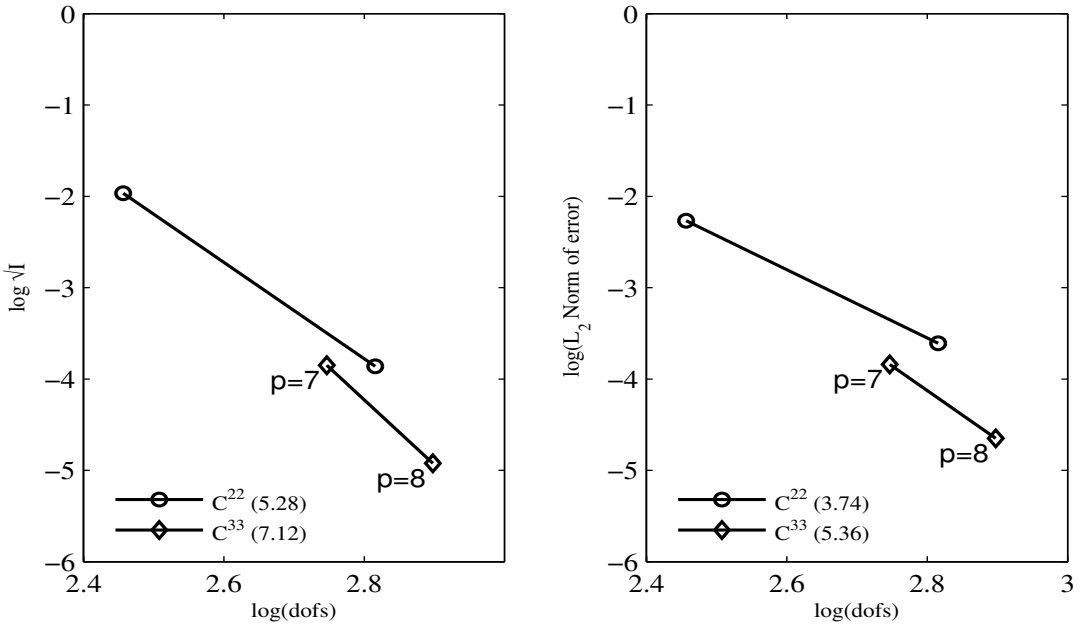

(a) $\sqrt{I}$ versus dofs

(b) L_2 norm of error in u versus dofs

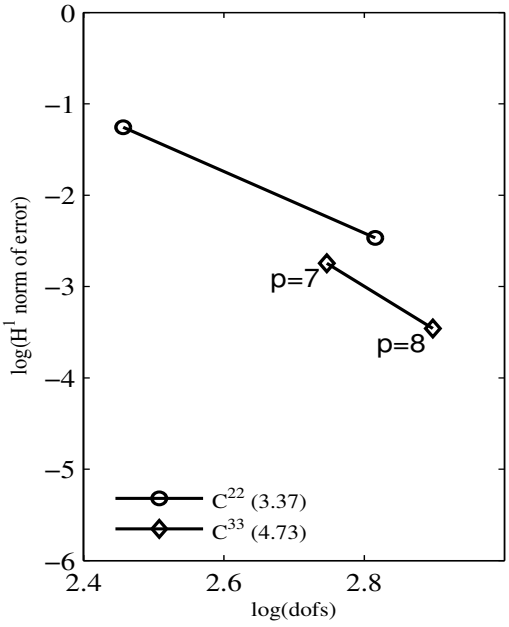

(c) H^1 norm of error in u versus dofs

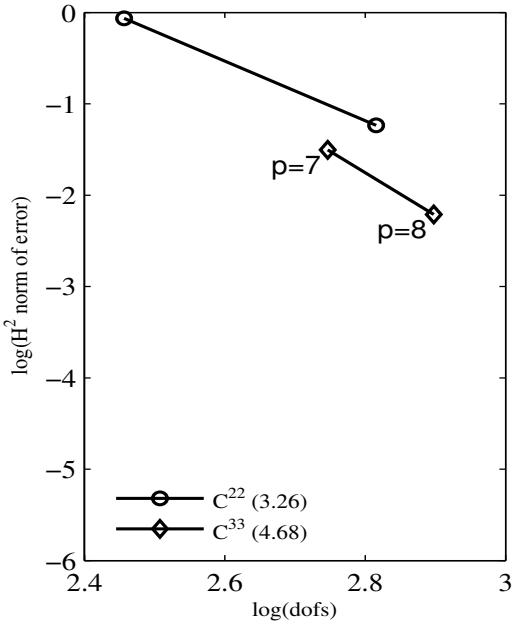

(d) H^2 norm of error in u versus dofs

Figure 4.83: Comparison of C^{ij} Distorted HGDA elements for 2-D Convection-diffusion equation : $\boldsymbol{C^{22}}$ ($\boldsymbol{k = 3}$), $\boldsymbol{C^{33}}$ ($k = 4$), **16 element Distorted discretization**

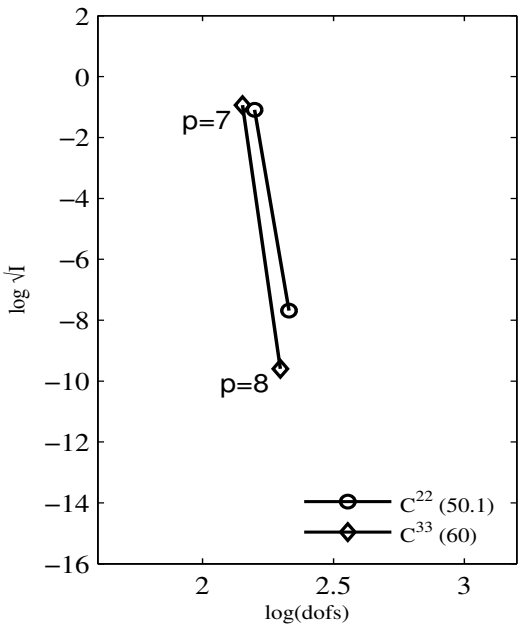

(a) √I versus dofs

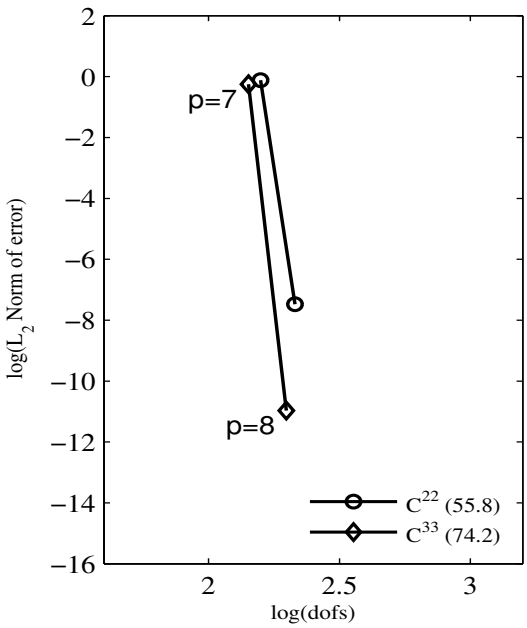

(b) L_2 norm of error in u versus dofs

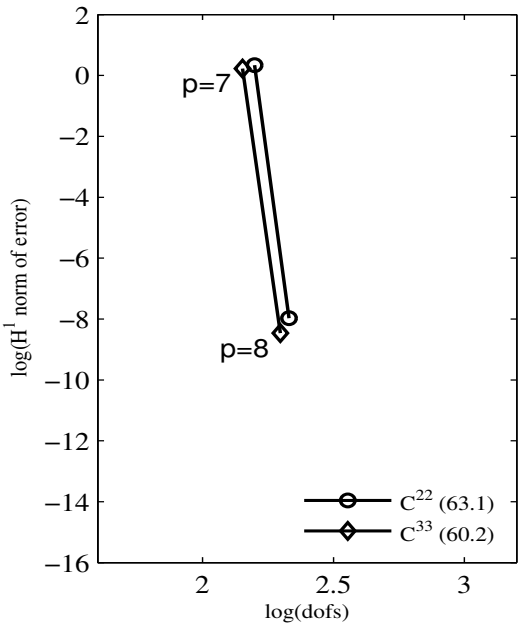

(c) H^1 norm of error in u versus dofs

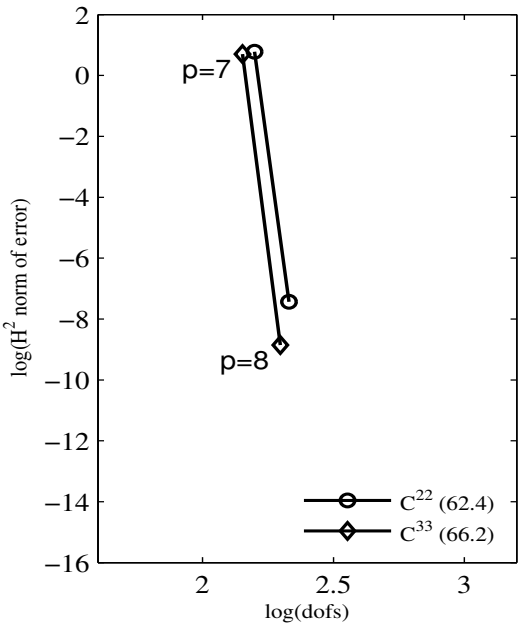

(d) H^2 norm of error in u versus dofs

Figure 4.84: Comparison of C^{ij} Distorted HGDA elements for 2-D non-linear Poisson's equation : $\boldsymbol{C^{22}}$ **(**$\boldsymbol{k=3}$**)**, $\boldsymbol{C^{33}}$ $(k=4)$**, 4 element Distorted discretization**

4.6 Summary

In this chapter, numerical studies for model problems defined by self-adjoint (2-D Poisson's equation), non self-adjoint (2-D Convection-diffusion equation) and non-linear (2-D non-linear Poisson's equation) differential operators are solved using the HGDA elements developed in Chapter 2. The studies are conducted with rectangular as well as non-rectangular discretizations. For rectangular meshes, solution is computed with HGDA as well as tensor product elements and a comparison of their convergence rates is made. For rectangular discretizations, tensor product elements have best performance and hence can be considered as benchmark results. For (rectangular or non-rectangular discretization), we conduct two studies: (i) h-convergence (ii) p-convergence. Galerkin method with weak form (GAL) and Least squares processes (LSP) are used for self-adjoint operators whereas only Least squares processes is utilized for non self-adjoint and non-linear operators In all the numerical studies presented here, various of interest are computed to assess performance of the developed HGDA elements.

Chapter 5

Summary, Conclusions and Future work

This thesis presents a general framework and a systematic procedure for the development of higher order global differentiability local approximations for 2-D and 3-D distorted element geometries. Although, global differentiability has been recognized as an important aspect in all numerical computations, very little has been done to design mathematical and computational processes in which higher-order global smoothness is achievable. In chapter 1, a brief literature review of the work done in developing higher order global differentiability elements is presented.

Surana et al. [5] have shown that when the element geometry is rectangular, higher order global differentiability approximations (HGDA) can be easily derived using tensor product of 1-D higher order continuity approximations. When the element geometries are distorted, the tensor product approach cannot be utilized in deriving these approximation functions. Thus, the derivation of HGDA for 2-D and 3-D distorted elements in xy and xyz space requires a fundamentally different approach.

The curved element in 2-D xy or 3-D xyz physical coordinate space is mapped to a master element in $\xi\eta$ or $\xi\eta\zeta$ natural coordinate space. We borrow appropriate degrees of freedom and corresponding approximation functions from a standard set of 2-D C^{00} or 3-D C^{000} p-version hierarchical local approximations to derive the desired derivative degrees of freedom at the corner nodes of the new 2-D or 3-D HGDA element being

generated. The new derivative degrees of freedom at the corner nodes of a C^{ij} or C^{ijk} HGDA element are chosen in such a way that these can be transformed from natural coordinate space to the physical coordinate space using Jacobians of transformations for the derivatives of various orders. Pascal rectangle, Pascal triangle and Pascal pyramid provided a systematic selection process for accomplishing this selection process for 2-D rectangular, 2-D triangular and 3-D hexahedral geometries respectively.

The framework to derive higher order global differentiability local approximations for 2-D distorted element geometries is presented in Chapter 2. We consider 2-D distorted quadrilateral elements as well as triangular elements. C^{00} p-version hierarchical approximations are used as a basis in deriving HGDA elements. The required degrees of freedom are borrowed from the mid-side nodes and center node of C^{00} hierarchical element and the Jacobians of transformation presented. The degrees of freedom are borrowed from the hierarchical nodes in such a way that (i) lowest degree admissible functions (corresponding to a lower p-level) are selected first (ii) a symmetric pattern is maintained in selecting the approximation functions.

In Chapter 3, the framework presented in Chapter 2 is extended to 3-D distorted elements of hexahedral geometry. C^{000} p-version hierarchical approximations are used as a basis in deriving the desired HGDA elements. The rules of borrowing degrees of freedom from the hierarchical nodes (mid-side and face nodes) remain the same as in case of 2-D HGDA elements.

Numerical studies are presented in Chapter 4. Various quantities of interest (least squares error or quadratic functional, L_2 norm, H_1 norm, H_2 norm of error in the solution) are computed for model problems described by self-adjoint, non self-adjoint and non-linear differential operators. For self-adjoint operator, we consider Galerkin method with weak form as well as Least squares processes while only Least squares process is considered for non self-adjoint and non-linear operators [1–4]. The model problems considered are 2-D steady state Poisson's equation, Convection-diffusion equation and non-linear Poisson's equation. The numerical studies assess the performance of the developed HGDA elements of distorted geometries as well as those based on tensor product.

Surana et al. [1–4] have shown that higher order global differentiability local approximations:

(1) allow us to incorporate the desired physics in the design of a computational process

(2) eliminate the need for auxiliary equations and auxiliary variables in least squares processes, thereby reducing the number of variables significantly, especially for 2-D and 3-D cases.

(3) with the proper choices of the order k of the approximation space all integrals in the formulation become Riemann integrals as apposed to Lebesgue integrals.

(4) provide improved accuracy for the same number of degrees of freedom compared to C^0 processes.

With the development of a general framework to derive desired order global differentiability local approximations for distorted element geometries, the objective of applying hpk framework to irregular domains of definitions of boundary value problems or initial value problems is made possible. In conclusion, higher order global differentiability local approximations is rather a natural way to design a computational process with desired continuity and differentiability features that are dictated by the physics.

Future work

The work presented here demonstrates that C^{11} HGDA elements for quadrilateral shapes need further work. The C^{11} local approximations derived using the approach presented here are such that center node approximation functions remain the same as those for C^{00} local approximations. The same holds in case of C^{11} triangular HGDA local approximations. In addition, numerical studies need to be performed for C^{11} HGDA triangular elements. The infrastructure for C^{11} triangular elements including quadrature has been tested and appears to perform well. A complete infrastructure for deriving 3-D HGDA hexahedral family of elements of distorted shape has also been

presented. The C^{111} and C^{222} HGDA local approximations for these elements also seem to have the same problem as C^{11} HGDA elements and need further investigation. The numerical studies for the 3-D hexahedron family of HGDA elements need to be performed. An extension of the infrastructure presented for triangular elements needs to be considered for 3-D tetrahedron family.

Appendix A

Numerical Integration

Irregular or curved domains in Finite element method are accurately represented by distorted or non-rectangular elements. The derivation of local approximation functions for irregular elements is complicated and hence these elements are mapped into master elements over which these interpolations can be easily derived. For example, in two dimensions, quadrilateral elements are usually mapped into a 2-unit square and triangular elements are mapped into a 2-unit equilateral triangle. In computing stiffness matrices in finite element method, integral statements defined over these distorted geometries are transformed into expressions involving natural coordinate axes. This transformation results in complex expressions and the integrals are generally solved using numerical integration techniques (such as Gauss-Legendre numerical integration scheme).

Integral expressions are usually of the form:

$$I = \int \int_{\Omega_e} F(x, y) dx dy \tag{A.1}$$

where Ω_e represents a typical finite element. The integrand is a function of the global coordinates x and y and may contain not only functions but also derivatives with respect to the global coordinates. The integrand is rewritten in terms of coordinates ξ and η of the master element. The mapping $x = \sum_{i=1}^{n} N_i(\xi, \eta) x_i$, $y = \sum_{i=1}^{n} N_i(\xi, \eta) y_i$ transforms the element so that the integration is performed on the standard element

Ω_{st}. Under this mapping, the above integral can be rewritten as

$$I = \int \int_{\Omega_{st}} F(\xi, \eta)|J| \, d\xi d\eta \tag{A.2}$$

where $|J|$ is the determinant of the Jacobian matrix defined by

$$[J] = \begin{bmatrix} \frac{\partial x}{\partial \xi} & \frac{\partial y}{\partial \xi} \\ \frac{\partial x}{\partial \eta} & \frac{\partial y}{\partial \eta} \end{bmatrix} \tag{A.3}$$

Integration over a master rectangular element [47]

Standard quadrature rules for integrals over a rectangular master element Ω_{st} are derived from the one-dimensional quadrature formulae. We have

$$I = \int \int_{\Omega_{st}} F(\xi, \eta)|J| \, d\xi d\eta \approx \sum_{i=1}^{m} \sum_{j=1}^{n} F(\xi_i, \eta_j) W_i W_j |J| \tag{A.4}$$

where m and n denote the number of quadrature points in the natural coordinate axes ξ and η, ξ_i, η_j denote gauss points and W_i and W_j denote the corresponding Gauss weights [47]. The number of points are selected in such a way that the expression can be integrated exactly. A polynomial of degree p is integrated exactly with $(p+1)/2$ points in both ξ and η and therefore $m = n$.

Integration over a master triangular element [26]

In case of triangles, the mapping functions are usually in terms of area coordinates L_1, L_2, L_3. In general, the quadrature rules using area coordinates [50] should be used. However, the area coordinates L_1, L_2, L_3 can be related to the orthogonal natural coor-

dinates ξ, η, through the relations introduced by Szabo [26].

$$\begin{aligned} L_1 &= \tfrac{1}{2}(1-\xi-\tfrac{\eta}{\sqrt{3}}) \\ L_2 &= \tfrac{1}{2}(1+\xi-\tfrac{\eta}{\sqrt{3}}) \\ L_3 &= \tfrac{\eta}{\sqrt{3}} \end{aligned} \tag{A.5}$$

Szabo [26] introduced the following mapping to transform the standard quadrilateral element into the standard triangular element by collapsing the side $\eta = 1$ of the standard quadrilateral element into the point $\xi_t = 0$, $\eta = \sqrt{3}$.

$$\xi = \frac{1}{2}\xi_r(1-\eta_r)\ ,\ \eta = \frac{\sqrt{3}}{2}(1+\eta_r) \tag{A.6}$$

where ξ_r and η_r are the natural coordinates of the master element corresponding to quadrilateral elements. For this mapping, we have the following transformation of the derivatives with respect to natural coordinates corresponding to master rectangular and triangular elements.

$$\left\{ \begin{array}{c} \frac{\partial}{\partial \xi_r} \\ \frac{\partial}{\partial \eta_r} \end{array} \right\} = \left\{ \begin{array}{cc} \frac{1-\eta_r}{2} & 0 \\ -\frac{1}{2\xi_r} & \frac{\sqrt{3}}{2} \end{array} \right\} \left\{ \begin{array}{c} \frac{\partial}{\partial \xi} \\ \frac{\partial}{\partial \eta} \end{array} \right\} \tag{A.7}$$

Let the determinant of the Jacobian of transformation in the above equation be denoted by $|J_1|$.

For the integration of the finite element integrals over the master triangular elements, we have the following:

$$I = \int\int_{\Omega_{st^t}} F(\xi,\eta)\ |J|\ d\xi d\eta = \int\int_{\Omega_{st^r}} F(\xi_r,\eta_r)\ |J|\ |J_1|\ d\xi_r d\eta_r \tag{A.8}$$

where Ω_{st^t} and Ω_{st^r} represent standard triangular and rectangular master elements.

This is less efficient than the integration rules employing area coordinates [50] but allows us to utilize the quadrature rules for standard rectangular elements.

Bibliography

[1] KS. Surana, AR. Ahmadi, and JN. Reddy. The k-version of Finite Element Method for Self-Adjoint Operators in BVP. *International Journal of Computational Engineering Science (IJCES)*, 3(2):155–218, 2002.

[2] KS. Surana, AR. Ahmadi, and JN. Reddy. The k-Version Of Finite Element Method For Non-Self-Adjoint Operators In BVP. *International Journal of Computational Engineering Science (IJCES)*, 4(4):737–812, 2003.

[3] KS. Surana, AR. Ahmadi, and JN. Reddy. k–version of Finite Element Method for Non-Linear Operators in BVP. *International Journal of Computational Engineering Science (IJCES)*, 5(1):133–207, 2004.

[4] KS. Surana, S. Allu, and JN. Reddy. k–version of Finite Element Method for Initial Value Problems: Mathematical and Computational Framework. *International Journal of Computational Engineering Science (IJCES)*, 8(3):123–136, 2007.

[5] KS. Surana, SR. Petti, AR. Ahmadi, and JN. Reddy. On p-version hierarchical interpolation functions for higher-order continuity finite element models. *International Journal of Computational Engineering Science*, 2(4):653–673, 2001.

[6] C. Johnson. *Numerical solution of Partial Differential Equations by the Finite Element Method*. Cambridge University Press, Cambridge, UK, 1987.

[7] PG. Ciarlet. *The Finite Element Method for Elliptic Problems*. North Holland, The Netherlands, 1978.

[8] GF. Carey and JT. Oden. *Finite Elements, Mathematical Aspects*. Prentice Hall, Englewood Cliffs, NJ, 1984.

[9] G. Strang and G. Fix. *An Analysis of The Finite Element Method*. Prentice Hall, Englewood Cliffs, NJ, 1973.

[10] JN. Reddy. *Functional Analysis and Variational Methods in Engineering*. McGraw-Hill, New York, 1986.

[11] OC. Zienkiewicz and CJ. Parekh. Transient Field Problems: Two-Dimensional and Three-Dimensional Analysis by Isoparametric Finite Elements. *International Journal of Numerical Method of Engineering*, 2:61–71, 1970.

[12] WK. Liu and T. Belytschko. Efficient linear and nonlinear heat conduction with a quadrilateral element. *International Journal for Numerical Methods in Engineering*, 20:931–948, 1984.

[13] P. Silvester. High-order polynomial triangular finite elements for potential problems. *Int. J. Eng. Sci*, 7:849–861, 1969.

[14] RL. Taylor. On completeness of shape functions for finite element analysis. *International Journal for Numerical Methods in Engineering*, 4(1):17–22, 1972.

[15] OC. Zienkiewicz, BM. Irons, FC. Scott, and J. Campbell. Three dimensional stress analysis. *Proc. IUTAM Symp. on High Speed Computing of Elastic Structures*, pages 413–433, 1971.

[16] I. Babuska and MR. Dorr. Error estimates for the combined h and p versions of the finite element method. *Numerische Mathematik*, 37(2):257–277, 1981.

[17] B. Guo and I. Babuska. The hp-version of the finite element method. Part 1: The basic approximation results. Part 2: General results and applications. *Comput. Mech*, 1:21–41, 203–226, 1986.

[18] W. Gui and I. Babuška. The h, p and hp versions of the finite element method in 1 dimension. Part 1. The error analysis of the p-version. *Numerische Mathematik*, 49(6):577–612, 1986.

[19] I. Babuska and BQ. Guo. The hp Version of the Finite Element Method with Curved Boundary. *SIAM J. Numer. Anal*, 24:837–861, 1988.

[26] BA. Szabo and I. Babuska. *Finite Element Analysis*. Wiley-Interscience, 1991.

[20] A. Peano. Efficient high order finite elements for shells. *Meccanica*, 11(1):42–47, 1976.

[21] MP. Rossow, JC. Lee, and KC. Chen. Computer implementation of the constraint method(finite element structural analysis). *Computers and Structures*, 6:203–209, 1976.

[22] KS. Surana and NJ. Orth. Completely hierarchical axisymmetric shell element based on p-version for heat conduction in laminated composites. *Computers and Structures*, 38(4), 1991.

[23] KS. Surana and RM. Sorem. p-version hierarchical three dimensional curved shell element for elastostatics. *International Journal for Numerical Methods in Engineering*, 31:649–676, 1991.

[24] KS Surana and Y. Guo. p-Version axisymmetric solid element for heat conduction. *Comp. Struct.*, 38(4):415–428, 1991.

[25] D. Winterscheidt and KS. Surana. p-version least squares finite element formulation for convection-diffusion problems. *International Journal for Numerical Methods in Engineering*, 36(1):111–133, 1993.

[27] S. Adjerid, M. Aiffa, and JE. Flaherty. Hierarchical finite element bases for triangular and tetrahedral elements. *Computer Methods in Applied Mechanics and Engineering*, 190(22):2925–2941, 2001.

[28] P. Tong. Simplex elements of C^0 continuity with varying polynomial degrees. *International journal for numerical methods in engineering*, 11:27–38, 1977.

[29] P. Rahulkumar, S. Saigal, and S. Yunus. Singular p-version finite elements for stress intensity factor computations. *International Journal for Numerical Methods in Engineering*, 40(6):1091–1114, 1997.

[30] P. Carnevali, RB. Morris, Y. Tsuji, and G. Taylor. New basis functions and computational procedures for p-version finite element analysis. *International Journal for Numerical Methods in Engineering*, 36:3759–3779, 1993.

[31] G. Strang. Variational crimes in the finite element method. *Annals of Mathematics Study*, 33, Priceton University Press, Princeton, NJ, 1954.

[32] GP. Bazeley, YK. Cheung, BM. Irons, and OC. Zienkiewics. Triangular elements in plate bending- conforming and non-conforming solutions(Stiffness characteristics of triangular plate elements in bending, and solutions). *Conference on Matrix Methods in Structural Mechanics, Air Force Institute of Technology*, pages Air Force Institute of Technology, Wright–Patterson, Ohio, 1965.

[33] B. Nayroles, G. Touzot, and P. Villon. Generalizing the finite element method: Diffuse approximation and diffuse elements. *Computational Mechanics*, 10(5):307–318, 1992.

[34] T. Belytschko, YY. Lu, and L. Gu. Element-free Galerkin methods. *International Journal for Numerical Methods in Engineering*, 37(2):229–256, 1994.

[35] J. Patera and FT. Pettman. Isoparametric Hermite elements. *International Journal for Numerical Methods in Engineering*, 37:3489–3519, 1994.

[36] AG. Peano. *Hierarchies of conforming finite elements*. PhD thesis, Washington University, 1975.

[37] DW. Wang, IN. Katz, and BA. Szabo. Implementation of a C^1 triangular element based on the p-version of the finite element method(structural analysis computer code). *Computers and Structures*, 19(3):381–392, 1984.

[38] A. Overhauser. Analytic definilion of curves and surfaces by parabolic blending, Technical Report SL 68-40, Ford Motor Company, 1968.

[39] H. Hashemolhosseini, N. Sadati, and M. Farzin. A new class of C^n interpolations and its application to the finite element method. *Int. J. Numer. Meth. Engng*, 53:1781–1800, 2002.

[40] B. Bigdeli and DW. Kelly. C^*-convergence in the finite element method. *International Journal for Numerical Methods in Engineering*, 40(23):4405–4425, 1997.

[41] J. Kratochvil, A. Zenisek, and M. Zlamal. A simple algorithm for the stiffness matrix of triangular plate bending elements(Stiffness matrix algorithm for triangular plate bending elements using hierarchy of interpolation polynomials). *International journal for numerical methods in engineering*, 3:553–563, 1971.

[42] KS. Surana and DG. Van Dyne. Non-weak strong solutions in gas dynamics: a C^{11} p-version STLSFEF in Lagrangian frame of reference using; u; p primitive variables. *Int. J. Numer. Meth. Engng*, 53:1025–1050, 2002.

[43] KS Surana and DG. Van Dyne. Non-weak strong solutions in gas dynamics: a C^{11} p-version STLSFEF in Eulerian frame of reference using; u; p primitive variables. *Int. J. Numer. Meth. Engng*, 53:1051–1099, 2002.

[44] HV Nayak. Solutions of class C^{00} and C^{11} of Two dimensional Newtonian and Polymer flows. *Ph.D. Dissertation*, University of Kansas, 2001.

[45] KS Surana and M. Bona. Non-weak/strong solutions of linear and non-linear hyperbolic and parabolic equations resulting from a single constitutive law. *Int. J. Comp. Eng. Sci.*, 1(2):299–330, 2000.

[46] A. Ahmadi, KS. Surana, and JN. Reddy. Higher order global differentiability approximations for 2D distorted element geometries. *7th World Congress on Computational Mechanics*, July 16-22, Los Angeles, CA, 2006.

[47] J.N. Reddy. *An introduction to the finite element method*. McGraw-Hill Singapore, 1993.

[48] F.Murnaghan. *Finite Deformation of an Elastic solid*. Dover, New York, 1951.

[49] G. Dhondt and G.D.C. Dhondt. *The Finite Element Method for Three-Dimensional Thermomechanical Applications*. John Wiley and Sons, 2004.

[50] DA. Dunavant. High Degree Efficient Symmetric Gaussian Quadrature Rules for the Triangle. *International Journal for Numerical Methods in Engineering*, 21:1129–1148, 1985.